University of Nevada, Reno

miR-10b Rescues Diabetes and GI Dysmotility Associated with a Leaky Gut

A dissertation submitted in partial fulfillment of the requirements for the degree of

Doctor of Philosophy in Cellular and Molecular Biology

by

Hannah Zogg

Seungil Ro, Ph.D. – Dissertation Advisor

December 2022

THE GRADUATE SCHOOL

We recommend that the dissertation
prepared under our supervision by

Hannah Zogg

entitled

miR-10b Rescues Diabetes and GI Dysmotility Associated with a Leaky Gut

be accepted in partial fulfillment of the
requirements for the degree of

DOCTOR OF PHILOSOPHY

Seungil Ro, Ph.D.
Advisor

Caroline Cobine, Ph.D.
Committee Member

Brian Perrino, Ph.D.
Committee Member

Sal Baker, Ph.D.
Committee Member

Subhash Verma, Ph.D.
Committee Member

Cyprian Rossetto, Ph.D.
Graduate School Representative

Markus Kemmelmeier, Ph.D., Dean
Graduate School

December, 2022

ABSTRACT

Of all microorganisms in the human body, the largest and most complex population resides in the gastrointestinal (GI) tract. The gut microbiota continuously adapts to the host environment and serves multiple critical functions for their hosts, including regulating host immunity, procuring energy from food, and preventing the colonization of pathogens. Mounting evidence has suggested gut immune dysfunction, impaired barrier function, and gut dysmotility play a key role in the development of metabolic disorders and disorders of gut-brain interactions (DGBIs).

In reference to the Rome IV criteria, the most common DGBIs, include functional dyspepsia (FD) and irritable bowel syndrome (IBS). Additionally, there is substantial overlap of these disorders and other specific GI motility disorders such as gastroparesis. These disorders are heterogeneous and are intertwined with several proposed pathophysiological mechanisms, such as altered gut motility, intestinal barrier dysfunction, gut immune dysfunction, visceral hypersensitivity, altered GI secretion, presence and degree of bile acid malabsorption, microbial dysbiosis, and alterations to the gut-brain axis. The currently available therapies lack long-term effectiveness and safety for their use to treat motility disorders and DGBIs. Additionally, currently available treatment options simply treat the symptoms and not the pathological mechanism causing the disorder. Pharmacological agents that are developed based on the cellular and molecular mechanisms underlying the pathologies of these disorders might provide the best avenue for future pharmaceutical development.

Current advances in RNA-based therapies have substantial promise in treating and preventing many human diseases and disorders through fixing the pathology instead of merely treating the symptomology, like traditional therapeutics. Although many RNA therapeutics have made it to clinical trials, only a few have been FDA-approved thus far. Additionally, the results of clinical trials for RNA therapeutics have been ambivalent to date, with some studies demonstrating potent efficacy, whereas others have limited effectiveness and/or toxicity. Momentum is building

in the clinic for RNA therapeutics; future clinical care of human diseases will likely be comprised of promising RNA therapeutics.

There has been phenomenal progress in understanding the cellular and molecular mechanisms of DGBIs. However, the precise cellular and molecular pathogeneses of gut dysfunctions are yet enigmatic. Important regulatory mechanisms are mediated through mircoRNAs (miRNAs) and they play an essential role in gut health. miRNAs are small non-coding RNA molecules that post-transcriptionally regulate gene expression by binding to specific mRNA targets to repress their translation and/or promote the target mRNA degradation. Dysregulation of miRNAs might impair gut physiological functions leading to DGBIs and gut motility disorders. Studies have shown miRNAs regulate gut functions such as visceral sensation, gut immune response, GI barrier function, enteric neuronal development, and GI motility. These biological processes are highly relevant to the gut where neuroimmune interactions are key contributors in controlling gut homeostasis and functional defects lead to DGBIs. The therapeutic targeting of miRNAs represents an attractive approach for the treatment of DGBIs because they offer new insights into disease mechanisms and have great potential to be used in the clinic as diagnostic markers and therapeutic targets. Additionally, miRNAs might be beneficial for the treatment of DGBIs because they might be able to return functionality of key cells in the maintenance of normal gut homeostasis such as interstitial cells of Cajal (ICCs), enterochromaffin (EC cells), enteric neurons, smooth muscle cells, gut immune cells, etc. that are normally dysregulated in these conditions.

Our previous studies demonstrated that depletion of miR-10b in KIT^{+} cells has been shown to cause the development of diabetes and gut dysmotility through the KLF11-KIT pathway. Recent studies have also shown that the leaky gut is connected to both diabetes and gut dysmotility; however, there is no direct evidence indicating whether or not the leaky gut is the linking mechanism between these conditions. Here we aimed to elucidate if global loss of miR-10b leads to the development of the leaky gut and if this is the linking mechanism between hyperglycemia and gut dysmotility. First, we created a *mir-10b* global KO (gKO) mouse model using CRISPR-Mb3Cas12a/Mb3Cpf1. Using

both loss-of-function and gain-of-function studies we found that the leaky gut phenotype is a core pathophysiological mechanism linking the hyperglycemic and gut dysmotility phenotypes. Finally, we found that treating the mice with a miR-10b mimic rescues these phenotypes and might have substantial therapeutic potential for the treatment of diabetes, gut dysmotility, and the leaky gut.

Dedication

I would like to dedicate my dissertation to the following individuals who have impacted my life in such a huge way:

Dillon Zogg, none of this would be possible without your endless support. You have believed in me since day one and I cannot thank you enough for that.

Dena Zeidner, you taught me the importance of education and inspired my passion for learning.

Chris Phillips, I owe every ounce of my inquisitive brain to you. No question of mine ever went unanswered, which allowed my curiosity, a key asset for a scientist, to flourish.

Daniel Zogg, this is all for you. You encouraged me to keep pursuing this degree, be the best role model for you, and give you the best life possible.

Janet Spencer, for being the first teacher to believe in my future as a scientist. Without your class I likely would have given up on my dream of becoming a biologist.

Dr. Kelly McDonald, for being the absolute most amazing role model throughout my undergraduate program at Sacramento State University. You helped foster my confidence in myself, which was essential in my decision to go on to pursue this graduate degree.

Acknowledgments

I would like to thank Dr. Seungil Ro for his constant support over the last five years. None of this work would have been possible without him. His mentorship has helped me hone my scientific writing and systematic exploration skills.

I would also like to thank the other members of my exceptional committee: Dr. Subash Verma, Dr. Sal Baker, Dr. Brian Perrino, Dr. Caroline Cobine, and Dr. Cyprian Rossetto for always critically analyzing my work and challenging me in the best ways throughout this program.

I owe so much to the following people for their encouragement and guidance during my time in the CMB PhD program: Dr. Rajan Singh, for not only being the most amazing mentor, but also one of my best friends; Dr. Seeun Ha, for being extremely supportive and always helping me whenever I ran into any problems; Dr. Brian Jorgensen, for truly inspiring my confidence in myself; Dr. Byungchang Jin for always being the calm in the storm; Dr. Lai Wei, for helping me become a master of cloning; Mariah Ha, Mirabel Dafinone, Tylar Batalon, and Nick Hoeberg, for always being there to help when I needed an extra set of hands. Most importantly, for allowing me to develop my mentorship abilities; Sushmita Debnath M.B.B.S, for your invaluable assistance with lab work during this writing process; and Sandra Poudrier, for her exceptional support all throughout my PhD.

Additionally, I would like to thank my friends for their constant encouragement and support. Juliana Velasquez, Leah MacNiven, Andrew Zareie, Erin Zareie, Allison Bartlett, Alex Henrikson, Jasen Brooks Frizzell, and Sam Brooks Frizzell, and Dr. Nicci Abbott, your friendship has helped me grow into the scientist and person I am today.

Finally, I want to acknowledge my family for inspiring me to follow my dreams and helping me achieve my goals every step of the way. Dillon Zogg, Carissa Alcantar, Bobby Alcantar, Emily Croson, Dena Zeidner, Chris Phillips, Michelle Phillips, Liam Priestley, Phil Zeidner, Diane Keppel, Kim North, Wesley North, Chrissie Bowen, Jay Bowen, Jason Bowen, Jeremy Bowen,

Daryl Zogg, Tina Zogg, and Maddison Zogg, your never wavering belief in me has enabled me to complete this work and I am fortunate to have each and every one of you in my life.

Table of Contents

List of Tables

List of Figures

CHAPTER ONE: Gut Microbial Dysbiosis in the Pathogenesis of Gastrointestinal Dysmotility and Metabolic Disorders

Introduction

Trillions of microorganisms live inside every human.[1, 2] Not surprisingly, these microbial inhabitants outnumber all of the human cells in the entire body by approximately one order of magnitude (10^{14} *vs.* 10^{13}, respectively).[3] To better grasp the role that gut microbes play in health and disease, scientists around the globe are investigating gut microbiota and their metabolites that play a fundamental role in modulating metabolic, developmental, and physiological aspects.[1, 4] Many human diseases originate from distorted gut microbiota composition (dysbiosis) leading to dysregulation of physiological and metabolic processes.[3-5] The gut microbial dysbiosis has been implicated in functional gastrointestinal (GI) disorders including irritable bowel syndrome (IBS), functional dyspepsia (FD), and inflammatory bowel diseases (Crohn's disease, and ulcerative colitis).[6-9]

In 2019 there were approximately 463 million people suffering from type 2 diabetes (T2D) and 4.2 million deaths due to T2D-related complications.[10] Currently, T2D is projected to affect 700 million people worldwide by 2045, which could become greater burden to the medical community already facing grim statistics.[10] Approximately 50% of diabetic patients also suffer from GI motility disorders including but not limited to diarrhea, fecal incontinence, constipation, dyspepsia, and gastroparesis.[11-13] GI motility disorders are also extremely common, with approximately 40% of adults suffering from functional bowel disorders worldwide.[14] There is a great need to understand the molecular mechanisms that occurs in conditions associated with dysbiosis and how these altered pathways contribute to the development of GI motility disorders and T2D. There are currently many studies on creating a deeper understanding of microbiota-related mechanisms of disease pathogenesis with hope that it will lead to the development of effective, preventative and therapeutic interventions.[15-19] Here, we summarize the impact that the gut microbiome and its metabolites have on both GI motility disorders and metabolic diseases. Although, extensive review

of current literature identifies a lack of knowledge, the question persists as to whether the disruption of gut microbial communities is a consequence or cause of chronic GI and metabolic diseases.

Function, composition, and the dysbiosis of the gut microbiota

The GI tract is home to vast microbial communities including bacteria, fungi, archaea and viruses.[1, 20] The microbe population is more sparse in the upper gut (stomach, duodenum, and jejunum) with approximately10^3 bacteria per mL of aspirate, where there are approximately 10^7-10^{12} bacteria per mL of aspirate in the lower gut (ileum and proximal colon).[21] Gut microbiota perform many diverse functions, such as aiding in the digestion of food, production of essential vitamins, synthesis of metabolites, prevention of pathogenic bacteria colonization, gut-immune regulation, drug metabolism, detoxification, and maintenance of GI physiological homeostasis (Figure 1).[20, 22, 23] Hence, maintaining a healthy proportion of beneficial microbes, also called eubiosis, is essential for human health.

Gut microbial imbalance, known as dysbiosis, can include an increase in the proportion of small bowel bacteria, alteration in the relative proportion of benevolent microbes to pathogenic ones, as well as the translocation of colonic bacteria.[4, 24] At a fundamental level, there are many contributing factors for the progression of a diseased states including microbe-microbe interactions, microbial metabolites, host immune response, host physiology, diet, and the host environment.[5, 25, 26]

Gut microbiota composition and relative abundance changes throughout the varying microenvironments of the GI tract[27] and over 50 bacterial phyla have been identified in the human GI tract so far.[28] In the healthy host *Bacteroidetes* and *Firmicutes* are the most predominantly found phyla in the gut, while *Proteobacteria, Verrucomicrobia, Actinobacteria, Fusobacteria,* and *Cyanobacteria* are found in much smaller proportions.[29] Generally, the various segments of the GI tract are colonized by different microbial communities; Gram-positive bacteria are prevalent in the small intestine while Gram-negative bacteria are predominate in the large intestine.[21] Approximately 95% of bacteria presiding in the colon are strict anaerobes, which is determined by

the available nutrients.[30] Small intestinal bacterial overgrowth is largely determined by intrinsic and extrinsic factors.[31] The most notable intrinsic factors preventing this overgrowth of bacteria are gastric acid and bile acid secretion, peristaltic movement, normal gut defense mechanisms, the production of mucin, gut antibacterial peptides, and prevention of bacterial retrograde translocation from the lower gut to the upper gut *via* the ileocecal valve.[32, 33] Extrinsic factors include nutrient intake and diet, bacterial and viral infection, medications altering motility (prokinetics), and drugs modulating the gut microbiota, for instance, pre- and probiotics, proton pump inhibitors (PPIs), H2 blockers, and antibiotics.[34-36] If any one of the extrinsic factors cause imbalance to off-set the many protective mechanisms set in place, commensal and pathogenic gut microbiota may colonize disproportionately and lead to dysbiosis. One example of dysbiosis is the development of small intestinal bacterial overgrowth (SIBO), diagnosed by overall bacterial overgrowth equal to or greater than 10^5 colony forming units (CFU) per mL of upper gut (*e.g.*, jejunal) aspirate culture.[37] However, overgrowth of bacteria equal to or greater than 10^3 CFU/mL of upper gut aspirate has also been included in the diagnosis of SIBO recently.[38] Based on jejunal aspirate cultures, one study showed that *Escherichia coli, Streptococcus species, Pseudomonas aeruginosa*, *Staphylococcus species*, *Acinetobacter baumannii, Acinetobacter lwoffii, Enterococcus faecium, Klebsiella pneumoniae*, and *Enterococcus faecalis* were predominantly found in patients with SIBO who suffered altered GI motility.[39]

Gut microbiota affects host physiology

The gut microbiota provides its host with essential health benefits primarily by maintaining healthy gut homeostasis.[4, 5] Currently, scientists are investigating what makes a healthy gut microbiome and exploring the molecular mechanisms and signaling pathways that allow for crosstalk between gut microorganisms and the host. Many studies have shown that pathogens have the ability to impair the epithelial barrier dysfunction.[40-42] In contrast, commensal gut microbiota have been found to act as gatekeepers to protect epithelial cell integrity from penetration and disease caused by pathogens.[43] Other beneficial effects of commensal gut microbiota include micronutrient production, such as vitamin K and folate.[44] Colonic bacteria ferment unabsorbed

carbohydrates to SCFAs, which can be subsequently absorbed through the colonic mucosa and used as an additional energy source.[45] Most importantly, commensal gut microbiota is essential to prevent colonization and translocation with pathogenic bacteria at the intestinal epithelial barrier.[46]

SIBO has been found to lead to several complications in affected hosts,[28, 47] including destruction of microvilli and heightened epithelial inflammatory response, which many times results in impaired absorption.[48, 49] The bacteria responsible for the harmful effects of SIBO are often aerobes; however, in a healthy gut the small intestine primarily houses facultative anaerobes.[50] This microbial shift in patients with SIBO leads to the malabsorption of fat and a deficiency in the fat-soluble vitamins D, E, A and K.[51] Common symptoms of SIBO are abdominal discomfort, gas, distension and bloating and are likely caused by the dysregulated fermentation of carbohydrates and bacterial colonization in the small intestine, which produce methane (CH_4), carbon dioxide (CO_2) and hydrogen (H_2).[52, 53]

Gut microbial alterations in GI dysmotility and metabolic disorders

Gut microbial alterations and GI dysmotility:

Peristaltic movements are of paramount importance for the foods to properly travel through the gut.[54] Peristalsis is generated by a coordination of both contraction and relaxation of the circular and longitudinal smooth muscles of the muscularis externa[55] and are regulated by the enteric nervous system (ENS), GI smooth muscle cells (SMCs), pacemaker cells called interstitial cells of Cajal (ICCs), enterochromaffin (EC) cells, as well as other factors.[56-60] In addition to host-specific genetic predispositions, diet and microbiota are critical regulators of GI physiology.[16, 17, 61] Furthermore, altered microbiota composition of the lumen and mucus layer covering the epithelium often accompany GI disorders.[7] As the complexities of the gut microbiota are being increasingly understood, it has revealed that microbe-host interaction, including immune and metabolic responses, are extremely important pathological factors of GI motility disorders. Previous research has shown significant changes in the gut microbiota of patients with IBS when compared to that of healthy individuals, which may contribute significantly to altered bowel habits caused by impaired

colonic transit.[62, 63] However, it is still inconclusive whether the gut microbial signature is different between IBS patients and healthy controls. Also, more robust future studies are warranted to confirm whether this is an association and/or causation. A microbiome 'signature' for diseases like IBS has been proposed and based upon previous literature would generally include reduced overall microbial diversity as well as an abundance of methanogenic or *Clostridiales* species, which are more commonly associated with increasing severity IBS symptoms.[64] *Clostridiales* spp have been shown to adversely affect normal GI activity due to their role in serotonin synthesis, although more research is needed to confirm the causative relationship.[6] Immune dysregulation, intestinal barrier dysfunction, and altered gut microbial signaling have been at the forefront of understanding the microbiome-related pathogenesis of GI disease.[7, 15, 65]

Further evidence of the relationship between microbial dysbiosis and GI motility is demonstrated by the association between SIBO and GI dysfunction. Proper GI motility allows for a constant flow of luminal material through the GI tract, which prevents bacterial overgrowth of in the small intestine.[66] However, patients presenting with GI dysmotility have a stagnant flow of luminal material, contributing to the development of SIBO.[67] For example, patients with malabsorption syndromes have delayed upper gut motility and later also developed SIBO.[67] Additionally, SIBO predisposes dysfunctional defense mechanisms of the gut.[68] Gut defense mechanisms that prevent SIBO are mediated *via* secretory immuno-globulin (Ig)-A, gastric acid, duodenal bile, and defensins.[69] Defensins are host antimicrobial peptides, which contribute to the innate immunity of the gut and as one type of microbicidal agent, the adequate concentration of defensin plays a vital role in inhibiting pathogenic organism colonization and maintaining commensal bacteria.[70, 71] For instance, SIBO-induced GI dysfunction is a result of several mechanisms including disproportionate immune activation and inflammation, inadequate GI motility, intestinal epithelial barrier dysfunction, dysregulated BA deconjugation and serotonergic modulation.[20, 72, 73] Individuals with SIBO often contain bacteria that is commonly found in the colon, including the Gram-negative, carbohydrate-fermenting, facultative aerobes and anaerobes such as *Escherichia coli*, *Klebsiella pneumonia*, *Enterococcus spp,* and *Proteus mirabilis*.[31, 52, 74-76] Not surprisingly, in patients with SIBO versus

those without, the small intestinal luminal contents had different metabolomic profiles[77] and in another study patients with malabsorption syndrome had higher quantities of total BAs, lactate, acetate, and formate compared to controls.[78] A similar study in subjects with SIBO found that patients were also unable to properly absorb these substances.[35] Additionally, patients with malabsorption syndrome were found to have a positive correlation with the quantity of acetate and the degree of symptom severity of SIBO. [35] In the same study, unconjugated BAs positively correlated with the degree of steatorrhea, or malabsorption of fat in the intestine.[35] Indicating that bacteria commonly found in the small intestine of SIBO patients contributes to the excess production of acetate and deconjugated BA, leading to malabsorption of fat. The inability of intestinal epithelial cells to absorb short-chain fatty acids (SCFAs) leads to further damage in small intestinal epithelial cells, inducing barrier dysfunction, ileal brake, and leading to stasis and eventually bacterial colonization.[24]

Gut microbial alterations and metabolic disorders:

There have been many studies demonstrating how gut microbiota contribute to the regulation of metabolic homeostasis and through microbial dysbiosis, can lead to metabolic dysregulation and diseases; mechanisms include but are not limited to changes to gut barrier function and metabolic inflammation.[5, 79, 80] Furthermore, there is surmounting evidence of the importance of the microbiota in regulating body weight and in the development of T2D. For example, fecal microbiota transplantation (FMT) with healthy gut bacteria improves insulin sensitivity and weight loss in mice and human subjects.[81] The gut microbiota are able to produce and absorb host metabolism signaling molecules by regulating available energy extracted from indigestible carbohydrates to the host.[82, 83] While the primary phyla of the healthy gut remain relatively stable, colonization can be modified by diet, including prebiotics, and with probiotics and antibiotics, which have an effect on the production of microbial metabolites.[84] Still, future studies are warranted to confirm the occurrence of a gut microbial shift caused by the administration of prebiotics and probiotics. Antibiotics have the ability to decimate microbial populations and have been associated with the development of metabolic disease especially with early life exposure.[80]

Conversely, there has been recent evidence that the use of antibiotics may help regulate metabolic function by improving peripheral insulin sensitivity in obese patients.[84] A considerable amount of experimental data has been produced backing the role of microbiota in metabolic regulation and in the genesis of obesity.[85-87] Therefore, it should not be unexpected that several studies have found SIBO as a comorbidity in obese and diabetic patients alike.[88] Further, among individuals with T2D, the presence of SIBO has been associated with delayed gut transit, indicating an association between gut microbial dysbiosis, GI dysmotility, and metabolic disorder.[89] However, present knowledge is lacking robust and highly-controlled human studies examining the effects of microbial mechanisms on host metabolism. As discussed, these studies provide evidence that changes in the gut microbiota might provide an auspicious platform to treat diabetes-related metabolic disorders.

Microbial signaling uncovers pathogenesis of GI dysmotility and metabolic disease

Microbial signaling *via* metabolites or structural components of bacteria are transmitted across the intestinal epithelium to communicate with distant organs.[26] Once these signals are transmitted, they are able to affect organs through subsequent signaling *via* nerves or hormones.[90] Metabolic signaling from the gut microbiota have the potential to significantly affect the host, influencing health status.

Immune signals:

Immune signaling begins with the recognition of microbe-associated molecular patterns (MAMPs) which can include structural components such as lipopolysaccharide (LPS), flagellin and peptidoglycan by pattern-recognition receptors (PRRs). While there are many different types of PRRs, commonly used by host-microbe immune interactions are the Toll-like receptors (TLRs), RIG-1-like receptors (RLRs), or NOD-like receptors (NLRs) located on epithelial and immune cells.[91] In addition, the aryl hydrocarbon receptor (AHR), which is a transcription factor important for coordinating cellular responses to external stimuli, is stimulated by the *Lactobacilli* tryptophan ligand, indole-3-aldehyde.[92] Remarkably, it has been shown that in the dysbiosis-associated

conditions, the microbiota fail to generate AHR ligands contributing to the pathogenesis of GI and metabolic disorders[93, 94] as a recent study showed that AHR functions as a biosensor that connect the environment of the intestinal lumen to programming of the ENS *via* intestinal motility.[17] The ENS regulates most aspects of gut physiology through intrinsic neural networks which innervate throughout the GI system and is commonly called the second brain.[57] Distinct neuronal transcriptomes have been identified in various delineations of the GI tract as well as microbiota communities in mice. These transcriptome data led to the discovery that AHR has a defined role in regulating microbe-associated intestinal peristalsis in the surveillance pathway of the ENS.[17] Murine studies have also found that AHR deficiency enhances insulin sensitivity and reduces Peroxisome proliferator-activated receptor-α (PPAR-α), a key metabolic protein.[95] Thus, modulating AHR signaling independently or though gut microbiota modulation could help to treat conditions commonly associated with impaired gut motility and metabolic diseases. Taken together, the studies reviewed demonstrate that gut microbial dysbiosis alters host immune signals, which is a central pathogenic mechanism for GI dysmotility and metabolic disorders.

Short-chain fatty acids (SCFAs):

Butyrate, propionate, and acetate are the three most commonly studied SCFAs and are the major fermentation metabolites generated from gut microbial degradation of dietary fiber and help to provide up to 10% of the total energy required by the host.[96] Butyrate, propionate, and acetate are also important multifunctional signals produced by the gut microbiota and can bind to the G-protein-coupled receptors (GPCR) GPR43 and GPCR41, also known as free fatty acid receptor 2 and 3 (FFAR2 and FFAR3), respectively. SCFAs binding to FFAR3 induces expression of the hormone peptide YY (PYY) in enteroendocrine L-cells, which has been shown to normalize gut motility allowing for an increase in available energy harvested from food in mice.[97] Binding of SCFAs to FFAR2 and FFAR3 in the epithelial cells of small intestine and colon activates secretion glucagon-like peptide (GLP)-1 by L-cells, substantially impacting overall pancreatic function and insulin release, and hormonal effects regulating appetite.[98, 99] Independently, SCFAs perform a wide range of metabolic functions; propionate and butyrate are able to stimulate expression of

intestinal gluconeogenic enzymes and propionate is able to independently act as a precursor as intestinal gluconeogenesis.[100] All three major SCFAs are able to activate FFAR2 in mouse WAT, suppressing insulin signaling and therefore decreasing fat accumulation and further stimulating energy expenditure in hepatocytes and myocytes.[19, 101]

A study by Reigstad *et al*. demonstrated that gut microbiota derived metabolites in human and mouse trigger *Tph1* gene expression and serotonin (5-HT) production in the colon through stimulation of EC cells *via* SCFAs.[102] In this study, to explore the association between intestinal microbes, gut contractility, and serotonergic gene expression, germ-free (GF) or humanized (HM; ex-GF mice colonized with human gut microbiota) mice were used. Findings showed that the microbiota from conventionally raised mice (CR) and HM mice had caused a significant increase in colonic mRNAs of TPH1 compared to the GF mice.[102] These studies demonstrate that GI and metabolic homeostasis rely on SCFA production by the gut microbiota, which play a central role in regulating GI motility and metabolic functions.

Tryptamine:

Similar to 5-HT, tryptamine is a monoamine metabolite produced from tryptophan by gut bacteria, particularly *Ruminococcus gnavus* and *Clostridium sporogenes*, and is found abundantly in human and rodent stool samples.[103] In a study reported by Bhattarai *et al*., investigators determined that the role of tryptamine in the GI tract is facilitated by the 5-HT_4 receptor (5-HT_4R) that is only found in colonic epithelium.[16] Tryptamine produced by both GF and HM mice were shown to increase movement across the colonic epithelium as well as fluid secretions in colonoids, validating the importance of tryptamine for proper intestinal secretion. Additionally, improved GI motility was seen in GF mice that were colonized with tryptamine-producing engineered *Bacteroides thetaiotaomicron microbes*.[16] This study demonstrates that bacterial metabolites are able to control different facets of host physiology and could be used for localized treatments for GI disorders associated with constipation.

The aforementioned studies provide evidence that metabolites and byproducts essential to gut microbiome signaling fill a specific niche to maintain proper GI function and metabolic regulation. Further, these findings give insight into gut microbiota and host crosstalk alluding to future potential therapeutic options for GI dysmotility and metabolic disorders.

The gut-brain axis and gut microbiota: GI dysmotility and metabolic syndrome

The endocrine and nervous system are able to conduct and coordinate with absolute synergy each organ system in the body in order to maintain homeostasis.[104] The processes between the brain and the gut are bi-directional; as the brain modulates gut physiology, the gut is also able to influence brain function.[105] This bi-directional interaction has been demonstrated through the improvement in patients with hepatic encephalopathy after gut-microbiota directed antibiotic treatment.[106] Moreover, animal and human studies have demonstrated how the gut microbiota is able to affect brain function. For example, the study by De Palma *et. al* demonstrated that GF mice have altered hippocampal brain-derived neurotrophic factors (BDNF), dysregulated hypothalamic pituitary stress responses, impaired neurotransmission, diminished tryptophan availability and dysregulated metabolism further demonstrating a connection between the gut microbiota and the gut-brain axis.[107]

Bi-directional gut-brain interactions serve as important modulators of GI functionality influencing motility, gastric secretions, blood flow, immune activity, and visceral sensations.[108] Brain-to-gut bidirectional signaling can also affect the GI tract through indirect signaling between the gut microbiota and the host. Microbial organisms residing in the GI tract can cause increased intestinal epithelial permeability and modulate the mucosal immune response, leading to changes in host physiology.[109] Some evidences support that communication between the gut microbiota and intestinal epithelial cells occurs through luminal release from neurons, Paneth cells, and EC cells.[110] The perception of gut stimuli and modulation of various gut functions are conducted through the emotional motor system. The emotional motor system is described as complimentary parallel outflow systems which includes the sympathetic and parasympathetic branches of the autonomic system, and endogenous pain-modulation systems.[108] A bi-directional gut-brain microbiota axis is

established through the gut microbiota interactions with gut based effector systems and visceral afferent pathways.[108] Also, current research demonstrates that the host serotonin is synthesized in the gut *via* microbial-derived metabolites; these findings add further weight to the concept of a gut microbiota-gut-brain axis and its influence on GI homeostasis.[111]

Connecting the dots between the gut microbiota, brain, and metabolic control of insulin secretion, Perry and colleagues explored a pathway involving the 'rest-and-digest' and 'feed-and-breed' processes.[19] In this study, rats fed a high-fat diet had greater production and turnover of the SCFA, acetate, compared to normal control diet (NCD) rats. They found that by exposing stomachs of NCD rats with acetate, glucose-stimulated insulin secretion (GSIS) was increased, indicating a relationship between microbiota-derived acetate and insulin secretion.[19] The vagus nerve largely controls parasympathetic activity through motor inputs which are sent to various organs and is able to control heart rate, regulate GI movement, aid in the digestion of food, and enhance insulin secretion. Perry *et al.* demonstrated this by using parasympathetic blockers, atropine or methylatropine, or surgically severing portions of the vagus nerve connecting the gut, to prevent acetate from increasing GSIS.[19] This indicates that the beneficial effects of acetate-inducing GSIS is controlled through the vagus nerve and parasympathetic nervous system. To elucidate the role of microbiota acetate turnover in this study, Perry *et al*. performed FMT from NCD or high-fat diet donor rats into recipients on the opposite diet. Results showed that acetate levels and GSIS levels from the donor groups were transferred to recipient groups, implying that changes in the microbiota regulate acetate turnover and therefore GSIS. These powerful findings confirmed the gut microbiota–gut–brain axis influences metabolic homeostasis (Figure 2).

Strong pre-clinical data highlights that the gut microbiota is important for bi-directional interactions of the gut-brain axis in health and in disease. Therefore, gut microbial dysbiosis has pathophysiological effects on gut-brain bidirectional interactions leading to GI dysmotility and metabolic disorders. An emerging area that should be further explored is how the gut-brain axis is affected by the gut microbiota and their derived metabolites leading to metabolic benefits.

Gut microbiota mediated immune dysregulation in GI dysmotility and metabolic disease

The most important function of the GI tract is to take in food particles, digest these to smaller molecules, absorb nutrients, and excrete the undigested byproducts. The GI tract also harnesses the benefits of commensal microbiota, which play a part in regulating the host metabolism and directing proper immunity.[112] Like proper heart function, the functions of the GI tract, such as gut motility, are necessary for life. Current literature suggests proper gut motility is dependent on the interacting forces between the microbiome and ENS with the help of immune cells, like the tissue-resident muscularis macrophages (MMs). [113] MMs are in close proximity to the myenteric plexus of GI smooth muscle.[114] One study explored the functional role of MMs under normal physiological conditions and homeostatic crosstalk between ENS neurons and MMs.[114] Muller *et al.* showed that MMs are a unvarying subset of CX3CR1^{+} CD11cloMHCIIhi cells, dependent on CSF-1R, a cytokine receptor.[115] By using a low-dose anti-CSF-1R antibody blocking intraperitoneal injection they specifically depleted 80% of MMs, leaving stromal cells and other GI resident macrophage populations unharmed. By depleting this specific subset of macrophages, gastric emptying was accelerated, and colonic emptying was reduced in mice. Further, *in vitro* experiments demonstrated the homeostatic role of MMs in regulating peristalsis showing signs of deregulated and hyperreactive, contractions of the muscularis externa. In addition to the distinctive role of MMs, to establish the molecular mechanisms contributing to these effects, researchers analyzed the nonimmune MM transcripts, and found novel expression of bone morphogenetic protein 2 (BMP2) that is known to stimulate the BMP receptors I and II (BMPRI and BMPRII). Neuronal and smooth muscle development relies on BMP receptors indicating BMP2 may be a candidate for MM-mediated control of peristalsis. It is well established that the intestinal microbiota possess the ability to instruct mucosal immune cells and therefore influence the composition of the gut microbiota.[112] Studies have also shown that GF mice and mice treated with antibiotics experience GI dysmotility.[115] However, how is it possible for the intestinal microbiota to influence MM function given the distance between the intestinal lumen and MMs? To answer this question, Muller *et al.* treated mice with antibiotics and found decreased expression of BMP2, CSF1, and

decreased numbers of MMs, alluding to reliance on the microbiome. Notably, treated mice also developed delayed GI transit. These findings advance our understanding of communication that occurs during inflammation between the nervous system and immune system and shows the significance of bi-directional neuroimmune communication for maintaining proper human body functions.[116] An important component of this study was also in the identification of BMP2 as an additional neurotrophic factor produced by macrophages, in addition to BDNF[117] . From this we can deduce that the intestinal microbiota is an essential component in the neuroimmune crosstalk and MMs act as intermediaries between the ENS and the gut microbiota (Figure 2).

Metabolic disorders, as in obesity and T2D, are associated with low-grade chronic inflammation in adipose tissue, liver, skeletal muscle, pancreas, brain, and intestines.[118] Elevated levels of the circulating pro-inflammatory cytokines tumor necrosis factor a (TNF- α), interleukin (IL)- 1β, and IL-6 were found in high fat diet induced obese mice and humans and was found to lead to insulin resistance and T2D.[119] In obesity, there can be a disproportionate amount of visceral adipose tissue (VAT) caused by the accumulated pro-inflammatory immune cells and reduced of anti-inflammatory ones, which leads to chronic, low-grade inflammation. VAT, which is hormonally active, can be considered as a major driver of insulin resistance in obese animal models and humans.[118, 120, 121] Other organs also develop low-grade inflammation, which also contributes to insulin resistance.[118, 122] Billions of microbes are constantly interacting with epithelial mucosa in the gut, which keeps intestinal immune system incessantly active. Intestinal barrier dysfunction is widely accepted as one of the first events in GI dysmotility and metabolic disorders and leads to immune cell infiltration and low-grade inflammation of the gut mucosa.[118] Mainly, intestinal barrier dysfunction caused by microbial dysbiosis plays a critical component in the development of immune dysregulation leading to GI and metabolic disease.[123] Recently in a study published in *Science* by Thaiss *et al.*, T2D and obesity mouse models showed that hyperglycemia led to intestinal barrier dysfunction through transcriptional restructuring of GLUT2-dependent intestinal epithelial cells and altered tight junction and adherence protein integrity.[124] As a consequence of hyperglycemia-mediated epithelial barrier disruption, a systemic influx of microbial products can enhance allocation

of intestinal microbiome products leading to enteric infection. However, barrier function is restored, and the microbiota is contained upon treatment and management of hyperglycemia, intestinal epithelial-specific GLUT2 deletion, or by inhibition of glucose metabolism.[124] Glycemic control, indicated by glycated hemoglobin levels, was shown to correlate with the systemic influx of intestinal microbiome products. Collectively, these results provide a mechanistic connection of the hyperglycemic condition and intestinal barrier dysfunction with the systemic inflammatory and potentially infectious consequences of obesity and T2D. Most importantly, this study shows that metabolic syndrome revolves around the gut, supports the hypothesis that imbalances in metabolic processes may begin in the gut, and highlights intestinal barrier dysfunction, mediated by gut microbial dysbiosis, as a core pathophysiology of GI dysmotility and metabolic disease (Figure 2).

Gut microbial dysbiosis connects GI dysmotility with metabolic disorders

GI dysmotility is commonly diagnosed in patients with metabolic disorders.[11, 13] Accumulating evidence has shown that gut microbial dysbiosis and the resulting intestinal barrier dysfunction link these two conditions. For example, a recent study showed how duodenal microbial dysbiosis is linked with enteropathy and intestinal barrier dysfunction in the environmental enteric dysfunction (EED) condition.[125] EED is a subclinical syndrome characterized by intestinal villous blunting, reduced absorptive capacity, and increased intestinal inflammation.[125, 126] Furthermore, there have been several metabolic consequences, such as malnutrition and stunting, in patients with EED. However, findings from this study raise additional questions: Is environmental enteropathy caused by a form of bacterial overgrowth in the small intestine? If so, how does SIBO alter GI motility? In response to these questions, we reviewed an article published on tropical sprue (TS), a type of malabsorption syndrome which has clinical and histological features similar to EED.[67] This study demonstrated that there was increased intestinal bacterial colonization in patients with TS. Furthermore, there is a vicious cycle of SIBO and small intestinal stasis due to the ileal brake induced by unabsorbed fat passing through the ileum.[127] SIBO also deconjugates bile acids, which further caused fat malabsorption and may even change gut motility. Malabsorption

of fat induces ileal brake by liberating gut hormones such as peptide YY and neurotensin.[67] Therefore, orocecal transit time (OCTT) was found to be longer in patients with TS than in controls.

Further evidence supporting intestinal barrier dysfunction as a pathogenic mechanism for metabolic disorders is illuminated by two recent studies. One study demonstrated that hyperglycemia drives intestinal barrier dysfunction and increases the risk for enteric infection.[124] In contrast, a second study showed loss of the gut barrier integrity triggers activation of islet-reactive T cells and autoimmune diabetes.[128] While it is currently unclear whether intestinal barrier dysfunction or metabolic disorder comes first, it is clear that there is a direct connection between these two conditions. Interestingly, research over the past few decades has indicated that intestinal barrier dysfunction is a major pathophysiological mechanism for the development of GI dysmotility and functional bowel disorders.[129] Further studies provided evidence for this connection by demonstrating that the development of IBS follows acute infective gastroenteritis, a condition known as post-infectious IBS (PI-IBS).[130] Taken together, the aforementioned studies indicated that intestinal barrier dysfunction is associated with gut microbial dysbiosis and is likely a key pathophysiological mechanism that links metabolic disorders with GI dysmotility.

Furthermore, we reviewed some proof-of-concept studies that provide a direct connection between metabolic and GI motility disorders through microbial dysbiosis. Landmark studies have demonstrated that altering the gut microbiota during stages of critical developmental has lasting metabolic consequences.[131, 132] A large retrospective cohort study reported that prescription for antibiotics within the first 2 years of life is associated with the development of early childhood obesity.[133] Also, antibiotic-induced depletion of the gut microbiota has been shown to induce changes in serotonin biosynthesis and to delay GI motility.[134] Moreover, studies have demonstrated that gut microbial alterations, especially alterations leading to increased abundance of methanogens, leads to the development of slow transit constipation.[135] These state-of-the-art studies clearly indicate that intestinal barrier dysfunction brought about by gut microbial dysbiosis is a central pathogenic mechanism for metabolic as well as GI motility disorders.

Treatment options for gut microbial dysbiosis

Current management options for gut microbial dysbiosis include antibiotics, fecal microbiota transplantation (FMT), as well as diet and probiotic interventions (Figure 3).

Antibiotics:

Minimally absorbed antibiotics neomycin and rifaximin led to improved colonic motility as evidenced in clinical trials in patients with IBS.[136, 137] In addition, several studies have shown that exposure to a combination of antibiotics for approximately 4-8 weeks in obesity mouse models or high-fat diet fed mice substantially improves metabolic parameters including: increased glucose tolerance, reduction in fat mass, and lowered hepatic steatosis in hepatic and systemic inflammation; these changes are also associated with changes in gut microbiota composition, gut barrier dysfunction, and metabolic endotoxemia.[4, 138] However, we desperately need well-designed human clinical trials to test if the efficacy of these intervention techniques are applicable to humans and may lead to manipulation of the gut microbiota contributing to hampered metabolism and the manifestation of metabolic disorders. The most studied treatment for patients with SIBO is rifaximin, a non-systemic antibiotic.[139] A systematic review and meta-analysis (26 studies) of rifaximin reported that SIBO was improved or resolved in 70.8% of patients.[140] However, systemic antibiotics, such as norfloxacin, have also been reported to also eradicate SIBO.[52] A meta-analysis (10 prospective clinical studies) of non-systemic antibiotics found more normal H_2-breath tests in patients with SIBO that had been treated with an antibiotic compared to patients that received a placebo (51.1% *vs.* 9.8%, respectively).[141]

FMT:

FMT is also thought to be beneficial in treating microbial dysbiosis as it could restore ‘healthy’ microbes in diseased patients.[142] However, whether FMT as a treatment for IBS is a panacea or placebo, is still debatable. A double-blind randomized controlled trial including 165 patients with IBS showed that after FMT, IBS symptom severity significantly improved when compared to a placebo control group, although there were no outstanding changes in the degree

of overall dysbiosis.[143] In a recent metanalysis, data pooled from five different randomized controlled trials found no significant improvements in IBS symptoms of patients who received FMT *vs.* placebo.[144] However, larger and more rigorous trials are needed; studies included in this metanalysis were small and included potential for a high-risk of bias.[145] Interestingly, FMT eliminated SIBO in 71% of patients with chronic intestinal pseudo-obstruction.[146] Another study demonstrated the effect of a lean donor (allogenic) versus own (autologous) FMT to recipients with metabolic syndrome.[147] Changes in blood plasma metabolites, such as g-aminobutyric acid, indicate metabolic responses responsible for the observed improved insulin sensitivity in the allogenic FMT group. However, this improvement is dependent on the fact that the patient had decreased fecal microbial diversity at the start of the study. Further, changes in intestinal microbiota composition is associated with the beneficial effects on glucose metabolism seen in patients in the allogenic group and may be predicted from fecal microbiota composition before treatment.[147]

Probiotics:

Probiotics, live microorganisms, are believed to have favorable effects on the gut microbiota.[148] However, there have only been a few clinical studies examining this option, and they lack consistency. Recently, a meta-analysis found that improved clearance of SIBO was associated with probiotic use.[149] Probiotics have also been shown to confer health benefits in patients with IBS although the mechanism responsible for improved symptomology needs more studies.[150] Another study found that probiotics from fermented camel milk significantly restored blood glucose and lipid levels back to healthy levels in the db/db T2D mouse model.[151] In addition, researchers found that insulin secretion was improved in probiotic treated diabetic mice due to upregulation of GPR43/41, which improved glucose-triggered GLP-1 secretion.[151] Taken together, the studies presented show promise for probiotic treatment in GI motility disorders as well as metabolic disease.

Dietary intervention:

'You and your microbiome are what you eat'.[152, 153] Our gut microbiome is largely influenced by our diet because it modulates the richness of specific colonizers and their individual and collective functions. Microbial community changes facilitated by diet could have a detrimental effect for host health due to the essential role that the microbiome plays in regulating host physiology.[154] A superlative option for a low-risk treatment intended to modulate the microbiome would be to change the patients' diet. Therefore, utilizing diet and diet-based studies to change microbial communities could present novel therapeutic strategies for conditions in which the gut microbiota and its associated metabolic products have been shown to harm the host or be key in disease pathogenesis. An exciting question arises of whether the presence of the individual's specific microbiome fingerprint can actually influence dietary preferences of the host, and therefore influencing positive feedback loops. In a study in which patients with obesity were assigned several different control diets, researchers found that the fecal microbiota profiles associated more by individual than by diet.[155] On the contrary, in response to the dietary changes, marked changes were found in the relative abundance of dominant microbial phylotypes.[155] Wu *et al*. reported a correlation between long-term dietary habits and two enterotypes that were defined in 96 adults.[156] High fiber intake conferred a 'Prevotella-type' community and high protein intake was associated with a 'Bacteroides-type' community. This implies that dietary patterns may influence the enterotypes found in the host. Another interesting study found that populations of Italian and African children had significant differences in fecal microbiota, which can be explained due to different dietary habits.[157] In these samples, Italian children had higher intakes of starch and proteins compared to African populations and showed a higher proportion of *Bacteroides spp.* and *Firmicutes*, suggesting that both short-term and long-term dietary shifts can lead to compositional changes of the gut microbiota.

Dietary intervention has the potential to be a powerful tool in helping patients overcome microbial dysbiosis.[86] In patients suffering from conditions as a result of gut dysbiosis, translocated colonic bacteria residing in the small bowel ferment carbohydrates causing excessive gas, abdominal pain, and bloating. Therefore, with the temporary restriction of dietary components, such

as diets low in fermentable oligo-di-monosaccharides and polyols, hence the (FODMAP), has been suggested to improve symptoms of IBS and of dysbiosis.[158] Low FODMAP diets have been associated with reduced absolute abundance of bacteria, which may have significant beneficial effects in the treatment of SIBO or other dysbiosis conditions.[159] Moreover, a diet high in complex carbohydrates preferentially encourages the growth of less pathogenic bacteria than a diet rich in fats or protein.[152] Primarily vegetarian diets abundant in fiber lead to increased production of SCFAs, which inhibit potentially invasive bacteria from colonizing the gut.[160] While there is accumulating evidence supporting the role of diet on gut microbial composition, more research is needed to accurately deduce the effect of different diets on gut microbiota.

Conclusions and further directions

Constant communication between the gut microbiota derived metabolites and human body systems regulates physiological aspects of health and disease. Current literature demonstrates that metabolic syndrome is highly influenced by the gut and supports the hypothesis that metabolic disorders might begin there. Metabolic disease is a multi-factorial condition that makes it difficult to unravel a causative effect of the microbiome on the pathogenesis of this condition. Further, gut microbiota mediated immune dysregulation and intestinal barrier dysfunction emerges as a core pathophysiology of GI dysmotility and metabolic disease. However, it should be noted that these disorders are not mutually inclusive; patients may have GI dysmotility without the co-occurrence of metabolic disorders and vice versa.

Evidence has emerged demonstrating a potential position of the gut microbiome in GI dysmotility and metabolic disorders (Figure 4). A major challenge in studying the gut microbiota is in translating and applying data into physiologically relevant mechanisms. One way to go about facing this challenge is to isolate specific bacterial strains or, analyze how they are affected by specific macronutrients commonly found in humans, and using the information obtained to elucidate biomarkers that may be used to find better treatments for GI dysmotility and metabolic diseases. These biomarkers may also allow for the identification of mechanisms in which the microbial

metabolites lead to or prevent the development of disease states. Also, due to obscure small intestinal microbiome research, more attention is needed on the pathogenesis of SIBO in GI dysmotility and metabolic diseases. Using next generation sequencing techniques to explore small intestinal microbiome, together with better sampling of the small bowel aspirate, may allow us to prevent cases of antibiotic resistance and help better understand the microbial pathogenesis of SIBO.

The collaborative work between microbiologists, gastroenterologists, endocrinologists, and epidemiologists along with improvements in the analysis of microbial markers, microbial metabolites, and molecular signals will lead to thrilling discoveries in the future. The closer we can get to the microbial pathogenesis of the gut microbial alterations and exploring crosstalk with the host, the more effectively we can treat and manage GI dysmotility and related metabolic manifestations. The statement from Hippocrates that “all disease begins in the gut” is becoming progressively more accepted with increasing knowledge of the gut microbiota-gut-brain axis and its influence on human health and disease when altered.

References:

1. Brody H. The gut microbiome. Nature 2020;577:S5.
2. Cani PD. Human gut microbiome: hopes, threats and promises. Gut 2018;67:1716-1725.
3. Prakash S, Rodes L, Coussa-Charley M, et al. Gut microbiota: next frontier in understanding human health and development of biotherapeutics. Biologics 2011;5:71-86.
4. Cani PD. Gut microbiota: Changes in gut microbes and host metabolism: squaring the circle? Nat Rev Gastroenterol Hepatol 2016;13:563-4.
5. Lynch SV, Pedersen O. The Human Intestinal Microbiome in Health and Disease. N Engl J Med 2016;375:2369-2379.
6. Pittayanon R, Lau JT, Yuan Y, et al. Gut Microbiota in Patients With Irritable Bowel Syndrome-A Systematic Review. Gastroenterology 2019;157:97-108.
7. Barbara G, Feinle-Bisset C, Ghoshal UC, et al. The Intestinal Microenvironment and Functional Gastrointestinal Disorders. Gastroenterology 2016.
8. Ghoshal UC. Marshall and Warren Lecture 2019: A paradigm shift in pathophysiological basis of irritable bowel syndrome and its implication on treatment. J Gastroenterol Hepatol 2020;35:712-721.
9. Pittayanon R, Lau JT, Leontiadis GI, et al. Differences in Gut Microbiota in Patients With vs Without Inflammatory Bowel Diseases: A Systematic Review. Gastroenterology 2020;158:930-946 e1.
10. Cho NH, Shaw JE, Karuranga S, et al. IDF Diabetes Atlas: Global estimates of diabetes prevalence for 2017 and projections for 2045. Diabetes Res Clin Pract 2018;138:271-281.
11. Choung RS, Locke GR, 3rd, Schleck CD, et al. Risk of gastroparesis in subjects with type 1 and 2 diabetes in the general population. Am J Gastroenterol 2012;107:82-8.
12. Halland M, Bharucha AE. Relationship Between Control of Glycemia and Gastric Emptying Disturbances in Diabetes Mellitus. Clin Gastroenterol Hepatol 2016;14:929-36.
13. Camilleri M, Chedid V, Ford AC, et al. Gastroparesis. Nat Rev Dis Primers 2018;4:41.

14. Sperber AD, Bangdiwala SI, Drossman DA, et al. Worldwide Prevalence and Burden of Functional Gastrointestinal Disorders, Results of Rome Foundation Global Study. Gastroenterology 2020.

15. Ohman L, Tornblom H, Simren M. Crosstalk at the mucosal border: importance of the gut microenvironment in IBS. Nat Rev Gastroenterol Hepatol 2015;12:36-49.

16. Bhattarai Y, Williams BB, Battaglioli EJ, et al. Gut Microbiota-Produced Tryptamine Activates an Epithelial G-Protein-Coupled Receptor to Increase Colonic Secretion. Cell Host Microbe 2018;23:775-785 e5.

17. Obata Y, Castano A, Boeing S, et al. Neuronal programming by microbiota regulates intestinal physiology. Nature 2020;578:284-289.

18. Kimura I, Miyamoto J, Ohue-Kitano R, et al. Maternal gut microbiota in pregnancy influences offspring metabolic phenotype in mice. Science 2020;367.

19. Perry RJ, Peng L, Barry NA, et al. Acetate mediates a microbiome-brain-beta-cell axis to promote metabolic syndrome. Nature 2016;534:213-7.

20. Cani PD. Gut microbiota - at the intersection of everything? Nat Rev Gastroenterol Hepatol 2017;14:321-322.

21. Ghoshal UC, Ghoshal U. Small Intestinal Bacterial Overgrowth and Other Intestinal Disorders. Gastroenterol Clin North Am 2017;46:103-120.

22. Eisenstein M. The hunt for a healthy microbiome. Nature 2020;577:S6-S8.

23. Backhed F, Ley RE, Sonnenburg JL, et al. Host-bacterial mutualism in the human intestine. Science 2005;307:1915-20.

24. Ghoshal UC, Srivastava D. Irritable bowel syndrome and small intestinal bacterial overgrowth: meaningful association or unnecessary hype. World J Gastroenterol 2014;20:2482-91.

25. Shreiner AB, Kao JY, Young VB. The gut microbiome in health and in disease. Curr Opin Gastroenterol 2015;31:69-75.

26. Schroeder BO, Backhed F. Signals from the gut microbiota to distant organs in physiology and disease. Nat Med 2016;22:1079-1089.

27. Shin A, Preidis GA, Shulman R, et al. The Gut Microbiome in Adult and Pediatric Functional Gastrointestinal Disorders. Clin Gastroenterol Hepatol 2019;17:256-274.

28. Dukowicz AC, Lacy BE, Levine GM. Small intestinal bacterial overgrowth: a comprehensive review. Gastroenterol Hepatol (N Y) 2007;3:112-22.

29. Eckburg PB, Bik EM, Bernstein CN, et al. Diversity of the human intestinal microbial flora. Science 2005;308:1635-8.

30. Lagier JC, Million M, Hugon P, et al. Human gut microbiota: repertoire and variations. Front Cell Infect Microbiol 2012;2:136.

31. Ghoshal UC, Shukla R, Ghoshal U. Small Intestinal Bacterial Overgrowth and Irritable Bowel Syndrome: A Bridge between Functional Organic Dichotomy. Gut Liver 2017;11:196-208.

32. Gabrielli M, D'Angelo G, Di Rienzo T, et al. Diagnosis of small intestinal bacterial overgrowth in the clinical practice. Eur Rev Med Pharmacol Sci 2013;17 Suppl 2:30-5.

33. Riordan SM, McIver CJ, Wakefield D, et al. Small intestinal mucosal immunity and morphometry in luminal overgrowth of indigenous gut flora. Am J Gastroenterol 2001;96:494-500.

34. Erdogan A, Rao SS, Gulley D, et al. Small intestinal bacterial overgrowth: duodenal aspiration vs glucose breath test. Neurogastroenterol Motil 2015;27:481-9.

35. Peralta S, Cottone C, Doveri T, et al. Small intestine bacterial overgrowth and irritable bowel syndrome-related symptoms: experience with Rifaximin. World J Gastroenterol 2009;15:2628-31.

36. Ziegler TR, Cole CR. Small bowel bacterial overgrowth in adults: a potential contributor to intestinal failure. Curr Gastroenterol Rep 2007;9:463-7.

37. Ghoshal UC, Goel A, Quigley EMM. Gut microbiota abnormalities, small intestinal bacterial overgrowth, and non-alcoholic fatty liver disease: An emerging paradigm. Indian J Gastroenterol 2020;39:9-21.

38. Ghoshal UC, Baba CS, Ghoshal U, et al. Low-grade small intestinal bacterial overgrowth is common in patients with non-alcoholic steatohepatitis on quantitative jejunal aspirate culture. Indian J Gastroenterol 2017;36:390-399.

39. Ghoshal UC, Srivastava D, Ghoshal U, et al. Breath tests in the diagnosis of small intestinal bacterial overgrowth in patients with irritable bowel syndrome in comparison with quantitative upper gut aspirate culture. Eur J Gastroenterol Hepatol 2014;26:753-60.

40. Odenwald MA, Turner JR. The intestinal epithelial barrier: a therapeutic target? Nat Rev Gastroenterol Hepatol 2017;14:9-21.

41. Vancamelbeke M, Vermeire S. The intestinal barrier: a fundamental role in health and disease. Expert Rev Gastroenterol Hepatol 2017;11:821-834.

42. Luissint AC, Parkos CA, Nusrat A. Inflammation and the Intestinal Barrier: Leukocyte-Epithelial Cell Interactions, Cell Junction Remodeling, and Mucosal Repair. Gastroenterology 2016;151:616-32.

43. Kohler H, McCormick BA, Walker WA. Bacterial-enterocyte crosstalk: cellular mechanisms in health and disease. J Pediatr Gastroenterol Nutr 2003;36:175-85.

44. Jorgensen JR, Fitch MD, Mortensen PB, et al. In vivo absorption of medium-chain fatty acids by the rat colon exceeds that of short-chain fatty acids. Gastroenterology 2001;120:1152-61.

45. Shindo K, Machida M, Koide K, et al. Deconjugation ability of bacteria isolated from the jejunal fluid of patients with progressive systemic sclerosis and its gastric pH. Hepatogastroenterology 1998;45:1643-50.

46. Gorbach SL. Probiotics and gastrointestinal health. Am J Gastroenterol 2000;95:S2-4.

47. Baumler AJ, Sperandio V. Interactions between the microbiota and pathogenic bacteria in the gut. Nature 2016;535:85-93.

48. Kaufman SS, Loseke CA, Lupo JV, et al. Influence of bacterial overgrowth and intestinal inflammation on duration of parenteral nutrition in children with short bowel syndrome. J Pediatr 1997;131:356-61.

49. Ament ME, Shimoda SS, Saunders DR, et al. Pathogenesis of steatorrhea in three cases of small intestinal stasis syndrome. Gastroenterology 1972;63:728-47.

50. Riepe SP, Goldstein J, Alpers DH. Effect of secreted Bacteroides proteases on human intestinal brush border hydrolases. J Clin Invest 1980;66:314-22.

51. Giannella RA, Rout WR, Toskes PP. Jejunal brush border injury and impaired sugar and amino acid uptake in the blind loop syndrome. Gastroenterology 1974;67:965-74.

52. Sachdev AH, Pimentel M. Gastrointestinal bacterial overgrowth: pathogenesis and clinical significance. Ther Adv Chronic Dis 2013;4:223-31.

53. Dibaise JK, Young RJ, Vanderhoof JA. Enteric microbial flora, bacterial overgrowth, and short-bowel syndrome. Clin Gastroenterol Hepatol 2006;4:11-20.

54. Sanders KM, Koh SD, Ro S, et al. Regulation of gastrointestinal motility--insights from smooth muscle biology. Nat Rev Gastroenterol Hepatol 2012;9:633-45.

55. Sanders KM. Spontaneous Electrical Activity and Rhythmicity in Gastrointestinal Smooth Muscles. Adv Exp Med Biol 2019;1124:3-46.

56. Sanders KM, Kito Y, Hwang SJ, et al. Regulation of Gastrointestinal Smooth Muscle Function by Interstitial Cells. Physiology (Bethesda) 2016;31:316-26.

57. Spencer NJ, Hu H. Enteric nervous system: sensory transduction, neural circuits and gastrointestinal motility. Nat Rev Gastroenterol Hepatol 2020;17:338-351.

58. Spencer NJ, Nicholas SJ, Robinson L, et al. Mechanisms underlying distension-evoked peristalsis in guinea pig distal colon: is there a role for enterochromaffin cells? Am J Physiol Gastrointest Liver Physiol 2011;301:G519-27.

59. Keating DJ, Spencer NJ. What is the role of endogenous gut serotonin in the control of gastrointestinal motility? Pharmacol Res 2019;140:50-55.

60. Grover M, Farrugia G, Stanghellini V. Gastroparesis: a turning point in understanding and treatment. Gut 2019;68:2238-2250.

61. Dickson I. Microbiota modulate ENS maturation. Nat Rev Gastroenterol Hepatol 2018;15:454-455.

62. Shukla R, Ghoshal U, Dhole TN, et al. Fecal Microbiota in Patients with Irritable Bowel Syndrome Compared with Healthy Controls Using Real-Time Polymerase Chain Reaction: An Evidence of Dysbiosis. Dig Dis Sci 2015;60:2953-62.

63. Malinen E, Rinttila T, Kajander K, et al. Analysis of the fecal microbiota of irritable bowel syndrome patients and healthy controls with real-time PCR. Am J Gastroenterol 2005;100:373-82.

64. Tap J, Derrien M, Tornblom H, et al. Identification of an Intestinal Microbiota Signature Associated With Severity of Irritable Bowel Syndrome. Gastroenterology 2017;152:111-123 e8.

65. Salem AE, Singh R, Ayoub YK, et al. The gut microbiome and irritable bowel syndrome: State of art review. Arab J Gastroenterol 2018;19:136-141.

66. Ghoshal UC, Ghoshal U, Das K, et al. Utility of hydrogen breath tests in diagnosis of small intestinal bacterial overgrowth in malabsorption syndrome and its relationship with oro-cecal transit time. Indian J Gastroenterol 2006;25:6-10.

67. Ghoshal UC, Ghoshal U, Ayyagari A, et al. Tropical sprue is associated with contamination of small bowel with aerobic bacteria and reversible prolongation of orocecal transit time. J Gastroenterol Hepatol 2003;18:540-7.

68. Nakamura K, Sakuragi N, Takakuwa A, et al. Paneth cell alpha-defensins and enteric microbiota in health and disease. Biosci Microbiota Food Health 2016;35:57-67.

69. Simeonova D, Ivanovska M, Murdjeva M, et al. Recognizing the Leaky Gut as a Trans-diagnostic Target for Neuroimmune Disorders Using Clinical Chemistry and Molecular Immunology Assays. Curr Top Med Chem 2018;18:1641-1655.

70. Ghosh D, Porter E, Shen B, et al. Paneth cell trypsin is the processing enzyme for human defensin-5. Nat Immunol 2002;3:583-90.

71. Salzman NH, Ghosh D, Huttner KM, et al. Protection against enteric salmonellosis in transgenic mice expressing a human intestinal defensin. Nature 2003;422:522-6.

72. Ghoshal UC, Shukla R, Ghoshal U, et al. The gut microbiota and irritable bowel syndrome: friend or foe? Int J Inflam 2012;2012:151085.

73. Pimentel M, Kong Y, Park S. IBS subjects with methane on lactulose breath test have lower postprandial serotonin levels than subjects with hydrogen. Dig Dis Sci 2004;49:84-7.

74. Mackie RI, Sghir A, Gaskins HR. Developmental microbial ecology of the neonatal gastrointestinal tract. Am J Clin Nutr 1999;69:1035S-1045S.

75. Bouhnik Y, Alain S, Attar A, et al. Bacterial populations contaminating the upper gut in patients with small intestinal bacterial overgrowth syndrome. Am J Gastroenterol 1999;94:1327-31.

76. Sachdev AH, Pimentel M. Antibiotics for irritable bowel syndrome: rationale and current evidence. Curr Gastroenterol Rep 2012;14:439-45.

77. Posserud I, Stotzer PO, Bjornsson ES, et al. Small intestinal bacterial overgrowth in patients with irritable bowel syndrome. Gut 2007;56:802-8.

78. Bala L, Ghoshal UC, Ghoshal U, et al. Malabsorption syndrome with and without small intestinal bacterial overgrowth: a study on upper-gut aspirate using 1H NMR spectroscopy. Magn Reson Med 2006;56:738-44.

79. Gilbert JA, Blaser MJ, Caporaso JG, et al. Current understanding of the human microbiome. Nat Med 2018;24:392-400.

80. Nicholson JK, Holmes E, Kinross J, et al. Host-gut microbiota metabolic interactions. Science 2012;336:1262-7.

81. Kootte RS, Levin E, Salojarvi J, et al. Improvement of Insulin Sensitivity after Lean Donor Feces in Metabolic Syndrome Is Driven by Baseline Intestinal Microbiota Composition. Cell Metab 2017;26:611-619 e6.

82. Muscogiuri G, Balercia G, Barrea L, et al. Gut: A key player in the pathogenesis of type 2 diabetes? Crit Rev Food Sci Nutr 2018;58:1294-1309.

83. Bouter KE, van Raalte DH, Groen AK, et al. Role of the Gut Microbiome in the Pathogenesis of Obesity and Obesity-Related Metabolic Dysfunction. Gastroenterology 2017;152:1671-1678.

84. Johnson AM, Olefsky JM. The origins and drivers of insulin resistance. Cell 2013;152:673-84.

85. Roland BC, Lee D, Miller LS, et al. Obesity increases the risk of small intestinal bacterial overgrowth (SIBO). Neurogastroenterol Motil 2018;30.

86. Sonnenburg JL, Backhed F. Diet-microbiota interactions as moderators of human metabolism. Nature 2016;535:56-64.

87. Tremaroli V, Backhed F. Functional interactions between the gut microbiota and host metabolism. Nature 2012;489:242-9.

88. Adamska A, Nowak M, Pilacinski S, et al. Small intestinal bacterial overgrowth in adult patients with type 1 diabetes: its prevalence and relationship with metabolic control and the presence of chronic complications of the disease. Pol Arch Med Wewn 2016;126:628-634.

89. Rana SV, Malik A, Bhadada SK, et al. Malabsorption, Orocecal Transit Time and Small Intestinal Bacterial Overgrowth in Type 2 Diabetic Patients: A Connection. Indian J Clin Biochem 2017;32:84-89.

90. Sekirov I, Russell SL, Antunes LC, et al. Gut microbiota in health and disease. Physiol Rev 2010;90:859-904.

91. Medzhitov R. Recognition of microorganisms and activation of the immune response. Nature 2007;449:819-26.

92. Zelante T, Iannitti RG, Cunha C, et al. Tryptophan catabolites from microbiota engage aryl hydrocarbon receptor and balance mucosal reactivity via interleukin-22. Immunity 2013;39:372-85.

93. Xu CX, Wang C, Zhang ZM, et al. Aryl hydrocarbon receptor deficiency protects mice from diet-induced adiposity and metabolic disorders through increased energy expenditure. Int J Obes (Lond) 2015;39:1300-1309.

94. Bock KW. Aryl hydrocarbon receptor (AHR) functions in NAD(+) metabolism, myelopoiesis and obesity. Biochem Pharmacol 2019;163:128-132.

95. Wang C, Xu CX, Krager SL, et al. Aryl hydrocarbon receptor deficiency enhances insulin sensitivity and reduces PPAR-alpha pathway activity in mice. Environ Health Perspect 2011;119:1739-44.

96. Bergman EN. Energy contributions of volatile fatty acids from the gastrointestinal tract in various species. Physiol Rev 1990;70:567-90.

97. Samuel BS, Shaito A, Motoike T, et al. Effects of the gut microbiota on host adiposity are modulated by the short-chain fatty-acid binding G protein-coupled receptor, Gpr41. Proc Natl Acad Sci U S A 2008;105:16767-72.

98. Tolhurst G, Heffron H, Lam YS, et al. Short-chain fatty acids stimulate glucagon-like peptide-1 secretion via the G-protein-coupled receptor FFAR2. Diabetes 2012;61:364-71.

99. Fava S. Glucagon-like peptide 1 and the cardiovascular system. Curr Diabetes Rev 2014;10:302-10.

100. De Vadder F, Kovatcheva-Datchary P, Goncalves D, et al. Microbiota-generated metabolites promote metabolic benefits via gut-brain neural circuits. Cell 2014;156:84-96.

101. Kimura I, Ozawa K, Inoue D, et al. The gut microbiota suppresses insulin-mediated fat accumulation via the short-chain fatty acid receptor GPR43. Nat Commun 2013;4:1829.

102. Reigstad CS, Salmonson CE, Rainey JF, 3rd, et al. Gut microbes promote colonic serotonin production through an effect of short-chain fatty acids on enterochromaffin cells. FASEB J 2015;29:1395-403.

103. Williams BB, Van Benschoten AH, Cimermancic P, et al. Discovery and characterization of gut microbiota decarboxylases that can produce the neurotransmitter tryptamine. Cell Host Microbe 2014;16:495-503.

104. Ghoshal UC. Gut Microbiota-Brain Axis Modulation by a Healthier Microbiological Microenvironment : Facts and Fictions. J Neurogastroenterol Motil 2018;24:4-6.

105. Quigley EMM. Microbiota-Brain-Gut Axis and Neurodegenerative Diseases. Curr Neurol Neurosci Rep 2017;17:94.

106. Garcovich M, Zocco MA, Roccarina D, et al. Prevention and treatment of hepatic encephalopathy: focusing on gut microbiota. World J Gastroenterol 2012;18:6693-700.

107. De Palma G, Collins SM, Bercik P. The microbiota-gut-brain axis in functional gastrointestinal disorders. Gut Microbes 2014;5:419-29.

108. Rhee SH, Pothoulakis C, Mayer EA. Principles and clinical implications of the brain-gut-enteric microbiota axis. Nat Rev Gastroenterol Hepatol 2009;6:306-14.

109. Sharkey KA, Beck PL, McKay DM. Neuroimmunophysiology of the gut: advances and emerging concepts focusing on the epithelium. Nat Rev Gastroenterol Hepatol 2018;15:765-784.

110. Salzman NH, Underwood MA, Bevins CL. Paneth cells, defensins, and the commensal microbiota: a hypothesis on intimate interplay at the intestinal mucosa. Semin Immunol 2007;19:70-83.

111. Fung TC, Vuong HE, Luna CDG, et al. Intestinal serotonin and fluoxetine exposure modulate bacterial colonization in the gut. Nat Microbiol 2019;4:2064-2073.

112. Clemente JC, Ursell LK, Parfrey LW, et al. The impact of the gut microbiota on human health: an integrative view. Cell 2012;148:1258-70.

113. Robinette ML, Colonna M. GI motility: microbiota and macrophages join forces. Cell 2014;158:239-240.

114. Mikkelsen HB. Interstitial cells of Cajal, macrophages and mast cells in the gut musculature: morphology, distribution, spatial and possible functional interactions. J Cell Mol Med 2010;14:818-32.

115. Muller PA, Koscso B, Rajani GM, et al. Crosstalk between muscularis macrophages and enteric neurons regulates gastrointestinal motility. Cell 2014;158:300-313.

116. Olofsson PS, Rosas-Ballina M, Levine YA, et al. Rethinking inflammation: neural circuits in the regulation of immunity. Immunol Rev 2012;248:188-204.

117. Parkhurst CN, Yang G, Ninan I, et al. Microglia promote learning-dependent synapse formation through brain-derived neurotrophic factor. Cell 2013;155:1596-609.

118. Winer DA, Luck H, Tsai S, et al. The Intestinal Immune System in Obesity and Insulin Resistance. Cell Metab 2016;23:413-26.

119. Olefsky JM, Glass CK. Macrophages, inflammation, and insulin resistance. Annu Rev Physiol 2010;72:219-46.

120. Lumeng CN, Bodzin JL, Saltiel AR. Obesity induces a phenotypic switch in adipose tissue macrophage polarization. J Clin Invest 2007;117:175-84.

121. Brestoff JR, Kim BS, Saenz SA, et al. Group 2 innate lymphoid cells promote beiging of white adipose tissue and limit obesity. Nature 2015;519:242-6.

122. Garidou L, Pomie C, Klopp P, et al. The Gut Microbiota Regulates Intestinal CD4 T Cells Expressing RORgammat and Controls Metabolic Disease. Cell Metab 2015;22:100-12.

123. Cani PD, Bibiloni R, Knauf C, et al. Changes in gut microbiota control metabolic endotoxemia-induced inflammation in high-fat diet-induced obesity and diabetes in mice. Diabetes 2008;57:1470-81.

124. Thaiss CA, Levy M, Grosheva I, et al. Hyperglycemia drives intestinal barrier dysfunction and risk for enteric infection. Science 2018;359:1376-1383.

125. Chen RY, Kung VL, Das S, et al. Duodenal Microbiota in Stunted Undernourished Children with Enteropathy. N Engl J Med 2020;383:321-333.

126. Gehrig JL, Venkatesh S, Chang HW, et al. Effects of microbiota-directed foods in gnotobiotic animals and undernourished children. Science 2019;365.

127. Ghoshal UC, Srivastava D, Verma A, et al. Tropical sprue in 2014: the new face of an old disease. Curr Gastroenterol Rep 2014;16:391.

128. Sorini C, Cosorich I, Lo Conte M, et al. Loss of gut barrier integrity triggers activation of islet-reactive T cells and autoimmune diabetes. Proc Natl Acad Sci U S A 2019;116:15140-15149.

129. Camilleri M. Leaky gut: mechanisms, measurement and clinical implications in humans. Gut 2019;68:1516-1526.

130. Barbara G, Grover M, Bercik P, et al. Rome Foundation Working Team Report on Post-Infection Irritable Bowel Syndrome. Gastroenterology 2019;156:46-58 e7.

131. Jess T. Microbiota, antibiotics, and obesity. N Engl J Med 2014;371:2526-8.

132. Cox LM, Yamanishi S, Sohn J, et al. Altering the intestinal microbiota during a critical developmental window has lasting metabolic consequences. Cell 2014;158:705-721.

133. Scott FI, Horton DB, Mamtani R, et al. Administration of Antibiotics to Children Before Age 2 Years Increases Risk for Childhood Obesity. Gastroenterology 2016;151:120-129 e5.

134. Yano JM, Yu K, Donaldson GP, et al. Indigenous bacteria from the gut microbiota regulate host serotonin biosynthesis. Cell 2015;161:264-76.

135. Shah A, Morrison M, Holtmann G. A novel treatment for patients with constipation: Dawn of a new age for translational microbiome research? Indian J Gastroenterol 2018;37:388-391.

136. Low K, Hwang L, Hua J, et al. A combination of rifaximin and neomycin is most effective in treating irritable bowel syndrome patients with methane on lactulose breath test. J Clin Gastroenterol 2010;44:547-50.

137. Ghoshal UC, Srivastava D, Misra A. A randomized double-blind placebo-controlled trial showing rifaximin to improve constipation by reducing methane production and accelerating colon transit: A pilot study. Indian J Gastroenterol 2018;37:416-423.

138. Reijnders D, Goossens GH, Hermes GD, et al. Effects of Gut Microbiota Manipulation by Antibiotics on Host Metabolism in Obese Humans: A Randomized Double-Blind Placebo-Controlled Trial. Cell Metab 2016;24:63-74.

139. Rao SSC, Bhagatwala J. Small Intestinal Bacterial Overgrowth: Clinical Features and Therapeutic Management. Clin Transl Gastroenterol 2019;10:e00078.

140. Gatta L, Scarpignato C. Systematic review with meta-analysis: rifaximin is effective and safe for the treatment of small intestine bacterial overgrowth. Aliment Pharmacol Ther 2017;45:604-616.

141. Shah SC, Day LW, Somsouk M, et al. Meta-analysis: antibiotic therapy for small intestinal bacterial overgrowth. Aliment Pharmacol Ther 2013;38:925-34.

142. Khoruts A, Sadowsky MJ. Understanding the mechanisms of faecal microbiota transplantation. Nat Rev Gastroenterol Hepatol 2016;13:508-16.

143. El-Salhy M, Hatlebakk JG, Gilja OH, et al. Efficacy of faecal microbiota transplantation for patients with irritable bowel syndrome in a randomised, double-blind, placebo-controlled study. Gut 2020;69:859-867.

144. Ianiro G, Eusebi LH, Black CJ, et al. Systematic review with meta-analysis: efficacy of faecal microbiota transplantation for the treatment of irritable bowel syndrome. Aliment Pharmacol Ther 2019;50:240-248.

145. Xu D, Chen VL, Steiner CA, et al. Efficacy of Fecal Microbiota Transplantation in Irritable Bowel Syndrome: A Systematic Review and Meta-Analysis. Am J Gastroenterol 2019;114:1043-1050.

146. Park JH. Clinical Usefulness of Fecal Microbiota Transplantation. J Neurogastroenterol Motil 2017;23:149-150.

147. Vrieze A, Van Nood E, Holleman F, et al. Transfer of intestinal microbiota from lean donors increases insulin sensitivity in individuals with metabolic syndrome. Gastroenterology 2012;143:913-6 e7.

148. Hemarajata P, Versalovic J. Effects of probiotics on gut microbiota: mechanisms of intestinal immunomodulation and neuromodulation. Therap Adv Gastroenterol 2013;6:39-51.

149. Zhong C, Qu C, Wang B, et al. Probiotics for Preventing and Treating Small Intestinal Bacterial Overgrowth: A Meta-Analysis and Systematic Review of Current Evidence. J Clin Gastroenterol 2017;51:300-311.

150. Enck P, Aziz Q, Barbara G, et al. Irritable bowel syndrome. Nat Rev Dis Primers 2016;2:16014.

151. Wang Y, Dilidaxi D, Wu Y, et al. Composite probiotics alleviate type 2 diabetes by regulating intestinal microbiota and inducing GLP-1 secretion in db/db mice. Biomed Pharmacother 2020;125:109914.

152. Zmora N, Suez J, Elinav E. You are what you eat: diet, health and the gut microbiota. Nat Rev Gastroenterol Hepatol 2019;16:35-56.

153. Pulipati P, Sarkar P, Jakkampudi A, et al. The Indian gut microbiota-Is it unique? Indian J Gastroenterol 2020.

154. Delzenne NM, Bindels LB. Food for thought about manipulating gut bacteria. Nature 2020;577:32-34.

155. Walker AW, Ince J, Duncan SH, et al. Dominant and diet-responsive groups of bacteria within the human colonic microbiota. ISME J 2011;5:220-30.

156. Wu GD, Chen J, Hoffmann C, et al. Linking long-term dietary patterns with gut microbial enterotypes. Science 2011;334:105-8.

157. De Filippo C, Cavalieri D, Di Paola M, et al. Impact of diet in shaping gut microbiota revealed by a comparative study in children from Europe and rural Africa. Proc Natl Acad Sci U S A 2010;107:14691-6.

158. Mehtab W, Agarwal A, Singh N, et al. All that a physician should know about FODMAPs. Indian J Gastroenterol 2019;38:378-390.

159. Altobelli E, Del Negro V, Angeletti PM, et al. Low-FODMAP Diet Improves Irritable Bowel Syndrome Symptoms: A Meta-Analysis. Nutrients 2017;9.

160. Tomova A, Bukovsky I, Rembert E, et al. The Effects of Vegetarian and Vegan Diets on Gut Microbiota. Front Nutr 2019;6:47.

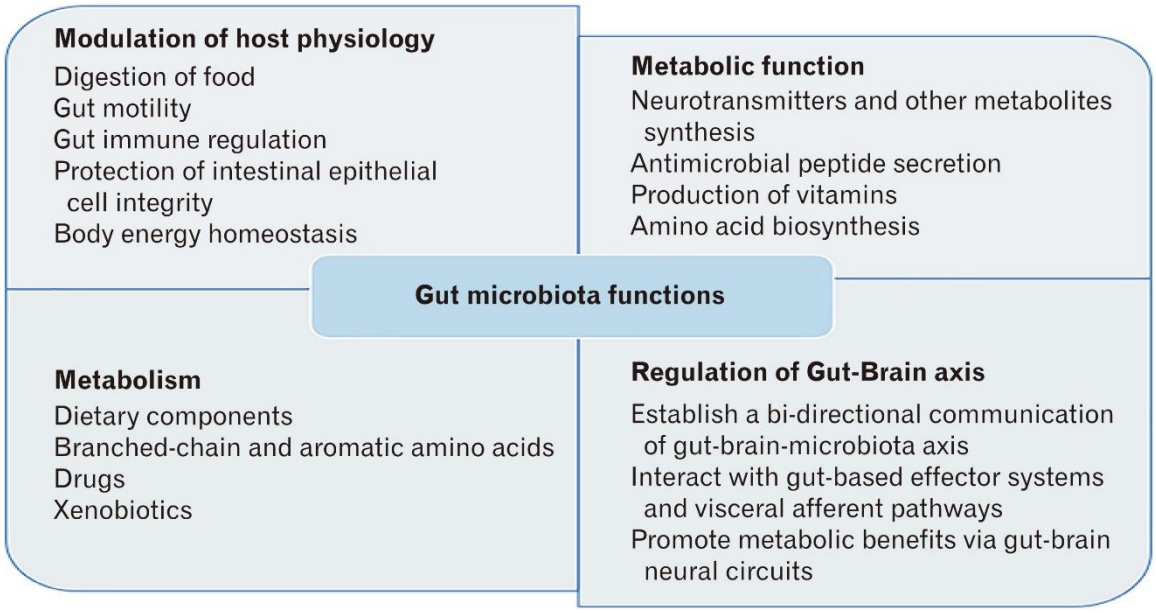

Figure 1: Functions of the gut microbiota.

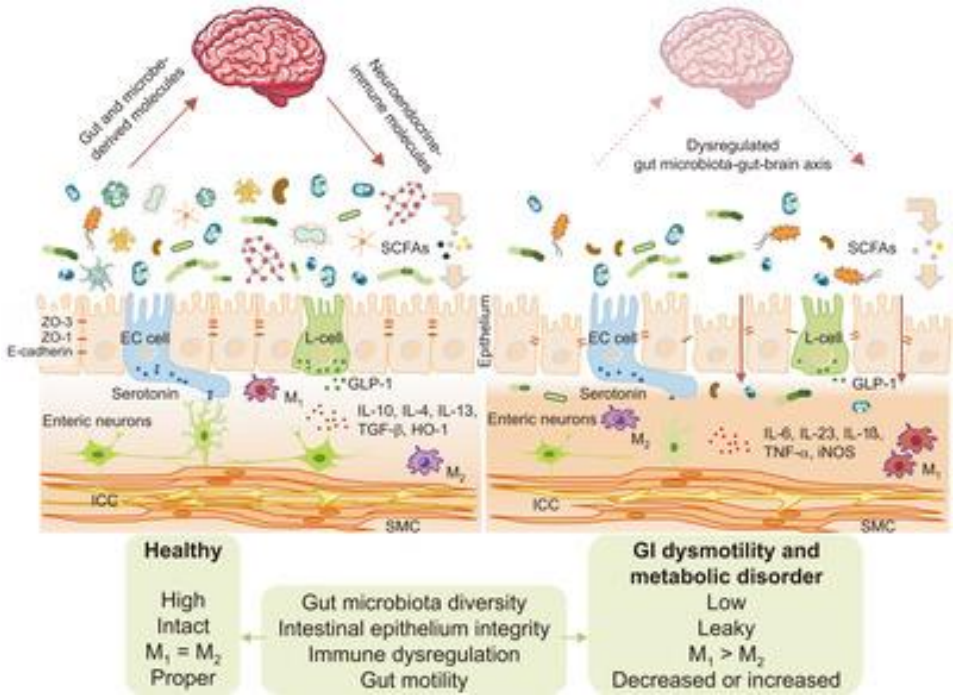

Figure 2: Intestinal barrier dysfunction as a core pathophysiology of gastrointestinal (GI) dysmotility and metabolic disorder. SCFAs, short-chain fatty acids; ZO, zonula occludens; E-cadherin, epithelial cadherin; EC, enterochromaffin; GLP-1, glucagon-like peptide-1; IL, interleukin; M1, classically activated macrophages; M2, alternatively activated macrophages; TGF-β, transforming growth factor beta; HO-1, heme oxygenase-1; TNF-α, tumor necrosis factor alpha; iNOS, inducible nitric oxide synthase; ICC, interstitial cell of Cajal; SMC, smooth muscle cell; L-cell, enteroendocrine cell.

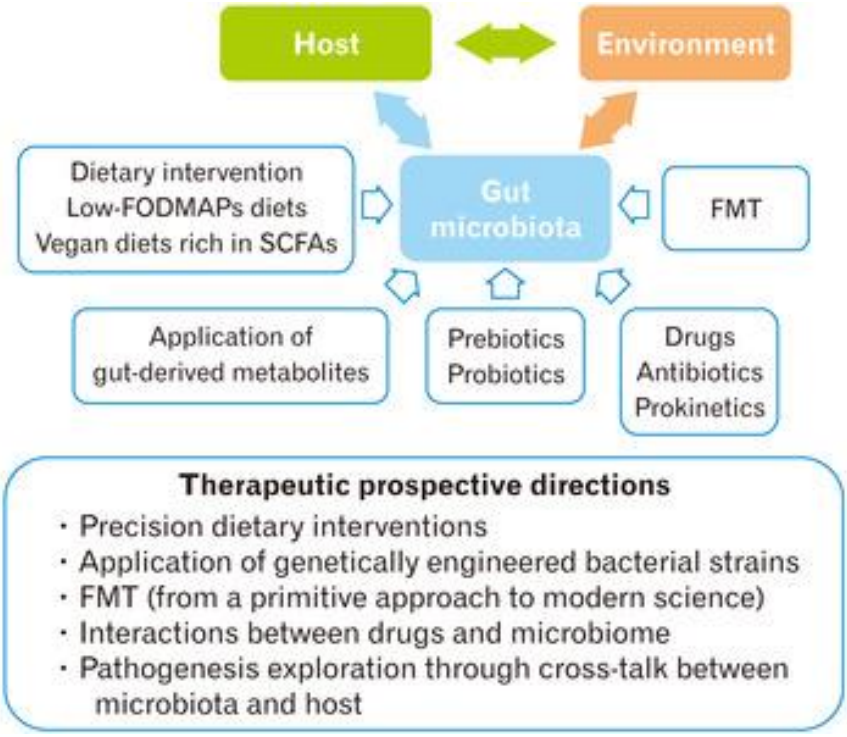

Figure 3: Therapeutic modulations of gut microbiota. FODMAPs, fermentable oligosaccharides, disaccharides, monosaccharides, and polyols; SCFAs, short-chain fatty acids; FMT, fecal microbiota transplantation.

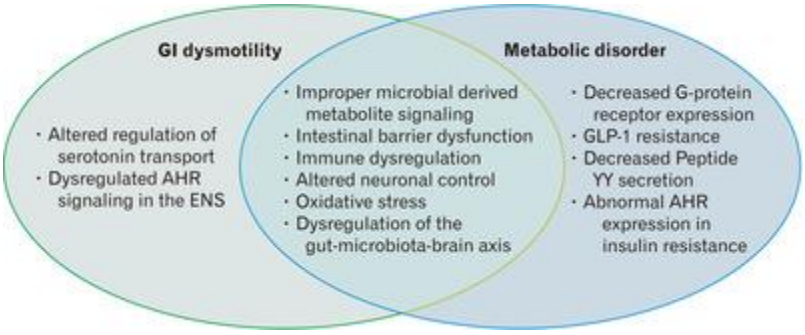

Figure 4: Pathogenesis in gastrointestinal (GI) dysmotility and metabolic disorder. AHR, aryl hydrocarbon receptor; ENS, enteric nervous system; GLP-1, glucagon-like peptide-1.

CHAPTER TWO: Current Advances in RNA Therapeutics for Human Diseases

Introduction

For years it was believed that DNA was transcribed into RNA and that this RNA (messenger RNA) was then translated into a protein; however, this all became more complicated when RNA interference (RNAi) was discovered.[1,2] RNAi is a conserved biological process in which there is repression of gene expression caused by small RNAs [i.e., microRNAs (miRNAs) and synthetic small interfering RNAs (siRNAs)] interacting with protein complexes, such as the RNA-induced silencing complex (RISC).[3,4] Once bound, the small RNAs can then bind to their respective target mRNA in a sequence-specific manner to either stop translation or target the mRNA for degradation.[5] This discovery led to a huge increase in research focused on treatments for diseases that would exploit RNAi instead of traditional treatments focused on utilizing small molecules and proteins.

Most drugs currently on the market are either small molecules or proteins. Small molecule-based drugs are commonly competitive inhibitors of their target proteins, while protein-based drugs are commonly used to bind to target proteins, replace non-functional target proteins, or supplement for an inadequate amount of a target protein.[6-8] A serious issue with protein-based drugs is that most proteins are too large to enter their target cells and therefore are only effective when their target molecule is extracellular or excreted.[9] While small molecule- and protein-based drugs have been found to be effective in many cases, there are still a plethora of diseases that are unable to be treated using either small molecules or proteins. For example, many diabetic patients develop insulin resistance, and supplementing additional insulin is no longer effective in lowering their blood glucose levels. However, RNA-based treatments may have therapeutic potential for diseases, such as diabetes, cancer, and Huntington's disease.[2,10-13] RNA therapies may provide better treatment options to target the pathophysiological mechanisms of these disorders, which may lead to better outcomes for patients. Additionally, many RNA therapies have already been approved by the US

Food and Drug Administration (FDA) with more therapies in various phases of clinical trials demonstrating the validity of such RNA therapies for various diseases. This review will cover the mechanisms of RNA therapy design, current FDA-approved RNA therapies, RNA therapies in clinical trials, and RNAs with clinical potential for treating patients suffering from various conditions.

RNA Therapeutics

RNAs as therapeutic agents have been vastly studied over the past few decades, as they are more cost-effective and easier to develop than traditional small molecule or protein-based therapeutics.[2] As of now, there are five different categories of RNA therapeutics (Figure 1): 1) messenger RNAs (mRNAs) encode for proteins, 2) antisense oligonucleotides (ASOs) are small (~15-25 nucleotides) single-stranded RNAs (or DNAs, but for the purposes of this review we focus only on RNA ASOs) that can either promote or repress their targets expression, 3) silencing RNAs (siRNAs) are very similar to ASOs in size, however, they are double-stranded and primarily cause translational repression of their target protein, 4) microRNAs (miRNAs) are small RNAs that can either inhibit protein synthesis when they bind to an mRNA target (miRNA mimics), or free up mRNA by binding to the miRNA that represses the translation of that particular mRNA (miRNA inhibitors), and 5) aptamers are short single-stranded nucleic acids that form secondary and tertiary structures and interact with a specific enzyme or molecule and therefore can promote or inhibit many different molecular pathways. Within these five categories there are a handful of already U.S. FDA-approved medications (Table 1), many that are in clinical trials (Table 2), and an enormous amount that have been found to have possible therapeutic potential but are not yet in clinical trials. It is important to note that while RNA therapeutics seem to have immense potential, there are many hurdles that need to be surmounted when they are developed clinically to make them effective potential treatment options.

Before RNAs were used therapeutically there were many challenges that had to be overcome in order to make them feasible treatment options for human diseases. For example, nucleic acids are negatively charged and do not passively cross the hydrophobic lipid barrier of the

cell. Further, exogenous RNAs are degraded very rapidly by RNases once they are injected into the host. Finally, some exogenous RNAs cause an immune response that hampers the translation of the target protein or causes the development of a toxic cell environment. Luckily, scientists over the past couple of decades have substantially overcome these barriers with the use of many unique delivery methods, such as nanoparticles, that protect the RNA and enable cell-specific delivery of the therapeutic agent.

mRNA therapeutics and functional implications:

mRNA is coding RNA that is transcribed using genomic DNA as a template and serves to encode proteins.[14] mRNAs are typically around 2kb in length and characteristically contain a 5' cap, 5' UTR, coding region, 3' UTR, and poly(A) tail (Figure 1A).[15] mRNAs are excellent candidates for the treatment of diseases with a known genetic component. Traditionally, mRNAs have been used for replacement therapy when diseases are caused by a lack of expression of a particular protein.[16] Additionally, CRISPR-Cas-based mRNA therapies can be used to repair DNA mutations that cause non-functional downstream products.[17] In 1990, Wolff et al. were one of the first groups to induce expression of a protein *in vivo* through the injection of a synthetic mRNA that encoded beta-galactosidase, chloramphenicol, or luciferase into the skeletal muscle of mice.[18] Further, Jirikowski et al. used mRNA to treat diabetes insipidus in Brattleboro rats that have reduced levels of vasopressin.[19] Synthetic or *in vitro* exogenous vasopressin mRNA was able to rescue diabetes insipidus when injected in these rats. These initial reports implicated mRNAs as possible therapeutic options for treating/preventing human diseases.

mRNA vaccines:

mRNAs that encode either adjuvants or antigens have also been proposed as possible vaccine candidates that may be able to prevent many diseases. In 1993 Martinon et al. reported that there was induction of anti-influenza cytotoxic T lymphocytes following immunization with liposome-complexed mRNA encoding influenza virus nucleoproteins in a murine model.[20] This was

the first report highlighting the possible use of mRNAs as vaccines to prevent many infectious diseases. While this study was conducted decades ago, mRNA vaccines have become more common in recent years, especially since the COVID-19 pandemic. Further, this pandemic also highlighted the speediness of the development of mRNA vaccines when compared to many of the traditional vaccine technologies. The first vaccines to receive emergency use authorization from the FDA were mRNA vaccines.

Currently, there are two mRNA vaccines that are FDA-approved and one that is in clinical trials. The first mRNA vaccine approved by the FDA was BNT162b2.[21] This vaccine was produced in collaboration between Pfizer and BioNTech to create immunogenicity and antibody response to SARS-CoV-2, which causes COVID-19. This vaccine candidate was clinically tested in Germany and the US and was found to significantly decrease the risk of contracting COVID-19. BNT162b2 encodes for the full-length membrane-anchored spike (S) protein that includes two minor mutations to increase conformational stability. The second FDA-approved mRNA vaccine is mRNA-1273 which encodes the perfusion stabilized S protein of SARS-CoV-2 as well as a S1-S2 cleavage site.[22] Similar to BNT162b2, the mRNA-1273 vaccine was manufactured by Moderna to prevent the contraction of COVID-19. Both FDA-approved mRNA COVID-19 vaccines include 1-methyl-pseudouridine to hamper innate immune sensing, while also increasing the translational ability of the mRNA. Additionally, they both are encapsulated by lipid nanoparticles. Further, both vaccines have shown to provide significant immunity against SARS-CoV-2 infection, while also maintaining high safety standards. It should be noted the exceptional speed at which both vaccines were developed. To date no other vaccine has been developed with such swiftness, while also maintaining efficacy. This highlights the clinical advantage of using RNA based vaccines in treating deadly diseases.

Along with the two FDA-approved mRNA vaccines, there are two additional vaccine candidates. The first is CVnCoV, which is currently in phase III clinical trials.[23] This vaccine candidate is produced by CureVac AG and is a chemically unmodified mRNA that encodes the full-

length S protein of SARS-CoV-2 and utilizes the RNActive mRNA vaccine platform.[23] CVnCoV induces a robust immune response and provides immunity against SARS-CoV-2 infection. The second vaccine candidate is CV7202 and is in phase I clinical trials for rabies prevention.[24] This vaccine is composed of rabies virus glycoprotein mRNA to induce a rabies neutralizing antibody response. Additionally, there are many mRNA vaccine candidates that are currently in pre-clinical trials or that have pre-clinical potential.[20,25-30]

To date, there are several mRNA drug candidates in clinical trials for various human diseases: 1) AZD8601 is a vascular endothelial growth factor A (VEGF-A) drug candidate manufactured by Astrazeneca for ischemic heart disease.[31] VEGF-A has been promising in preclinical trials for increased vessel collateralization.[32] This study suggested VEGF-A might be a good drug candidate for treating ischemic heart disease. However, studies found that treatment with VEGF-A DNA or viral vectors was safe, but not effective in treating ischemic heart disease.[33,34] Therefore, it was hypothesized that VEGF-A mRNA drug candidates may be a more efficacious way of treating this disease. AZD8601 is currently being evaluated in phase II clinical trials. 2) MRT5005 is manufactured by Translate Bio and is currently in phase I/II clinical trials for the treatment of cystic fibrosis (CF) lung disease.[35] CF is caused by mutations in the CF transmembrane conductance regulator (*CFTR*) gene. This mutation leads to the buildup of mucous in many organs, especially the lungs.[36] MRT5005 encodes for CFTR and can be delivered through nebulization. 3) mRNA-3704 is in phase I/II clinical trials for the treatment of methylmalonic aciduria and is manufactured by Moderna.[37,38] Methylmalonic aciduria is a life-threatening genetic disorder in which there is an inability to break down certain proteins and fats, causing a buildup of methylmalonic acid.[39] This disorder is caused by a plethora of mutations in the methylmalonyl-CoA mutase gene. mRNA-3704 encodes for a fully functional methylmalonyl-CoA mutase enabling the breakdown of proteins and fats that were previously unable to be broken down.[37,38] 4) BNT111, manufactured by BioNTech SE, is currently in dose-escalation phase I clinical trials for the treatment of advanced melanoma.[40] This drug targets NY-ESO-1, MAGEA3, tyrosinase, and TPTE, which are tumor-associated antigens predominantly found in melanoma. This therefore should

cause an immune response leading to the destruction of tumor cells. It should also be noted that there is a plethora of other mRNA drug candidates in the preclinical pipeline.[41-45]

ASO therapeutics and functional implications:

ASOs are synthetic small single-stranded nucleic acid sequences composed of RNA, DNA, or RNA-DNA heteroduplexes that are typically 8-50 bp long.[46] The study of ASOs really began in the late 1970s when it was found that synthesized oligonucleotides were able to inhibit Rous sarcoma virus replication.[47] This was achieved through viral protein translation inhibition due to the binding of the synthesized complementary oligonucleotide sequence to the viral 35S mRNA. This study paved the way for ASO-based therapeutics.

Since their discovery, there have been a plethora of other mechanisms of action for ASOs. While there are many different ASOs, they all belong to one of two major categories: RNase H dependent ASOs and RNase H independent/steric block ASOs.[48] RNase H is an endogenous enzyme that catalyzes the degradation of RNA that is part of an RNA-DNA heteroduplex. Therefore, ASOs composed of DNA or both RNA and DNA (gapmers) typically belong to the RNase H dependent category. Once they bind their complementary target mRNA strand, RNase H recognizes the DNA-RNA heteroduplex and catalyzes the degradation of the mRNA. This leads to downregulation of the target mRNA, which can be a useful tool in therapeutic approaches for the treatment of diseases caused by overexpression of certain genes,[49] such as homozygous familial hypercholesterolemia.[50]

RNase H independent/steric block ASOs are typically composed of only RNA and act by binding directly to the target pre-mRNA or mature mRNA to cause inhibition of mRNA translation (Figure 1B), alternative splicing, promotion of mRNA translation, or alternative polyadenylation. When the ASO binds to the pre-mRNA at a splice recognition site, it will cause alternative splicing of the target RNA. This approach can be extremely useful for treatment of disorders that are caused by mutations that can be avoided by selective alternative splicing.[51] In general, this type of ASO

can also lead to increased expression of the target protein;[52] however, they can also be used to cause exon skipping in order to block translation of the target mRNA.[53] This approach is also known as splice corruption. ASOs have also been known to bind regions of the mRNA, such as the translation initiation codon, to inhibit translation of the mRNA.[54] Further, ASOs that bind regulatory regions upstream of the open reading frame (ORF) have been shown to promote target translation.[55] This is caused by the blocking of regulatory regions typically responsible for translational suppression. ASOs also have been shown to cause alternative polyadenylation by blocking certain polyadenylation sites.[56] This commonly leads to shorter transcripts that contain less destabilized segments, typically leading to increased stability of the mRNA. The many molecular mechanisms of ASOs have enabled their use for many different therapeutic approaches to treat human diseases.

FDA-approved ASOs:

The first FDA-approved ASO was fomivirsen, which is also known as Vitravene. Formivirsen was developed to treat patients with cytomegalovirus (CMV) retinitis, a serious viral eye infection.[57] This ASO therapeutic is composed of 21 phosphorothioate oligodeoxynucleotides that target CMV immediate-early-2 mRNA, which is essential for viral replication.[58] Clinical trials showed that injections of this drug into the vitreous humor delayed the disease progression when compared to untreated controls. Successful clinical trials led to fomivirsen obtaining FDA approval in 1999.[57] However, it is important to note that disease progression was still inevitable. This, along with the discovery of anti-retroviral therapies made this medication less pertinent and it was eventually taken off the market in 2006.

Mipomersen was approved by the FDA in 2013 for the treatment of homozygous familial hypercholesterolemia.[59] This genetic disorder is characterized by increased levels of low-density lipoprotein (LDL) cholesterol due to decreased liver uptake of plasma LDL.[60] This condition leads to premature cardiovascular disease even when treated with previously established lipid-lowering therapies, such as statin therapy.[61] However, treatment with mipomersen, a gapmer 20

oligonucleotides long that targets and reduces expression of the ApoB mRNA, led to significantly reduced LDL levels.[50] ApoB is an essential protein for the clearance of LDL and aids in the production of very low-density lipoprotein (VLDL), which is a precursor of LDL.[61] Therefore, reduction of ApoB likely leads to the reduced plasma levels of LDL following mipomersen treatment.

In 2016, nusinersen was approved by the FDA for the treatment of spinal muscular atrophy (SMA).[62] This disorder is caused by deletions or mutations in the survival motor neuron 1 (*SMN1*) gene. This leads to inadequate SMN protein expression, causing weakness and atrophy of skeletal and respiratory muscles.[63] Nusinersen modulates splicing of *SMN2*, which varies only from *SMN1* in that it undergoes alternative splicing and excludes exon 7.[64] This exclusion results in a truncated protein that only has 5 to 10% functionality. However, nusinersen regulates alternative splicing so that exon 7 is included, resulting in fully functional SMN leading to improved motor function in patients with SMA.

Eteplirsen was approved by the FDA in 2016 for the treatment of Duchenne muscular dystrophy (DMD).[65] Mutations in the DMD gene encoding the dystrophin protein leads to the development of DMD.[66] The most common mutation resulting in DMD is located in exon 51, therefore, eteplirsen (a 30-mer ASO), targets exon 51 of the DMD gene causing this exon to be excluded during alternative splicing.[67] This prevents frame shift mutations that lead to the production of non-functional dystrophin. The resulting dystrophin protein is slightly shorter than its wildtype counterpart but maintains its functionality.[68]

Inotersen received FDA approval in 2018 for the treatment of familial amyloid polyneuropathy. This disorder is caused by autosomal dominant mutations in the transthyretin (*TTR*) gene. These mutations disrupt the TTR tetramer leading to aggregation of TTR monomers into amyloid deposits throughout the body.[69] In order to combat the buildup of TTR, inotersen targets the 3' UTR of the *TTR* mRNA preventing the production of TTR, thus inhibiting disease progression.[70] Clinical trials demonstrated the efficacy and safety of inotersen for the reduction of circulating TTR levels.[71]

Another ASO that has been FDA approved for the treatment of DMD is golodirsen. This drug behaves similarly to eteplirsen, in that it enables exon skipping; however, it leads to the exclusion of exon 53 instead of exon 51.[72] This results in functional dystrophin and improves symptomology of patients with DMD caused by mutations that are acquiescent to exon 53 skipping.[73]

Milasen was developed in less than a year to treat Mila Makovec's *CLN7* gene mutation leading to the development of Batten disease. This is a rare disease caused by one of at least thirteen known mutations to the *CLN* gene that affects the cell's ability to get rid of waste, such as excess proteins and lipids.[74] This disease eventually is fatal if left untreated. After genomic sequencing of Mila Makovec's unique *CLN7* gene mutation, it was clear that this form of Batten disease was caused by improper exon splicing and the resulting premature translational termination.[75] Milasen targets a specific *CLN7* splice site restoring proper splicing and function of CLN7. It eventually received FDA approval in 2018.

The FDA approved the use of casimersen in 2021 for the treatment of DMD caused by a mutation in the *DMD* gene that is amenable to exon 45 skipping.[76] Again, the mechanism of action of this drug is very similar to that of golodirsen and eteplirsen.

ASOs in clinical trials:

ISS 1018 is in Phase II clinical trials for its synergistic effect with rituximab for the treatment of Non-Hodgkin's Lymphoma (NHL).[77] NHL is a very common cancer that begins in the lymphatic system and eventually spreads to other organs.[78] Rituximab has been extremely successful in treating many forms of NHL; however, there are still some forms that do not see any improvement following rituximab treatment. ISS 1018 was thought to have a beneficial effect when given to patients simultaneously with rituximab treatment. This drug can illicit immunostimulatory effects by signaling through the Toll-like receptor 9 and leads to proliferation and immunoglobulin production by B cells and the induction of tumor necrosis factor α (TNF-α), interleukin-12 (IL-12), interferon-α

(IFN-α), and IFN-β by plasmacytoid dendritic cells.[77] The production of these cytokines triggers a powerful response in various other immune cell types that are not targeted directly by ISS 1018. Further, ISS 1018 can cause the maturation of dendritic cells that in turn cause initiation of NK-cell and T-cell responses to tumor antigens.[79,80] To date clinical trials have shown promise for 1018 ISS when used in conjunction with rituximab for the treatment of NHL.[81]

Apatorsen (OGX-427) is in Phase I/II clinical trials for the treatment of castration-resistant prostate cancer (CRPC) or other metastatic cancers that have been demonstrated to express Hsp27, such as ovarian, breast, bladder, and non-small-cell lung cancers.[82] Apatorsen works by inhibiting the expression of Hsp27 by binding to and blocking translation of its mRNA.[82] Studies have shown effectiveness and tolerance of apatorsen in high doses in clinical trials so far, with many patients showing decreased expression of cancer markers.[82]

Phase II clinical trials of cenersen (EL625) have been conducted to test the efficacy of the drug for the treatment of acute myeloid leukemia.[83] Cenersen targets mutated p53, which is a proto-oncogene and leads to degradation of the p53 mRNA. This allows for cancer cells to respond to DNA damaging agents that once were not sensitive to such agents. So far, clinical trials have shown patients that had not responded to standard chemotherapy or had relapsed shortly after standard chemotherapy had significantly better clinical outcomes following additional treatment with cenersen.[83]

ARRx (AZD5312) has undergone Phase I/II testing for the treatment of CRPC.[84] ARRx was designed to target the androgen receptor (AR), which plays an important role in CRPC disease development and progression.[85] Preclinical trials demonstrated the efficacy of this drug when used in conjunction with the pan-AKT inhibitor, AZD5363, for treating CRPC in a murine model.[84]

Custirsen (OGX-011) is in Phase I/II clinical trials for treatment of advanced non-small-cell lung cancer that has previously been left untreated.[86] Custirsen targets the mRNA clusterin, which encodes for a chaperone protein that enables cell survival and causes resistance to various

treatments.[87] Custirsen was shown to have minimal toxicity while significantly reducing the expression of clusterin in primary prostate tumors.[86]

siRNA therapeutics and functional implications:

siRNAs are double-stranded RNAs that are relatively small (~21-25 nucleotides) and function to silence gene expression (Figure 1C).[88] They occur naturally or can be chemically synthesized. Naturally occurring siRNAs originate from endogenous or viral precursor siRNAs. These precursors are roughly around 100 nucleotides long and are cleaved by Dicer into their mature siRNA structures [89]. Dicer leaves a 3' overhang of two nucleotides that allows the siRNA to interact with the RISC complex where it will initiate gene silencing.[90] Once it is bound, the RISC protein argonaute 2 (AGO) carries out cleavage of the sense strand.[91] This allows for the antisense strand to bind its target mRNA. Once the target RNA is bound to the antisense strand its phosphodiester backbone is cleaved by AGO2. This leads to sequence specific knockdown of the target mRNA and therefore, causes gene silencing. Synthetic or naturally occurring siRNAs can therefore be used to knockdown the expression of a single protein coding gene. The use of the double stranded siRNA to reduce expression of a target gene was first utilized in 1998 to target hlh-1, unc-54, unc-22, and fem1 in C. elegans.[1] This groundbreaking work by Fire *et al*. eventually led to a Nobel prize award. Most importantly, they found that double-stranded RNAs (siRNAs) are more effective in downregulating their target mRNA than their single-stranded counterparts (ASOs).[1] This highlights the advantage of siRNA technology over ASOs for the treatment of most human diseases.

FDA-approved siRNAs:

The very first siRNA therapeutic approved for use by the FDA was Patisiran.[92] It was approved in 2018 for the treatment of polyneuropathy caused by hereditary transthyretin-mediated (hATTR) amyloidosis.[93] hATTR amyloidosis is a genetic disorder that causes the buildup of abnormal TTR, which generally causes polyneuropathy when the build-up occurs in the peripheral

nervous system.[94] Patisiran is an siRNA drug that targets the mutated *TTR* mRNA leading to mRNA degradation and decreased TTR protein expression.[93] This has been shown to greatly reduce TTR deposition in patients with polyneuropathy caused by hATTR amyloidosis.[93]

Givosiran was the second FDA-approved siRNA therapeutic and is used to treat acute hepatic porphyria.[95] This disorder is caused by a plethora of deficiencies in enzymes involved in heme production and leads to a toxic buildup of porphobilinogen (PBG) and delta-aminolevulinic acid (ALA).[96] Givosiran targets the mRNA of ALA synthase 1 in the liver and reduces the levels of disease-causing neurotoxic intermediates aminolevulinic acid and porphobilinogen.[97]

Lumasiran was approved by the FDA for the treatment of primary hyperoxaluria type 1 (PH1) in 2020.[98] Various mutations in the enzyme alanine-glyoxylate aminotransferase causes increased oxalate concentrations and calcium oxalate crystal formation leading to the development of PH1.[99] Lumasiran targets the mRNA that encodes glycolate oxidase leading to the depletion of the substrate for oxalate synthesis and sufficiently reduces oxalate concentrations.[98]

In December 2021, inclisiran was approved by the FDA for the treatment of atherosclerotic cardiovascular disease (ASCVD) or heterozygous familial hypercholesterolemia (HeFH) (https://www.fda.gov/drugs/news-events-human-drugs/fda-approves-add-therapy-lower-cholesterol-among-certain-high-risk-adults). These conditions are characterized by high LDL-C levels. Inclisiran works to lower LDL-C levels by targeting the mRNA encoding for proprotein convertase subtilsin/kexin type 9 (PCSK9), which is involved in lipid metabolism and the regulation of cholesterol levels.[100] Inclisiran has been shown to reduce LDL-C levels in patients that were unable to reduce these levels with statins alone.[100] Additionally, inclisiran has demonstrated increased efficacy in lowering LDL-C levels when administered in conjunction with statins in patients that statins alone have been partially effective in lowering LDL-C levels.[100]

siRNAs in clinical trials:

TKM-080301 is in Phase I/II clinical trials for the treatment of hepatocellular carcinoma (HCC).[101] HCC is typically characterized by the overexpression of Polo-like kinase 1 (PLK1).[102] Therefore, targeting PLK1 may have beneficial effects for the treatment of HCC. To date, clinical trials have shown limited antitumor effects of TKM-080301 in patients with HCC.[101]

Atu027 is in Phase I/II clinical trials for the treatment of advanced solid tumors and pancreatic adenocarcinoma.[103,104] It is designed to target the mRNA encoding protein kinase N3 (PKN3) in order to reduce the metastatic activity of tumors. Clinical trials have demonstrated the safety and efficacy of Atu027 in preventing adverse outcomes in patients with metastatic cancer.[104]

siG12D LODER is in Phase I/IIa clinical trials for the treatment of pancreatic tumors in combination with chemotherapy.[105] It is a biodegradable implant containing a siRNA that targets the mRNA of the mutated *KRAS* oncogene, which can be surgically embedded in pancreatic tumors.[106] Mutated *KRAS* has been implicated in the development of most pancreatic cancers and is correlated with a worse prognosis for the patient.[107] Clinical studies have shown the potential efficacy of siG12D LODER in preventing tumor progression.[105]

ARO-HIF2 is in Phase I clinical trials for the treatment of clear cell renal cell carcinoma (NCT04169711). This form of carcinoma is the most diagnosed form of kidney cancer.[108] In addition, it is associated with the inactivation of von Hippel–Lindau tumor-suppressor protein (pVHL) propelled by hypoxia-inducible factor 2 (HIF2) transcription factor deregulation.[109] Therefore, ARO-HIF2 aims to target the mRNA of HIF2 to inhibit tumor growth.

APN401 is currently in Phase I clinical trials to test its efficacy in treating patients with either metastatic or recurrent colorectal cancer, pancreatic cancer, or other solid tumors that are not surgically accessible.[110] It works by targeting casitas-B-lineage lymphoma protein-b (Cbl-b) that has been shown to limit lymphocyte activation.[111] Preclinical studies using murine tumor models demonstrated that Cbl-b inhibition enhances natural killer cell and T cell-mediated antitumor activity.[111,112]

Vutrisiran (ALN-TTRSC02) is in Phase III clinical trials for the treatment of transthyretin (ATTR) mediated amyloidosis with (NCT04153149) or without (NCT03759379) cardiomyopathy. ATTR-mediated amyloidosis is a condition caused by a buildup of TTR either caused by mutations in the *TTR* gene or not.[113] By targeting the *TTR* mRNA, vutrisiran is able to reduce TTR protein expression, leading to better outcomes in patients with ATTR-mediated amyloidosis.[114]

miRNA therapeutics and functional implications:

miRNAs are non-coding RNAs that consist of ~20 nucleotides that are highly conserved between eukaryotic species. miRNAs were discovered in Caenorhabditis elegans by Ambros in 1993.[115] That same year, Ruvkun found the first miRNA target genes.[116] The discovery that miRNAs can be used to downregulate target genes paved the way for miRNA therapeutics. miRNAs have excellent therapeutic potential due to their extraordinary targeting capability. For example, one miRNA can target anywhere from ten to hundreds of genes. Additionally, they tend to target multiple genes within the same pathway. miRNAs are naturally occurring molecules endogenous to our cells. Therefore, there is less chance for immunogenic response with miRNA therapeutics than their other synthetic RNA counterparts. Further, miRNA inhibitors and mimics can be used to restore or inhibit protein synthesis, respectively (Figure 1D).

Inhibition of protein synthesis or mRNA degradation is achieved through the miRNA associating with a variety of AGO proteins and modulating gene expression through the activity of the RISC complex.[117] When the miRNA is associated with AGO and the RISC complex is formed, the miRNA guides AGO to its target mRNA.[118] The seed sequence of the miRNA binds to the mRNA and causes either translational repression or mRNA degradation.[119] This leads to reduced target protein expression and therefore plays a key role in post-transcriptional gene regulation. This pathway can be enhanced by the supplementation of a miRNA mimic that is identical in sequence to the endogenous miRNA duplex. Restoring miRNA levels will lead to the repression of mRNAs that are overexpressed in certain conditions.

In contrast, restoration of protein synthesis is achieved by administering a miRNA inhibitor, a single-stranded miRNA that is complementary to a target miRNA. Once the miRNA inhibitor binds to the miRNA it prevents the miRNA from associating with AGO. Therefore, miRNA inhibitors block the mRNA targeting ability of miRNAs and restore protein synthesis. This approach can be used to treat disorders caused by overexpression of a miRNA that leads to downregulation of certain disease preventing mRNAs.

miRNAs in clinical trials:

While there are currently no miRNAs that are FDA-approved, there are many in clinical development. For example, miravirsen has completed Phase II clinical trials for the treatment of Hepatitis (Hep) C.[120] Miravirsen is a miR-122 inhibitor, that sequesters miR-122, which has been implicated in the promotion of the Hep C virus (HCV) life cycle.[121] Clinical trials to date have shown a significant reduction of HCV viral load in patients treated with miravirsen.[120]

RG-012, also known as lademirsen, is in Phase II clinical trials for treatment of Alport syndrome (NCT02855268). This condition is caused by various mutations in the genes encoding collagen IV and leads to kidney disease as well as both ocular and hearing deficiencies.[122] This syndrome is associated with increased levels of miR-21; therefore, it was hypothesized that a miR-21 inhibitor may work in treating this condition. Pre-clinical trials have demonstrated that a miR-21 inhibitor is extremely successful in preventing the onset of Alport syndrome, thus highlighting the therapeutic potential for this drug.[123]

Cobomarsen is currently in clinical development for the treatment of various leukemias and lymphomas, such as adult T-cell leukemia/lymphoma (ATLL), chronic lymphocytic leukemia (CLL), the mycosis fungoides (MF) subtype of cutaneous T-cell lymphoma (CTCL), and the activated B-cell (ABC) subtype of diffuse large B-cell lymphoma (DLBCL).[124] It works by targeting miR-155, which is associated with inflammation and the development of various leukemias and lymphomas.[124-127] Phase II clinical trials were initiated following successful Phase I trials

(NCT02580552); however, they were terminated early due to business reasons unassociated with safety or efficacy (NCT03713320).

MRG-110 has completed Phase I clinical trials to test the safety efficacy of the miR-92a inhibitor in healthy patients (NCT03603431). Treatment with this inhibitor was found to significantly reduce miR-92a expression in these individuals when compared to patients treated with a placebo.[128] Additionally, increased expression of miR-92a has been associated with poor wound healing.[129] Further, miR-92a inhibition has been shown to improve wound healing *in vivo* in preclinical models.[130] Therefore, MRG-110 may be effective in treating impaired wound healing in conditions such as diabetes.

RG-125 (AZD4076) completed Phase I/IIa clinical trials for the treatment of Type 2 Diabetes (T2D) and Non-Alcoholic Fatty Liver Disease (NAFLD) (NCT02826525). This drug inhibits miR-103/107, in which overexpression of these miRNAs has been shown to correlate with the development of T2D and NAFLD.[131] Further, preclinical studies have demonstrated that a miR-103/107 inhibitor can improve insulin sensitivity in obese mice.[132] This along with successful Phase I/IIa clinical trials emphasizes the therapeutic potential of miR-103/107 inhibitors for the treatment of T2D and NAFLD.

RGLS4326 completed Phase 1b clinical trials for the treatment of autosomal dominant polycystic kidney disease (ADPKD) (NCT04536688). This disease is caused by mutations in *PKD1* and *PKD2* resulting in decreased expression of PC1 and PC2.[133] miR-17 has been shown to bind and downregulate *PKD1* and *PKD2* gene expression, while miR-17 inhibitors have been shown to restore *PKD1* and *PKD2* expression.[134] Finally, inhibition of miR-17 by RGLS4326 in humans was also shown to significantly increase PC1 and PC2 levels in patients with ADPKD (NCT04536688).

CDR132L has completed Phase I clinical trials for the treatment of heart failure of ischemic origin (NCT04045405). Hypertrophy of cardiomyocytes has been shown to be caused by overexpression of miR-212/132 family, leading to heart failure.[135] Further, preclinical studies have

shown that inhibiting miR-132 can improve heart function in animal models of heart failure.[136,137] Finally, initial clinical studies have shown exceptional efficacy of CDR132L for treating patients with heart failure (NCT04045405).

TargomiRs has been studied as either a second- or third-line treatment for recurrent malignant pleural mesothelioma and non-small cell lung cancer. Downregulation of miR-16 has been implicated in the development of many types of cancer, such as chronic lymphocytic leukemia and non-small cell lung cancer.[138,139] Additionally, miR-16 mimics act to increase miR-16 levels in order to target and downregulate multiple oncogenes and lead to tumor regression.[140] TargomiRs, a miR-16 mimic, has shown substantial preclinical efficacy in the treatment of many types of cancer.[141,142] Finally, initial clinical trials have shown TargomiRs has antitumor effects in patients with malignant pleural mesothelioma.[143]

Remlarsen has completed Phase II clinical trials for the treatment of keloid scars. Keloid scars are caused by a fibroproliferative disorder that causes excess production of extracellular matrix proteins and collagen.[144] Interestingly, miR-29 has been shown to negatively regulate multiple genes involved in the fibrotic response[145,146] and therefore reduces fibrosis.[147] Further, remlarsen, a miR-29 mimic, has shown a significant reduction in collagen expression and fibrosis in skin wounds.[148] Therefore, remlarsen may have therapeutic potential in treating keloid scars as well as scleroderma.

There have been some miRNA drug candidates that have demonstrated severe adverse effects. For example, MRX34 is a miR-34 mimic that showed success in preclinical trials for the treatment of cancer.[149-151] Expression of miR-34 has been shown to be significantly reduced in many different types of cancer.[152-154] Further, miR-34 targets many different oncogenes and, therefore can theoretically hamper tumor progression.[155-157] While early Phase I clinical trials were successful in reducing the miR-34a target oncogenes in a dose dependent manner,[158,159] they were eventually halted after several patients had severe adverse reactions to treatment.[159]

Finally, there are multiple miRNA therapeutics that have demonstrated substantial preclinical efficacy for various disorders. For example, miR-10b-5p is in preclinical development for the treatment of diabetes and associated gut motility disorders.[13] Additionally, a miR-101-3p inhibitor in combination with chemotherapeutic agents has been shown to effectively reduce CRC cell proliferation.[160] Further, miR-221 is another possible target for many different types of cancer as its expression is increased in glioblastoma, osteosarcoma, CRC, etc.[161-163] The therapeutic potential of miRNAs is limitless and will likely lead to improved treatment options for many different diseases, particularly ones with multiple underlying pathophysiological mechanisms.

Aptamer therapeutics and functional implications:

Aptamers are single-stranded RNA, DNA, or RNA-DNA hybrids that have often been classified as chemical antibodies. They often are around 20-100 base pairs long and fold into specific tertiary structures that allow them to specifically bind to their respective targets (Figure 1E).[164] Aptamers can be designed to target carbohydrates, peptides, proteins, and various other molecules making them an attractive therapeutic option for various diseases.

Aptamers are generated using the systematic evolution of ligands by exponential enrichment (SELEX) method. This procedure uses a randomized library that contains ~4^N individual sequences that can be tested simultaneously.[165] While aptamers have been synthesized containing 8-228 nucleotides, most are around 20 nucleotides long.[166] This large library allows for trillions of sequences to be tested to find ones that are able to bind the target molecule. These sequences then continue on to further rounds of selection. Thus, increasing the population of aptamers that are able to bind the target with high affinity. Eventually, there are specific sequences that dominate the population of library species. Finally, it is important to note that this process is extremely fast in comparison to traditional peptide synthesis strategies.

Aptamers can act through three main mechanisms of action: 1) aptamers that are specific to a particular cell type can deliver other therapeutic agents to the target tissue or cells; 2) aptamers

can act as an agonist and thus functionally activate their target molecules; 3) or aptamers work as antagonists and block the interaction of molecules in pathways associated with disease development.[164]

FDA-approved aptamers:

Pegaptanib was the first-ever FDA-approved aptamer and is used for the treatment of neovascular age-related macular degeneration. This disease is characterized by retinal degeneration, causing vision loss.[167] Increased vascular endothelial growth factor (VEGF) has been associated with this condition.[168] Therefore, anti-VEGF treatment was thought to be an efficient method of treating this disease. Pegaptanib was found to have high affinity for VEGF and caused it to be sequestered preventing it from binding to its receptor. After successful clinical trials showing that pegaptanib improved or halted vision loss,[169] it was approved for use by the FDA in 2004.

Defibrotide was approved by the FDA in 2020 for the treatment of hepatic veno-occlusive disease/sinusoidal obstruction syndrome.[170] This can be a life-threatening complication caused by chemotherapy and hematopoietic stem cell transplant (HSCT) conditioning.[171] Defibrotide has been reported to stabilize endothelial cells via reduced endothelial-cell activation.[172] This protects endothelial cells from further damage and rescues this condition. Both FDA-approved medicines have very minimal side effects and highlight the promise of aptamer-based therapeutics.

Aptamers in clinical trials:

NOX-A12 is an RNA aptamer that is in clinical trials for the treatment of various types of cancers; for example, pancreatic cancer, colorectal cancer, and multiple myeloma.[173-175] This drug works by neutralizing CXCL12, which leads to an increase in circulating tumor-infiltrating T-cells.[176] To date, clinical trials have demonstrated the potential of NOX-A12 in the treatment of various types of cancer.[173-175]

NOX-E36 has completed Phase I clinical trials for the treatment of diabetes and albuminuria (NCT01547897). Increased HbA1c and albumin/creatinine ratio (ACR) are hallmarks of these conditions. NOX-E36 has been shown to reduce these levels in patients with diabetes and albuminuria[177] by binding to CCL2, a proinflammatory cytokine, with high affinity.[178] Therefore, this therapeutic drug may have beneficial effects on the treatment of diabetes and related conditions.

There are other aptamers in clinical trials for various human diseases that are composed of DNA. For example, AS1411 is a DNA aptamer for the treatment of cancers such as acute myeloid leukemia.[179] However, since the purpose of this review is to highlight the potential of RNA therapeutics, we will not be discussing these aptamers in detail.

Conclusions and Future Perspectives

RNA molecules are multi-functional and are extremely versatile. State-of-the-art studies have demonstrated considerable promise for the clinical use of RNA therapeutics to treat and prevent human diseases. Further, RNA therapeutics are relatively cheaper, easier, and faster to develop than traditional protein and small molecule-based drugs. RNA therapeutic approaches vary in how they treat different clinical conditions. For example, siRNAs are highly specific with only one mRNA target; therefore, they are good for the treatment of diseases where pathologies are caused by the alternations of only one single gene. However, miRNAs have the virtue of targeting multiple mRNAs; consequently, they are suitable for the treatment of diseases in which various pathologies and/or alternations of many genes are involved. The current challenges for RNA therapeutics include: (i) Cell specificity; ideally, the best RNA therapeutic molecule would have on-target cell-specificity without off-target and undesired on-target effects. (ii) Cell-specific delivery agents, one of the most significant challenges in the RNA therapeutics is efficient and stable delivery of the molecule to the cell type of interest and being functionally active to perform their role.

Clinical trials should focus heavily on early study design to prevent possible adverse outcomes such as acute toxicity. Additionally, this early study design should focus on *in vivo*

functional assays rather than *in vitro* functional assays alone. Further, the most critical step in RNA therapeutics development is to compare the clinical outcomes in their ability to fix the mechanistic parameters. To accomplish this goal, the RNA therapeutic candidates must be rigorously examined, particularly for their immune tolerance, pharmacokinetics, and pharmacodynamics. But it is important to note that RNA therapeutic agents are likely developed based on the cellular and molecular mechanisms underlying pathologies of the diseases; thereby, these molecules are placed in a prime position for future clinical trials. The current knowledge gaps warrant a modern approach to better understand the pathologies at the cellular and molecular level that will enable us to tackle the therapeutic approaches to treat the disease, not only improving the symptomology, but also fixing the exact cause.

While there are currently challenges to RNA therapeutic development, unprecedented interdisciplinary approaches, the promising developments of modern science, along with improved early study design for clinical trials will overcome these obstacles in the foreseeable future. This will provide substantial hope for the clinical utility of RNA therapeutics for different disease conditions and lead to a better quality of life for millions of patients.

References

1. Fire A, Xu S, Montgomery MK, et al. Potent and specific genetic interference by double-stranded RNA in Caenorhabditis elegans. Nature 1998;391:806-11.
2. Winkle M, El-Daly SM, Fabbri M, et al. Noncoding RNA therapeutics - challenges and potential solutions. Nat Rev Drug Discov 2021;20:629-651.
3. Rand TA, Ginalski K, Grishin NV, et al. Biochemical identification of Argonaute 2 as the sole protein required for RNA-induced silencing complex activity. Proc Natl Acad Sci U S A 2004;101:14385-9.
4. Singh R, Zogg H, Ro S. Role of microRNAs in Disorders of Gut-Brain Interactions: Clinical Insights and Therapeutic Alternatives. J Pers Med 2021;11.
5. Matranga C, Tomari Y, Shin C, et al. Passenger-strand cleavage facilitates assembly of siRNA into Ago2-containing RNAi enzyme complexes. Cell 2005;123:607-20.
6. Zhong L, Li Y, Xiong L, et al. Small molecules in targeted cancer therapy: advances, challenges, and future perspectives. Signal Transduct Target Ther 2021;6:201.
7. Lu H, Zhou Q, He J, et al. Recent advances in the development of protein-protein interactions modulators: mechanisms and clinical trials. Signal Transduct Target Ther 2020;5:213.
8. Dimitrov DS. Therapeutic proteins. Methods Mol Biol 2012;899:1-26.
9. Bruno BJ, Miller GD, Lim CS. Basics and recent advances in peptide and protein drug delivery. Ther Deliv 2013;4:1443-67.
10. Bajan S, Hutvagner G. RNA-Based Therapeutics: From Antisense Oligonucleotides to miRNAs. Cells 2020;9.
11. Komatsu H. Innovative Therapeutic Approaches for Huntington's Disease: From Nucleic Acids to GPCR-Targeting Small Molecules. Front Cell Neurosci 2021;15:785703.
12. Hanna J, Hossain GS, Kocerha J. The Potential for microRNA Therapeutics and Clinical Research. Front Genet 2019;10:478.

13. Singh R, Ha SE, Wei L, et al. miR-10b-5p Rescues Diabetes and Gastrointestinal Dysmotility. Gastroenterology 2021;160:1662-1678 e18.
14. Mignone F, Gissi C, Liuni S, et al. Untranslated regions of mRNAs. Genome Biol 2002;3:REVIEWS0004.
15. Leppek K, Das R, Barna M. Functional 5' UTR mRNA structures in eukaryotic translation regulation and how to find them. Nat Rev Mol Cell Biol 2018;19:158-174.
16. Da Silva Sanchez A, Paunovska K, Cristian A, et al. Treating Cystic Fibrosis with mRNA and CRISPR. Hum Gene Ther 2020;31:940-955.
17. Musunuru K, Chadwick AC, Mizoguchi T, et al. In vivo CRISPR base editing of PCSK9 durably lowers cholesterol in primates. Nature 2021;593:429-434.
18. Wolff JA, Malone RW, Williams P, et al. Direct gene transfer into mouse muscle in vivo. Science 1990;247:1465-8.
19. Jirikowski GF, Sanna PP, Maciejewski-Lenoir D, et al. Reversal of diabetes insipidus in Brattleboro rats: intrahypothalamic injection of vasopressin mRNA. Science 1992;255:996-8.
20. Martinon F, Krishnan S, Lenzen G, et al. Induction of virus-specific cytotoxic T lymphocytes in vivo by liposome-entrapped mRNA. Eur J Immunol 1993;23:1719-22.
21. Polack FP, Thomas SJ, Kitchin N, et al. Safety and Efficacy of the BNT162b2 mRNA Covid-19 Vaccine. N Engl J Med 2020;383:2603-2615.
22. Baden LR, El Sahly HM, Essink B, et al. Efficacy and Safety of the mRNA-1273 SARS-CoV-2 Vaccine. N Engl J Med 2021;384:403-416.
23. Kremsner PG, Ahuad Guerrero RA, Arana-Arri E, et al. Efficacy and safety of the CVnCoV SARS-CoV-2 mRNA vaccine candidate in ten countries in Europe and Latin America (HERALD): a randomised, observer-blinded, placebo-controlled, phase 2b/3 trial. Lancet Infect Dis 2021.

24. Aldrich C, Leroux-Roels I, Huang KB, et al. Proof-of-concept of a low-dose unmodified mRNA-based rabies vaccine formulated with lipid nanoparticles in human volunteers: A phase 1 trial. Vaccine 2021;39:1310-1318.
25. Petsch B, Schnee M, Vogel AB, et al. Protective efficacy of in vitro synthesized, specific mRNA vaccines against influenza A virus infection. Nat Biotechnol 2012;30:1210-6.
26. Aliprantis AO, Shaw CA, Griffin P, et al. A phase 1, randomized, placebo-controlled study to evaluate the safety and immunogenicity of an mRNA-based RSV prefusion F protein vaccine in healthy younger and older adults. Hum Vaccin Immunother 2021;17:1248-1261.
27. Schnee M, Vogel AB, Voss D, et al. An mRNA Vaccine Encoding Rabies Virus Glycoprotein Induces Protection against Lethal Infection in Mice and Correlates of Protection in Adult and Newborn Pigs. PLoS Negl Trop Dis 2016;10:e0004746.
28. Medina-Magues LG, Gergen J, Jasny E, et al. mRNA Vaccine Protects against Zika Virus. Vaccines (Basel) 2021;9.
29. John S, Yuzhakov O, Woods A, et al. Multi-antigenic human cytomegalovirus mRNA vaccines that elicit potent humoral and cell-mediated immunity. Vaccine 2018;36:1689-1699.
30. Webster H, Valencia S, Kumar A, et al. Pre-existing immunity to cytomegalovirus in macaques influences human CMV vaccine responses in preclinical models. Vaccine 2021;39:5358-5367.
31. Anttila V, Saraste A, Knuuti J, et al. Synthetic mRNA Encoding VEGF-A in Patients Undergoing Coronary Artery Bypass Grafting: Design of a Phase 2a Clinical Trial. Mol Ther Methods Clin Dev 2020;18:464-472.
32. Conklin LD, McAninch RE, Schulz D, et al. HIV-based vectors and angiogenesis following rabbit hindlimb ischemia. J Surg Res 2005;123:55-66.
33. Giacca M, Zacchigna S. VEGF gene therapy: therapeutic angiogenesis in the clinic and beyond. Gene Ther 2012;19:622-9.

34. Gaffney MM, Hynes SO, Barry F, et al. Cardiovascular gene therapy: current status and therapeutic potential. Br J Pharmacol 2007;152:175-88.
35. Yan Z, McCray PB, Jr., Engelhardt JF. Advances in gene therapy for cystic fibrosis lung disease. Hum Mol Genet 2019;28:R88-R94.
36. Butnariu LI, Tarca E, Cojocaru E, et al. Genetic Modifying Factors of Cystic Fibrosis Phenotype: A Challenge for Modern Medicine. J Clin Med 2021;10.
37. Chandler RJ, Venditti CP. Gene Therapy for Methylmalonic Acidemia: Past, Present, and Future. Hum Gene Ther 2019;30:1236-1244.
38. An D, Schneller JL, Frassetto A, et al. Systemic Messenger RNA Therapy as a Treatment for Methylmalonic Acidemia. Cell Rep 2017;21:3548-3558.
39. Fraser JL, Venditti CP. Methylmalonic and propionic acidemias: clinical management update. Curr Opin Pediatr 2016;28:682-693.
40. Sahin U, Oehm P, Derhovanessian E, et al. An RNA vaccine drives immunity in checkpoint-inhibitor-treated melanoma. Nature 2020;585:107-112.
41. Connolly B, Isaacs C, Cheng L, et al. SERPINA1 mRNA as a Treatment for Alpha-1 Antitrypsin Deficiency. J Nucleic Acids 2018;2018:8247935.
42. Cao J, An D, Galduroz M, et al. mRNA Therapy Improves Metabolic and Behavioral Abnormalities in a Murine Model of Citrin Deficiency. Mol Ther 2019;27:1242-1251.
43. Porciuncula A, Morgado M, Gupta R, et al. Spatial Mapping and Immunomodulatory Role of the OX40/OX40L Pathway in Human Non-Small Cell Lung Cancer. Clin Cancer Res 2021;27:6174-6183.
44. Hewitt SL, Bailey D, Zielinski J, et al. Intratumoral IL12 mRNA Therapy Promotes TH1 Transformation of the Tumor Microenvironment. Clin Cancer Res 2020;26:6284-6298.
45. Zhu X, Yin L, Theisen M, et al. Systemic mRNA Therapy for the Treatment of Fabry Disease: Preclinical Studies in Wild-Type Mice, Fabry Mouse Model, and Wild-Type Non-human Primates. Am J Hum Genet 2019;104:625-637.

46. Evers MM, Toonen LJ, van Roon-Mom WM. Antisense oligonucleotides in therapy for neurodegenerative disorders. Adv Drug Deliv Rev 2015;87:90-103.
47. Stephenson ML, Zamecnik PC. Inhibition of Rous sarcoma viral RNA translation by a specific oligodeoxyribonucleotide. Proc Natl Acad Sci U S A 1978;75:285-8.
48. Roberts TC, Langer R, Wood MJA. Advances in oligonucleotide drug delivery. Nat Rev Drug Discov 2020;19:673-694.
49. Wu H, Lima WF, Zhang H, et al. Determination of the role of the human RNase H1 in the pharmacology of DNA-like antisense drugs. J Biol Chem 2004;279:17181-9.
50. Santos RD, Raal FJ, Donovan JM, et al. Mipomersen preferentially reduces small low-density lipoprotein particle number in patients with hypercholesterolemia. J Clin Lipidol 2015;9:201-9.
51. Wan L, Dreyfuss G. Splicing-Correcting Therapy for SMA. Cell 2017;170:5.
52. Lim KH, Han Z, Jeon HY, et al. Antisense oligonucleotide modulation of non-productive alternative splicing upregulates gene expression. Nat Commun 2020;11:3501.
53. Ward AJ, Norrbom M, Chun S, et al. Nonsense-mediated decay as a terminating mechanism for antisense oligonucleotides. Nucleic Acids Res 2014;42:5871-9.
54. Boiziau C, Kurfurst R, Cazenave C, et al. Inhibition of translation initiation by antisense oligonucleotides via an RNase-H independent mechanism. Nucleic Acids Res 1991;19:1113-9.
55. Liang XH, Shen W, Sun H, et al. Translation efficiency of mRNAs is increased by antisense oligonucleotides targeting upstream open reading frames. Nat Biotechnol 2016;34:875-80.
56. Vickers TA, Wyatt JR, Burckin T, et al. Fully modified 2' MOE oligonucleotides redirect polyadenylation. Nucleic Acids Res 2001;29:1293-9.
57. Piascik P. Fomiversen sodium approved to treat CMV retinitis. J Am Pharm Assoc (Wash) 1999;39:84-5.
58. Jabs DA, Griffiths PD. Fomivirsen for the treatment of cytomegalovirus retinitis. Am J Ophthalmol 2002;133:552-6.

59. Won JI, Zhang J, Tecson KM, et al. Balancing Low-density Lipoprotein Cholesterol Reduction and Hepatotoxicity With Lomitapide Mesylate and Mipomersen in Patients With Homozygous Familial Hypercholesterolemia. Rev Cardiovasc Med 2017;18:21-28.
60. Cesaro A, Fimiani F, Gragnano F, et al. New Frontiers in the Treatment of Homozygous Familial Hypercholesterolemia. Heart Fail Clin 2022;18:177-188.
61. Gouni-Berthold I, Berthold HK. Mipomersen and lomitapide: Two new drugs for the treatment of homozygous familial hypercholesterolemia. Atheroscler Suppl 2015;18:28-34.
62. Aartsma-Rus A. FDA Approval of Nusinersen for Spinal Muscular Atrophy Makes 2016 the Year of Splice Modulating Oligonucleotides. Nucleic Acid Ther 2017;27:67-69.
63. Burr P, Reddivari AKR. Spinal Muscle Atrophy. StatPearls. Treasure Island (FL), 2022.
64. Mercuri E, Darras BT, Chiriboga CA, et al. Nusinersen versus Sham Control in Later-Onset Spinal Muscular Atrophy. N Engl J Med 2018;378:625-635.
65. Aartsma-Rus A. FDA Approval of Nusinersen for Spinal Muscular Atrophy Makes 2016 the Year of Splice Modulating Oligonucleotides. Nucleic Acid Ther 2017;27:67-69.
66. Chamberlain JR, Chamberlain JS. Progress toward Gene Therapy for Duchenne Muscular Dystrophy. Mol Ther 2017;25:1125-1131.
67. Mendell JR, Rodino-Klapac LR, Sahenk Z, et al. Eteplirsen for the treatment of Duchenne muscular dystrophy. Ann Neurol 2013;74:637-47.
68. De Angelis FG, Sthandier O, Berarducci B, et al. Chimeric snRNA molecules carrying antisense sequences against the splice junctions of exon 51 of the dystrophin pre-mRNA induce exon skipping and restoration of a dystrophin synthesis in Delta 48-50 DMD cells. Proc Natl Acad Sci U S A 2002;99:9456-61.
69. Sekijima Y. Hereditary Transthyretin Amyloidosis. In: Adam MP, Ardinger HH, Pagon RA, Wallace SE, Bean LJH, Gripp KW, Mirzaa GM, Amemiya A, eds. GeneReviews((R)). Seattle (WA), 1993.
70. Mahfouz M, Maruyama R, Yokota T. Inotersen for the Treatment of Hereditary Transthyretin Amyloidosis. Methods Mol Biol 2020;2176:87-98.

71. Benson MD, Waddington-Cruz M, Berk JL, et al. Inotersen Treatment for Patients with Hereditary Transthyretin Amyloidosis. N Engl J Med 2018;379:22-31.
72. Iftikhar M, Frey J, Shohan MJ, et al. Current and emerging therapies for Duchenne muscular dystrophy and spinal muscular atrophy. Pharmacol Ther 2021;220:107719.
73. Scaglioni D, Catapano F, Ellis M, et al. The administration of antisense oligonucleotide golodirsen reduces pathological regeneration in patients with Duchenne muscular dystrophy. Acta Neuropathol Commun 2021;9:7.
74. Brudvig JJ, Weimer JM. On the cusp of cures: Breakthroughs in Batten disease research. Curr Opin Neurobiol 2021;72:48-54.
75. Kim J, Hu C, Moufawad El Achkar C, et al. Patient-Customized Oligonucleotide Therapy for a Rare Genetic Disease. N Engl J Med 2019;381:1644-1652.
76. Shirley M. Casimersen: First Approval. Drugs 2021;81:875-879.
77. Friedberg JW, Kim H, McCauley M, et al. Combination immunotherapy with a CpG oligonucleotide (1018 ISS) and rituximab in patients with non-Hodgkin lymphoma: increased interferon-alpha/beta-inducible gene expression, without significant toxicity. Blood 2005;105:489-95.
78. Schmitz-Feuerhake I, Frentzel-Beyme R, Wolff R. Non-Hodgkin lymphomas and ionizing radiation: case report and review of the literature. Ann Hematol 2022;101:243-250.
79. Fernandez NC, Lozier A, Flament C, et al. Dendritic cells directly trigger NK cell functions: cross-talk relevant in innate anti-tumor immune responses in vivo. Nat Med 1999;5:405-11.
80. Banchereau J, Steinman RM. Dendritic cells and the control of immunity. Nature 1998;392:245-52.
81. Friedberg JW, Kelly JL, Neuberg D, et al. Phase II study of a TLR-9 agonist (1018 ISS) with rituximab in patients with relapsed or refractory follicular lymphoma. Br J Haematol 2009;146:282-91.

82. Chi KN, Yu EY, Jacobs C, et al. A phase I dose-escalation study of apatorsen (OGX-427), an antisense inhibitor targeting heat shock protein 27 (Hsp27), in patients with castration-resistant prostate cancer and other advanced cancers. Ann Oncol 2016;27:1116-1122.
83. Cortes J, Kantarjian H, Ball ED, et al. Phase 2 randomized study of p53 antisense oligonucleotide (cenersen) plus idarubicin with or without cytarabine in refractory and relapsed acute myeloid leukemia. Cancer 2012;118:418-27.
84. De Velasco MA, Kura Y, Sakai K, et al. Targeting castration-resistant prostate cancer with androgen receptor antisense oligonucleotide therapy. JCI Insight 2019;4.
85. Yamamoto Y, Loriot Y, Beraldi E, et al. Generation 2.5 antisense oligonucleotides targeting the androgen receptor and its splice variants suppress enzalutamide-resistant prostate cancer cell growth. Clin Cancer Res 2015;21:1675-87.
86. Laskin JJ, Nicholas G, Lee C, et al. Phase I/II trial of custirsen (OGX-011), an inhibitor of clusterin, in combination with a gemcitabine and platinum regimen in patients with previously untreated advanced non-small cell lung cancer. J Thorac Oncol 2012;7:579-86.
87. Chi KN, Eisenhauer E, Fazli L, et al. A phase I pharmacokinetic and pharmacodynamic study of OGX-011, a 2'-methoxyethyl antisense oligonucleotide to clusterin, in patients with localized prostate cancer. J Natl Cancer Inst 2005;97:1287-96.
88. Fakhr E, Zare F, Teimoori-Toolabi L. Precise and efficient siRNA design: a key point in competent gene silencing. Cancer Gene Ther 2016;23:73-82.
89. Song MS, Rossi JJ. Molecular mechanisms of Dicer: endonuclease and enzymatic activity. Biochem J 2017;474:1603-1618.
90. Iwakawa HO, Tomari Y. Life of RISC: Formation, action, and degradation of RNA-induced silencing complex. Mol Cell 2022;82:30-43.
91. Niaz S. The AGO proteins: an overview. Biol Chem 2018;399:525-547.
92. Hoy SM. Patisiran: First Global Approval. Drugs 2018;78:1625-1631.
93. Adams D, Gonzalez-Duarte A, O'Riordan WD, et al. Patisiran, an RNAi Therapeutic, for Hereditary Transthyretin Amyloidosis. N Engl J Med 2018;379:11-21.

94. Kaku M, Berk JL. Neuropathy Associated with Systemic Amyloidosis. Semin Neurol 2019;39:578-588.
95. de Paula Brandao PR, Titze-de-Almeida SS, Titze-de-Almeida R. Leading RNA Interference Therapeutics Part 2: Silencing Delta-Aminolevulinic Acid Synthase 1, with a Focus on Givosiran. Mol Diagn Ther 2020;24:61-68.
96. Syed YY. Givosiran: A Review in Acute Hepatic Porphyria. Drugs 2021;81:841-848.
97. Balwani M, Sardh E, Ventura P, et al. Phase 3 Trial of RNAi Therapeutic Givosiran for Acute Intermittent Porphyria. N Engl J Med 2020;382:2289-2301.
98. Scott LJ, Keam SJ. Lumasiran: First Approval. Drugs 2021;81:277-282.
99. Liebow A, Li X, Racie T, et al. An Investigational RNAi Therapeutic Targeting Glycolate Oxidase Reduces Oxalate Production in Models of Primary Hyperoxaluria. J Am Soc Nephrol 2017;28:494-503.
100. Lamb YN. Inclisiran: First Approval. Drugs 2021;81:389-395.
101. El Dika I, Lim HY, Yong WP, et al. An Open-Label, Multicenter, Phase I, Dose Escalation Study with Phase II Expansion Cohort to Determine the Safety, Pharmacokinetics, and Preliminary Antitumor Activity of Intravenous TKM-080301 in Subjects with Advanced Hepatocellular Carcinoma. Oncologist 2019;24:747-e218.
102. Andrisani OM, Studach L, Merle P. Gene signatures in hepatocellular carcinoma (HCC). Semin Cancer Biol 2011;21:4-9.
103. Schultheis B, Strumberg D, Santel A, et al. First-in-human phase I study of the liposomal RNA interference therapeutic Atu027 in patients with advanced solid tumors. J Clin Oncol 2014;32:4141-8.
104. Schultheis B, Strumberg D, Kuhlmann J, et al. Safety, Efficacy and Pharcacokinetics of Targeted Therapy with The Liposomal RNA Interference Therapeutic Atu027 Combined with Gemcitabine in Patients with Pancreatic Adenocarcinoma. A Randomized Phase Ib/IIa Study. Cancers (Basel) 2020;12.

105. Golan T, Khvalevsky EZ, Hubert A, et al. RNAi therapy targeting KRAS in combination with chemotherapy for locally advanced pancreatic cancer patients. Oncotarget 2015;6:24560-70.

106. Zorde Khvalevsky E, Gabai R, Rachmut IH, et al. Mutant KRAS is a druggable target for pancreatic cancer. Proc Natl Acad Sci U S A 2013;110:20723-8.

107. Buscail L, Bournet B, Cordelier P. Role of oncogenic KRAS in the diagnosis, prognosis and treatment of pancreatic cancer. Nat Rev Gastroenterol Hepatol 2020;17:153-168.

108. Wolf MM, Kimryn Rathmell W, Beckermann KE. Modeling clear cell renal cell carcinoma and therapeutic implications. Oncogene 2020;39:3413-3426.

109. Krieg M, Haas R, Brauch H, et al. Up-regulation of hypoxia-inducible factors HIF-1alpha and HIF-2alpha under normoxic conditions in renal carcinoma cells by von Hippel-Lindau tumor suppressor gene loss of function. Oncogene 2000;19:5435-43.

110. Triozzi P, Kooshki M, Alistar A, et al. Phase I clinical trial of adoptive cellular immunotherapy with APN401 in patients with solid tumors. J ImmunoTherapy Cancer 2015;3:175.

111. Bachmaier K, Krawczyk C, Kozieradzki I, et al. Negative regulation of lymphocyte activation and autoimmunity by the molecular adaptor Cbl-b. Nature 2000;403:211-6.

112. Paolino M, Choidas A, Wallner S, et al. The E3 ligase Cbl-b and TAM receptors regulate cancer metastasis via natural killer cells. Nature 2014;507:508-12.

113. Sekijima Y, Wiseman RL, Matteson J, et al. The biological and chemical basis for tissue-selective amyloid disease. Cell 2005;121:73-85.

114. Habtemariam BA, Karsten V, Attarwala H, et al. Single-Dose Pharmacokinetics and Pharmacodynamics of Transthyretin Targeting N-acetylgalactosamine-Small Interfering Ribonucleic Acid Conjugate, Vutrisiran, in Healthy Subjects. Clin Pharmacol Ther 2021;109:372-382.

115. Lee RC, Feinbaum RL, Ambros V. The C. elegans heterochronic gene lin-4 encodes small RNAs with antisense complementarity to lin-14. Cell 1993;75:843-54.

116. Wightman B, Ha I, Ruvkun G. Posttranscriptional regulation of the heterochronic gene lin-14 by lin-4 mediates temporal pattern formation in C. elegans. Cell 1993;75:855-62.
117. Fabian MR, Sonenberg N. The mechanics of miRNA-mediated gene silencing: a look under the hood of miRISC. Nat Struct Mol Biol 2012;19:586-93.
118. Schirle NT, Sheu-Gruttadauria J, MacRae IJ. Structural basis for microRNA targeting. Science 2014;346:608-13.
119. Jonas S, Izaurralde E. Towards a molecular understanding of microRNA-mediated gene silencing. Nat Rev Genet 2015;16:421-33.
120. Janssen HL, Reesink HW, Lawitz EJ, et al. Treatment of HCV infection by targeting microRNA. N Engl J Med 2013;368:1685-94.
121. Panigrahi M, Thibault PA, Wilson JA. miR-122 affects both the initiation and maintenance of Hepatitis C Virus infections. J Virol 2021:JVI0190321.
122. Kashtan CE. Alport Syndrome: Achieving Early Diagnosis and Treatment. Am J Kidney Dis 2021;77:272-279.
123. Gomez IG, MacKenna DA, Johnson BG, et al. Anti-microRNA-21 oligonucleotides prevent Alport nephropathy progression by stimulating metabolic pathways. J Clin Invest 2015;125:141-56.
124. Witten L, Slack FJ. miR-155 as a novel clinical target for hematological malignancies. Carcinogenesis 2020;41:2-7.
125. Seto AG, Beatty X, Lynch JM, et al. Cobomarsen, an oligonucleotide inhibitor of miR-155, co-ordinately regulates multiple survival pathways to reduce cellular proliferation and survival in cutaneous T-cell lymphoma. Br J Haematol 2018;183:428-444.
126. Anastasiadou E, Seto AG, Beatty X, et al. Cobomarsen, an Oligonucleotide Inhibitor of miR-155, Slows DLBCL Tumor Cell Growth In Vitro and In Vivo. Clin Cancer Res 2021;27:1139-1149.
127. Bedewy AML, Elmaghraby SM, Shehata AA, et al. Prognostic Value of miRNA-155 Expression in B-Cell Non-Hodgkin Lymphoma. Turk J Haematol 2017;34:207-212.

128. Abplanalp WT, Fischer A, John D, et al. Efficiency and Target Derepression of Anti-miR-92a: Results of a First in Human Study. Nucleic Acid Ther 2020;30:335-345.
129. Bonauer A, Carmona G, Iwasaki M, et al. MicroRNA-92a controls angiogenesis and functional recovery of ischemic tissues in mice. Science 2009;324:1710-3.
130. Gallant-Behm CL, Piper J, Dickinson BA, et al. A synthetic microRNA-92a inhibitor (MRG-110) accelerates angiogenesis and wound healing in diabetic and nondiabetic wounds. Wound Repair Regen 2018;26:311-323.
131. Rottiers V, Naar AM. MicroRNAs in metabolism and metabolic disorders. Nat Rev Mol Cell Biol 2012;13:239-50.
132. Trajkovski M, Hausser J, Soutschek J, et al. MicroRNAs 103 and 107 regulate insulin sensitivity. Nature 2011;474:649-53.
133. Kim DY, Park JH. Genetic Mechanisms of ADPKD. Adv Exp Med Biol 2016;933:13-22.
134. Lee EC, Valencia T, Allerson C, et al. Discovery and preclinical evaluation of anti-miR-17 oligonucleotide RGLS4326 for the treatment of polycystic kidney disease. Nat Commun 2019;10:4148.
135. Ucar A, Gupta SK, Fiedler J, et al. The miRNA-212/132 family regulates both cardiac hypertrophy and cardiomyocyte autophagy. Nat Commun 2012;3:1078.
136. Foinquinos A, Batkai S, Genschel C, et al. Preclinical development of a miR-132 inhibitor for heart failure treatment. Nat Commun 2020;11:633.
137. Batkai S, Genschel C, Viereck J, et al. CDR132L improves systolic and diastolic function in a large animal model of chronic heart failure. Eur Heart J 2021;42:192-201.
138. Calin GA, Dumitru CD, Shimizu M, et al. Frequent deletions and down-regulation of micro-RNA genes miR15 and miR16 at 13q14 in chronic lymphocytic leukemia. Proc Natl Acad Sci U S A 2002;99:15524-9.
139. Bandi N, Zbinden S, Gugger M, et al. miR-15a and miR-16 are implicated in cell cycle regulation in a Rb-dependent manner and are frequently deleted or down-regulated in non-small cell lung cancer. Cancer Res 2009;69:5553-9.

140. Bonci D, Coppola V, Musumeci M, et al. The miR-15a-miR-16-1 cluster controls prostate cancer by targeting multiple oncogenic activities. Nat Med 2008;14:1271-7.
141. Reid G, Pel ME, Kirschner MB, et al. Restoring expression of miR-16: a novel approach to therapy for malignant pleural mesothelioma. Ann Oncol 2013;24:3128-35.
142. Chava S, Reynolds CP, Pathania AS, et al. miR-15a-5p, miR-15b-5p, and miR-16-5p inhibit tumor progression by directly targeting MYCN in neuroblastoma. Mol Oncol 2020;14:180-196.
143. van Zandwijk N, Pavlakis N, Kao SC, et al. Safety and activity of microRNA-loaded minicells in patients with recurrent malignant pleural mesothelioma: a first-in-man, phase 1, open-label, dose-escalation study. Lancet Oncol 2017;18:1386-1396.
144. Grabowski G, Pacana MJ, Chen E. Keloid and Hypertrophic Scar Formation, Prevention, and Management: Standard Review of Abnormal Scarring in Orthopaedic Surgery. J Am Acad Orthop Surg 2020;28:e408-e414.
145. Cheng J, Wang Y, Wang D, et al. Identification of collagen 1 as a post-transcriptional target of miR-29b in skin fibroblasts: therapeutic implication for scar reduction. Am J Med Sci 2013;346:98-103.
146. Zhu Y, Li Z, Wang Y, et al. Overexpression of miR-29b reduces collagen biosynthesis by inhibiting heat shock protein 47 during skin wound healing. Transl Res 2016;178:38-53 e6.
147. Montgomery RL, Yu G, Latimer PA, et al. MicroRNA mimicry blocks pulmonary fibrosis. EMBO Mol Med 2014;6:1347-56.
148. Gallant-Behm CL, Piper J, Lynch JM, et al. A MicroRNA-29 Mimic (Remlarsen) Represses Extracellular Matrix Expression and Fibroplasia in the Skin. J Invest Dermatol 2019;139:1073-1081.
149. Liu C, Kelnar K, Liu B, et al. The microRNA miR-34a inhibits prostate cancer stem cells and metastasis by directly repressing CD44. Nat Med 2011;17:211-5.
150. Jiang L, Hermeking H. miR-34a and miR-34b/c Suppress Intestinal Tumorigenesis. Cancer Res 2017;77:2746-2758.

151. Ji Q, Hao X, Zhang M, et al. MicroRNA miR-34 inhibits human pancreatic cancer tumor-initiating cells. PLoS One 2009;4:e6816.

152. Sun D, Wu Y, Zhang S, et al. Distinct roles of miR-34 family members on suppression of lung squamous cell carcinoma. Biomed Pharmacother 2021;142:111967.

153. Schmid G, Notaro S, Reimer D, et al. Expression and promotor hypermethylation of miR-34a in the various histological subtypes of ovarian cancer. BMC Cancer 2016;16:102.

154. Zou Y, Huang Y, Yang J, et al. miR-34a is downregulated in human osteosarcoma stem-like cells and promotes invasion, tumorigenic ability and self-renewal capacity. Mol Med Rep 2017;15:1631-1637.

155. Raver-Shapira N, Marciano E, Meiri E, et al. Transcriptional activation of miR-34a contributes to p53-mediated apoptosis. Mol Cell 2007;26:731-43.

156. Chen C, Zhao S, Karnad A, et al. The biology and role of CD44 in cancer progression: therapeutic implications. J Hematol Oncol 2018;11:64.

157. Tarasov V, Jung P, Verdoodt B, et al. Differential regulation of microRNAs by p53 revealed by massively parallel sequencing: miR-34a is a p53 target that induces apoptosis and G1-arrest. Cell Cycle 2007;6:1586-93.

158. Beg MS, Brenner AJ, Sachdev J, et al. Phase I study of MRX34, a liposomal miR-34a mimic, administered twice weekly in patients with advanced solid tumors. Invest New Drugs 2017;35:180-188.

159. Siu L, Brody J, Gupta S, et al. Safety and clinical activity of intratumoral MEDI9197 alone and in combination with durvalumab and/or palliative radiation therapy in patients with advanced solid tumors. J Immunother Cancer 2020;8.

160. Tao L, Xu C, Shen W, et al. HIPK3 Inhibition by Exosomal hsa-miR-101-3p Is Related to Metabolic Reprogramming in Colorectal Cancer. Front Oncol 2021;11:758336.

161. Chang L, Yin L, Zhang D, et al. MicroRNA-221 promotes tumor progression by targeting HHIP in human glioblastoma. Transl Cancer Res 2021; 10: 1073-1081.

162. Zhao H, Yan P, Wang J et al. Clinical significance of tumor miR-21, miR-221, miR-143, and miR-106a as biomarkers in patients with osteosarcoma. Int J Biol Markers 2019; 2, 184-193.

163. Iida M, Hazama S, Tsunedomi R, et al. Overexpression of miR-221 and miR-222 in the cancer stroma is associated with malignant potential in colorectal cancer. Oncol Rep 2018; 40, 1621-1631.

164. Zhou J, Rossi J. Aptamers as targeted therapeutics: current potential and challenges. Nat Rev Drug Discov 2017;16:181-202.

165. Tuerk C, Gold L. Systematic evolution of ligands by exponential enrichment: RNA ligands to bacteriophage T4 DNA polymerase. Science 1990;249:505-10.

166. Li-Ping Z, Ge Y, Xiao-Min Z, et al. Development of Aptamer Screening against Proteins and Its Applications Chinese J. Anal. Chem 2020;48:560-572.

167. Ricci F, Bandello F, Navarra P, et al. Neovascular Age-Related Macular Degeneration: Therapeutic Management and New-Upcoming Approaches. Int J Mol Sci 2020;21.

168. Jager RD, Mieler WF, Miller JW. Age-related macular degeneration. N Engl J Med 2008;358:2606-17.

169. Gragoudas ES, Adamis AP, Cunningham ET, Jr., et al. Pegaptanib for neovascular age-related macular degeneration. N Engl J Med 2004;351:2805-16.

170. Richardson PG, Smith AR, Triplett BM, et al. Defibrotide for Patients with Hepatic Veno-Occlusive Disease/Sinusoidal Obstruction Syndrome: Interim Results from a Treatment IND Study. Biol Blood Marrow Transplant 2017;23:997-1004.

171. Kernan NA, Grupp S, Smith AR, et al. Final results from a defibrotide treatment-IND study for patients with hepatic veno-occlusive disease/sinusoidal obstruction syndrome. Br J Haematol 2018;181:816-827.

172. Richardson PG, Riches ML, Kernan NA, et al. Phase 3 trial of defibrotide for the treatment of severe veno-occlusive disease and multi-organ failure. Blood 2016;127:1656-65.

173. Steurer M, Montillo M, Scarfo L, et al. Olaptesed pegol (NOX-A12) with bendamustine and rituximab: a phase IIa study in patients with relapsed/refractory chronic lymphocytic leukemia. Haematologica 2019;104:2053-2060.

174. Park EJ, Choi J, Lee KC, et al. Emerging PEGylated non-biologic drugs. Expert Opin Emerg Drugs 2019;24:107-119.

175. Suarez-Carmona M, Williams A, Schreiber J, et al. Combined inhibition of CXCL12 and PD-1 in MSS colorectal and pancreatic cancer: modulation of the microenvironment and clinical effects. J Immunother Cancer 2021;9.

176. Zboralski D, Hoehlig K, Eulberg D, et al. Increasing Tumor-Infiltrating T Cells through Inhibition of CXCL12 with NOX-A12 Synergizes with PD-1 Blockade. Cancer Immunol Res 2017;5:950-956.

177. Menne J, Eulberg D, Beyer D, et al. C-C motif-ligand 2 inhibition with emapticap pegol (NOX-E36) in type 2 diabetic patients with albuminuria. Nephrol Dial Transplant 2017;32:307-315.

178. Oberthur D, Achenbach J, Gabdulkhakov A, et al. Crystal structure of a mirror-image L-RNA aptamer (Spiegelmer) in complex with the natural L-protein target CCL2. Nat Commun 2015;6:6923.

179. Mongelard F, Bouvet P. AS-1411, a guanosine-rich oligonucleotide aptamer targeting nucleolin for the potential treatment of cancer, including acute myeloid leukemia. Curr Opin Mol Ther 2010;12:107-14.

180. Vitravene Study G. A randomized controlled clinical trial of intravitreous fomivirsen for treatment of newly diagnosed peripheral cytomegalovirus retinitis in patients with AIDS. Am J Ophthalmol 2002;133:467-74.

181. Wagner KR, Kuntz NL, Koenig E, et al. Safety, tolerability, and pharmacokinetics of casimersen in patients with Duchenne muscular dystrophy amenable to exon 45 skipping: A randomized, double-blind, placebo-controlled, dose-titration trial. Muscle Nerve 2021;64:285-292.

182. Clemens PR, Rao VK, Connolly AM, et al. Safety, Tolerability, and Efficacy of Viltolarsen in Boys With Duchenne Muscular Dystrophy Amenable to Exon 53 Skipping: A Phase 2 Randomized Clinical Trial. JAMA Neurol 2020;77:982-991.

183. Lee TB, Yang K, Ko HJ, et al. Successful defibrotide treatment of a patient with veno-occlusive disease after living-donor liver transplantation: A case report. Medicine (Baltimore) 2021;100:e26463.

184. Steegmaier M, Hoffmann M, Baum A, et al. BI 2536, a potent and selective inhibitor of polo-like kinase 1, inhibits tumor growth in vivo. Curr Biol 2007;17:316-22.

185. Cho H, Kaelin WG. Targeting HIF2 in Clear Cell Renal Cell Carcinoma. Cold Spring Harb Symp Quant Biol 2016;81:113-121.

186. Taubel J, Hauke W, Rump S, et al. Novel antisense therapy targeting microRNA-132 in patients with heart failure: results of a first-in-human Phase 1b randomized, double-blind, placebo-controlled study. Eur Heart J 2021;42:178-188.

187. Cushing L, Kuang PP, Qian J, et al. miR-29 is a major regulator of genes associated with pulmonary fibrosis. Am J Respir Cell Mol Biol 2011;45:287-94.

Table 1. FDA-approved RNA therapeutics in clinical care.

Product	Route of delivery	Target	Mechanism of action	Disease/clinical outcome	Company	Approval status	References
ASO							
Fomivirsen	IVT	CMV mRNA	Downregulates IE2	Cytomegalovirus (CMV) retinitis	Ionis Pharmaceutical, Novartis	FDA (1998)	[180]
Mipomersen	SC	apo-B-100 mRNA	Downregulates ApoB	Homozygous familial hypercholesterolemia	Kastle Therapeutics, Ionis Pharmaceuticals, Genzyme	FDA (2013)	[50]
Nusinersen	ITH	SMN2 pre-mRNA	Splicing modulation	Spinal muscular atrophy	Ionis Pharmaceuticals, Biogen	FDA (2016)	[64]
Eteplirsen	IV	Exon 51 of DMD	Splicing modulation	Duchenne muscular dystrophy	Sarepta Therapeutics	FDA (2016)	[67]
Inotersen	SC	TTR mRNA	Downregulates transthyretin mRNA	Familial amyloid polyneuropathy	Ionis Pharmaceuticals	FDA (2018)	[71]

Golodirsen	IV	Exon 53 of DMD	Splicing modulation	Duchenne muscular dystrophy	Sarepta Therapeutics	FDA (2019)	[73]
Milasen	Intrathecal	CLN7	Splicing modulation	Mila Makovec's *CLN7* gene associated with Batten disease	Boston Children's Hospital	FDA (2018)	[75]
Casimersen	IV	Exon 45 of DMD	Splicing modulation	Duchenne muscular dystrophy	Sarepta Therapeutics	FDA (2021)	[76,181,182]
siRNA							
Patisiran	IV	TTR mRNA	Downregulation of transthyretin	Polyneuropathy caused by hATTR amyloidosis	Alnylam	FDA (2018)	[93]
Givosiran	SC	ALS1 mRNA	Downregulation of ALAS1	Acute hepatic porphyria	Alnylam	FDA (2020)	[97]
Lumasiran	SC	HAO1 mRNA	Downregulation of glycolate oxidase	Primary hyperoxaluria type 1	Alnylam	FDA (2020)	[99]

Inclisiran	SC	PCSK9	Downregulation of proprotein convertase subtilsin/kexin type 9	Atherosclerotic cardiovascular disease	Novartis	FDA (2021)	[100]
Aptamer							
Pegaptanib	Intravitreal	Heparin-binding domain of VEGF-165	Blocking VEGF-165	Neovascular age-related macular degeneration	OSI Pharmaceuticals	FDA (2004)	[169]
Defibrotide	IV	Adenosine A1/A2 receptor	Activating Adenosine A1/A2 receptor	Veno-occlusive disease in liver	Jazz Pharmaceuticals	FDA (2020)	[170] [183]
mRNA							
BNT162b2	IM	Immunogenicity and antibody response to SARS-CoV-2 S antigens	SARS-CoV-2 S antigens' expression	COVID-19	BioNTech and Pfizer	FDA (2020)	[21]
mRNA-1273	IM	Immunogenicity and antibody response	SARS-CoV-2 S antigens' expression	COVID-19	Moderna	FDA (2020)	[22]

		to SARS-CoV-2 S antigens					

Table 2. RNA therapeutics in clinical development.

Oligonucleotide Therapeutics	Route of delivery	Target	Mechanism of action	Disease/ clinical outcome	Company	Clinical trial status	References
ASO							
1018 ISS	IV	TLR9	Enhancement of cytotoxic effector mechanisms	Non-Hodgkin's Lymphoma	Dana-Farber Cancer Institute, Brigham and Women's Hospital, Massachusetts General Hospital, University of Rochester	NCT00251394 (Phase II)	[77,81]
Apatorsen (OGX-427)	IV	HSP27	Inhibits expression of heat shock protein (Hsp27)	Urologic Cancer, Bladder Cancer, Prostate Cancer,	Achieve Life Sciences PRA Health Sciences	NCT00487786, NCT01454089 (Phase I/II)	[82]

				Urothelial Cancer, Non-Small Cell Lung Cancer			
Cenersen (EL625)	IV	TP53	Blocks the effects of p53	Acute Myelogenous Leukemia, Lymphoma	Eleos, Inc.	NCT00074737 (Phase II)	[83]
ARRx (AZD5312)	IV	AR	Suppression of human AR expression	Prostate Cancer	AstraZeneca	NCT02144051, (Phase I/II)	[84]
Custirsen (OGX-011)	IV	ApoJ	Inhibiton of clusterin expression	Prostate Cancer, Breast Cancer, Non-Small Cell Lung Cancer	NCIC Clinical Trials Group, Achieve Life Sciences	NCT00054106, NCT00138658, (Phase I/II)	[86,87]
siRNA							

TKM-080301	Intra-arterial/IV	PLK1	Inhibition of PLK1 activity	Cancer with hepatic metastases, Hepatocellular Cancer	National Cancer Institute, Arbutus Biopharma Corporation	NCT01437007, NCT02191878, (Phase I/II)	[101,184]
Atu027	IV	PNK3	Silences expression of PNK3	Solid Tumors, Pancreatic Cancer	Silence Therapeutics GmbH, Granzer Regulatory Consulting & Services	NCT00938574, NCT01808638 (Phase I/II)	[103,104]
siG12D LODER	Locally implanted through EUS biopsy procedure	KRASG12D	Inhibits KRAS expression	Pancreatic Cancer	Silenseed Ltd	NCT01676259, NCT01188785 (PhaseI/II)	[105,106]
ARO-HIF2	IV	HIF2A	Deregulation of HIF2A	Clear Cell Renal Cell	Arrowhead Pharmaceuticals	NCT04169711 (Phase I)	[185]

				Carcinoma			
APN401	IV	CBLB	Inhibition of Cbl-b enhances natural killer cell and T cell mediated antitumor activity	Brain Cancer, Melanoma, Pancreatic Cancer, Renal Cell Cancer	Wake Forest University Health Sciences, National Cancer Institute	NCT03087591, NCT02166255 (Phase I)	[110]
Vutrisiran	SQ	TTR	Reduces TTR protein expression	Transthyretin mediated amyloidosis with or without cardiomyopathy	Alnylam Pharmaceuticals	NCT03759379 NCT04153149 (Phase 3)	[113,114]
Aptamer							
NOX-A12	IV	CXCL12	Disrupts CXCR4-CXCL12 interactions	Pancreatic Cancer, Colorectal Cancer, Multiple myeloma	NOXXON Pharma AG, Merck Sharp & Dohme Corp.	NCT01521533, NCT01521533, NCT03168139 (Phase I/II)	[174]

NOX-E36	IV/SQ	CCL2	Specifically binds and inhibits the pro-inflammatory chemokine CCL2	Diabetic nephropathy	NOXXON Pharma AG	Phase I	[177]
mRNA							
CVnCoV	IM	Immunogenicity and antibody response to SARS-CoV-2 S antigens	SARS-CoV-2 S antigens' expression	COVID-19	CureVac AG	NCT04652102 (Phase III)	[23]
AZD8601	Epicardial	VEGF-A	Restores VEGF-A expression	Ischemic heart disease	Astrazeneca	NCT03370887 (Phase II)	[31]
MRT5005	Inhalation	CFTR	Restores CFTR expression	Cystic Fibrosis	Translate Bio	NCT03375047 (Phase I/II)	[35]

mRNA-3704	IV	MUT	Restores MUT expression	Methylmalonic aciduria	Moderna	NCT03810690 (Phase I/II)	[37,38]
BNT111	IV	Targets four non-mutated, TAAs (NY-ESO-1, MAGE A3, tyrosinase and TPTE	Induction of immune response against the four selected malignant melanoma-associated antigens [New York-ESO 1 (NY-ESO-1), tyrosinase, Melanoma-associated antigen A3 (MAGE-A3), and Trans-membrane phosphatase with tensin homology (TPTE)]	Advanced Melanoma	BioNTech SE	NCT02410733 (Phase I)	[40]
miRNA							

Miravirsen	SC	miR-122	miRNA-inhibitor	HCV	Roche/Santaris	NCT01200420 (Phase II)	[120]
RG-012 (lademirsen)	SC	miR-21	miRNA-inhibitor	Alport Syndrome	Sanofi	NCT03373786 (Phase II)	[123]
Cobomarsen	IV/SQ	miR-155	miRNA-inhibitor	Cutaneous T-Cell Lymphoma/Mycosis Fungoides	miRagen	NCT03713320, NCT02580552 (Phase II)	[127]
MRG-110	Intradermal	miR-92a	miRNA-inhibitor	Wound healing	miRagen	NCT03603431 (Phase I)	[129]
AZD4076	SC	miR-103/107	miRNA-inhibitor	T2D with NAFLD	AstraZeneca	NCT02826525 (Phase I/IIa)	[132]
RGLS4326	SC	miR-17	miRNA-inhibitor	Autosomal dominant polycystic kidney disease	Regulus Therapeutics Inc.	NCT04536688 (Phase I)	[134]
CDR132L	IV	miR-132	miRNA-inhibitor	Heart Failure	Cardior Pharmaceu	NCT04045405 (Phase I)	[186]

					ticals GmbH		
TargomiRs	IV	miR-16	miRNA-mimic	Malignant Pleural Mesothelioma	EnGeneIC Limited	NCT02369198 (Phase I)	[143]
Remlarsen	Intradermal	miR-29	miRNA-mimic	Keloids, scleroderma	miRagen	NCT03601052 (Phase II)	[187]
MRX34	IV	miR-34a	miRNA-mimic	Melanoma	miRNA Therapeutics, Inc.	NCT01829971 (Phase I)	[158]

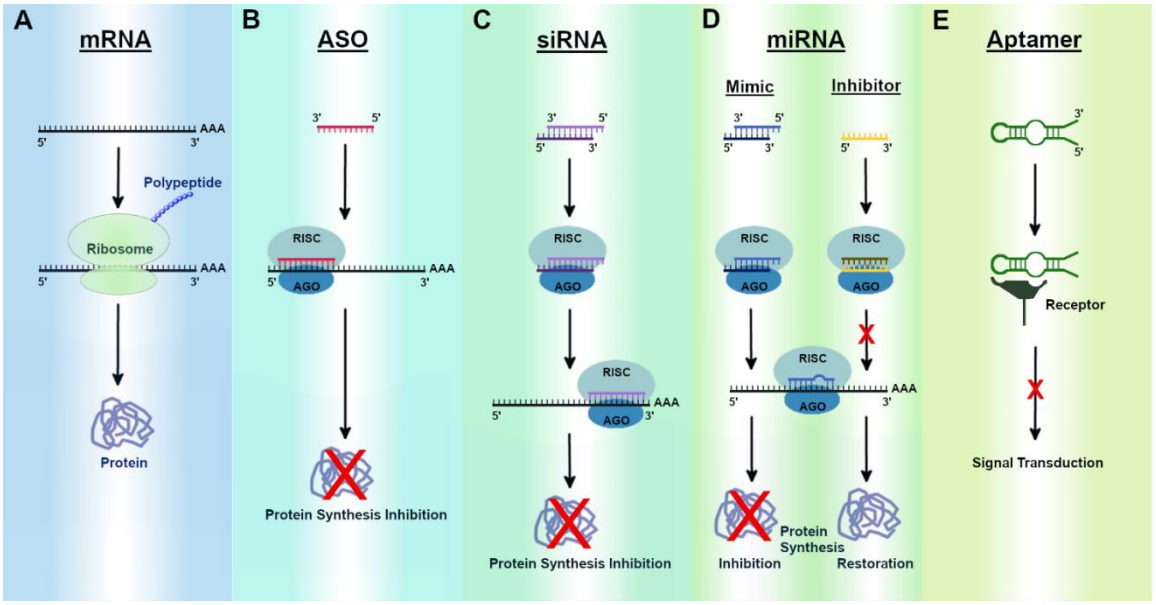

Figure 1. Schematic of RNA therapeutic approaches. A) Ribosomes translate mature mRNAs into proteins, the building blocks for life. B) ASOs are small single-stranded RNA molecules that have exact complementarity to a target mRNA. Once bound they induce gene silencing by preventing translation of the mRNA. C) siRNAs are small double-stranded RNA molecules that have exact complementarity to a target mRNA. Once associated with the RISC complex it binds to its target mRNA and induces gene silencing by preventing translation of the mRNA. D) miRNA mimics are small double-stranded RNA molecules that associate with and guide the RISC complex to its target mRNA. The mimic will bind with imperfect complementarity to its target mRNA and translation will be blocked or the mRNA will be degraded leading to gene silencing. miRNA inhibitors are small single-stranded RNAs that bind to and suppress their target miRNA. This results in restored mRNA translation. E) Aptamers are RNA, DNA, or RNA/DNA hybrids that form tertiary structures and bind to a target molecule either suppressing or enhancing the pathway that the target molecule is involved in.

CHAPTER THREE: MiR-10b-5p Rescues Diabetes and Gastrointestinal Dysmotility

Introduction

Over 451 million people had diabetes worldwide in 2017.[1] Type 1 diabetes (T1D) develops due to a lack of insulin production by pancreatic β cells, whereas type 2 diabetes (T2D) which accounts for over 95% cases, attributes to increased insulin resistance in the body's cells.[2] T1D and T2D culminate in the degeneration of β cells, requiring insulin therapy.[3] Pathophysiological mechanisms underlying diabetes remain elusive, making it difficult to produce effective treatments that ameliorate the symptoms of diabetes.[4] Moreover, effective treatments for diabetes have been developed; however, many of them are inadequate for prolonged use due to poor tolerance and negative ramifications.[5]

Approximately half of patients with diabetes have gastrointestinal (GI) motility disorders, such as gastroparesis and constipation.6 GI motility disorders are conditions in which GI muscular movements become abnormal, leading to delayed gastric emptying and slowed colonic transit.[7] GI motility patterns are initiated by the pacemaker activity of interstitial cells of Cajal (ICCs) and neural inputs from enteric motor neurons which are transduced, in part, by ICCs.[8] Hyperglycemia in patients with diabetes leads to the reconfiguration of the mechanisms controlling GI motility,[7] often leading to the dysfunction of ICCs in the stomach and intestines of diabetic animals and humans.[9, 10] ICCs express the receptor tyrosine kinase (KIT), essential for their development and functioning[11] where a loss of KIT leads to non-functional ICCs in diabetic mice, with similar patterns being found in patients with diabetes.[9] However, the underlying mechanisms behind KIT loss in ICCs of patients with diabetes is largely undetermined which prompted us to explore the molecular mechanisms underpinning diabetic GI motility disorders.

microRNAs (miRNAs) are small non-coding regulatory RNAs that mediate post-transcriptional gene repression by inhibiting translation and are master regulators of cell differentiation, proliferation, and apoptosis.[12] Dysregulated miRNAs lead to cellular dysfunction and diseases such as diabetes and GI dysmotility.[13, 14] For example, miR-10b-5p expression is reduced

in diabetic patients and animals.[12, 13] Therefore, it is imperative to track the mechanistic pathway at the cellular level to elucidate how miRNAs modulate diabetes and GI motility disorders.

Dysregulation of miR-10b-5p in pancreatic β cells and ICCs might be a potential pathogenic factor leading to the dysfunction of these cells through specific gene target regulation. Krüppel-like factors (KLF) are a family of transcription factors acting as either transcriptional activators or repressors, regulating cellular metabolism.[15] Most KLF isoforms are associated with the regulation of metabolic pathways and energetic homeostasis.[15] KLF11, specifically, regulates insulin production and sensitivity, lipid metabolism, and obesity.[16] Based on these clinical and molecular observations we hypothesized a novel molecular mechanism regulating glucose homeostasis and GI motility through miR-10b-5p mediated KLF11 repression.

In the present study, we found that miR-10b-5p is highly expressed in ICCs from healthy mice and selectively depleted in ICCs from diabetic mice. Using both loss- and gain-of-function studies in mice, we demonstrate that miR-10b-5p regulates both glucose homeostasis and GI motility through the miR-10b-5p-KLF11-KIT pathway. The loss of miR-10b-5p in KIT+-ICCs and β cells causes GI dysmotility and diabetes in mice, while restoring miR-10b-5p expression rescues these conditions. Notably, we found the murine miR-10b-5p-KLF11-mediated KIT regulation data to be consistent with the findings in patients with diabetic and idiopathic gastroparesis. Additionally, we demonstrated that the miR-10b-5p mimic is more efficacious in improving diabetic symptoms and GI functions in diabetic mice when compared to the widely used antidiabetic and prokinetic medications.

Materials and Methods

Mice:

All procedures that include animal subjects were approved by the Institutional Animal Care and Use Committee (IACUC) at University of Nevada, Reno (UNR).

Human Specimens:

Plasma samples and clinical data were obtained from Stanford University from patients with idiopathic or diabetic gastroparesis along with healthy controls. All human subjects provided informed consent, and all study procedures were approved by Stanford University and UNR Institutional Review Boards.

miRNA Sequencing:

Small RNA libraries were generated using an Illumina TruSeq Small RNA Preparation Kit (Illumina) following manufacturer's instructions. The cDNA libraries were sequenced following vendor's instructions.

In vivo Functional GI Motility Tests:

Gastric emptying test (GET), total GI transit time (TGITT) and colonic transit time (CTT) were performed on mice fasted overnight. GET was performed using the fluorescent imaging agent GastroSense750 on IVIS Lumina III system.[17] Fluorescence images were analyzed using Living Image software. Evans blue semiliquid solution was orally gavaged in mice to measure TGITT.[18] TGTT was assessed as the time taken from the gavage until the first observation of the blue fecal pellet. CTT was measured through the bead expulsion test.[18]

Construction of Luciferase Reporter and Klf11 Expression Plasmids:

For the generation of the luciferase reporter constructs, the miR-10b-hKLF11, miR-10b-mKlf11, miR-10b-mKlf11-mut, and scrambled complementary oligonucleotides were synthesized and cloned into the expression vector. All vectors were confirmed by sequencing at the Nevada Genomics Center.

Drug Comparison Study:

miR-10b-5p mimic (In vivo-jetPEI/miRNA complexes), Metformin, Sitagliptin, Liraglutide, Insulin, and Prucalopride were used for comparing the efficacy for the treatment of metabolic and GI motility conditions in HFHSD-fed C57 male mice.

Statistics:

The experimental data are shown as the mean ± SEM. Two-tailed unpaired Student's t-test, Mann-Whitney U test, area under the curve calculations, and one-way or two-way ANOVA were used for all mouse and human experiments using GraphPad Prism.

Results

miR-10b Is Suppressed in KIT+-ICCs in Male Diabetic and Obese Mice:

To identify abnormally expressed miRNAs in ICCs in diabetes, KitcopGFP/+;Lepob/ob (ob/ob) mice were generated.19 ob/ob males significantly gained more weight and had higher fasting blood glucose levels (>250 mg/dL) by 10-12 weeks than their wild type (WT) KitcopGFP/+;Lep+/+ (+/+) male counterparts (Figure 1A and B). KIT expression has been shown to be regulated by miRNAs,20 we obtained a miRNA expression profile from isolated colonic and jejunal copGFP+ ICCs (CICCs and JICCs) from diabetic ob/ob mice and healthy +/+ mice through miRNA-seq (Supplementary Table 1). miRNA expression patterns within ob/ob and +/+ CICCs and JICCs were quite different (Figure 1C). The most dynamically expressed miRNAs from both CICCs and JICCs of ob/ob, and +/+ mice were shown in Figure 1D. miR-10a-5p, miR-143-3p, and miR-10b-5p were the most highly expressed in +/+ ICCs and were substantially decreased in ob/ob ICCs. Among these three miRNAs, miR-10b-5p displayed the most substantial diabetes-dependent reduction in diabetic ob/ob ICCs (Figure 1E). Furthermore, we confirmed the diabetes-dependent reduction of miR-10b expression in gastric ICCs from +/+ and ob/ob mice by qPCR (Figure 1F). We reinforced previously reported findings that during hyperglycemia the numbers of copGFP+ ICCs in the small intestine and colon were reduced in ob/ob males,[19] by demonstrating reduced KIT expression in ob/ob males through Western blot (Figure 1G and H).

KIT+ Cell mir-10b Knockout (KO) in Male Mice Results in ICC loss:

To determine the functional role of mir-10b in ICCs, we generated tamoxifen-inducible KIT+ cell-specific KitCreERT2/+;mir-10blox/lox (mir-10b KO) mice (Supplementary Figure 1A). We

examined the number of ICCs in the jejunum and colon of mir-10b KO mice and found that ICCs (CD117+ CD45–) were decreased in the jejunum and colon of mir-10b KO mice (Supplementary Figure 1B). The reduction of mir-10b was confirmed through qPCR (Supplementary Figure 1C), which showed that miR-10b-5p expression was significantly decreased not only in the jejunum and colon, but also in the pancreas and blood of mir-10b KO mice. In the jejunum and colon of mir-10b KO mice, KIT protein expression was also decreased (Supplementary Figure 1D and E). Another gene that is potentially regulated by miR-10b-5p is Klf11, the evolutionarily conserved metabolic regulator,[21] as it is predicted to have a miR-10b-5p target site in its 3' UTR.22 KLF11 expression was increased in mir-10b KO tissues (Supplementary Figure 1D and E), suggesting that miR-10b-5p may target KLF11. mir-10b is encoded within the intronic region of two overlapping genes, Hoxd3 and Hoxd4 (Supplementary Figure 1A). We confirmed that the deletion of mir-10b did not disrupt the expression of these two genes in mir-10b KO mice (Supplementary Figure 1D and E). Additionally, immunohistochemistry showed that the density of ICCs in the deep muscular plexus of the jejunum and along the submucosal surface of the circular muscle layer in the colon was reduced in mir-10b KO tissues (Supplementary Figure 1F). Taken together, these results demonstrate that a deficiency of miR-10b-5p in KIT+-ICCs leads to degeneration of jejunal and colonic ICCs. In addition to KIT+-ICCs in the GI tract, miR-10b-5p may also regulate the development of KIT+-β cells in the pancreas linking miR-10b-5p to the diabetic phenotype.

mir-10b KO Male Mice Develop Diabetes and GI Dysmotility:

Further, we investigated whether mir-10b loss leads to the development of diabetes and GI dysmotility. We found male mir-10b KO mice became moderately obese and developed characteristic manifestations of diabetes such as hyperglycemia (blood glucose >200 mg/dL), after 24 weeks post-tamoxifen injection (PTI) (Figure 2A-C), while female mir-10b KO mice did not (Supplementary Figure 2A-D). Male mir-10b KO mice developed an impaired glucose tolerance after 7 months PTI, while WT mice cleared the glucose efficiently (Figure 2D and E). mir-10b KO mice showed reduced fasting blood insulin levels as compared to WT mice (Figure 2F).

Furthermore, mir-10b KO mice developed insulin resistance after 7 months PTI as compared to WT mice (Figure 2G and H).

Unlike the male dominant diabetic phenotype, both mir-10b KO males and females developed gastroparesis and constipation. The mir-10b KO males and females showed prolonged total GI transit time (TGITT) starting 1-month PTI which was progressively delayed over a 7-month period. (Figure 2I; Supplementary Figure 2E). Gastric emptying was also delayed in mir-10b KO males and females at 3, 6, and 7 months PTI compared to WT mice (Figure 2J and K; Supplementary Figure 2F and G). Additionally, colonic transit time (CTT), fecal pellet frequency and fecal pellet output in mir-10b KO males and females was significantly delayed and reduced, respectively, compared to WT mice (Figure 2L-N; Supplementary Figure 2H). These data suggest that KIT+ cell-specific mir-10b KO male mice developed diabetes and GI dysmotility, while the mir-10b KO females only developed GI dysmotility.

Depletion of KIT+ Cells in Male Mice Results in the Development of Diabetes and GI Dysmotility:

To study the role of KIT+-cells in the pancreas, we generated tamoxifen-induced KIT+-cell depleted mice, KitCreERT2/+;Rosa26DTA/+ (Kit-DTA) and fluorescent protein-labeled, KitCreERT2/+;Rosa26tdTom/+ (Kit-tdTom) mice. KIT+-cell depleted male mice gained weight and developed characteristic manifestations of diabetes (Supplementary Figure 3A and B). Glucose tolerance tests (GTT) and insulin tolerance tests (ITT) in Kit-DTA mice were impaired at 2 and 5 months PTI (Supplementary Figure 3C and D). miR-10b was reduced in the blood of Kit-DTA mice at 7 days and 5 months PTI (Supplementary Figure 3E). Consistent with miR-10b reduction, insulin and C-peptide levels were reduced in Kit-DTA mice at 7 days and 5 months PTI (Supplementary Figure 3F). Next, we investigated the distribution of KIT+-cells in the pancreas of Kit-tdTom mice. Kit-tdTom mice showed an abundance of tdTom+-cells in the pancreas at 7 days PTI (Supplementary Figure 3G). tdTom+-cells were co-labelled with the primary antibody of insulin in islets at 7 days PTI, but few appeared to be tdTom+ 5 months PTI. This implies that β cells may derive from KIT+-cells and most of the ones that originate from the KIT+ pancreatic β cell

progenitors[23] were lost and replaced with new mature β cells 5 months PTI. Also, β cells (Insulin+-cells) were substantially depleted in Kit-DTA mice as compared to Kit-tdTom mice. (Supplementary Figure 3G and H). KLF11 levels were increased in the pancreas, colon, and blood of Kit-DTA mice at 7 days and 5 months PTI, while KIT expression was reduced (Supplementary Figure 3I and J).

Further, Kit-DTA mice displayed delayed TGITT at 2 and 5 months PTI (Supplementary Figure 3K). Collectively, these data show that there are KIT+-cells located in pancreatic islets and loss of these cells results in depletion of β cells, leading to diabetes. Reduction of miR-10b-5p and KIT with subsequent elevation of KLF11 in Kit-DTA mice are consistent with results found in mir-10b KO mice. Thus, using mir-10b KO and Kit-DTA mouse models we demonstrated miR-10b-5p likely regulates KIT+-ICCs in the GI tract and KIT+-β cells in the pancreas and miR-10b-5p deficiency results in the development of diabetes and GI dysmotility.

MiR-10b-5p Mimic Injection Rescues Diabetes and GI Dysmotility in mir-10b KO Male Mice:

The synthesized miR-10b-5p duplex (miR-10b-5p mimic) was tested in vivo in mir-10b KO mice with diabetes and GI dysmotility. Diabetic mir-10b KO mice gradually lost weight over the first 4 weeks post-injection (PI) with the miR-10b-5p mimic, while the scramble RNA negative control and non-injected mice did not lose weight (Figure 3A). The reduced body weight was maintained in miR-10b-5p mimic-injected mice for 10 weeks PI. More importantly, miR-10b-5p mimic-injected mice dramatically lowered fasting glucose levels to normal (about 100 mg/dL) at 1 week PI and maintained the healthy levels for 8 weeks (Figure 3B). We compared fasting and glucose stimulated insulin levels between mir-10b KO mice injected with the miR-10b-5p mimic 1 week PI, no injection, and scramble injection (Figure 3C). Fasting insulin levels were restored in miR10b KO mice 1 week PI with the miR-10b-5p mimic as compared to mir-10b KO mice with no injection or scramble injection. Furthermore, the pattern of glucose stimulated insulin levels in the mir-10b KO mice injected with the miR-10b-5p mimic was similar to that in WT mice (Figure 3C). Glucose and insulin tolerance were significantly improved in the miR-10b-5p mimic-injected mice (Figure 3D-G). Furthermore, GI motility was gradually improved to normal levels in the miR-10b-5p mimic-injected

mice at 2 and/or 4 weeks PI (Figure 3H-J). We confirmed that miR-10b-5p was increased in the blood, pancreas, jejunum and colon 1 week PI of the miR-10b-5p mimic (Figure 3K). KIT and KLF11 protein expression were dysregulated in the pancreas and colon of mir-10b KO mice, but their protein levels were partially restored after 1 week in the miR-10b-5p mimic-injected mice (Figure 3L and M). ICCs were degenerated in the mir-10b KO diabetic mice but readily detected after 1 week in the jejunum and colon of mice injected with the miR-10b-5p mimic (Figure 3N). These data demonstrate that the miR-10b-5p mimic injection reversed diabetic symptoms and GI dysmotility in mir-10b KO male mice.

MiR-10b-5p Mimic Rescues Diabetes and GI Dysmotility in Multiple Diabetic Mouse Models:

We next evaluated metabolic and/or GI motility parameters to test the effect of the miR-10b-5p mimic on several diabetic mouse models [(High-fat, high-sucrose diet (HFHSD)-induced C57 male, HFHSD-fed ovariectomized (OVX) C57 female, ob/ob and TALLYHO male mice]. HFHSD-fed mice became obese and hyperglycemic compared to normal diet (ND)-fed mice (Figure 4A and B). The HFHSD-fed mice significantly lost weight and displayed a marked reduction in fasting blood glucose levels PI of the miR-10b-5p mimic compared to ND-fed mice (Figure 4A and B). The first miR-10b-5p mimic injection lowered blood glucose to normal levels, which returned to pre-diabetic levels 5 weeks PI. A second miR-10b-5p mimic injection lowered glucose to normal levels for an additional 6 weeks. In addition, TGITT and fecal output were restored in HFHSD-fed mice injected with miR-10b-5p mimic 4 weeks post-second injection (Figure 4C and D). miR-10b-5p expression was substantially reduced in the blood of diabetic HFHSD-fed mice (Figure 4E). miR-10b-5p levels were restored to approximately 60% of the healthy level following miR-10b-5p mimic injection at 1 week PI and gradually decreased (Figure 4E). Insulin levels were restored 1 week PI with miR-10b-5p mimic, following a similar pattern to the level of miR-10b-5p in the blood from HFHSD-fed mice (Figure 4F). Hemoglobin A1C (A1C) levels in HFHSD-fed mice were also improved by miR-10b-5p mimic (Figure 4G). KLF11 levels were increased in the blood, pancreas, stomach, colon, and skeletal muscle of HFHSD-fed mice (Figure 4H and I). miR-10b-5p mimic treatment reduced KLF11 expression and, in turn, increased KIT expression in the tissues of

HFHSD-fed mice 3 weeks PI (Figure 4H and I). KIT+-ICCs were degenerated in HFHSD-fed mice, but KIT expression was restored in the stomach, jejunum, and colon 1 week PI with miR-10b-5p mimic (Figure 4J). Pancreatic islets were also reduced in size in HFHSD-fed mice; however, some islets were restored 1 week PI with miR-10b-5p mimic in HFHSD-fed mice (Figure 4K). These data demonstrate that miR-10b-5p mimic injection likely restores proper functioning of ICCs and β cells by increasing the expression of KIT and insulin in HFHSD-fed male mice, which leads to the reversal of GI dysmotility and diabetes.

Estrogen delays the onset of diabetes in female mice.[24] Therefore, we evaluated the effect of the miR-10b-5p mimic on HFHSD-fed OVX female diabetic mice, as the mir-10b KO mice in this study as well as mice from other murine studies demonstrated HFD-fed female mice do not develop hyperglycemia.[24, 25] OVX C57 female HFHSD-fed mice substantially lost estrogen, gained weight, and became hyperglycemic (Supplementary Figure 4). Injection with the miR-10b-5p mimic in OVX HFHSD-fed females reversed the diabetic phenotype, while maintaining the body weight (Supplementary Figure 4E-F).

Further, we tested the efficacy of the miR-10b mimic in rescuing the diabetic and GI dysmotility phenotypes in diabetic ob/ob and polygenic TALLYHO T2D male mice. Both ob/ob- and TALLYHO male mice injected with the miR-10b mimic were able to significantly lower blood glucose and improve TGITT (Supplementary Figure 5 and 6).

MiR-10b-5p Regulates Expression of KIT via KLF11:

To identify the underlying molecular mechanisms in miR-10b-5p-KLF11-KIT pathway, we searched for miR-10b-5p target genes associated with diabetes utilizing Ingenuity Pathway Analysis (IPA). IPA identified 44 miR-10b-5p targets directly linked to diabetes (Figure 5A). As KLF11 directly interacts with the insulin (INS) gene by inhibiting its promoter activity in β cells,[26] we next examined the targeting effect of miR-10b-5p on KLF11 in the human (Panc.10.05) and mouse (NIT-1) pancreatic β cell lines. We tested the miR-10b-5p mimic and its antisense RNA (miR-10b-

5p inhibitor) in these two β cell lines (Figure 5B). Western blots depicted that miR-10b-5p mimic transfection decreased KLF11 levels, while the miR-10b-5p inhibitor increased KLF11 levels in these cell lines (Figure 5C and D). KIT and INS expression was inversely regulated by the miR-10b-5p mimic and inhibitor. Expression of these two proteins was also augmented by transfection with the KLF11 siRNAs (siKLF11-1 and siKLF11-2), substantiating miR-10b-5p regulates expression of KIT and INS via KLF11 (Figure 5C and D). The miR-10b-5p targeting effect on KLF11 was further validated in β cell lines, transfected with plasmids containing the luciferase gene with the 3' UTR of KLF11 (human and mouse) miR-10b target site (TS), a target site mutation (TSM) or a scramble sequence (Figure 5E). Each cell line was transfected with mKlf11 miR-10b TS and TSM or hKLF11 miR-10b TS plasmids and then subsequently treated with different concentrations of miR-10b mimic or inhibitor. All treatments showed a respective dose-dependent reduction or induction of luciferase activity (Figure 5F). The expression of miR-10b-5p was reduced by the high glucose level (Figure 5G), which also affected KLF11 and KIT protein expression in NIT-1 cells (Figure 5H and I). A similar targeting effect on luciferase activity by high glucose levels was observed in both mouse and human β cell lines (Figure 5J). These data imply that miR-10b-5p targets and inhibits the expression of KLF11, which subsequently suppresses the expression of KIT and INS in β cells. Next, we examined whether the Klf11 siRNAs could rescue diabetes and slowed GI transit in HFHSD-fed male mice. Diabetic, obese, and GI dysmotility phenotypes were substantially rescued by Klf11 siRNA. (Supplementary Figure 7). Taken together, miR-10b-5p mimic can reverse diabetic, obese, and GI dysmotility phenotypes via the suppression of Klf11.

Patients with Diabetic and Idiopathic Gastroparesis Have Reduced miR-10b-5p Expression:

We examined plasma samples from patients with diabetic gastroparesis (DG) and idiopathic gastroparesis (IG) (Supplementary Table 2) to see whether the abnormal expression patterns of miR-10b-5p, KLF11, and KIT were similar to what we observed in our animal models. miR-10b-5p expression was high in the healthy control (HC) samples and reduced in IG and DG samples (Figure 6A). Based on the miR-10b-5p expression levels, we found two groups of IG: intermediate-high expression (IG-H) and intermediate-low expression (IG-L). miR-10b-5p

expression was low in DG samples. Consistent with our murine data, insulin, C-peptide, A1C levels and expression profiles of miR-10b-5p, KLF-11, and KIT were similar in the patient samples (Figure 6B-E). The IG-L group had significantly lower levels of miR-10b-5p, insulin and C-peptide compared to those of the HC group but had higher expression levels than the DG group, suggesting the IG-L group is at a prediabetic stage. Deep sequencing of miRNAs from the blood samples of HC, IG-H, IG-L, and DG identified differentially expressed miRNAs (Supplementary Table 3). The expression patterns of all of the 345 identified miRNAs and the top 70 most dynamically regulated miRNAs show similarity between HC and IG-H and between IG-L and DG (Figure 6F and G). miR-10b-5p levels were highest in HC, followed by IG-H, IG-L, & DG, respectively (Figure 6G). In addition, expression levels of miR-10b-5p were negatively correlated with gastric emptying scintigraphy percentage at 2 hours in gastroparesis as well as with A1C levels in diabetes (Figure 6H). Taken together, metabolic and gene expression profiles from HC, IG, and DG patient samples were analogous to our mouse data.

Efficacy Comparison of the miR-10b-5p Mimic with Antidiabetic and Prokinetic Drugs:

We next compared the effects of miR-10b-5p mimic on diabetes and GI dysmotility in HFHSD-fed C57 mice with antidiabetic medications (liraglutide, sitagliptin, metformin, and insulin) and a prokinetic medication, prucalopride (Figure 7A). miR-10b-5p mimic injections (2 doses of IP) into HFHSD-induced diabetic mice reduced body weight and rescued the hyperglycemic condition. Antidiabetic medications and prucalopride lowered blood glucose, but the efficacy and duration were lower and shorter than that of miR-10b-5p mimic (Figure 7B and C). Glucose and insulin tolerance were improved in miR-10b-5p mimic-injected mice for up to 8 weeks with two injections, while the medications only maintained improvement for 4 weeks after treatment (Figure 7D and E). Fasting insulin and C-peptide levels in mice treated with the medications and miR-10b-5p mimic were increased at 4 weeks (Supplementary Figure 8A and B). Glucose stimulated insulin secretion was significantly impaired in HFHSD-mice but was restored and maintained in mice injected with the miR-10b-5p mimic for 8 weeks (Figure 7F). In addition, GI motility was restored in miR-10b-5p mimic-injected mice for 8 weeks PI, while prucalopride improved GI motility for only 4 weeks.

(Figure 7G-I; Supplementary Figure 8C). Next, we examined other metabolic parameters (food, calorie, and water intake, urine and fecal output) and found that the mir-10b-5p mimic-injected mice have better control of symptoms such as polyphagia, polydipsia, and polyuria (Supplementary Figure 9). Taken together, these murine metabolic and GI motility data confirm the profound and prolonged efficacy of miR-10b mimic as compared to antidiabetic and prokinetic medications.

miR-10b-5p is almost identical to miR-10a-5p and only differ by one nucleotide in the middle of their sequence. Additionally, both of these miRNAs are predicted to target KLF11. miR-10a-5p is also highly expressed in ICCs from healthy mice and drastically reduced in ICCs from diabetic mice (Figure 1D and E). To interrogate the linkage mechanism leading to the three major phenotypes (GI dysmotility, diabetes and obesity), we further compared the efficacy of miR-10a-5p mimic and miR-10b-5p mimic in rescuing the diabetic and GI dysmotility phenotypes in HFHSD-fed C57 male mice. Both miR-10a-5p and miR-10b-5p had similar beneficial effects on the three associated phenotypes (Supplementary Figure 10A-J), but body weight was further reduced by miR-10a-5p (Supplementary Figure 10B). The substantial body weight loss (3.0 g) was due to a reduction of gonadal and inguinal adipose tissue (1.24 g) in the miR-10a injected mice (Supplementary Figure 10C). These results further support the miR-10-mediated regulatory linkage mechanism leading to the three major phenotypes.

As previous studies have shown that elevated miR-10b-5p levels may increase the risk of cancer,[27] we evaluated miR-10b levels in blood samples from diabetic C57 male mice injected with a series of doses of miR-10b-5p mimic (50-1,000 ng/g). Diabetic mice injected with 1,000 ng/g of the miR-10b-5p mimic, which is higher than the concentrations (250-500 ng/g) used in this study, greatly increased miR-10b-5p levels in the blood (Supplementary Figure 11A). However, miR-10b-5p levels were still significantly less in mice injected with the highest dose of the mimic than in healthy mice. In contrast, miR-10b-5p expression was approximately 12 times higher in liver tumors when compared to the healthy liver (Supplementary Figure 11B). These data suggest there is a low risk of cancer development when treating diabetic mice with the optimized doses (250-500 ng/g) of miR-10b-5p mimic.

Discussion

Diabetes and gastroparesis are phenotypically associated, however, a defined network of molecular mechanisms has yet to be unveiled. This study revealed that deficiency of miR-10b-5p in KIT+-cells (ICCs and pancreatic β cell progenitors) contributes to the development of GI motility disorders and diabetes via transcription factor, KLF11. Removal of mir-10b in KIT+-cells caused cellular degeneration, which triggered the onset of GI dysmotility and diabetes. Treatment of diabetic mice with a miR-10b-5p mimic reversed the diabetic and GI dysmotility phenotypes.

Our data suggest that diabetes and gastroparesis can develop due to the degeneration of ICCs and β cells, both caused by the lack of miR-10b-5p. Previous studies have shown that ICCs require stem cell factor and KIT signaling for proper growth and function.[28] It is widely accepted that loss of KIT in ICCs results in abnormal GI motility in animals, and ICC loss is also associated with GI motility disorders in humans.[10] However, the pathogenic factor leading to KIT loss in ICCs was elusive until now. Our mir-10b KO mice demonstrated that decreased miR-10b-5p levels lead to reduced KIT expression and subsequent degeneration of ICCs resulting in delayed gastric emptying as well as slowed colonic and total GI transit. Meanwhile, murine studies demonstrated the importance of KIT in glucose homeostasis.[29] Loss of KIT activity in pancreatic β cells in KitWv mutant mice resulted in decreased β cell proliferation and hyperglycemia,[30] while KIT overexpression in KitβTg mice prevented HFD-induced diabetes.[29] KIT+-cells serve as pancreatic β cell progenitors and cells derived from KIT+-cells are insulin-producing β cells.[31] Kit-DTA mice developed a diabetic phenotype due to ablation of KIT+ pancreatic β cells. Our findings confirmed that the loss of miR-10b in KIT+-cells (β cells and ICCs) in mir-10b KO mice lead to the co-occurrence of diabetes and GI dysmotility. Further investigation is warranted to elucidate if other pathogenic changes (dysregulation of immune cells, enteric neurons, and adipocytes) have a co-occurrence with degenerated KIT+ cells in the mir-10b KO diabetic and GI dysmotility model.

The diabetic phenotype in our mouse models (mir-10b KO and HFHSD-induced mice) was apparent in males, but not females. Likewise, this gender bias is also true in humans.[32] Diabetes

is more common in males ≤45 yrs old, while it is the reverse in females ≥45 yrs old due to the depletion of estrogen.[33] Estrogen protects rodent pancreatic β cells in vivo against multiple pro-apoptotic insults and this protection is conserved in human islets.[24, 34] This gender/age nexus to diabetes suggests that estrogen hormone therapy may reduce the incidence of T2D by protecting β cell function in post-menopausal women.[35] We confirmed HFHSD-fed OVX female mice developed diabetes similar to males. Furthermore, we demonstrated that the diabetes phenotype was rescued by the miR-10b mimic in both male and female mice. Future studies are warranted to enumerate the linkage between sexual dimorphism/estrogen levels and diabetes. Unlike the diabetic phenotype, both male and female mir-10b KO mice developed gastroparesis. Additionally, these mice developed slow transit constipation, which is consistent with recent data from patients with gastroparesis showing an overlap of approximately 60-70% with slow transit constipation.[36] This suggest our conditional mir-10b KO mouse is a good model to study diabetic and idiopathic gastroparesis.

Our data suggested that mir-10b is required for the survival, proper growth and function of KIT+-ICCs and KIT+-β cells. We confirmed the restoration of KIT in ICCs and β cells after miR-10b-5p mimic injections in mice with diabetes and GI dysmotility. miR-10b-5p mimic injections were also able to lower blood glucose levels for up to 10 weeks after a single injection, with significant improvements in GI motility. Further, miR-10b-5p mimic injections were able to reduce and maintain body weight reduction for up to 10 weeks in HFHSD-induced diabetic and obese mice. However, it is not clear how miR-10b-5p regulates β-cell function and tissue specific insulin sensitivity, which are required for further studies using cell-specific animal models.

This study showed miR-10b regulates three phenotypes: hyperglycemia, GI dysmotility, and obesity. However, unlike how diabetes and GI dysmotility were directly regulated by miR-10b-5p via KIT+-β-cell and ICCs, the obesity phenotype is likely only a secondary effect because it developed after the hyperglycemia and GI dysmotility phenotypes. This suggests the weight gain was likely due to complications caused by the diabetic phenotype (changed glucose and insulin

levels). Further studies are warranted to investigate the molecular mechanisms linking these three pathological phenotypes using cell- or tissue-specific KO animal models.

miRNAs are excellent diagnostic markers for diseases.[37] Our data showed that miR-10b-5p is highly expressed in ICCs from healthy mice but markedly reduced in ICCs from diabetic mice. Furthermore, we demonstrated reduced expression of miR-10b-5p in blood from mice with diabetes and GI dysmotility. The later was in conjunction with reduced expression of miR-10b-5p in patients with DG and IG. The reduced miR-10b-5p expression profile for mice and humans was consistent with the miRNA expression profiles of diabetic rats,[38] HFD-induced hepatic insulin-resistant mice,12 children with T1D[39] and twins with T2D.[13] Thus, we suggest the use of miR-10b-5p as a potential diagnostic marker for diabetes/GI motility disorders.

Overexpression of miR-10b-5p is linked to many cancer types and has also been shown to promote cell proliferation and migration.[27] In parallel, miR-10b-5p is highly expressed in proliferating stem cell lines,[40] suggesting they likely have a role in the proliferation of KIT+-ICCs and β cells. Injection of miR-10b-5p in mice may induce cancer development; however, we confirmed there was no indication of cancer development in miR-10b-5p mimic (500 ng/g) injected mice over a one-year period. This suggests that a low dose of the miRNA mimic is not enough to induce cancer. Further, we showed a single injection of the miR-10b-5p mimic into mice restored miR-10b-5p in blood to approximately 40-60% of healthy levels, but not to the elevated levels reported in cancers.[27] Therefore, it is unlikely that the miR-10b-5p mimic injections will lead to cancer development when used to treat diabetes and GI dysmotility caused by reduced miR-10b-5p expression.

Our study demonstrated a novel mechanistic pathway miR-10b-5p-KLF11-KIT in the regulation of glucose homeostasis and GI motility. We confirmed that miR-10b-5p mimic has targeting effects on KLF11 (using both mouse and human β cell lines) and demonstrated that expression of KIT is negatively regulated by KLF11, the metabolic regulator controlling multiple pathways attributed to diabetes and its early onset.[15] A congenital deletion of Klf11 in mice results

in decreased blood glucose levels and body weight, as well as protection against HFD-induced obesity and diabetes,[16] similar to what we found after injection of the miR-10b-5p mimic and Klf11 siRNAs. Binding of KLF11 to GC and CACCC boxes at the promoter of proinsulin gene INS suppresses transcriptional activation.[41] KLF11 recruits transcriptional repressor SIN3A and epigenetic gene silencers HDAC1/2 and HP1, which may silence INS and KIT genes in diabetes and GI dysmotility.[42]

Unlike antidiabetic drugs, such as GLP-1 agonists and metformin, that causes delayed GI motility as a side effect,[43, 44] miR-10b-5p mimic treatment reversed the GI dysmotility phenotype. Prolonged exposure to current antidiabetic medications such as metformin can lead to progressive β cell failure and increased insulin resistance,[5] while the miR-10b-5p mimic treatment restored glucose tolerance and insulin sensitivity. Our drug comparison study with the miR-10b-5p mimic depicted a compelling long-term efficacy in reversing the phenotypes of both diabetes and GI dysmotility when compared to commonly used antidiabetic and prokinetic medications. The beneficial and prolonged effects as seen with the use of the miR-10b-5p mimic in both diabetes and GI dysmotility suggest an opportunity for a new therapeutic approach. By restoring miR-10b-5p in these disease states, we may be able to attenuate symptoms and restore key cells detrimental for insulin production and GI motility, while additionally alleviating the burden for patents relying on insulin treatments.

References

1. Cho NH, Shaw JE, Karuranga S, et al. IDF Diabetes Atlas: Global estimates of diabetes prevalence for 2017 and projections for 2045. Diabetes Res Clin Pract 2018;138:271-281.
2. Holman N, Young B, Gadsby R. Current prevalence of Type 1 and Type 2 diabetes in adults and children in the UK. Diabet Med 2015;32:1119-20.
3. Halban PA, Polonsky KS, Bowden DW, et al. beta-cell failure in type 2 diabetes: postulated mechanisms and prospects for prevention and treatment. Diabetes Care 2014;37:1751-8.
4. Eizirik DL, Pasquali L, Cnop M. Pancreatic beta-cells in type 1 and type 2 diabetes mellitus: different pathways to failure. Nat Rev Endocrinol 2020;16:349-362.
5. Cherney DZI, Lam TKT. A Gut Feeling for Metformin. Cell Metab 2018;28:808-810.
6. Camilleri M, Chedid V, Ford AC, et al. Gastroparesis. Nat Rev Dis Primers 2018;4:41.
7. Bharucha AE, Kudva YC, Prichard DO. Diabetic Gastroparesis. Endocr Rev 2019.
8. Sanders KM, Ward SM, Koh SD. Interstitial cells: regulators of smooth muscle function. Physiol Rev 2014;94:859-907.
9. Grover M, Bernard CE, Pasricha PJ, et al. Clinical-histological associations in gastroparesis: results from the Gastroparesis Clinical Research Consortium. Neurogastroenterol Motil 2012;24:531-9, e249.
10. Sanders KM, Koh SD, Ro S, et al. Regulation of gastrointestinal motility--insights from smooth muscle biology. Nat Rev Gastroenterol Hepatol 2012;9:633-45.
11. Beckett EA, Ro S, Bayguinov Y, et al. Kit signaling is essential for development and maintenance of interstitial cells of Cajal and electrical rhythmicity in the embryonic gastrointestinal tract. Dev Dyn 2007;236:60-72.
12. Croce CM, Calin GA. miRNAs, cancer, and stem cell division. Cell 2005;122:6-7.
13. Bork-Jensen J, Scheele C, Christophersen DV, et al. Glucose tolerance is associated with differential expression of microRNAs in skeletal muscle: results from studies of twins with and without type 2 diabetes. Diabetologia 2015;58:363-73.

14. Mazzone A, Strege PR, Gibbons SJ, et al. microRNA overexpression in slow transit constipation leads to reduced NaV1.5 current and altered smooth muscle contractility. Gut 2020;69:868-876.

15. Pollak NM, Hoffman M, Goldberg IJ, et al. Kruppel-like factors: Crippling and un-crippling metabolic pathways. JACC Basic Transl Sci 2018;3:132-156.

16. Mathison A, Escande C, Calvo E, et al. Phenotypic Characterization of Mice Carrying Homozygous Deletion of KLF11, a Gene in Which Mutations Cause Human Neonatal and MODY VII Diabetes. Endocrinology 2015;156:3581-95.

17. McCann CJ, Cooper JE, Natarajan D, et al. Transplantation of enteric nervous system stem cells rescues nitric oxide synthase deficient mouse colon. Nat Commun 2017;8:15937.

18. Anitha M, Reichardt F, Tabatabavakili S, et al. Intestinal dysbiosis contributes to the delayed gastrointestinal transit in high-fat diet fed mice. Cell Mol Gastroenterol Hepatol 2016;2:328-339.

19. Ro S, Park C, Jin J, et al. A model to study the phenotypic changes of interstitial cells of Cajal in gastrointestinal diseases. Gastroenterology 2010;138:1068-78 e1-2.

20. Fan R, Zhong J, Zheng S, et al. MicroRNA-218 inhibits gastrointestinal stromal tumor cell and invasion by targeting KIT. Tumour Biol 2014;35:4209-17.

21. Lomberk G, Grzenda A, Mathison A, et al. Kruppel-like factor 11 regulates the expression of metabolic genes via an evolutionarily conserved protein interaction domain functionally disrupted in maturity onset diabetes of the young. J Biol Chem 2013;288:17745-58.

22. Agarwal V, Bell GW, Nam JW, et al. Predicting effective microRNA target sites in mammalian mRNAs. Elife 2015;4.

23. Feng ZC, Riopel M, Popell A, et al. A survival Kit for pancreatic beta cells: stem cell factor and c-Kit receptor tyrosine kinase. Diabetologia 2015;58:654-65.

24. Xu B, Allard C, Alvarez-Mercado AI, et al. Estrogens Promote Misfolded Proinsulin Degradation to Protect Insulin Production and Delay Diabetes. Cell Rep 2018;24:181-196.

25. Nyavor Y, Estill R, Edwards H, et al. Intestinal nerve cell injury occurs prior to insulin resistance in female mice ingesting a high-fat diet. Cell Tissue Res 2019;376:325-340.

26. Niu X, Perakakis N, Laubner K, et al. Human Kruppel-like factor 11 inhibits human proinsulin promoter activity in pancreatic beta cells. Diabetologia 2007;50:1433-41.

27. Sheedy P, Medarova Z. The fundamental role of miR-10b in metastatic cancer. Am J Cancer Res 2018;8:1674-1688.

28. Maeda H, Yamagata A, Nishikawa S, et al. Requirement of c-kit for development of intestinal pacemaker system. Development 1992;116:369-75.

29. Feng ZC, Li J, Turco BA, et al. Critical role of c-Kit in beta cell function: increased insulin secretion and protection against diabetes in a mouse model. Diabetologia 2012;55:2214-25.

30. Krishnamurthy M, Ayazi F, Li J, et al. c-Kit in early onset of diabetes: a morphological and functional analysis of pancreatic beta-cells in c-KitW-v mutant mice. Endocrinology 2007;148:5520-30.

31. Ma F, Chen F, Chi Y, et al. Isolation of pancreatic progenitor cells with the surface marker of hematopoietic stem cells. Int J Endocrinol 2012;2012:948683.

32. Menke A, Casagrande S, Geiss L, et al. Prevalence of and Trends in Diabetes Among Adults in the United States, 1988-2012. JAMA 2015;314:1021-9.

33. Wang WS, Wahlqvist ML, Hsu CC, et al. Age- and gender-specific population attributable risks of metabolic disorders on all-cause and cardiovascular mortality in Taiwan. BMC Public Health 2012;12:111.

34. Tiano JP, Mauvais-Jarvis F. Importance of oestrogen receptors to preserve functional beta-cell mass in diabetes. Nat Rev Endocrinol 2012;8:342-51.

35. Mauvais-Jarvis F, Manson JE, Stevenson JC, et al. Menopausal Hormone Therapy and Type 2 Diabetes Prevention: Evidence, Mechanisms, and Clinical Implications. Endocr Rev 2017;38:173-188.

36. Zikos TA, Kamal AN, Neshatian L, et al. High Prevalence of Slow Transit Constipation in Patients With Gastroparesis. J Neurogastroenterol Motil 2019;25:267-275.

37. Vasu S, Kumano K, Darden CM, et al. MicroRNA Signatures as Future Biomarkers for Diagnosis of Diabetes States. Cells 2019;8.

38. Herrera BM, Lockstone HE, Taylor JM, et al. Global microRNA expression profiles in insulin target tissues in a spontaneous rat model of type 2 diabetes. Diabetologia 2010;53:1099-109.

39. Samandari N, Mirza AH, Kaur S, et al. Influence of Disease Duration on Circulating Levels of miRNAs in Children and Adolescents with New Onset Type 1 Diabetes. Noncoding RNA 2018;4.

40. Guessous F, Alvarado-Velez M, Marcinkiewicz L, et al. Oncogenic effects of miR-10b in glioblastoma stem cells. J Neurooncol 2013;112:153-63.

41. Neve B, Fernandez-Zapico ME, Ashkenazi-Katalan V, et al. Role of transcription factor KLF11 and its diabetes-associated gene variants in pancreatic beta cell function. Proc Natl Acad Sci U S A 2005;102:4807-12.

42. Lomberk G, Mathison AJ, Grzenda A, et al. Sequence-specific recruitment of heterochromatin protein 1 via interaction with Kruppel-like factor 11, a human transcription factor involved in tumor suppression and metabolic diseases. J Biol Chem 2012;287:13026-39.

43. Nakatani Y, Maeda M, Matsumura M, et al. Effect of GLP-1 receptor agonist on gastrointestinal tract motility and residue rates as evaluated by capsule endoscopy. Diabetes Metab 2017;43:430-437.

44. Sato D, Morino K, Nakagawa F, et al. Acute Effect of Metformin on Postprandial Hypertriglyceridemia through Delayed Gastric Emptying. Int J Mol Sci 2017;18.

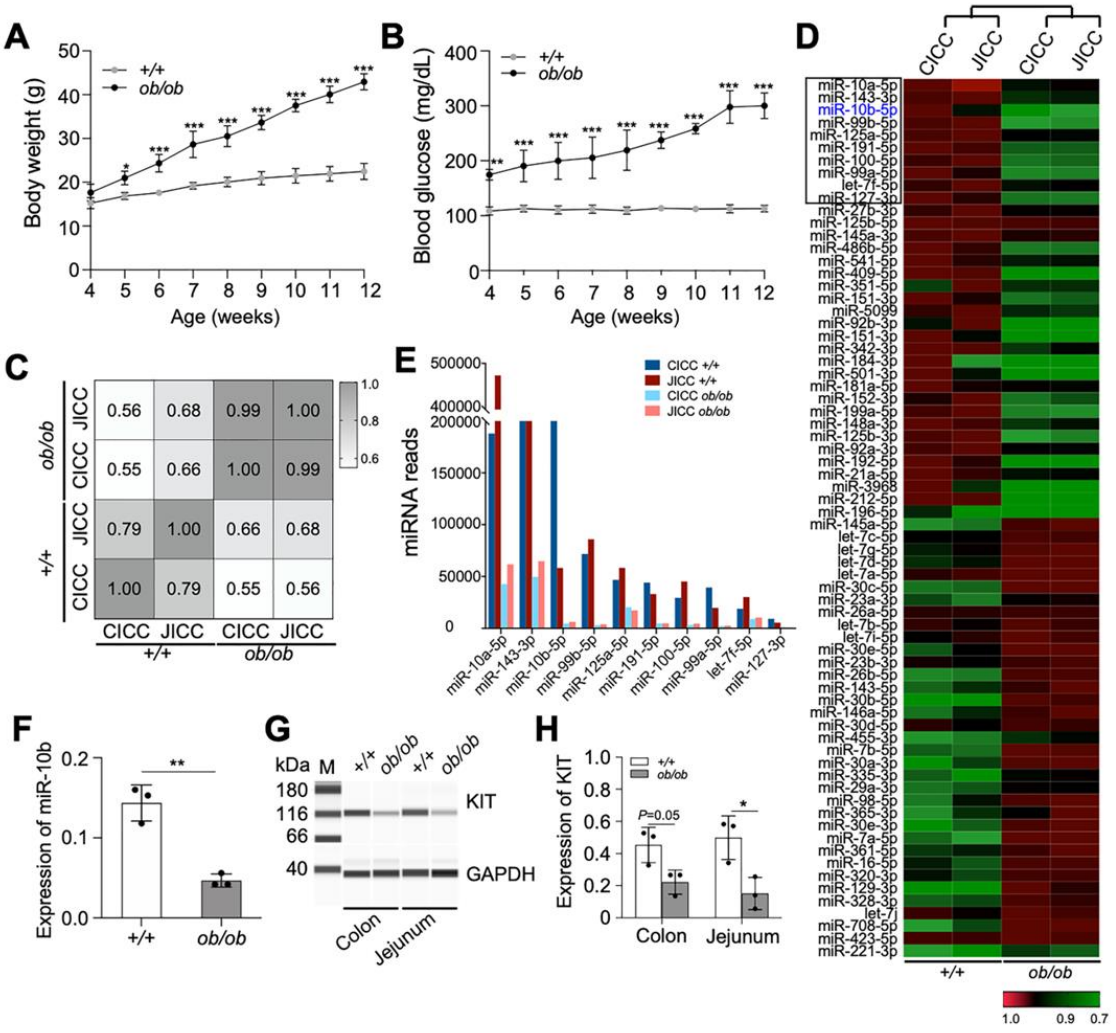

Figure 1. Expression of miR-10b-5p is drastically reduced in KIT+-ICCs in male diabetic KitcopGFP/+;Lepob/ob Mice. (A, B) Body weight and fasting blood glucose levels of KitcopGFP/+;Lep+/+ (+/+) and KitcopGFP/+;Lepob/ob (ob/ob) mice (Two-way ANOVA, n=8). (C) Pearson correlation analysis between miRNA-seq data obtained from colonic and jejunal ICC (CICC and JICC, respectively) isolated and pooled from diabetic ob/ob (n=30) and +/+ mice (n=20). (D) Heat map of the 70 most dynamically regulated miRNAs in CICC and JICC of diabetic ob/ob mice. (E) Expression levels of the ten most prominently reduced miRNAs in CICC and JICC of diabetic ob/ob mice from panel E (black box) obtained by miRNA-seq (n=20-30). (F) Expression of

miR-10b-5p in gastric ICCs of +/+ and ob/ob mice measured by qPCR (n=3). (G, H) Western blot and quantification of KIT in the jejunum and colon of +/+ and ob/ob mice (n=3). Error bar indicate SEM, unpaired t-test. *$p < 0.05$, **$p < 0.01$.

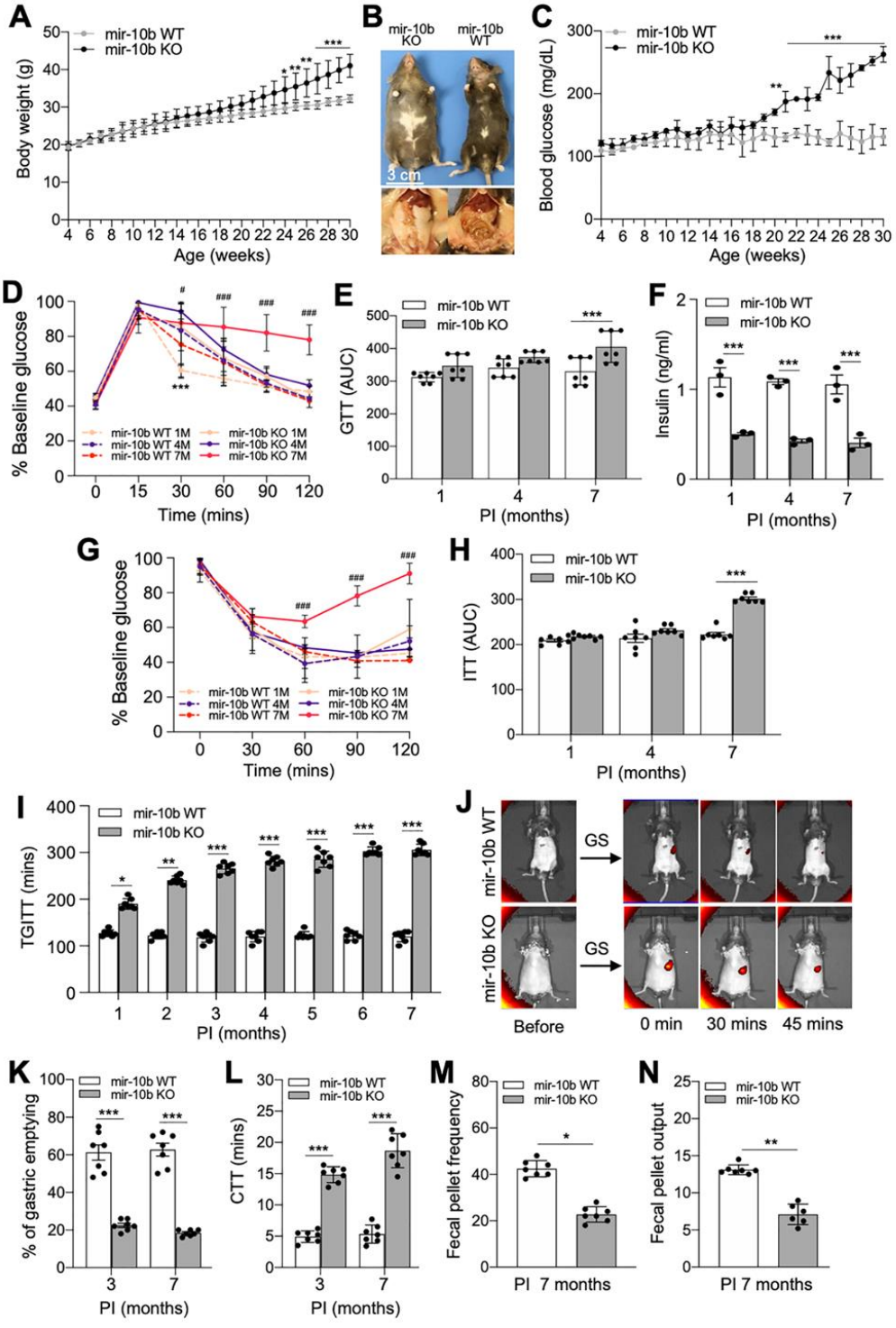
A
mir-10b WT
mir-10b KO
Body weight (g)
Age (weeks)
B
mir-10b KO
mir-10b WT
3 cm
C
mir-10b WT
mir-10b KO
Blood glucose (mg/dL)
Age (weeks)
D
% Baseline glucose
Time (mins)
mir-10b WT 1M
mir-10b WT 4M
mir-10b WT 7M
mir-10b KO 1M
mir-10b KO 4M
mir-10b KO 7M
E
GTT (AUC)
PI (months)
F
Insulin (ng/ml)
PI (months)
G
% Baseline glucose
Time (mins)
H
ITT (AUC)
PI (months)
I
TGITT (mins)
PI (months)
J
mir-10b WT
mir-10b KO
GS
Before
0 min
30 mins
45 mins
K
% of gastric emptying
PI (months)
L
CTT (mins)
PI (months)
M
Fecal pellet frequency
PI 7 months
N
Fecal pellet output
PI 7 months

Figure 2. Male KIT+ cell-specific mir-10b KO mice develop diabetes and GI dysmotility. KitCreERT2/+;mir-10blox/lox mice were injected with tamoxifen (mir-10b KO) or oil (mir-10b WT) at 4 weeks of age. (A) Body weight of mir-10b KO and WT male mice. (B) Gross anatomical images of 30 weeks old male mir-10b KO and WT mice. (C) Fasting blood glucose levels in mir-10b KO and WT male mice. (D) Glucose tolerance tests (GTT) in mir-10b KO and WT male mice. (E) GTT plot of the area under the curve (AUC) from (D). (F) Changes in blood insulin levels after 6 hrs fasting in mir-10b KO and WT male mice (n=3). (G) Insulin tolerance test (ITT) in mir-10b KO and WT male mice. (H) ITT plot of the AUC from (G). (I) Total GI transit time (TGITT). (J) Gastric emptying images of 7-month-old mir-10b KO and WT mice. (K) Quantification of gastric emptying at 30 min. (L) Colonic transit time (CTT). (M, N) Fecal pellet frequency and output within 24 hrs. (unpaired t-test). n=7 per condition for each experiment. Error bar indicate SEM, Two-way ANOVA. *$p < 0.05$, **$p < 0.01$, ***$p < 0.001$, ††$p < 0.01$, #$p < 0.05$, ###$p < 0.001$.

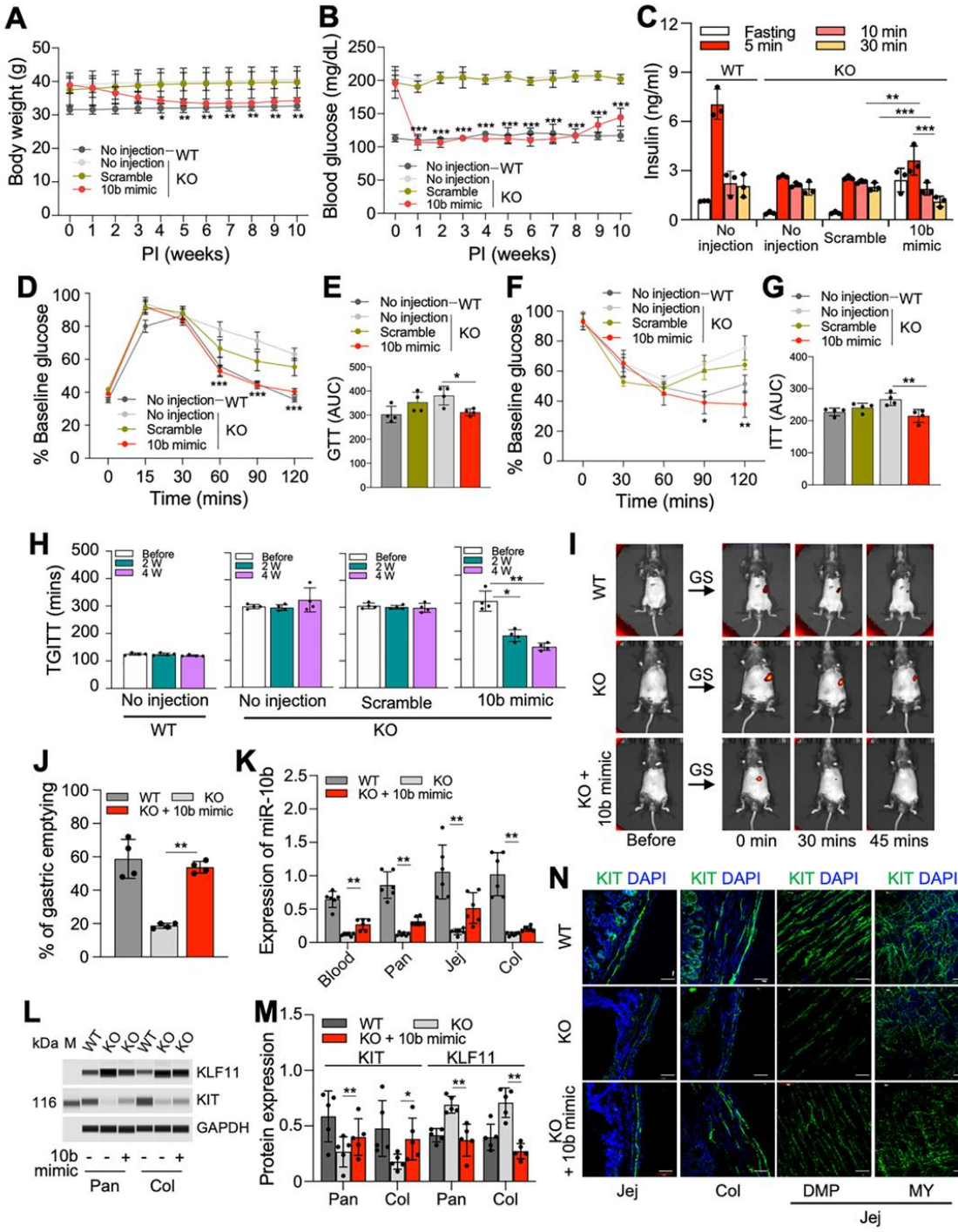
A
Body weight (g)
PI (weeks)
No injection
No injection
Scramble
10b mimic
WT
KO
B
Blood glucose (mg/dL)
PI (weeks)
C
Insulin (ng/ml)
Fasting
5 min
10 min
30 min
WT
KO
No injection
No injection
Scramble
10b mimic
D
% Baseline glucose
Time (mins)
E
GTT (AUC)
F
% Baseline glucose
Time (mins)
G
ITT (AUC)
H
TGITT (mins)
Before
2 W
4 W
No injection
No injection
Scramble
10b mimic
WT
KO
I
WT
KO
KO + 10b mimic
GS
Before
0 min
30 mins
45 mins
J
% of gastric emptying
WT
KO
KO + 10b mimic
K
Expression of miR-10b
Blood
Pan
Jej
Col
L
kDa M WT KO KO WT KO KO
KLF11
116
KIT
GAPDH
10b mimic
Pan
Col
M
Protein expression
KIT
KLF11
Pan
Col
Pan
Col
N
KIT DAPI
WT
KO
KO + 10b mimic
Jej
Col
DMP
MY
Jej

Figure 3. miR-10b-5p mimic injection rescues the diabetic and GI dysmotility phenotypes in male mir-10b KO mice. Male diabetic mir-10b KO mice were injected with miR-10b-5p (10b mimic), a negative control (scramble RNA), or given no injection, compared to WT mice. (A, B) Body weight and fasting blood glucose levels for 10 weeks post-injection (PI). (C) Comparison of insulin levels after 6 hrs fasting and after glucose injection in mir-10b KO and WT mice at 1 week post-injection (IP) (One-way ANOVA). (D and F) GTT and ITT at 1 week PI. (E and G) GTT and ITT plot of the AUC from (D and F) (One-way ANOVA). (H, I) TGITT (One-way ANOVA) at 2 and 4 weeks PI and gastric emptying test at 4 weeks PI. (J) Quantification of gastric emptying at 30 min (One-way ANOVA). (K) Quantification of miR-10b-5p in the blood, pancreas, jejunum, and colon in male WT and diabetic mir-10b KO mice 1 week after 10b mimic or no injection measured by qPCR (One-way ANOVA). (L, M) Western blot and quantification of KLF11 and KIT in the pancreas and colon in male WT and diabetic mir-10b KO mice 1 week after 10b mimic or no injection (One-way ANOVA). (N) Images of cross sections and whole mount tissue sections showing the restoration of ICCs (KIT+) in the jejunum and colon at 1 week PI. Scale bars are 50 μm. n=3-4 per condition for each experiment. Pan, pancreas; Col, colon; Jej, jejunum; DMP, deep muscular plexus; MY, myenteric plexus. Error bar indicate SEM, Two-way ANOVA (A-D). *$p < 0.05$, **$p < 0.01$, ***$p < 0.001$.

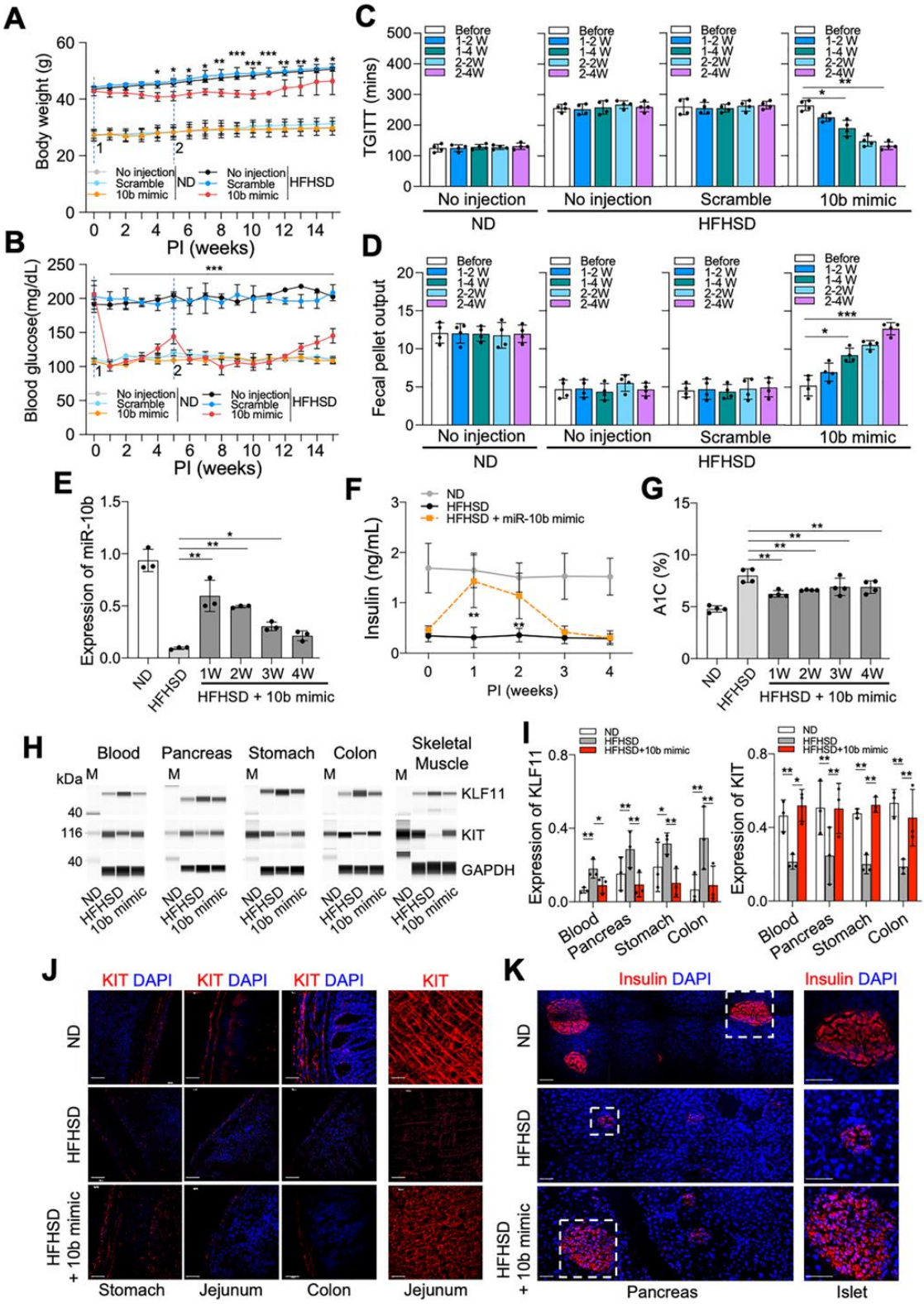
A
Body weight (g)
PI (weeks)
No injection
Scramble
10b mimic
ND
HFHSD
B
Blood glucose(mg/dL)
PI (weeks)
C
TGITT (mins)
Before
1-2 W
1-4 W
2-2W
2-4W
No injection
Scramble
10b mimic
ND
HFHSD
D
Fecal pellet output
E
Expression of miR-10b
ND
HFHSD
1W 2W 3W 4W
HFHSD + 10b mimic
F
Insulin (ng/mL)
ND
HFHSD
HFHSD + miR-10b mimic
PI (weeks)
G
A1C (%)
H
Blood
Pancreas
Stomach
Colon
Skeletal Muscle
kDa
M
40
116
40
KLF11
KIT
GAPDH
ND
HFHSD
10b mimic
I
Expression of KLF11
Expression of KIT
ND
HFHSD
HFHSD+10b mimic
Blood
Pancreas
Stomach
Colon
J
KIT DAPI
KIT
ND
HFHSD
HFHSD + 10b mimic
Stomach
Jejunum
Colon
Jejunum
K
Insulin DAPI
Pancreas
Islet

Figure 4. miR-10b-5p mimic rescues the diabetic and GI dysmotility phenotypes in male HFHSD-fed mice. Male C57 mice (at 4 weeks of age) were fed a HFHSD (diabetic) or ND (healthy controls) for 4 months and injected twice (second injection at 5 weeks) with either the miR-10b-5p mimic (10b mimic), a negative control (scramble RNA), or given no injection, over a 10 week period. (A, B) Body weight and fasting blood glucose level comparison (Two-way ANOVA). (C, D) TGITT and fecal pellet output. (E) Expression of miR-10b-5p in the blood from ND-fed healthy mice, HFHSD-fed diabetic mice, and 10b mimic-injected HFHSD-fed mice at 1-4 weeks PI measured by qPCR. (F) Changes in insulin levels (6 hrs fasting) and A1C levels in male mice fed a HFHSD or ND and injected with 10b mimic (Two-way ANOVA). (G) Changes in A1C levels in male mice fed a HFHSD or ND and injected with 10b mimic. (H, I) Western blot and quantification of KLF11 and KIT in blood, pancreas, stomach, colon and skeletal muscle from ND, HFHSD, and 10b mimic-injected HFHSD-fed mice at 3 weeks PI. (J, K) Images of cross sections and whole mount tissue sections showing the restoration of ICCs (KIT+) in the stomach, jejunum, and colon, as well as in β cells (Insulin+) in the pancreatic islets at 3 weeks PI. Scale bars are 100 μm. n=3-4 per condition for each experiment. Error bar indicate SEM, One-way ANOVA. *$p < 0.05$, **$p < 0.01$, ***$p < 0.001$.

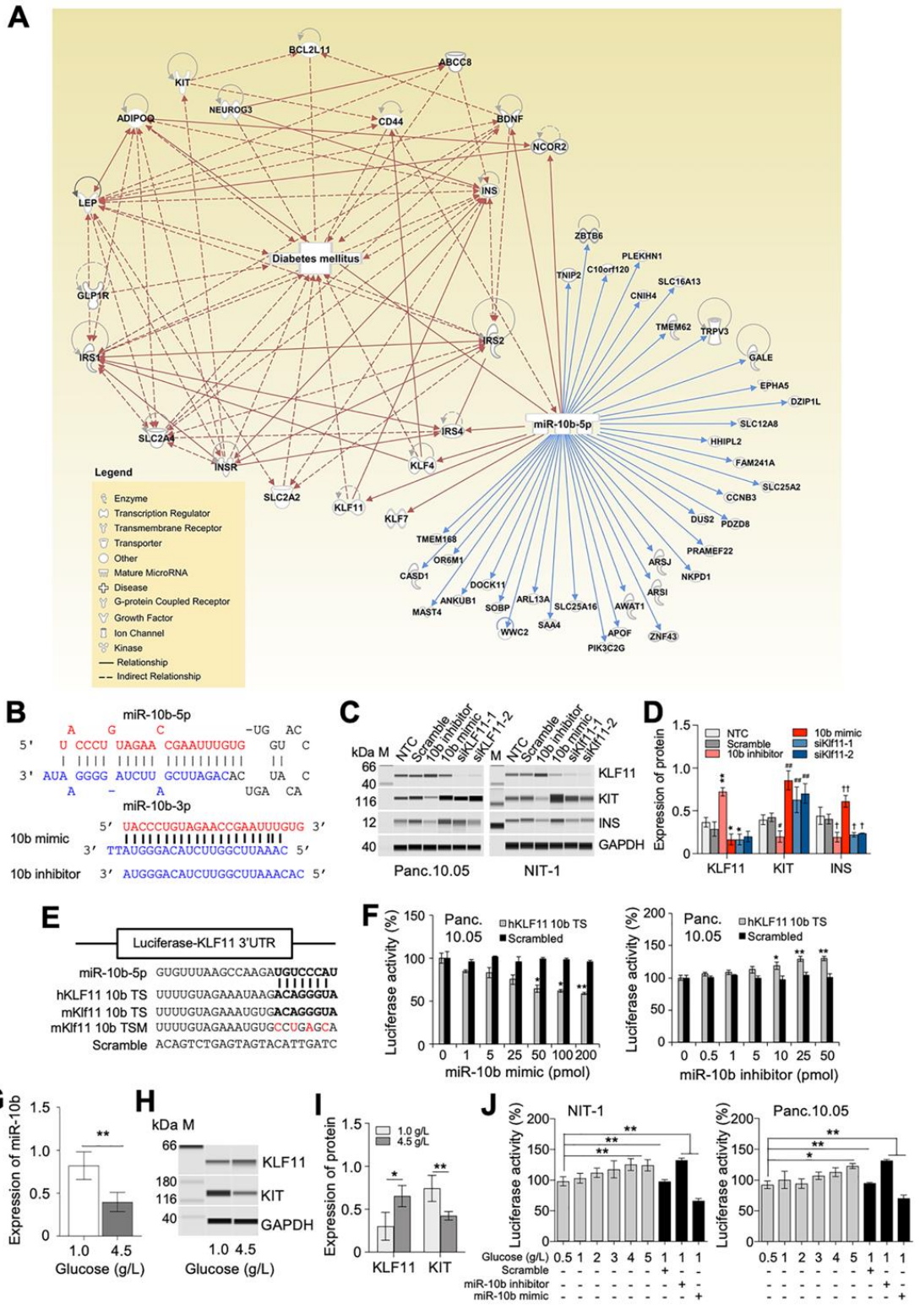
A
BCL2L11
ABCC8
KIT
NEUROG3
ADIPOQ
CD44
BDNF
NCOR2
INS
LEP
ZBTB6
PLEKHN1
C10orf120
TNIP2
SLC16A13
CNIH4
Diabetes mellitus
GLP1R
TMEM62
TRPV3
IRS2
IRS1
GALE
EPHA5
DZIP1L
IRS4
miR-10b-5p
SLC12A8
SLC2A4
HHIPL2
INSR
KLF4
FAM241A
SLC25A2
SLC2A2
KLF11
CCNB3
KLF7
DUS2
PDZD8
TMEM168
PRAMEF22
OR6M1
ARSJ
CASD1
NKPD1
DOCK11
ARSI
ANKUB1
ARL13A
SLC25A16
AWAT1
MAST4
SOBP
SAA4
WWC2
APOF
ZNF43
PIK3C2G
Legend
Enzyme
Transcription Regulator
Transmembrane Receptor
Transporter
Other
Mature MicroRNA
Disease
G-protein Coupled Receptor
Growth Factor
Ion Channel
Kinase
Relationship
Indirect Relationship
B
miR-10b-5p
5' U CCCU UAGAA CGAAUUUGUG GU C
3' AUA GGGG AUCUU GCUUAGACAC UA C
A A UGA CA
miR-10b-3p
10b mimic 5' UACCCUGUAGAACCGAAUUUGUG 3'
3' TTAUGGGACAUCUUGGCUUAAAC 5'
10b inhibitor 3' AUGGGACAUCUUGGCUUAAACAC 5'
C
kDa M
NTC
Scramble
10b inhibitor
10b mimic
siKLF11-1
siKLF11-2
66
40
116
12
40
KLF11
KIT
INS
GAPDH
Panc.10.05
NIT-1
D
Expression of protein
NTC
Scramble
10b inhibitor
10b mimic
siKlf11-1
siKlf11-2
KLF11
KIT
INS
E
Luciferase-KLF11 3'UTR
miR-10b-5p GUGUUUAAGCCAAGAUGUCCCAU
hKLF11 10b TS UUUUGUAGAAAUAAGACAGGGUA
mKlf11 10b TS UUUUGUAGAAAUGUGACAGGGUA
mKlf11 10b TSM UUUUGUAGAAAUGUGCCUGAGCA
Scramble ACAGTCTGAGTAGTACATTGATC
F
Panc. 10.05
hKLF11 10b TS
Scrambled
Luciferase activity (%)
miR-10b mimic (pmol)
miR-10b inhibitor (pmol)
G
Expression of miR-10b
Glucose (g/L)
H
kDa M
KLF11
KIT
GAPDH
Glucose (g/L)
I
1.0 g/L
4.5 g/L
Expression of protein
KLF11
KIT
J
NIT-1
Panc.10.05
Luciferase activity (%)
Glucose (g/L)
Scramble
miR-10b inhibitor
miR-10b mimic

Figure 5. Target identification and validation of miR-10b-5p in vitro. (A) Pathway analysis of miR-10b-5p and its target genes associated with diabetes mellitus according to Ingenuity Pathway Analysis. (B) The sequence and structure of the mouse miR-10b precursor (pre-miR-10b) encoding miR-10b-5p and miR-10b-3p, a synthetic miR-10b-5p molecule (miR-10b-5p mimic) and a synthetic miR-10b-5p antisense molecule (miR-10b-5p inhibitor). (C) Targeting of KLF11, KIT and INS by the miR-10b-5p mimic, miR-10b-5p inhibitor, and KLF11 siRNAs (siKLF11-1 and siKLF11-2 in human Panc.10.05 cells and siKlf11-1 and siKlf11-2 in mouse NIT-1 cells). A non-targeting (scramble) RNA and non-transfection control (NTC) were used as negative controls. A protein marker (M) with corresponding molecular weights (kDa) is shown. (D) Quantification of protein expression levels of KLF11, KIT and INS in Panc.10.05 cells. (E) Diagram of luciferase reporter plasmids with the miR-10b-5p target site (miR-10b-5p mimic binding site) of human and mouse KLF11 (hKLF11 10b TS and mKlf11 10b TS) and a mutant (mKlf11 10b TSM). (F) Target validation of KLF11 with the miR-10b-5p mimic and miR-10b-5p inhibitor in Panc.10.05 cells transfected with luciferase reporter plasmids (Two-way ANOVA). (G) Quantification of miR-10b-5p in NIT-1 cells incubated in media with different glucose concentrations (0, 1.0, and 4.5 mg/L). (H and I) Western blot and quantification of KLF11 and KIT expression at different glucose concentrations. (J) Target effects of KLF11 in NIT-1 and Panc.10.05 cells cultured at different glucose concentrations. n=3 per condition for each experiment. Error bar indicate SEM, One-way ANOVA. *$p < 0.05$, **$p < 0.01$.

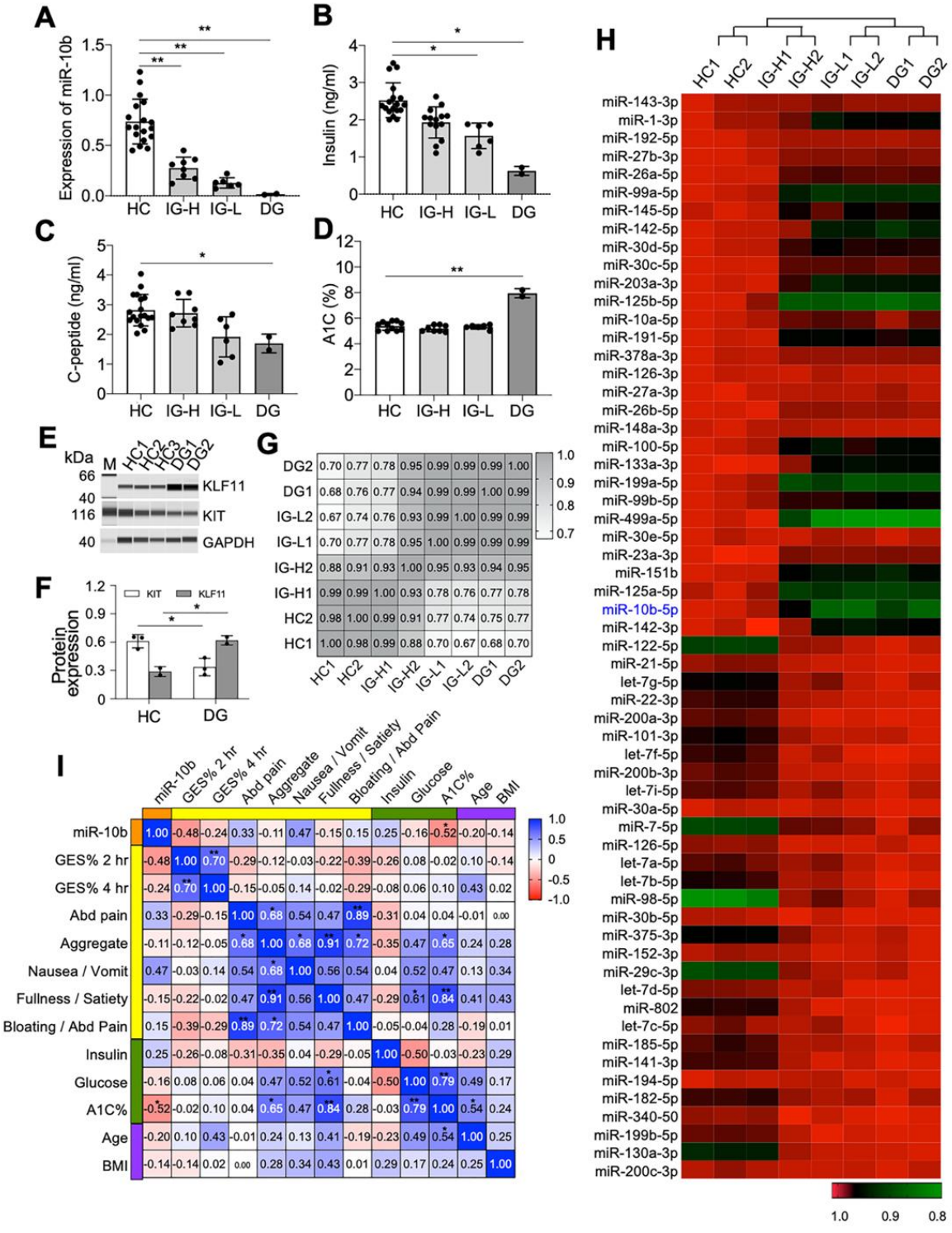
A
Expression of miR-10b
HC IG-H IG-L DG
B
Insulin (ng/ml)
C
C-peptide (ng/ml)
D
A1C (%)
E
kDa
M
HC1 HC2 HC3 DG1 DG2
66
40
116
40
KLF11
KIT
GAPDH
F
KIT
KLF11
Protein expression
G
DG2 0.70 0.77 0.78 0.95 0.99 0.99 0.99 1.00
DG1 0.68 0.76 0.77 0.94 0.99 0.99 1.00 0.99
IG-L2 0.67 0.74 0.76 0.93 0.99 1.00 0.99 0.99
IG-L1 0.70 0.77 0.78 0.95 1.00 0.99 0.99 0.99
IG-H2 0.88 0.91 0.93 1.00 0.95 0.93 0.94 0.95
IG-H1 0.99 0.99 1.00 0.93 0.78 0.76 0.77 0.78
HC2 0.98 1.00 0.99 0.91 0.77 0.74 0.75 0.77
HC1 1.00 0.98 0.99 0.88 0.70 0.67 0.68 0.70
HC1 HC2 IG-H1 IG-H2 IG-L1 IG-L2 DG1 DG2
1.0 0.9 0.8 0.7
H
HC1 HC2 IG-H1 IG-H2 IG-L1 IG-L2 DG1 DG2
miR-143-3p
miR-1-3p
miR-192-5p
miR-27b-3p
miR-26a-5p
miR-99a-5p
miR-145-5p
miR-142-5p
miR-30d-5p
miR-30c-5p
miR-203a-3p
miR-125b-5p
miR-10a-5p
miR-191-5p
miR-378a-3p
miR-126-3p
miR-27a-3p
miR-26b-5p
miR-148a-3p
miR-100-5p
miR-133a-3p
miR-199a-5p
miR-99b-5p
miR-499a-5p
miR-30e-5p
miR-23a-3p
miR-151b
miR-125a-5p
miR-10b-5p
miR-142-3p
miR-122-5p
miR-21-5p
let-7g-5p
miR-22-3p
miR-200a-3p
miR-101-3p
let-7f-5p
miR-200b-3p
let-7i-5p
miR-30a-5p
miR-7-5p
miR-126-5p
let-7a-5p
let-7b-5p
miR-98-5p
miR-30b-5p
miR-375-3p
miR-152-3p
miR-29c-3p
let-7d-5p
miR-802
let-7c-5p
miR-185-5p
miR-141-3p
miR-194-5p
miR-182-5p
miR-340-50
miR-199b-5p
miR-130a-3p
miR-200c-3p
1.0 0.9 0.8
I
miR-10b GES% 2 hr GES% 4 hr Abd pain Aggregate Nausea / Vomit Fullness / Satiety Bloating / Abd Pain Insulin Glucose A1C% Age BMI
miR-10b 1.00 -0.48 -0.24 0.33 -0.11 0.47 -0.15 0.15 0.25 -0.16 -0.52 -0.20 -0.14
GES% 2 hr -0.48 1.00 0.70 -0.29 -0.12 -0.03 -0.22 -0.39 -0.26 0.08 -0.02 0.10 -0.14
GES% 4 hr -0.24 0.70 1.00 -0.15 -0.05 0.14 -0.02 -0.29 -0.08 0.06 0.10 0.43 0.02
Abd pain 0.33 -0.29 -0.15 1.00 0.68 0.54 0.47 0.89 -0.31 0.04 0.04 -0.01 0.00
Aggregate -0.11 -0.12 -0.05 0.68 1.00 0.68 0.91 0.72 -0.35 0.47 0.65 0.24 0.28
Nausea / Vomit 0.47 -0.03 0.14 0.54 0.68 1.00 0.56 0.54 0.04 0.52 0.47 0.13 0.34
Fullness / Satiety -0.15 -0.22 -0.02 0.47 0.91 0.56 1.00 0.47 -0.29 0.61 0.84 0.41 0.43
Bloating / Abd Pain 0.15 -0.39 -0.29 0.89 0.72 0.54 0.47 1.00 -0.05 -0.04 0.28 -0.19 0.01
Insulin 0.25 -0.26 -0.08 -0.31 -0.35 0.04 -0.29 -0.05 1.00 -0.50 -0.03 -0.23 0.29
Glucose -0.16 0.08 0.06 0.04 0.47 0.52 0.61 -0.04 -0.50 1.00 0.79 0.49 0.17
A1C% -0.52 -0.02 0.10 0.04 0.65 0.47 0.84 0.28 -0.03 0.79 1.00 0.54 0.24
Age -0.20 0.10 0.43 -0.01 0.24 0.13 0.41 -0.19 -0.23 0.49 0.54 1.00 0.25
BMI -0.14 -0.14 0.02 0.00 0.28 0.34 0.43 0.01 0.29 0.17 0.24 0.25 1.00
1.0 0.5 0 -0.5 -1.0

Figure 6. Validation of altered expression of miR-10b-5p, KLF11, and KIT in patients with idiopathic and diabetic gastroparesis. (A) Expression of miR-10b-5p in blood samples collected from idiopathic gastroparesis patients (IG, n=14) and diabetic gastroparesis patients (DG, n=2) compared to healthy control subjects (HC, n=18). The IG group was divided into two groups with high miR-10b levels (IG-H, n=8) or low miR-10b levels (IG-L, n=6). (B-D) Comparison of insulin, C-peptide and A1C levels in the blood of the four groups. (E) Western blot of KLF11 and KIT in the blood samples of the HC and DG groups. (F) Pearson correlation analysis between miRNA-seq data obtained from the blood of HC, IG-H, IG-L, and DG (n=2). (G) Heat map of 70 most dynamically regulated miRNAs in blood plasma samples from HC, IG-H, IG-L, and DG (n=2). (H) The Spearman rank correlation between miR-10b-5p expression levels and metabolic parameters, clinical GI symptoms, and gastric emptying scintigraphy (GES) % at 2 and 4 hrs in gastroparesis. Error bar indicate SEM, One-Way ANOVA. *$p < 0.05$, **$p < 0.01$.

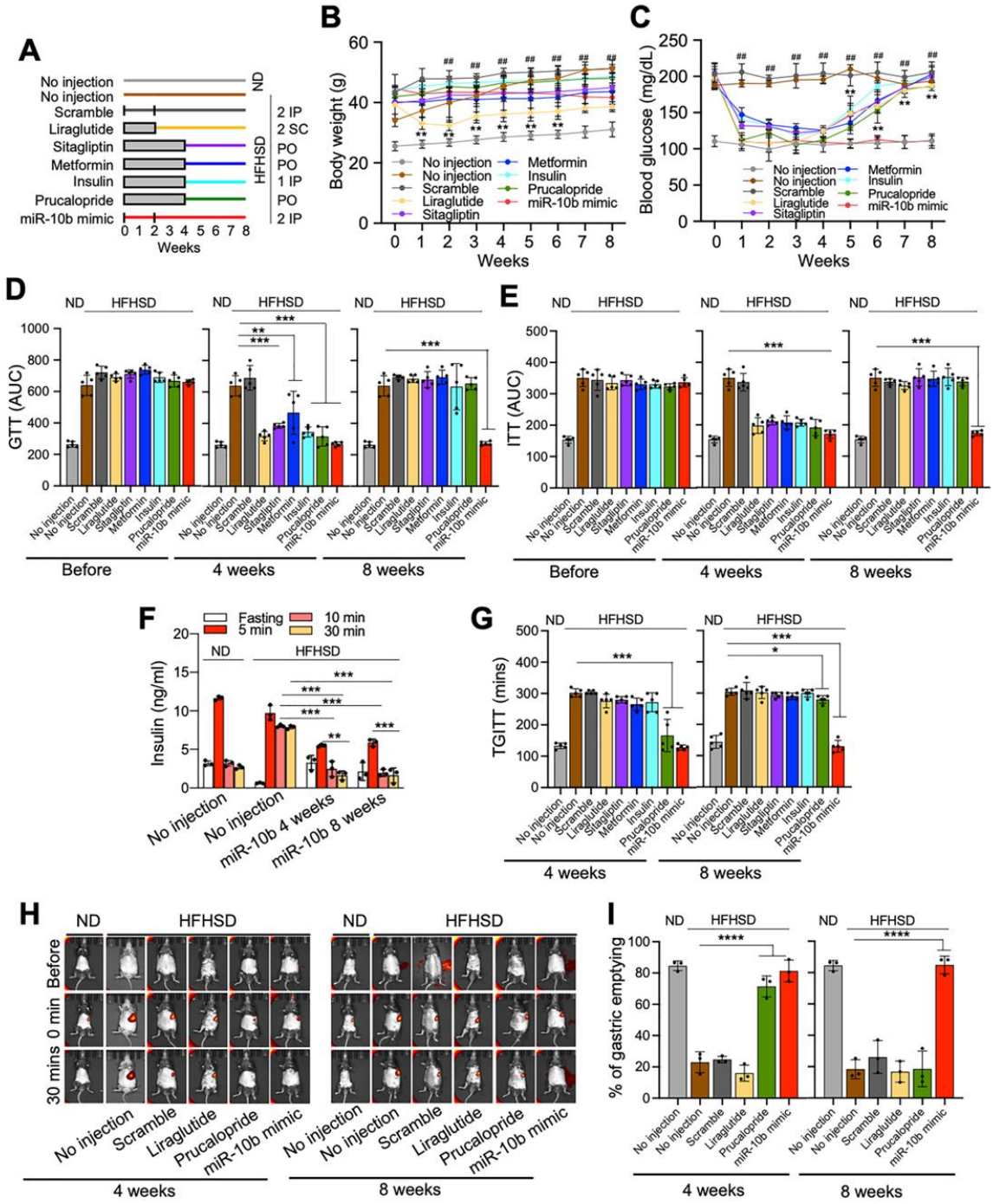
A
No injection
No injection
Scramble
Liraglutide
Sitagliptin
Metformin
Insulin
Prucalopride
miR-10b mimic
ND
HFHSD
2 IP
2 SC
PO
PO
1 IP
PO
2 IP
0 1 2 3 4 5 6 7 8
Weeks
B
Body weight (g)
Weeks
C
Blood glucose (mg/dL)
Weeks
D
GTT (AUC)
Before
4 weeks
8 weeks
E
ITT (AUC)
Before
4 weeks
8 weeks
F
Fasting
5 min
10 min
30 min
Insulin (ng/ml)
No injection
No injection
miR-10b 4 weeks
miR-10b 8 weeks
G
TGITT (mins)
4 weeks
8 weeks
H
Before
0 min
30 mins
No injection
Scramble
Liraglutide
Prucalopride
miR-10b mimic
4 weeks
8 weeks
I
% of gastric emptying
4 weeks
8 weeks

Figure 7. Efficacy comparison of miR-10b-5p mimic with antidiabetic and prokinetic medicines in HFHSD-fed diabetic C57 male mice. (A) A study design of drug effects in HFHSD-fed diabetic mice- or ND-fed healthy mice. miR-10b-5p, or scramble RNA were injected twice, at 0 and 2 weeks by IP injection; Metformin or Sitagliptin was provided daily PO for 4 weeks; Liraglutide was injected twice daily by SC injection for 2 weeks; Insulin was injected once daily by IP injection for 4 weeks; Prucalopride was provided daily PO for 4 weeks. (B, C) Body weight and fasting blood glucose levels for 8 weeks post treatment (Two-way ANOVA, n=5). (D, E) Comparison of GTT and ITT plot of AUC (n=5). (F) Comparison of insulin levels at 6 hrs fasting and after glucose injection (n=3). (G) TGITT comparison (n=5). (H, I) Gastric emptying images and quantification of stomach emptying (n=3). Error bar indicate SEM, One-way ANOVA. *p < 0.05, **p < 0.01, ***p < 0.001, ****p < 0.0001, #p < 0.05, ##p < 0.01.

Supplementary Material

Materials and Methods

Mice:

KitcopGFP/+, 1 Lepob/ob, 2 KitcreERT2/+, 3 mir-10bLacZ-FLP-lox/lox, 4 Rosa26 FLP/+, 5 Rosa26tdTom, 6 and Rosa26DTA 7 mouse lines were used in this study. KitcopGFP/+ mice were crossed with Lepob/+ mice to generate KitcopGFP/+;Lepob/+ mice. KitcopGFP/+;Lepob/+ heterozygote mice were backcrossed to generate KitcopGFP/+;Lepob/ob mice. Mir-10bLacZ-FLP-lox/+ mice were crossed with KitCreERT2/+ mice or Rosa26FLP/+ mice to generate KitCreERT2/+;mir-10bLacZ/LacZ (resulting in Kit¬ cell-specific mir-10b KO following tamoxifen injection and mir-10b WT following oil injection) mice and Rosa26FLP/+;mir-10blox/lox mice. Rosa26FLP/+;mir-10blox/lox mice were further crossed with KitCreERT2/+ mice to generate KitCreERT2/+;10blox/lox (resulting in Kit¬ cell-specific mir-10b KO following tamoxifen injection and mir-10b WT following oil injection) mice. Genotypes were confirmed through PCR. All primer sequences used can be found in Supplementary Table 4. mir-10bLacZ-FLP-lox/lox mice were crossbred with KitCreERT2/+ mice or Rosa26FLP/+ mice to generate KitCreERT2/+;mir-

10bLacZ/LacZ or KitCreERT2/+;10blox/lox mice. Rosa26tdTom and Rosa26DTA mice were crossbred with KitcreERT2/+ to generate KitcreERT2/+;Rosa26tdTom/+ or KitcreERT2/+;Rosa26DTA/+ mice. For the inducible studies, tamoxifen (Sigma-Aldrich) injections (1.0 mg/20g body weight daily) were given intraperitoneally for 5 consecutive days to 4-6 weeks old male and female mice to activate Cre activity. The control groups were given the same volume of sunflower oil (Sigma-Aldrich). Due to mouse genetic inheritance, the analysis was compiled from age-matched males and females from multiple litters. The colony of mice was housed in a centralized animal facility at the University of Nevada, Reno (UNR) Animal Resources. The animal protocol was approved by the Institutional Animal Care and Use Committee at the UNR Animal Resources. UNR is fully accredited by AAALAC International. Animals were air freighted to UNR, where they were housed in the transgenic facility at UNR, School of Medicine. All mice were housed under pathogen-free conditions on a 12 hrs light/dark cycle with food and water ad libitum. Mice were euthanized by inhaling CO2, followed by cervical dislocation. A ventral midline incision was made, and the whole GI tract was carefully excised. These procedures were in accordance with National Institutes of Health guidelines for the care and use of laboratory animals.

Human Specimens:

The research participants included in this study were adults 21-65 years of age (Supplementary Table 2). Cases were defined as patients that had been diagnosed by the Stanford Hospital and Clinics with gastroparesis after an upper GI endoscopy. Gastroparesis was confirmed based on well-accepted symptom criteria and delayed gastric emptying, defined as gastric retention of >10% at 4 hrs and/or >60% at 2 hrs when using the standard low fat, scrambled egg meal as described by Tougas.8, 9 Additionally, controls were defined as age-matched adults who underwent upper GI endoscopy, did not have a history of functional GI disorders, and did not experience symptoms such as abdominal pain, nausea, or vomiting. Subjects were excluded if they were actively using opiates, were found to have a recent or new diagnosis of Helicobacter pylori gastritis, or had active peptic ulcer disease according to endoscopy. Venous blood samples were collected into sodium heparin-containing vacutainer tubes (BD) by routine venipuncture. Plasma

was obtained from the tube supernatants after 10 min of ultracentrifugation (800 g) at room temperature, aliquoted, and frozen at -80°C until further use. All experiments with idiopathic and diabetic gastroparesis and control plasma samples and GCSI-dd were obtained from Stanford University School of Medicine. All human subjects provided informed consent, and all study procedures were approved by the Stanford University Institutional Review Board, and the Institutional Review Board at UNR. The human samples were obtained from 2 patients with diabetic gastroparesis (DGs), 14 patients with idiopathic gastroparesis (IGs), and 18 healthy controls (HCs).

Fluorescence-Activated Cell Sorting (FACS):

Interstitial cells of Cajal (ICCs) from the jejunum and colon of age-matched diabetic KitcopGFP/+;Lepob/ob (n=30) and healthy KitcopGFP/+;Lep+/+ WT mice (n=20) were isolated through FACS based on copGFP (KIT) expression as previously described.10 Each ICC group was pooled for the isolation of small RNAs.

Isolation of Small RNAs:

Blood (murine whole blood used for qPCR and human plasma used for miRNA sequencing and qPCR), jejunal, colonic, and pancreatic tissues were placed in Lysis/Binding buffer from the mirVana miRNA Isolation Kit (Ambion) and homogenized via bead beating in an air-cooled bead homogenizer (Bullet Blender Storm, Next Advance, Inc.). Isolated ICCs were centrifuged at 3,000 rpm for 5 min and directly lysed in Lysis/Binding buffer without bead beating. Small RNAs were isolated using the mirVana miRNA Isolation Kit as previously described.11 Extracted small RNAs were used for quantitative PCR (qPCR) or miRNA sequencing.

miRNA Sequencing:

Small RNA libraries were generated using an Illumina TruSeq Small RNA Preparation Kit (Illumina) according to the manufacturer’s instructions. The cDNA libraries were sequenced via Illumina GAIIx (Illumina) following the vendor’s instructions (LC Sciences). Sequence reads were extracted from the image files using Illumina’s Sequencing Control Studio software version 2.8

(SCS v2.8) following real-time sequencing image analysis and base-calling with Illumina's Real-Time Analysis version 1.8.70. A proprietary pipeline script, ACGT101-miR v4.2 (LC Sciences), was used for sequencing data analysis. All miRNAs were annotated from pre-miRNA and mature miRNA sequences listed in the latest (2019) release of miRbase.12 Comparative analysis of miRNA expression profiles was used for murine and human diabetic and/or idiopathic gastroparesis miRNAs and healthy control miRNAs after normalization to the total number of miRNAs.

Reverse Transcription Quantitative Polymerase Chain Reaction (RT-qPCR):

RNA quality and quantity were evaluated using a Nanodrop 2000 Spectrophotometer (Thermo Fisher Scientific), then RNAs were polyadenylated using Poly(A) Polymerase (Ambion) followed by reverse transcription using SuperScript IV Reverse Transcriptase (Thermo-Fisher). Thereafter, a TaqMan probe-based qPCR assay (Applied Biosystems) was performed. The following TaqMan Advanced MicroRNA Assay probes were used: hsa-miR-10b-5p (Gene ID: MI0000267) and mmu-snoRNA420 (Gene ID: AF357339). A standard qPCR protocol was followed on a 7900HT Fast Real-Time PCR System (Applied Biosystems). The comparative cycle threshold method was used to compare relative transcription levels. The transcription level of each miRNA was estimated as the relative fold-change over the control small nucleolar RNA (snoRNA) genes.11 All samples were run in triplicate for each assay.

Automated Western Blot:

Blood (murine whole blood and human plasma), murine stomach, jejunal, colonic, and pancreatic tissues were placed on ice for 5 min and then extracted with Pierce RIPA Buffer (Thermo-Fisher). The homogenates were then centrifuged at 12,000 rpm at 4°C for 20 mins, then supernatants were stored at -80°C. A Bradford assay was used to determine protein concentrations, and equal protein amounts (1 µg) were loaded for protein assay separation. Automated Western blots were performed using WES (ProteinSimple) on isolated blood, pancreas, stomach, jejunum, and colon samples from mice, as well as human blood samples. Quantification of banding patterns was performed using Compass software (v4.0.0) for WES (ProteinSimple).

Quantification of banding patterns was performed using Compass software (v4.0.0). All antibodies used are listed in Data Supplementary Table 5.

Immunohistochemical and Confocal Microscopy Analysis:

Murine stomach, jejunum, colon, and pancreas tissue were analyzed through whole mount and cryostat section staining. Slides were exposed to 1x Tris-buffered saline (TBS), followed by blocking in 4% milk/1x TBS/0.1–0.5% Triton X-114 (Sigma-Aldrich). The slides were then incubated at 4°C with primary antibody for 48 hrs. Next, the slides were incubated with a secondary antibody at room temperature for 2 hrs. After washing with 1x TBS and treated with Fluoroshield mounting medium with DAPI (Abcam). Images were collected using Fluoview FV10-ASW (Olympus) Viewer software (v3.1) on an Olympus FV1000 confocal laser scanning microscope. All antibodies used are listed in Supplementary Table 5.

Body Weight and Blood Glucose Measurements:

Body weight was monitored at the same time of day, once every week. Fasting blood glucose monitoring was performed in mice fasted for 6 hrs by collecting blood from the tail vein via a small needle prick using a blood glucose monitoring system on a weekly basis (ReliOnTM Prime). Mice were considered healthy (90–120 mg/dL), prediabetic (>120 to <180 mg/dL) or diabetic (≥ 180 mg/dL) based on 6 hrs fasting blood glucose levels. Blood glucose levels exceeding 500 mg/dL were considered the upper limit of the hyperglycemic state. Following established sub-therapeutic dosing procedures for insulin glargine [rDNA origin] injection (Lantus, Sanofi-Aventis), intraperitoneal injections via a 25-G needle were used when glucose levels were higher than 500 mg/dL to keep the diabetic mice alive.13 Additionally, diabetic mice were monitored to ensure that their glucose levels were below 500 mg/dL to prevent complications from the diabetic phenotype. For animal welfare purposes, mice showing two consecutive readings of 500 mg/dL or more over 48 hrs were euthanized.

Metabolic Procedures:

Glucose tolerance tests (GTTs) and insulin tolerance tests (ITTs) were conducted to confirm the onset of diabetes. For GTTs, intraperitoneal injections of glucose (Sigma-Aldrich) at a dose of 2 g/kg body weight were administered to mice fasted for 6 hrs. Then, blood glucose monitoring was performed on blood collected from the tail vein by a small needle prick using a blood glucose monitoring system (ReliOnTM Prime) before glucose injection (0 min) and at 15, 30, 60, 90, and 120 min after injection. ITTs were performed in mice fasted for 6 hrs through intraperitoneal injection of insulin glargine (0.75 IU/kg, Sanofi-Aventis). Blood glucose concentration was measured in blood collected from the tail vein by a small needle prick before insulin injection (0 min) and 30, 60, 90 and 120 min after insulin injection.

The area under curve (AUC) analysis for GTTs and ITTs were performed using GraphPad Prism. We presented the data for GTTs and ITTs with percentages of basal glucose, and the AUC for GTT and ITT was calculated with the area above baseline glucose and the area below baseline glucose, respectively, for each group of mice.14 For the comparison of AUC between the groups, we performed a two-way ANOVA analysis.

In Vivo Functional GI Tests:

The gastric emptying test (GET), total GI transit time (TGITT) test, and colonic transit time (CTT) test were performed on mice in vivo to evaluate changes in GI motility. For GETs, the gastric emptying of semi-solids and/or liquids was observed using the fluorescent imaging agent GastroSenseTM750 (a near-infrared fluorescent imaging agent used to monitor and quantify gastric emptying rates in murine models in vivo in real time) and an IVIS Lumina III system (PerkinElmer). GETs were performed on mice fasted overnight, which allows the stomach to empty the entirety of its food contents. IVIS fluorescence gastric imaging of each mouse was performed before ingestion of GastroSenseTM750 to ensure that there was no autofluorescence. Next, each mouse was given intragastric gavaged with 0.250 nmol GastroSenseTM750 mixed with crushed solid food in 1X Phosphate buffered saline (PBS) or 1X PBS solution. Fluorescence datasets were acquired by imaging the gastric region both before gavaging (0 min) and 15, 30, 45, 60, 90 and 120

min after intragastric gavage. After fluorescence imaging of each mouse, fluorescence in the stomach was measured using Living Image (PerkinElmer) software (v4.5.5). Percentage gastric emptying after 30 min in each mouse was quantified as: [1 - (stomach fluorescence/total fluorescence) × 100].15 For TGITT, mice fasted overnight were orally gavaged with 0.1 ml of a semiliquid solution containing 5% Evans blue in 0.9% NaCl and 0.5% methylcellulose. TGITT was calculated as the time between the intragastric gavage of the dye and the visualization of the first blue fecal pellet.16 For CTT, a 3 mm glass bead was placed in the colon (~3 cm from the anus) of an overnight fasted mouse using a plastic Pasteur pipette lightly lubricated with lubricating jelly. CTT was assessed by measuring the amount of time between bead placement and bead expulsion.16

Fecal Pellet Assessment:

Fecal pellets were collected weekly from each cage and weighed and counted to monitor any changes in defecation patterns (indicating changes in bowel function) of the mice. The cage bedding was replaced with an Alpha Pad (LBS Biotechnology) for the specified collection time (typically 24 hrs). The pellets were removed from the pad, and the mice were placed in a cage with normal bedding. The fecal pellet frequency was the number of pellets produced by one mouse in 24 hrs. The fecal pellet out was calculated as the fecal pellet number multiplied by the weight of the pellets (g) produced by the mouse within 24 hrs.

Ovariectomy Surgery:

Ovariectomy surgery was done on five-weeks-old C57BL/6J female mice weighing between 20-30 g. Surgery was performed in a room dedicated to surgical procedures. Mice were anesthetized with a mixture of isoflurane (5%) and oxygen (100-200 mL/min) until recumbent. During surgery anesthesia was delivered through a nosecone with 2-3% isoflurane and oxygen throughout the length of the procedure. Before the surgery start mice were injected pain medicine (Buprenorphine, 1 µg/g of body weight) intraperitonially away from the incision site. After completion of the procedure, mice received gentamicin (0.5mg/100 g body weight; 150 µL per 20-30 g mouse

body weight) by IP injection and mice were placed into a recovery cage with thermal support and monitored closely until fully recovered. Surgery protocol was approved by the Institutional Animal Care and Use Committee at the UNR Animal Resources.

Ingenuity Pathway Analysis:

Pathway analysis was performed on target gene candidates using the Ingenuity Pathway Analysis (IPA) program (Qiagen, http://www.ingenuity.com).17 Our target genes were those that had published evidence of a link to diabetes mellitus and an interaction with miR-10b-5p and KLF11. Within IPA, a network was graphically depicted to show gene relationships pertaining to diabetes mellitus, miR-10b-5p and KLF11. The IPA map was generated using experimentally validated targets" of miR-10b-5p. According to IPA, IPA's microRNA Target Filter functionality enables prioritization of experimentally validated and predicted mRNA targets. The microRNA Target Filter in IPA provides insights into the biological effects of microRNAs, using experimentally validated interactions from TarBase and miRecords, as well as predicted microRNA-mRNA interactions from TargetScan. Additionally, IPA includes a large number of microRNA-related findings from the peer-reviewed literature. We selected "experimentally validated targets", but not predicted mRNA targets in the IPA.

Construction of Luciferase Reporter and Klf11 Expression Plasmids:

For the generation of the luciferase reporter constructions, the miR-10b-hKLF11, miR-10b-mKlf11, miR-10b-mKlf11-mut, and scrambled complementary oligonucleotide were synthesized (IDT). The luciferase vector (pLenti-CMV-Luc-Puro, Addgene) was digested with XbaI. Each annealed oligonucleotide was ligated to the pLenti-CMV-Luc-Puro individually to make pLenti-CMV-Luc-10b-hKLF11, pLenti-CMV-Luc-10b mKlf11, pLenti-CMV-Luc-10b-mKlf11-mut, and pLent-CMV-Luc-scrambled construct. The mKlf11 cDNA (1655 bp, NM_178357.3) and hKLF11 (1685 bp, NM_003597.5), with restriction enzyme sites PshAI and XbaI were synthesized and inserted in pUC57 vectors (BioMatik). The pLenti-CMV-Luc-Puro, mKlf11-pUC57, and hKLF11-pUC57 were digested with PshAI and XbaI. Then pLenti-CMV-hKLF11 and pLenti-CMV-mKlf11

expression construct were generated by individual ligations. All the vectors were confirmed by Sanger sequencing at the Nevada Genomics Center (UNR).

Cell Culture and Stable Cell Line Generation:

The human and mouse cell lines HEK293T and NIH3T3, Panc 10.05, and NIT-1 (ATCC) were maintained at 37°C under 5% CO2 in DMEM or Ham's F-12K (Kaighn's) Medium (Gibco) supplemented with 10% heat-inactivated FBS (Gibco) and antibiotic-antimycotic (penicillin, streptomycin, amphotericin B, Gibco). Human and mouse cells were plated in 24-well plates 24 hrs before transfection and reached 80-90% confluency before transfection. Approximately 2.0 × 105 cells in each well were selected for transfection with pLenti-CMV-Luc-10b-hKLF11, pLenti-CMV-Luc-10b mKlf11, pLent-CMV-Luc-10b-mKlf11-mut, or pLent-CMV-Luc-scrambled (500 ng each) using Lipofectamine 2000 (Invitrogen) in accordance with the manufacturer's protocol. 24 hrs after transfection, the plated cells were incubated with fresh medium and a selective marker (2 mg/ml puromycin) for 24 hrs.

Transfection with RNA and Luciferase Reporter Assay:

The human and mouse cell lines were transfected with miR-10b mimic, miR-10b inhibitor, a mix of mouse siKlf11-1/2, a mix of human siKLF11-1/2, or a scrambled RNA (all, Thermo Fisher Scientific), at a final concentration of 50 nM. 48 hrs after transfection, KLF11 protein levels were detected through a WES (ProteinSimple) automated Western blot in each group. All cell transfections were performed using Lipofectamine RNAiMAX (Invitrogen) in accordance with the manufacturer’s instructions. Luciferase activity was determined using a TurboLuc Luciferase One-Step Glow Assay Kit (Thermo Fisher Scientific).

In vivo Delivery of MiRNA Mimic and silKF11:

Mice were grouped into either treatment or control groups and intraperitoneally injected with a chemically synthesized miR-10b mimic or mirVana miRNA mimic negative control and a mix of mouse siKLF11-1/2 (Thermo Fisher Scientific). In vivo-jetPEI (Polyplus-transfection) was used

as the delivery agent. In vivo-jetPEI/miRNA complexes were prepared according to the manufacturer's protocol, as previously described.18 Intraperitoneal injections were performed on mice using complexes equilibrated at room temperature.

Diet:

The mice were fed one of two purified Teklad diets, ad libitum, from ENVIGO: a purified control diet (TD.08806) containing 20.5% kcal from protein, 10.5% kcal from fat, and 69.1% kcal from carbohydrates; or a high-fat, high-sucrose diet (representative western diet) (TD.130784) containing 14.7% kcal from protein, 44.6% kcal from fat, and 40.7% kcal from carbohydrates.

ELISA:

Insulin, C-peptide, A1C and estrogen measurements were gathered from both mouse whole blood or serum and human plasma. The blood was centrifuged for 40 min at 2,000 rpm (4°C). Serum was collected and stored at -80°C. ELISAs were performed on blood serum using an Insulin ELISA Kit (Millipore), human and mouse C-Peptide ELISA Kit (Crystal Chem), Hemoglobin A1C (HbA1c) ELISA Kit (Crystal Chem) and Estradiol (mouse) ELISA kit. All kits were used according to the manufacturer's protocol.

Drug Comparison Study:

For the drug comparison study, male C57 mice were fed a high-fat, high-sucrose diet (HFHSD, (TD.130784) or a purified control normal diet (ND, TD.08806) for 4 months. Before the treatment start date HFHSD induced diabetic mice were confirmed for diabetic onset and GI dysmotility as compared to age matched healthy controls. At this point, the mice were divided into nine groups (n=5-8) and placed in separate cages with free access to HFHSD or ND and water. miR-10b mimic, or scramble RNA (Thermo Fisher Scientific) were injected twice, at 1 and 2 weeks by intraperitoneal injections (In vivo-jetPEI/miRNA complexes); Metformin (Ascend Laboratories, LLC) or Sitagliptin (Januvia, Merck) was provided daily per oral for 4 weeks; Liraglutide (Victoza, Novo Nordisk) was injected twice daily by subcutaneous injection for 2 weeks; Insulin (Lantus,

Sanofi-Aventis) was injected once daily by intraperitoneal injection for 4 weeks; Prucalopride (Motegrity, Takeda) was provided daily PO for 4 weeks as per IACUC approved protocol for doses and route of administration (Supplementary Table 6).

Mice were monitored for body weight and fasting blood glucose levels once every week, GTT, ITT, TGITT, GET, and CTT were performed once every 4 weeks over the 8 weeks study duration. Also, data was collected for other metabolic parameters (food, calorie, and water intake as well as urine and fecal output) during the dosing period using single housed metabolic cages (Tecniplast). For the metabolic data collection, mice were acclimated to the metabolic cages for three days prior to data collection. Each mouse was checked at least twice daily for behavioral signs of distress (e.g. excessively increased or decreased activity, reduced food or water intake, and hunched posture).

Statistics:

The experimental data are shown as the mean ± SEM. The data presented in the figures were collected from multiple independent experiments performed on different days using age-matched mice with both genders unless otherwise mentioned. Two-tailed unpaired t-test, area under the curve calculations, and one-way or two-way analysis of variance (ANOVA) with corrections for multiple comparisons were used for all mouse experiment comparisons. GraphPad Prism (v8.0) (GraphPad Software) was used for statistical analyses. For all tests, p-values less than 0.05 were considered statistically significant.

Data availability:

miRNA-seq data can be found in Supplementary Table 1 and 3. The miRNA-seq data from this study have been deposited to the NCBI GEO under accession number: GSE139577, miRNA sequencing profile of human plasma samples from healthy, diabetic, and gastroparesis patients (GSM4143924-GSM4143931), and GSE139577, miRNA sequencing profile of isolated Kit+ interstitial cells of Cajal (ICC) in Leptin mutant mice (GSM4143932-GSM4143935).

Supplementary References

1. Ro S, Park C, Jin J, et al. A model to study the phenotypic changes of interstitial cells of Cajal in gastrointestinal diseases. Gastroenterology 2010;138:1068-78 e1-2.
2. Ingalls AM, Dickie MM, Snell GD. Obese, a new mutation in the house mouse. J Hered 1950;41:317-8.
3. Klein S, Seidler B, Kettenberger A, et al. Interstitial cells of Cajal integrate excitatory and inhibitory neurotransmission with intestinal slow-wave activity. Nat Commun 2013;4:1630.
4. Brown SD, Moore MW. Towards an encyclopaedia of mammalian gene function: the International Mouse Phenotyping Consortium. Dis Model Mech 2012;5:289-92.
5. Raymond CS, Soriano P. High-efficiency FLP and PhiC31 site-specific recombination in mammalian cells. PLoS One 2007;2:e162.
6. Madisen L, Zwingman TA, Sunkin SM, et al. A robust and high-throughput Cre reporting and characterization system for the whole mouse brain. Nat Neurosci 2010;13:133-40.
7. Ivanova A, Signore M, Caro N, et al. In vivo genetic ablation by Cre-mediated expression of diphtheria toxin fragment A. Genesis 2005;43:129-35.
8. Camilleri M, Parkman HP, Shafi MA, et al. Clinical guideline: management of gastroparesis. Am J Gastroenterol 2013;108:18-37; quiz 38.
9. Tougas G, Eaker EY, Abell TL, et al. Assessment of gastric emptying using a low fat meal: establishment of international control values. Am J Gastroenterol 2000;95:1456-62.
10. Lee MY, Ha SE, Park C, et al. Transcriptome of interstitial cells of Cajal reveals unique and selective gene signatures. PLoS One 2017;12:e0176031.
11. Park C, Hennig GW, Sanders KM, et al. Serum response factor-dependent MicroRNAs regulate gastrointestinal smooth muscle cell phenotypes. Gastroenterology 2011;141:164-75.

12. Kozomara A, Birgaoanu M, Griffiths-Jones S. miRBase: from microRNA sequences to function. Nucleic Acids Res 2019;47:D155-D162.

13. Choi KM, Gibbons SJ, Sha L, et al. Interleukin 10 Restores Gastric Emptying, Electrical Activity, and Interstitial Cells of Cajal Networks in Diabetic Mice. Cell Mol Gastroenterol Hepatol 2016;2:454-467.

14. Ayala JE, Samuel VT, Morton GJ, et al. Standard operating procedures for describing and performing metabolic tests of glucose homeostasis in mice. Dis Model Mech 2010;3:525-34.

15. McCann CJ, Cooper JE, Natarajan D, et al. Transplantation of enteric nervous system stem cells rescues nitric oxide synthase deficient mouse colon. Nat Commun 2017;8:15937.

16. Anitha M, Reichardt F, Tabatabavakili S, et al. Intestinal dysbiosis contributes to the delayed gastrointestinal transit in high-fat diet fed mice. Cell Mol Gastroenterol Hepatol 2016;2:328-339.

17. Kramer A, Green J, Pollard J, Jr., et al. Causal analysis approaches in Ingenuity Pathway Analysis. Bioinformatics 2014;30:523-30.

18. Nezami BG, Mwangi SM, Lee JE, et al. MicroRNA 375 mediates palmitate-induced enteric neuronal damage and high-fat diet-induced delayed intestinal transit in mice. Gastroenterology 2014;146:473-83 e3.

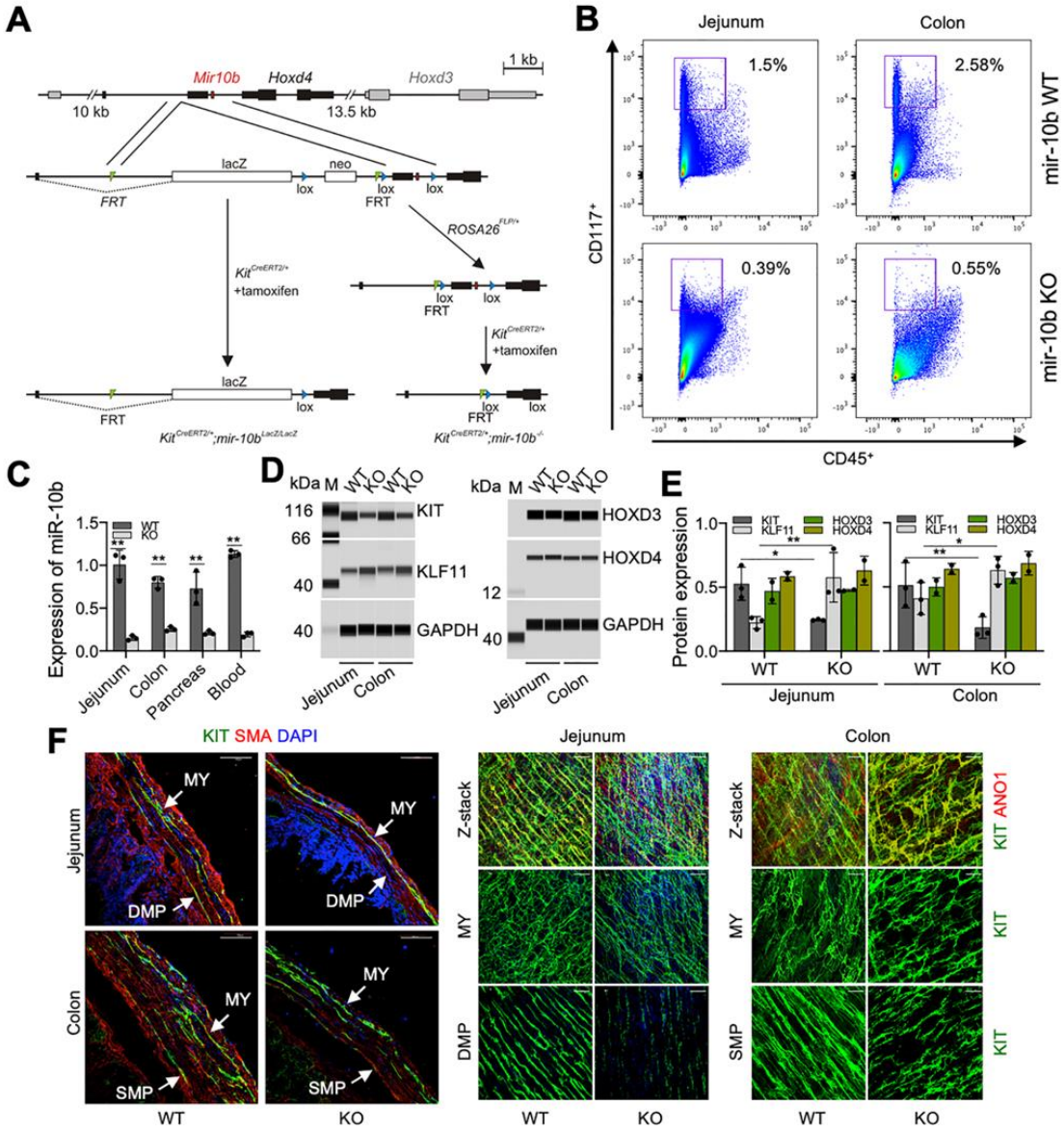

Supplementary Figure 1. Male KIT+ cell-specific mir-10b KO mice have reduced KIT expression in ICCs. (A) Genomic map of tamoxifen-inducible KitCreERT2/+;mir-10bLacZ/LacZ and KitCreERT2/+;mir-10b-/- mice. The mir-10b gene, generating mature miR-10b-5p, is located within the fifth intron of Hoxd4, which also overlaps with the first intron of Hoxd3. The mir-10bLacZ/+ mouse was crossed with the KitCreERT2/+ mouse to generate KitCreERT2/+;mir-10bLacZ/LacZ mice and the Rosa26FLP/+ mouse to generate Rosa26FLP/+;mir-10blox/lox mice, respectively. The Rosa26FLP/+;mir-10blox/lox mouse was further crossed with the KitCreERT2/+ mouse to

generate KitCreERT2/+;mir-10blox/lox mice. Both KitCreERT2/+;mir-10bLacZ/LacZ mice and KitCreERT2/+;mir-10blox/lox mice became KitCreERT2/+;mir-10b-/- mir-10b KO (KO) mice upon tamoxifen injection. (B) Cell number showing a reduction of ICCs (CD117+CD45–) in the jejunum and colon of mir-10b KO mice (n=5). (C) qPCR measurement of miR-10b-5p depletion in mir-10b KO mice (unpaired t-test, n=5). (D, E) Western blot and quantification of proteins regulated by miR-10b-5p (KLF11 and KIT), or of mir-10b host genes (Hoxd3/4) (One-Way ANOVA, n=3). (F) Images of cross sections, whole mount tissue optical stacks (Z-stacks), and separated images (ICC-DMP and ICC-SMP) of jejunal and colonic ICCs (KIT+ANO1+) in tamoxifen-injected mir-10b KO mice compared to oil-injected mir-10b WT (WT) mice (n=3). Scale bars are 50 μm. DMP, deep muscular plexus; SMP, submucosal plexus; MY, myenteric plexus. Error bar indicate SEM. *$p < 0.05$, **$p < 0.01$.

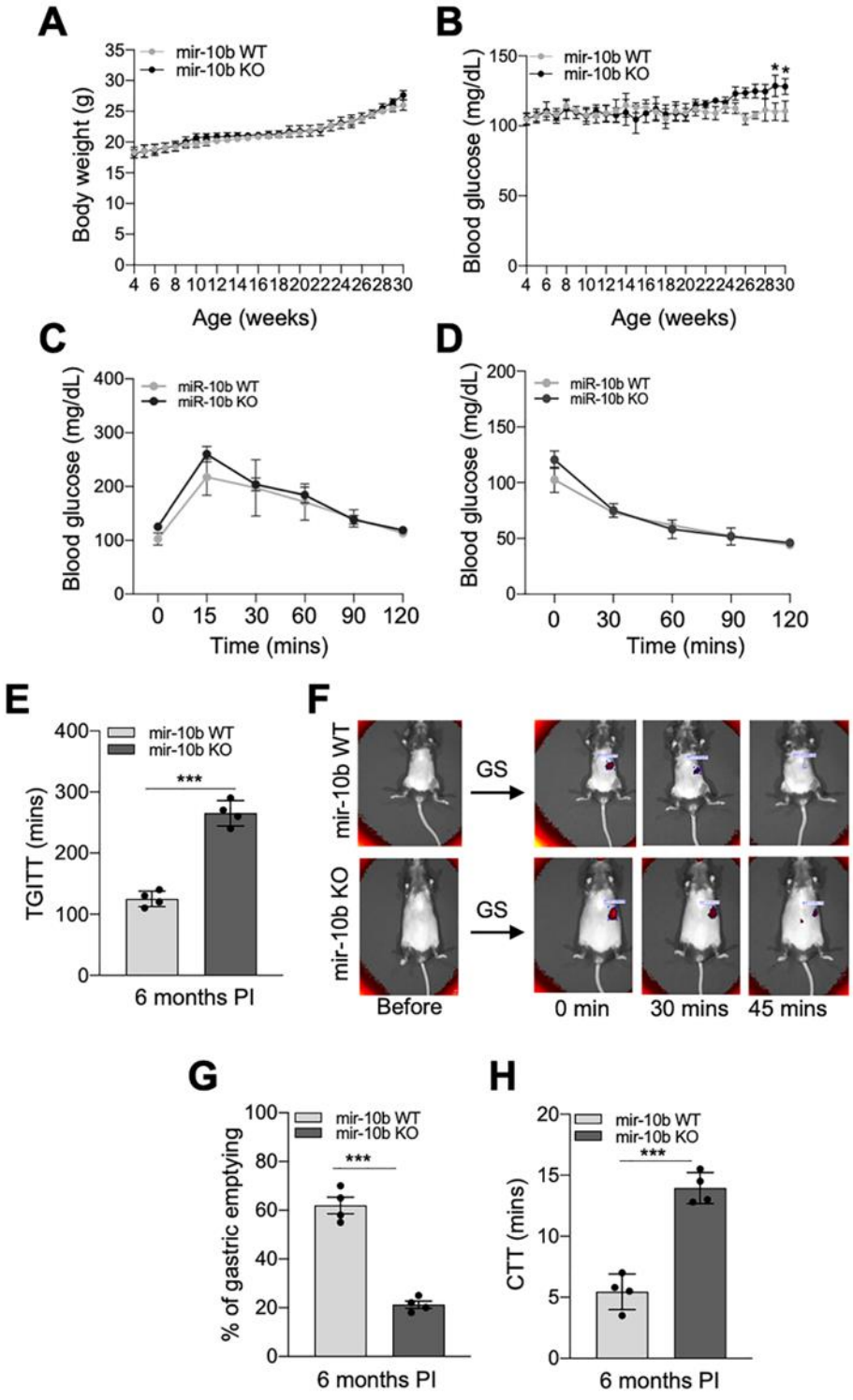

Supplementary Figure 2. Female KIT+ cell-specific mir-10b KO mice develop GI dysmotility but not diabetes. (A, B) Body weight and fasting blood glucose levels of mir-10b KO and WT female

mice (n=4). (C, D) GTT and ITT in mir-10b KO and WT female mice (n=4). (E) TGITT in mir-10b KO and WT female mice at 6 months PTI (n=4). (F) Gastric emptying images of mir-10b KO and WT female mice at 6 months PTI. (G) Quantification of gastric emptying after 30 min (unpaired t-test, n=4). (H) CTT at 6 months PTI (unpaired t-test, n=4). Error bar indicate SEM, Two-way ANOVA. *$p < 0.05$, ***$p < 0.001$.

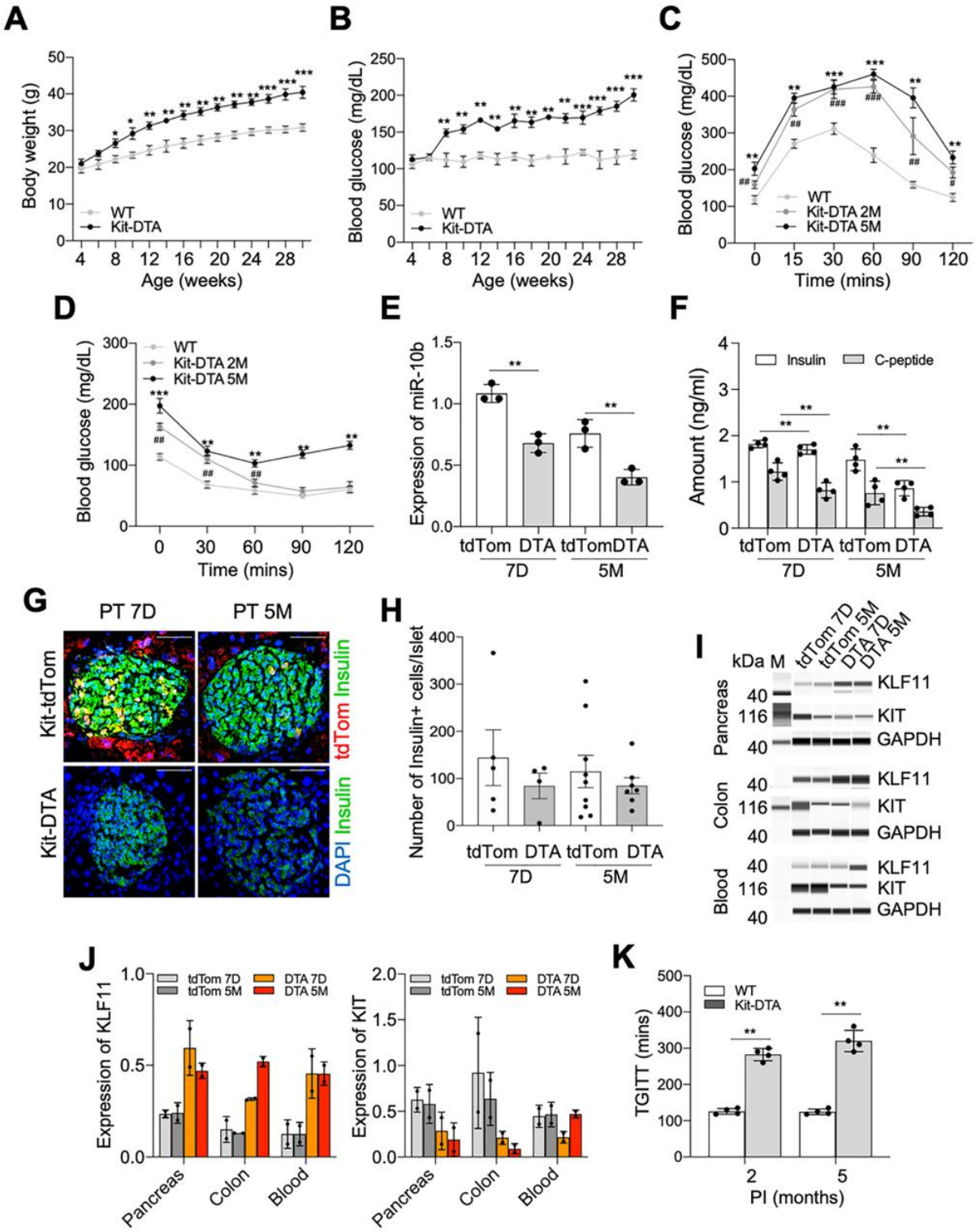
A
Body weight (g)
Age (weeks)
WT
Kit-DTA
B
Blood glucose (mg/dL)
Age (weeks)
WT
Kit-DTA
C
Blood glucose (mg/dL)
Time (mins)
WT
Kit-DTA 2M
Kit-DTA 5M
D
Blood glucose (mg/dL)
Time (mins)
WT
Kit-DTA 2M
Kit-DTA 5M
E
Expression of miR-10b
tdTom DTA tdTom DTA
7D 5M
F
Amount (ng/ml)
Insulin
C-peptide
tdTom DTA tdTom DTA
7D 5M
G
PT 7D
PT 5M
Kit-tdTom
Kit-DTA
tdTom Insulin
DAPI Insulin
H
Number of Insulin+ cells/Islet
tdTom DTA tdTom DTA
7D 5M
I
kDa M
tdTom 7D
tdTom 5M
DTA 7D
DTA 5M
Pancreas
Colon
Blood
KLF11
KIT
GAPDH
J
Expression of KLF11
Expression of KIT
tdTom 7D
tdTom 5M
DTA 7D
DTA 5M
Pancreas
Colon
Blood
K
TGITT (mins)
WT
Kit-DTA
PI (months)

Supplementary Figure 3. Conditional removal of KIT+ cells in male KitCreERT2/+; Rosa26DTA/+ (Kit-DTA) mice leads to development of a diabetic phenotype and slowed GI transit. KitCreERT2/+;Rosa26tdTom/+ (Kit-tdTom) and Kit-DTA mice were injected with tamoxifen at 4 weeks of age. (A, B) Body weight and fasting blood glucose levels comparing Kit-DTA and WT mice from 4 to 30 weeks PTI. (C, D) GTT and ITT in Kit-DTA mice at 2 months and 5 months PTI compared to WT mice. (E) Expression of miR-10b-5p measured by qPCR in Kit-DTA and Kit-tdTom mice at 7 days and 5 months PTI (One-way ANOVA). (F) Amount of insulin and C-peptide in the blood of Kit-DTA and Kit-tdTom mice at 7 days and 5 months PTI measured by ELISA (One-way ANOVA). (G, H) Identification of Kit-tdTom cells and INS+ β cells in the islets of Kit-tdTom mice compared to those of Kit-DTA mice at 7 days and 5 months PTI (One-way ANOVA). Scale bars are 200 μm. (I, J) Western blot and quantification of KLF11 and KIT in the pancreas, colon, and blood of Kit-tdTom and Kit-DTA mice at 7 days and 5 months PTI (One-way ANOVA). (K) TGITT in Kit-DTA mice at 2 and 5 months PTI (unpaired t-test). n=2-4 per condition for each experiment. Error bar indicate SEM, Two-way ANOVA. *$p < 0.05$, **$p < 0.01$, ***$p < 0.001$, #$p < 0.05$, ##$p < 0.01$, ###$p < 0.001$.

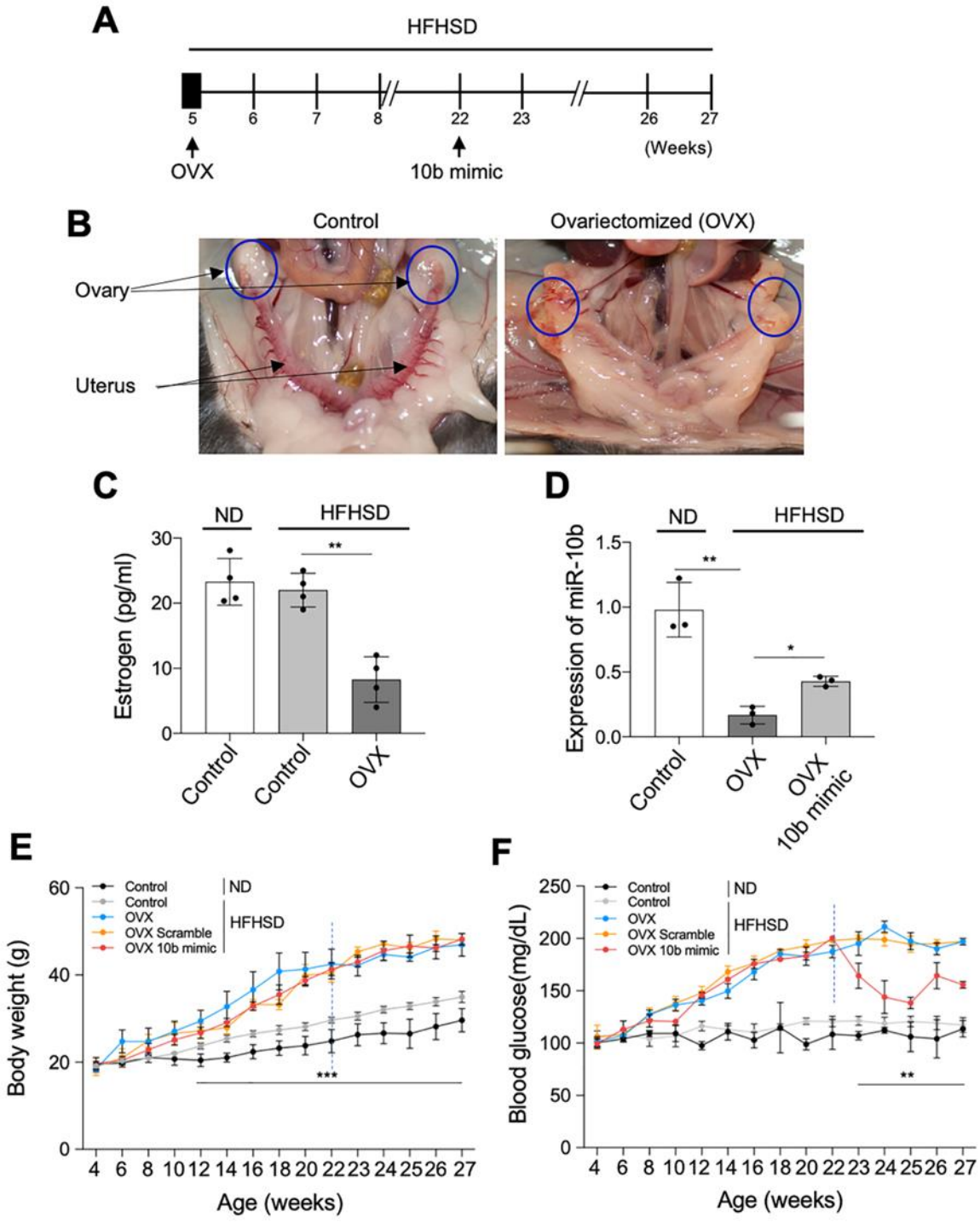

Supplementary Figure 4. miR-10b-5p mimic rescues diabetic phenotype in HFHSD-fed ovariectomized (OVX) female mice. HFHSD-fed diabetic female C57 mice were injected with miR-10b-5p (10b mimic), a negative control (scramble RNA), or given no injection, compared to control

mice. (A) An OVX surgery plan. (B) Ovariectomized and control female mice. (C) Estrogen levels in the blood through ELISA in OVX vs control mice (One-Way ANOVA). (D) miR-10b-5p expression in blood through qPCR in OVX and control mice (One-Way ANOVA). (E, F) Body weight and fasting blood glucose levels of HFHSD-fed OVX and control female. n=3 per condition for each experiment. Error bar indicate SEM, Two-way ANOVA. *$p < 0.05$, **$p < 0.01$.

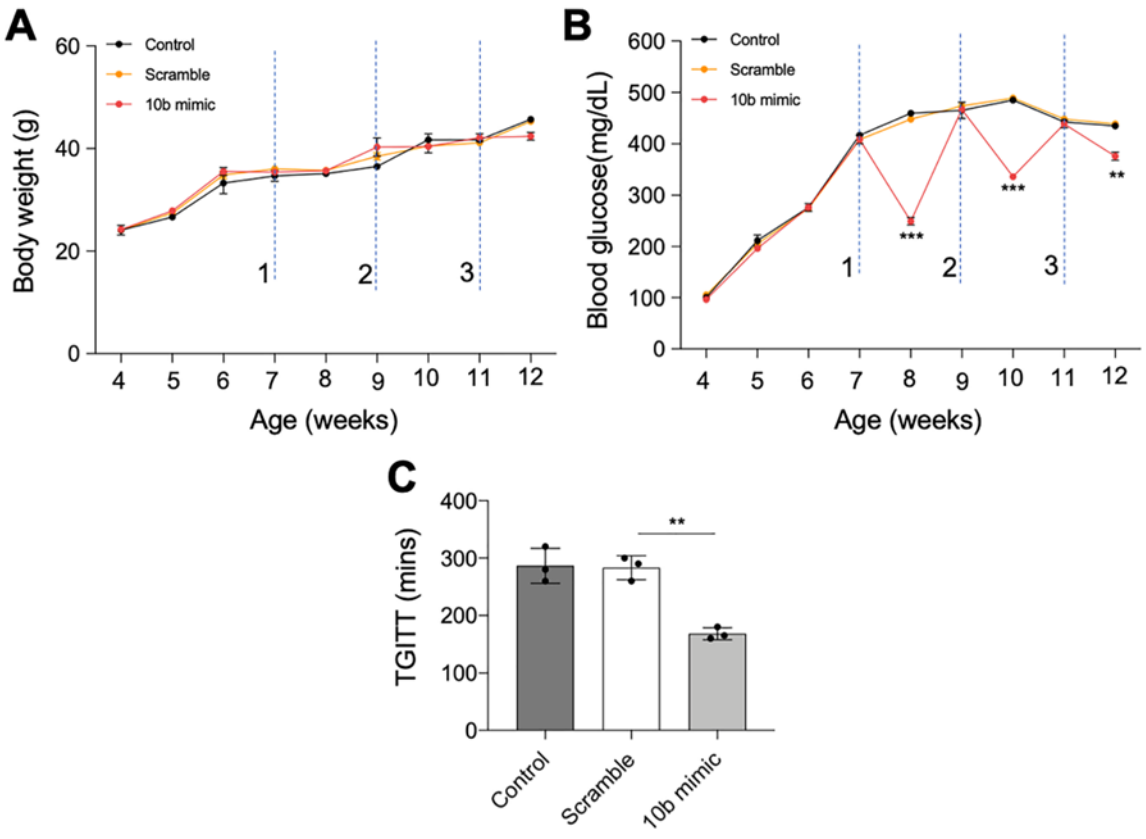

Supplementary Figure 5. miR-10b-5p mimic rescues diabetic and GI dysmotility phenotypes in diabetic ob/ob male mice. Diabetic ob/ob male mice were injected three different times with miR-10b-5p (10b mimic), a negative control (a scramble RNA) compared to diabetic ob/ob mice given no injection. (A, B) Body weight and fasting blood glucose levels comparison (Two-way ANOVA). (C) TGITT comparison. n=3 per condition for each experiment. Error bar indicate SEM, One-Way ANOVA. *p < 0.05, **p < 0.01.

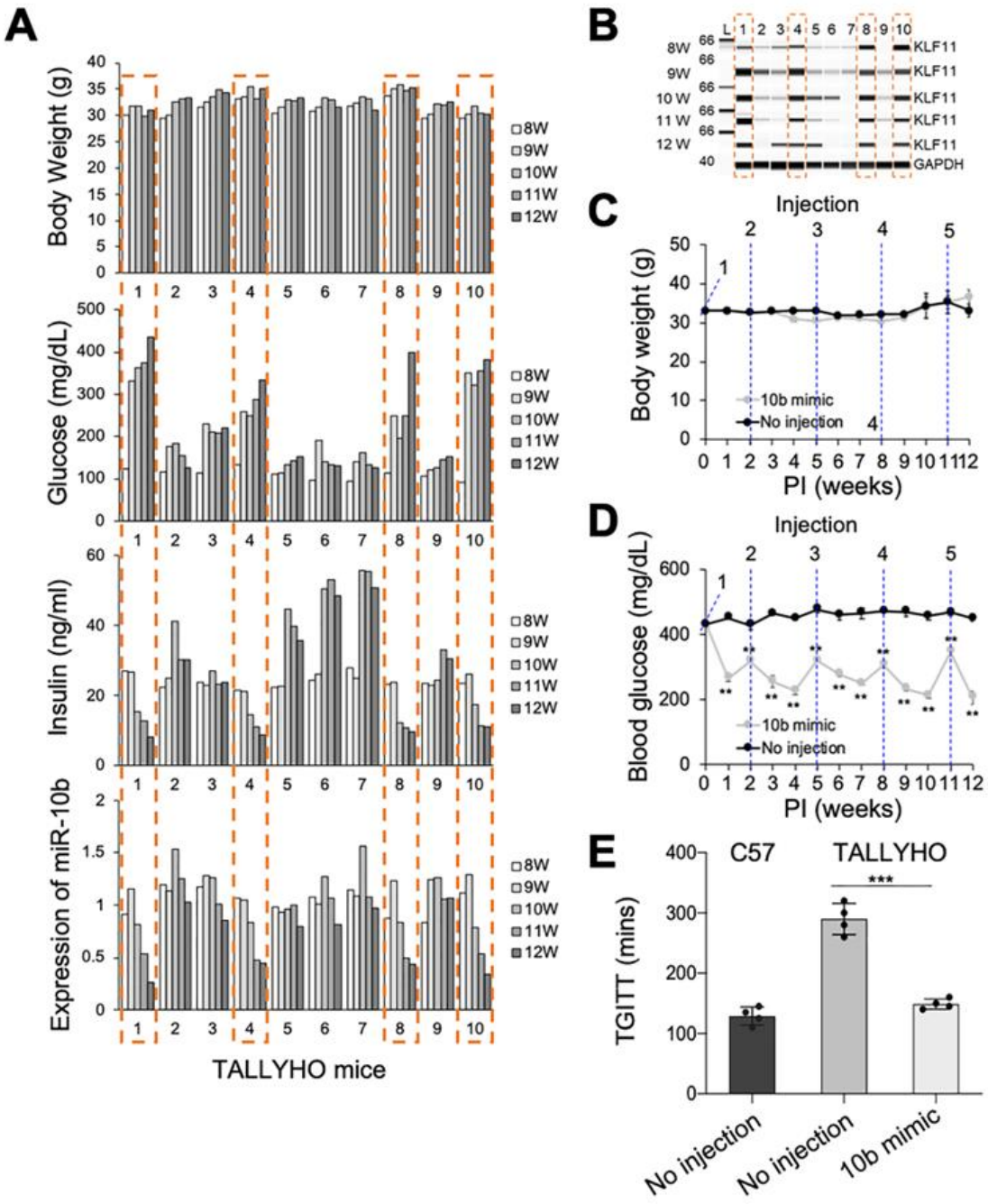

Supplementary Figure 6. miR-10b-5p mimic rescues the diabetic phenotype and slowed GI transit in TALLYHO/Jng (TH) mice (polygenic model for type 2 diabetes). (A) Individual mouse pattern (1-10) of body weight, fasting blood glucose, insulin level and miR-10b expression level in male TH mouse after onset of hyperglycemia at 8 weeks over 12 weeks of age (n=10) (B) Western blot of

KLF11 in the blood of individual TH mouse at 12 weeks (n=10). (C, D) Body weight and fasting blood glucose in diabetic TH mice injected with either the miR-10b-5p mimic or given no injection (Two-way ANOVA, n=4). (E) Total GI transit time in diabetic TH mice injected either the miR-10b-5p mimic or given no injection (One-way ANOVA, n=4). Error bar indicate SEM. *$p < 0.05$, **$p < 0.01$ and ***$p < 0.001$.

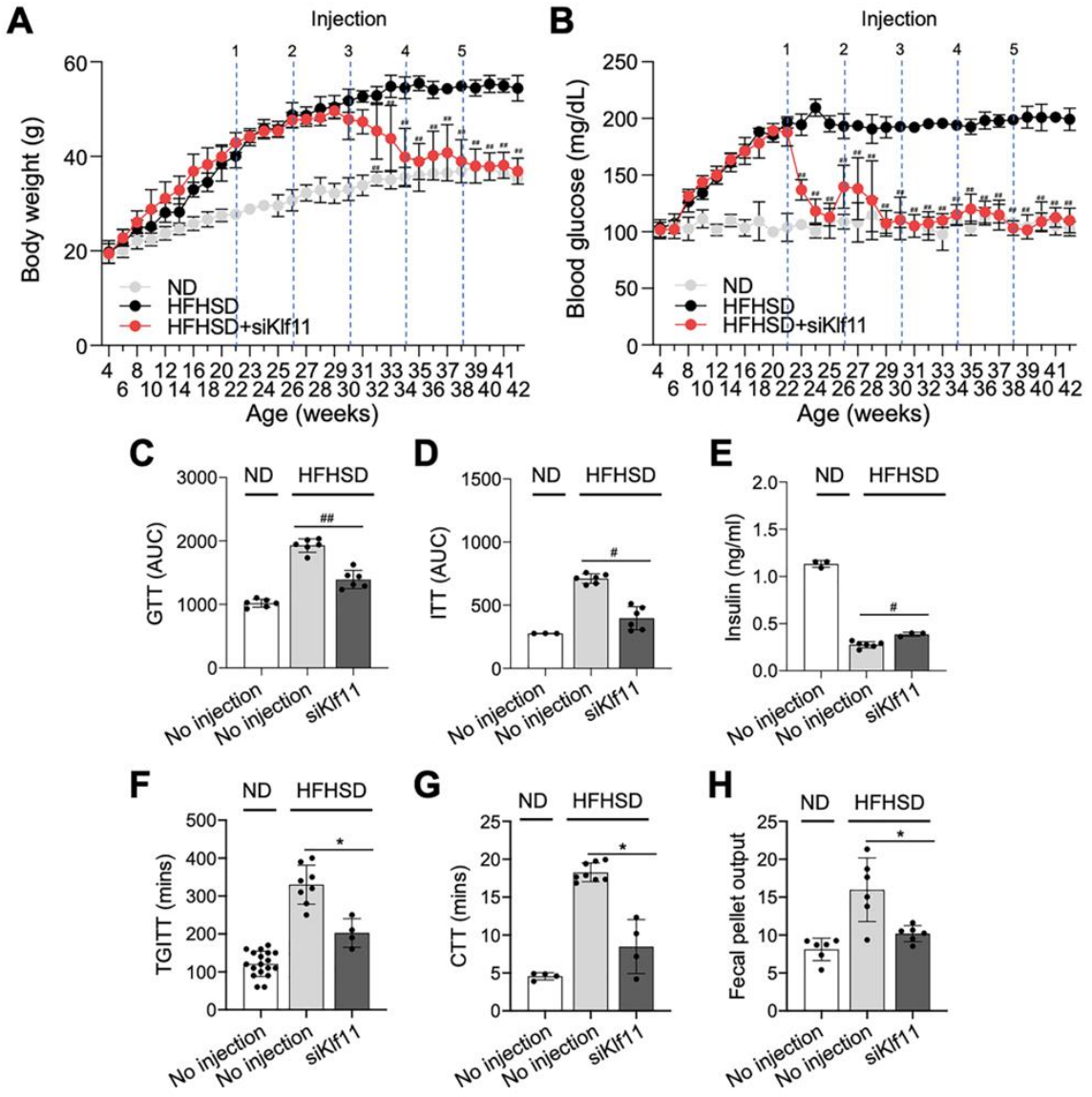

Supplementary Figure 7. siKlf11 rescues the diabetic and obese phenotype in male HFHSD-fed mice. (A, B) Body weight and fasting blood glucose levels comparison in male C57 mice fed a HFHSD or a ND for 18 weeks (4-22 weeks of age) and injected at 22, 26, 30, 34 and 38 weeks (5 injections) with either the siKlf11 mix (siKlf11-1 and siKlf11-2) or given no injection over a 20-week period post-injection (PI) (22-42 weeks of age) (Two-way ANOVA). (C, D) GTT and ITT in C57 mice fed a HFHSD (diabetic) with either the siKlf11 mix or given no injection at 4 weeks PI. (E), Insulin in C57 mice fed a HFHSD (diabetic) with either the siKlf11 mix or given no injection at 4 weeks PI.

(F-H) TGITT, CTT and fecal pellet output C57 mice fed a HFHSD (diabetic) with either the siKlf11 mix or given no injection at 4 weeks PI. n=6 per condition for each experiment. Error bar indicate SEM, One-Way ANOVA. *p < 0.05, #p < 0.05, ##p < 0.01.

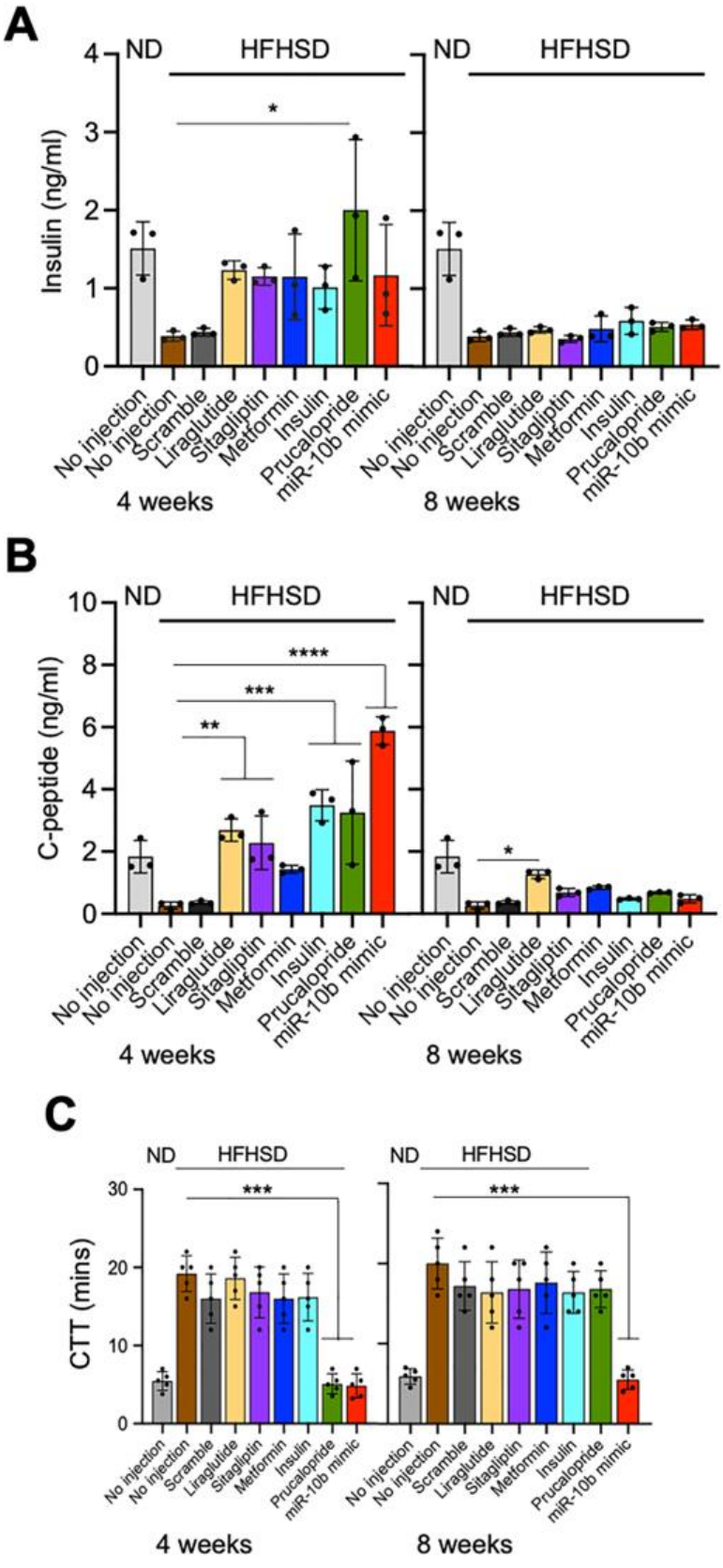
A
ND
HFHSD
ND
HFHSD
Insulin (ng/ml)
*
No injection
No injection
Scramble
Liraglutide
Sitagliptin
Metformin
Insulin
Prucalopride
miR-10b mimic
4 weeks
8 weeks
B
C-peptide (ng/ml)
**
***
****
*
C
CTT (mins)

Supplementary Figure 8. Comparison of blood insulin and C-peptide levels in HFHSD-fed diabetic male mice after treatment of miR-10b-5p mimic, antidiabetic drugs, or a prokinetic drug. (A, B) Comparison of basal insulin and C-peptide levels after 6 hrs of fasting in male mice fed a HFHSD (diabetic) before and after treatment at 4 weeks and 8 weeks with either the miR-10b-5p mimic, a negative control (scramble RNA), liraglutide, sitagliptin, metformin, insulin, prucalopride, or given no injection. ND fed mice given no injection were included as a healthy control (n=3). (C) CTT of male mice fed a HFHSD before and at 4 weeks and 8 weeks after treatment in groups (n=5). Error bar indicate SEM, One-Way ANOVA. **p < 0.01, ***p < 0.001, ****p < 0.0001.

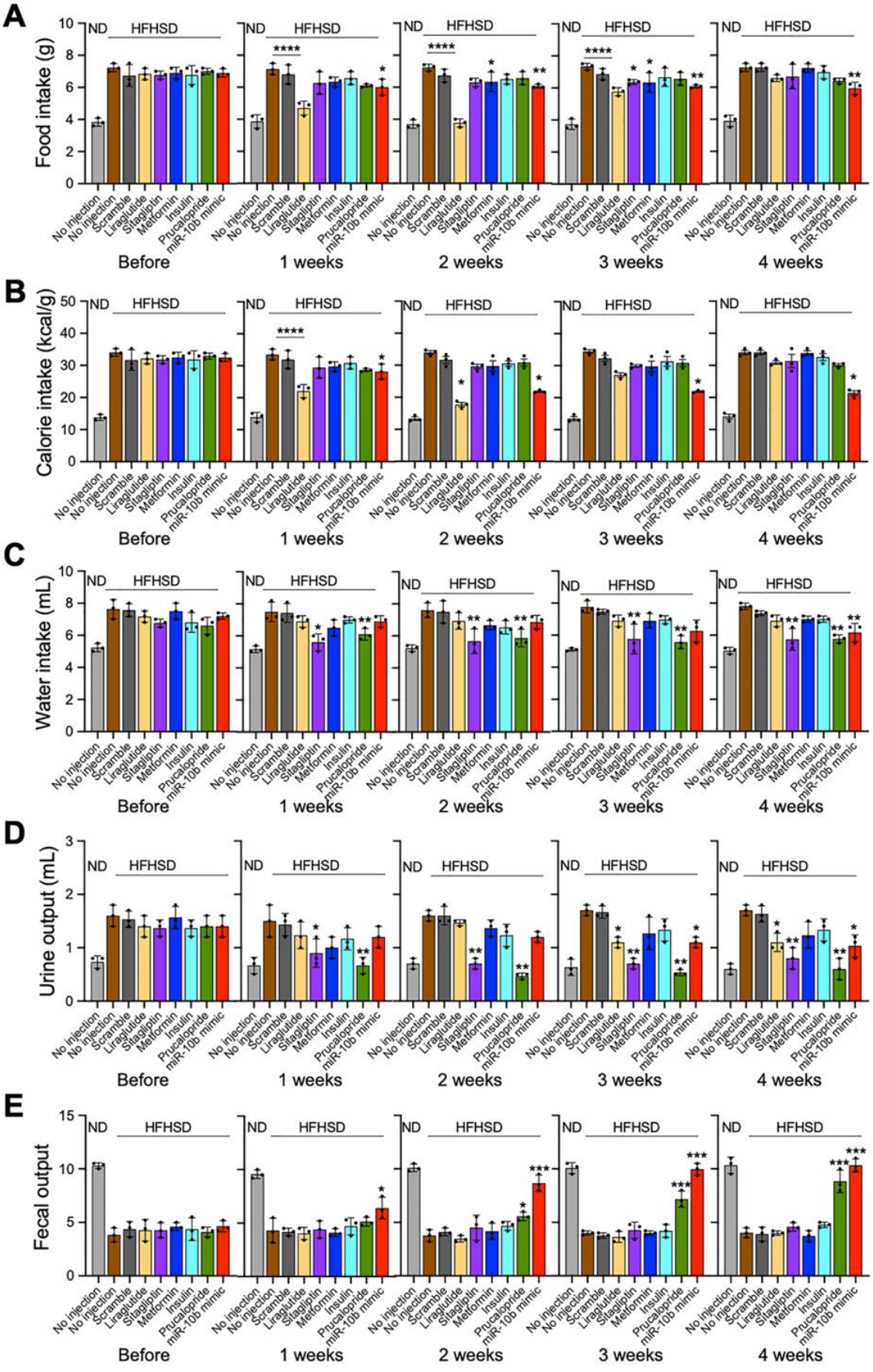
A
Food intake (g)
B
Calorie intake (kcal/g)
C
Water intake (mL)
D
Urine output (mL)
E
Fecal output
ND
HFHSD
Before
1 weeks
2 weeks
3 weeks
4 weeks
No injection
No injection
Scramble
Liraglutide
Sitagliptin
Metformin
Insulin
Prucalopride
miR-10b mimic

Supplementary Figure 9. Comparison of metabolic parameters in male HFHSD-fed diabetic mice treated with miR-10b-5p mimic, antidiabetic drugs, or a prokinetic drug. (A) Daily food intake, (B) Calorie intake, (C) Water intake, (D) Urine output, (E) Fecal output comparison of male HFHSD-fed diabetic mice and injected twice (second injection at 2 weeks) with either the miR-10b-5p mimic, a negative control (scramble RNA), liraglutide, sitagliptin, metformin, insulin, prucalopride, or given no injection, over a 4 weeks period. n=3 per condition for each experiment. Error bar indicate SEM, One-Way ANOVA. *p < 0.05, **p < 0.01, ***p < 0.001, ****p < 0.0001.

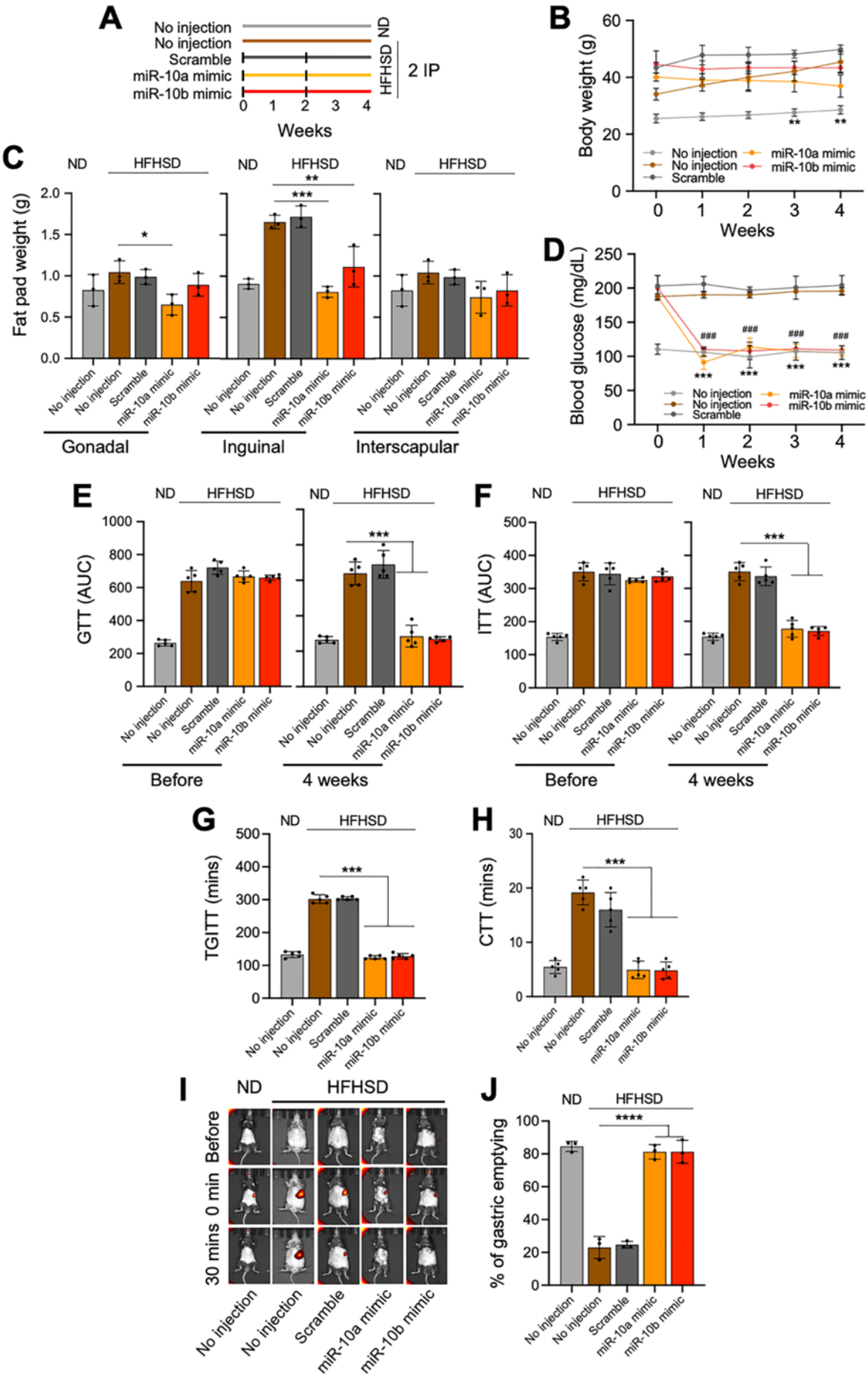
A
No injection
No injection
Scramble
miR-10a mimic
miR-10b mimic
ND
HFHSD
2 IP
0 1 2 3 4
Weeks
B
Body weight (g)
No injection
No injection
Scramble
miR-10a mimic
miR-10b mimic
Weeks
C
ND
HFHSD
Fat pad weight (g)
Gonadal
Inguinal
Interscapular
D
Blood glucose (mg/dL)
Weeks
E
GTT (AUC)
Before
4 weeks
F
ITT (AUC)
Before
4 weeks
G
TGITT (mins)
H
CTT (mins)
I
Before
30 mins
0 min
No injection
No injection
Scramble
miR-10a mimic
miR-10b mimic
J
% of gastric emptying

Supplementary Figure 10. Efficacy comparison of the miR-10b-5p mimic and the miR-10a-5p mimic in HFHSD-fed diabetic C57 male mice on metabolic and GI motility phenotypes. (A) A study design of drug effects in HFHSD-fed diabetic mice or ND-fed healthy mice. miR-10b-5p, or scramble RNA were administered twice, at 0 and 2 weeks by IP injection. (B) Body weight measurements for 4 weeks post injection (Two-way ANOVA, n=5). (C) Comparison of the fat pad weight measurements at 4 weeks post injection (n=3). (D) Fasting blood glucose levels for 4 weeks post injection (Two-way ANOVA, n=5). (E, F) Comparison of AUC for GTT and ITT before and at 4 weeks post injection (n=5). (G, H) TGITT and CTT comparison at 4 weeks post injection (n=5). (I, J) Gastric emptying images and quantification of stomach emptying at 4 weeks post injection (n=3). Error bars indicate SEM, One-Way ANOVA. *p < 0.05, **p < 0.01, ***p < 0.001, ****p < 0.0001, #p < 0.05, ##p < 0.01, ###p < 0.001.

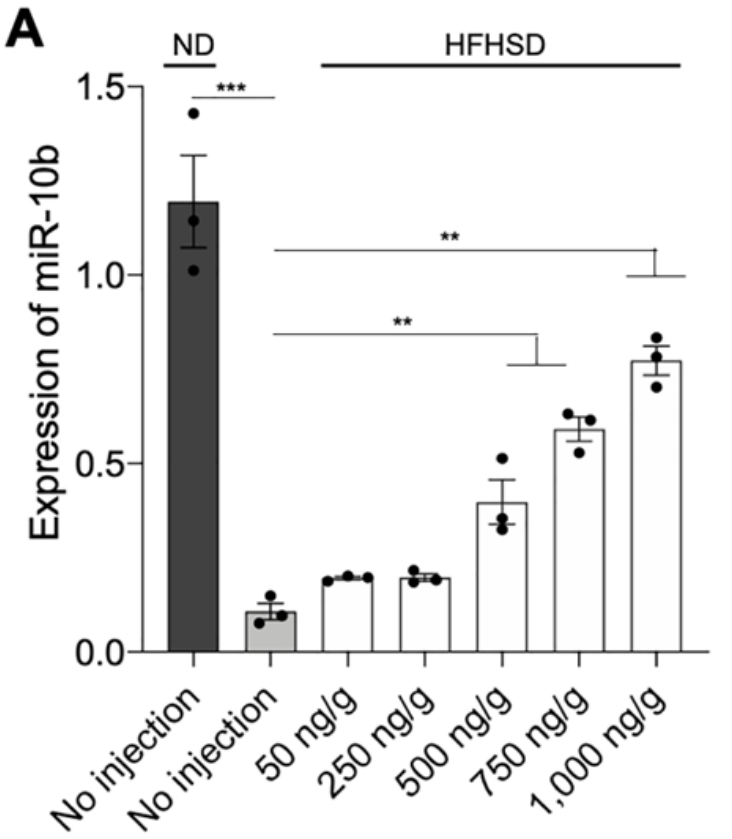
A
ND
HFHSD
***
**
**
Expression of miR-10b
1.5
1.0
0.5
0.0
No injection
No injection
50 ng/g
250 ng/g
500 ng/g
750 ng/g
1,000 ng/g

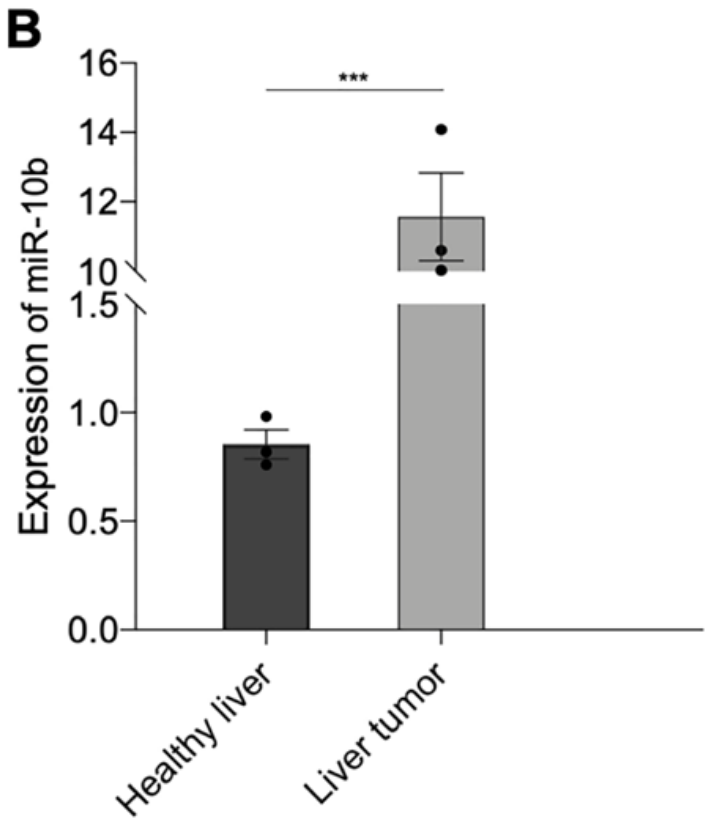
B
***
Expression of miR-10b
16
14
12
10
1.5
1.0
0.5
0.0
Healthy liver
Liver tumor

Supplementary Figure 11. HFHSD-fed diabetic male mice injected with the miR-10b-5p mimic have lower expression of miR-10b-5p in the blood when compared with ND-fed healthy mice and liver tumor tissue. HFHSD-fed diabetic C57 male mice were injected with four different doses of the miR-10b-5p mimic. (A) miR-10b-5p expression comparison in blood from mice injected with four different doses of the mimic vs control mice (ND-fed healthy and HFHSD-fed diabetic mice with no injection) (One-Way ANOVA). (B) miR-10b-5p expression in the healthy liver and in a liver tumor. n=3 per condition for each experiment. Error bar indicate SEM, unpaired t-test. **p < 0.01, ***p < 0.001.

Supplementary Table 1. Expression levels of miRNAs in jejunal ICCs and colonic ICCs from diabetic *Kit*$^{copGFP/+}$;*Lep*$^{ob/ob}$ and wild type *Kit*$^{copGFP/+}$;*Lep*$^{+/+}$ mice obtained by miRNA-seq

miRNA Name	Normalized Reads (Number)				Change of Reads (Number)
	WT		ob/ob		ob/ob-+/+
	CICC	JICC	CICC	JICC	
miR-10a-5p	188031.1	474072.5	42730.5	61758.1	-278807.5
miR-143-3p	281600.2	345646.5	49714.1	64861.5	-256335.5
miR-10b-5p	278419.5	58151.9	4421.7	6352.9	-162898.4
miR-99b-5p	71743.2	85929.8	3009.5	3763.0	-75450.3
miR-125a-5p	46778.6	58292.8	20161.8	17260.0	-33824.8
miR-191-5p	44092.8	33015.9	4624.1	4837.6	-33823.5
miR-100-5p	29431.4	45247.8	3353.4	4384.2	-33470.8
miR-99a-5p	39300.9	19739.1	2224.3	2567.2	-27124.2
let-7f-5p	18944.7	30199.5	8974.7	10519.0	-14825.3
miR-127-3p	9161.8	5452.7	1067.5	929.1	-6309.0
miR-27b-3p	8968.8	14149.8	6178.7	5993.4	-5473.2
miR-125b-5p	19859.0	17436.7	16305.4	14736.8	-3126.8
miR-145a-3p	6668.5	8023.7	4111.7	4487.5	-3046.4
miR-486b-5p	3152.6	2103.4	417.5	453.4	-2192.5
miR-541-5p	3841.6	2335.0	1347.4	1424.7	-1702.3
miR-409-5p	1791.7	1694.9	113.9	110.0	-1631.3
miR-351-5p	864.2	3498.5	1053.2	1058.0	-1125.7
miR-151-5p	1827.6	1056.4	292.6	370.1	-1110.7
miR-5099	1433.1	2067.0	711.6	591.2	-1098.7
miR-92b-3p	524.7	1262.0	102.8	111.1	-786.4
miR-151-3p	1178.5	543.4	94.9	110.0	-758.5
miR-342-3p	1183.3	1099.9	393.8	525.7	-681.9
miR-184-3p	1201.3	151.2	0.0	0.0	-676.2
miR-501-3p	1055.4	463.8	99.6	104.5	-657.6
miR-181a-5p	2068.4	1147.5	1067.5	896.8	-625.8
miR-152-3p	427.9	656.8	142.3	185.6	-378.4
miR-199a-5p	414.2	494.1	99.6	87.8	-360.4
miR-148a-3p	688.5	552.0	238.8	313.4	-344.1
miR-125b-3p	377.7	439.2	69.6	88.9	-329.2
miR-92a-3p_1	635.9	757.5	379.5	369.0	-322.5
miR-92a-3p_2	635.9	757.5	379.5	369.0	-322.5
miR-192-5p	344.2	247.4	14.2	20.0	-278.7
miR-21a-5p	663.4	471.8	300.5	321.2	-256.8

miR-3968	399.2	160.3	30.0	57.8	-235.9
miR-212-5p	249.8	242.8	0.0	31.1	-230.7
miR-196b-5p	443.4	6.3	7.9	0.0	-220.9
miR-214-3p	402.8	36.6	0.0	0.0	-219.7
miR-411-5p	221.1	220.4	0.0	6.7	-217.5
let-7e-5p	1482.2	2069.1	1609.9	1556.0	-192.7
miR-335-3p	349.0	156.3	56.9	64.5	-192.0
miR-484	259.4	307.5	117.0	80.0	-184.9
miR-322-3p	203.2	763.3	275.2	325.6	-182.8
miR-25-3p	297.6	285.1	112.3	106.7	-181.9
miR-215-5p	25.1	387.6	31.6	47.8	-166.7
miR-27a-3p	305.4	242.8	107.5	112.2	-164.2
miR-1a-3p	320.9	1678.5	638.9	1050.8	-154.9
miR-22-3p	702.8	1559.7	915.7	1042.4	-152.2
miR-101a-3p	147.0	140.3	0.0	20.0	-133.6
miR-199b-3p	299.2	83.6	51.7	71.5	-129.8
miR-200b-3p	164.9	80.4	7.9	0.0	-118.7
miR-434-5p	145.8	202.7	71.2	53.3	-112.0
miR-423-3p	194.8	134.6	52.2	54.5	-111.4
miR-10b-3p	224.7	11.5	11.1	12.2	-106.4
miR-139-3p	143.4	91.0	17.4	17.8	-99.6
miR-222-3p	271.3	35.5	58.5	62.2	-93.0
miR-181a-3p	47.8	148.9	9.5	15.6	-85.8
miR-615-3p	46.6	203.3	30.0	51.1	-84.4
miR-370-3p	46.6	125.4	7.9	0.0	-82.1
miR-6240	88.5	197.0	61.7	61.1	-81.3
miR-409-3p	89.6	129.4	33.2	24.4	-80.7
miR-204-5p	124.3	111.7	42.7	37.8	-77.7
miR-3470b	4.2	150.6	0.0	0.0	-77.4
miR-434-3p	193.6	191.2	117.0	124.5	-71.7
miR-136-3p	43.0	118.0	12.7	7.8	-70.3
miR-9-5p	155.0	29.8	25.3	21.1	-69.2
miR-128-3p	132.7	80.2	36.4	45.6	-65.5
miR-379-5p	117.1	77.3	30.0	37.8	-63.3
miR-1981-3p	65.7	64.1	14.2	0.0	-57.8
miR-126a-5p	89.6	114.5	50.6	44.5	-54.6
miR-377-3p	40.6	85.3	9.5	11.1	-52.7
miR-666-5p	66.9	28.6	0.0	0.0	-47.8
miR-146b-5p	161.4	39.5	34.8	74.5	-45.8
miR-574-3p	105.2	23.5	22.1	16.7	-44.9
miR-140-3p	135.1	105.9	56.9	101.1	-41.5
miR-411-3p	44.2	56.7	11.1	8.9	-40.5

miR-181b-5p	429.1	151.4	296.5	203.4	-40.3
miR-676-3p	95.6	61.8	30.0	50.0	-38.7
miR-674-3p	72.9	30.3	9.5	16.7	-38.6
miR-700-3p	38.2	37.8	0.0	0.0	-38.0
miR-182-5p	50.2	21.8	0.0	0.0	-36.0
miR-148b-3p	209.2	189.0	136.0	191.1	-35.5
miR-362-5p	88.5	48.1	36.4	35.6	-32.3
miR-124-3p	55.8	14.7	5.3	4.1	-30.6
miR-199b-5p	40.6	16.6	0.0	0.0	-28.6
miR-505-5p	50.2	14.9	7.9	0.0	-28.6
miR-329-3p	39.4	51.5	12.7	23.3	-27.5
miR-221-5p	59.8	10.9	9.5	10.0	-25.6
miR-195a-5p	101.6	53.8	41.1	64.5	-24.9
miR-375-3p	29.9	16.0	0.0	0.0	-23.0
miR-532-5p	17.9	30.9	0.0	5.6	-21.6
miR-671-3p	15.5	26.9	0.0	0.0	-21.2
miR-1943-5p	34.7	11.5	0.0	5.6	-20.3
miR-574-5p	37.1	2.9	0.0	0.0	-20.0
miR-28a-5p	71.7	108.2	61.7	78.3	-20.0
miR-342-5p	49.0	47.5	23.7	34.5	-19.2
miR-381-3p	14.3	33.2	9.5	0.0	-19.0
miR-1843b-3p	7.2	29.8	0.0	0.0	-18.5
miR-2137	13.1	21.8	0.0	0.0	-17.5
miR-877-5p	23.9	9.2	0.0	0.0	-16.5
miR-101b-3p	8.4	24.6	0.0	0.0	-16.5
miR-205-5p	32.3	0.0	0.0	0.0	-16.1
miR-149-5p	98.0	138.6	120.2	84.5	-16.0
miR-503-3p	75.3	282.9	178.7	148.9	-15.3
miR-3470a	0.0	30.3	0.0	0.0	-15.2
miR-1193-3p	14.3	41.2	7.9	17.8	-14.9
miR-126a-3p	113.6	228.5	180.3	132.2	-14.7
miR-669c-5p	38.2	20.6	14.2	15.6	-14.5
miR-300-3p	0.0	26.3	0.0	0.0	-13.2
miR-369-5p	22.7	3.4	0.0	0.0	-13.1
miR-203-3p	13.1	20.6	0.0	7.8	-13.0
miR-132-3p	41.8	38.9	20.6	34.5	-12.9
miR-30b-3p	25.1	20.6	7.9	15.6	-11.1
miR-93-3p	7.2	14.9	0.0	0.0	-11.0
miR-425-3p	9.6	11.5	0.0	0.0	-10.5
miR-378c	83.1	144.0	91.7	114.5	-10.4
miR-673-5p	7.2	10.3	0.0	0.0	-8.7

miR-582-3p	6.0	11.5	0.0	0.0	-8.7
miR-3057-5p	0.0	16.0	0.0	0.0	-8.0
miR-181c-5p	6.0	19.5	9.5	0.0	-8.0
miR-8114	15.5	0.0	0.0	0.0	-7.8
miR-136-5p	0.0	14.9	0.0	0.0	-7.4
miR-138-5p	6.6	8.3	0.0	0.0	-7.4
miR-410-3p	10.8	12.6	0.0	8.9	-7.2
miR-26b-3p	0.0	14.3	0.0	0.0	-7.2
miR-130b-5p	0.0	13.7	0.0	0.0	-6.9
miR-1843b-5p	0.0	13.7	0.0	0.0	-6.9
miR-20a-5p	7.2	6.3	0.0	0.0	-6.7
miR-873a-3p	6.0	7.4	0.0	0.0	-6.7
miR-1843a-3p	0.0	13.2	0.0	0.0	-6.6
miR-421-3p	0.0	12.6	0.0	0.0	-6.3
miR-23b-5p	10.8	18.3	0.0	16.7	-6.2
miR-668-3p	8.4	4.0	0.0	0.0	-6.2
miR-7019-3p	6.0	6.3	0.0	0.0	-6.1
miR-181c-3p	0.0	10.9	0.0	0.0	-5.4
miR-200a-3p	6.0	4.6	0.0	0.0	-5.3
miR-667-3p	0.0	18.3	7.9	0.0	-5.2
miR-181d-3p	0.0	10.3	0.0	0.0	-5.2
miR-339-3p	0.0	10.3	0.0	0.0	-5.2
miR-450a-1-3p	0.0	10.3	0.0	0.0	-5.2
miR-93-5p	9.6	19.5	7.9	11.1	-5.0
miR-196a-5p	14.3	4.6	6.3	3.3	-4.6
miR-467c-5p	0.0	9.2	0.0	0.0	-4.6
miR-194-5p	21.5	41.8	7.9	46.7	-4.4
miR-379-3p	0.0	8.6	0.0	0.0	-4.3
miR-493-5p	0.0	8.6	0.0	0.0	-4.3
miR-5126	0.0	8.6	0.0	0.0	-4.3
miR-25-5p	8.4	0.0	0.0	0.0	-4.2
miR-382-3p	0.0	8.0	0.0	0.0	-4.0
miR-200c-3p	7.2	5.4	0.0	5.6	-3.5
miR-345-5p	0.0	6.9	0.0	0.0	-3.4
miR-3475-3p	0.0	6.9	0.0	0.0	-3.4
miR-450b-5p	0.0	16.6	0.0	10.0	-3.3
miR-874-3p	12.0	0.0	0.0	5.6	-3.2
miR-140-5p	0.0	6.3	0.0	0.0	-3.1
miR-152-5p	0.0	6.3	0.0	0.0	-3.1
miR-712-5p	0.0	6.3	0.0	0.0	-3.1

miR-17-5p	6.0	0.0	0.0	0.0	-3.0
miR-21a-3p	6.0	0.0	0.0	0.0	-3.0
miR-301a-3p	6.0	0.0	0.0	0.0	-3.0
miR-504-5p	6.0	0.0	0.0	0.0	-3.0
miR-664-5p	6.0	0.0	0.0	0.0	-3.0
miR-486a-3p	0.0	12.6	0.0	6.7	-3.0
miR-28c	0.0	9.7	0.0	3.9	-2.9
miR-450b-3p	0.0	5.7	0.0	0.0	-2.9
miR-134-5p	15.5	3.4	7.9	5.6	-2.8
miR-148b-5p	0.0	5.2	0.0	0.0	-2.6
miR-383-5p	0.0	5.2	0.0	0.0	-2.6
miR-6538	0.0	5.2	0.0	0.0	-2.6
miR-9-3p	4.8	0.0	0.0	0.0	-2.4
miR-1187	0.0	4.6	0.0	0.0	-2.3
miR-6986-5p	0.0	4.6	0.0	0.0	-2.3
miR-1194	0.0	4.0	0.0	0.0	-2.0
miR-187-5p	0.0	4.0	0.0	0.0	-2.0
miR-341-3p	0.0	4.0	0.0	0.0	-2.0
miR-376b-5p	0.0	4.0	0.0	0.0	-2.0
miR-466g	0.0	4.0	0.0	0.0	-2.0
miR-5121	0.0	4.0	0.0	0.0	-2.0
miR-706	0.0	4.0	0.0	0.0	-2.0
miR-144-3p	0.0	3.4	0.0	0.0	-1.7
miR-3057-3p	0.0	3.4	0.0	0.0	-1.7
miR-323-5p	0.0	3.4	0.0	0.0	-1.7
miR-455-5p	0.0	3.4	0.0	0.0	-1.7
miR-615-5p	0.0	3.4	0.0	0.0	-1.7
miR-6944-3p	0.0	3.4	0.0	0.0	-1.7
miR-7047-3p	0.0	3.4	0.0	0.0	-1.7
miR-935	0.0	3.4	0.0	0.0	-1.7
miR-148a-5p	0.0	2.9	0.0	0.0	-1.4
miR-1947-5p	0.0	2.9	0.0	0.0	-1.4
miR-210-3p	0.0	2.9	0.0	0.0	-1.4
miR-331-3p	0.0	2.9	0.0	0.0	-1.4
miR-339-5p	0.0	2.9	0.0	0.0	-1.4
miR-361-3p	0.0	2.9	0.0	0.0	-1.4
miR-365-2-5p	0.0	2.9	0.0	0.0	-1.4
miR-467e-5p	0.0	2.9	0.0	0.0	-1.4
miR-541-3p	0.0	2.9	0.0	0.0	-1.4
miR-92b-5p	0.0	2.9	0.0	0.0	-1.4
miR-466e-3p	1.2	1.5	0.0	0.0	-1.3

miR-466p-3p	1.2	1.5	0.0	0.0	-1.3
miR-467b-5p	0.0	2.4	0.0	0.0	-1.2
miR-344d-3p	0.0	2.3	0.0	0.0	-1.1
miR-1843a-5p	0.0	8.6	0.0	6.7	-1.0
miR-323-3p	0.0	16.0	7.9	6.7	-0.7
miR-5128	0.0	1.4	0.0	0.0	-0.7
miR-133b-3p	0.0	1.3	0.0	0.0	-0.7
miR-3068-3p	0.0	6.9	0.0	5.6	-0.7
miR-378b	0.0	1.1	0.0	0.0	-0.6
miR-3473a	0.0	1.0	0.0	0.0	-0.5
miR-708-3p	0.0	8.0	7.9	0.0	-0.1
miR-144-5p	0.0	0.0	0.0	0.0	0.0
miR-155-5p	0.0	0.0	0.0	0.0	0.0
miR-183-5p	0.0	0.0	0.0	0.0	0.0
miR-19b-3p	0.0	0.0	0.0	0.0	0.0
miR-200b-5p	0.0	0.0	0.0	0.0	0.0
miR-206-3p	0.0	0.0	0.0	0.0	0.0
miR-216a-5p	0.0	0.0	0.0	0.0	0.0
miR-299a-3p	0.0	0.0	0.0	0.0	0.0
miR-299a-5p	0.0	0.0	0.0	0.0	0.0
miR-29c-3p	0.0	0.0	0.0	0.0	0.0
miR-326-3p	0.0	0.0	0.0	0.0	0.0
miR-34b-3p	0.0	0.0	0.0	0.0	0.0
miR-429-3p	0.0	0.0	0.0	0.0	0.0
miR-491-5p	0.0	0.0	0.0	0.0	0.0
miR-496a-3p	0.0	0.0	0.0	0.0	0.0
miR-540-3p	0.0	0.0	0.0	0.0	0.0
miR-543-5p	0.0	0.0	0.0	0.0	0.0
miR-547-3p	0.0	0.0	0.0	0.0	0.0
miR-671-5p	0.0	0.0	0.0	0.0	0.0
miR-674-5p	0.0	0.0	0.0	0.0	0.0
miR-96-5p	0.0	0.0	0.0	0.0	0.0
miR-672-5p	0.0	6.3	0.0	6.7	0.2
miR-669a-5p	2.7	0.0	4.3	0.0	0.8
miR-3473b	0.0	2.9	4.7	0.0	0.9
miR-3473e	0.0	2.9	4.7	0.0	0.9
miR-150-5p	7.2	2.9	12.7	0.0	1.3
miR-5100	0.0	2.9	0.0	5.6	1.3
miR-497a-5p	6.0	0.0	0.0	8.9	1.5
miR-30d-3p	0.0	3.4	0.0	6.7	1.6
miR-122-5p	0.0	13.7	9.5	7.8	1.8

miR-345-3p	0.0	4.0	0.0	7.8	1.9
miR-27b-5p	0.0	6.9	11.1	0.0	2.1
miR-132-5p	0.0	7.4	0.0	12.2	2.4
miR-193a-5p	0.0	0.0	0.0	6.7	3.3
miR-488-3p	0.0	0.0	0.0	6.7	3.3
miR-495-3p	0.0	0.0	0.0	6.7	3.3
miR-125a-3p	47.8	45.8	50.6	50.0	3.5
miR-652-3p	182.9	212.4	196.1	206.7	3.7
miR-29c-5p	0.0	0.0	0.0	7.8	3.9
miR-700-5p	0.0	0.0	7.9	0.0	4.0
miR-186-5p	210.4	214.1	218.2	214.5	4.1
miR-494-3p	0.0	3.4	0.0	12.2	4.4
miR-378a-5p	0.0	0.0	0.0	8.9	4.4
miR-337-5p	0.0	6.9	9.5	6.7	4.6
miR-29b-2-5p	0.0	0.0	9.5	0.0	4.7
miR-592-5p	0.0	0.0	9.5	0.0	4.7
miR-340-5p	8.4	10.9	12.7	16.7	5.0
let-7e-3p	0.0	4.0	9.5	5.6	5.5
let-7f-3p	0.0	6.3	11.1	7.8	6.3
miR-30c-3p	6.0	28.6	19.0	30.0	7.2
miR-384-5p	0.0	3.4	12.7	5.6	7.4
miR-543-3p	15.5	16.6	23.7	23.3	7.5
miR-29b-3p	0.0	0.0	5.5	9.4	7.5
miR-433-3p	26.3	34.4	52.2	24.4	8.0
miR-872-3p	0.0	18.9	19.0	16.7	8.4
miR-450a-5p	21.5	62.7	45.1	56.1	8.5
miR-1249-3p	0.0	14.9	19.0	14.4	9.3
miR-1198-5p	0.0	3.4	11.1	12.2	9.9
miR-218-5p	0.0	7.2	14.2	13.3	10.2
miR-142a-5p	0.0	7.4	9.5	20.0	11.0
miR-107-3p	0.0	3.4	0.0	25.6	11.1
miR-425-5p	6.0	17.8	17.4	28.9	11.3
miR-3068-5p	9.6	27.5	30.0	32.2	12.6
miR-382-5p	108.8	56.1	99.6	92.2	13.5
miR-340-3p	7.2	14.9	26.9	23.3	14.1
miR-485-5p	0.0	0.0	9.5	18.9	14.2
miR-329-5p	0.0	0.0	7.9	22.2	15.1
miR-322-5p	0.0	0.0	19.0	13.3	16.2
miR-330-3p	20.3	42.9	45.9	50.0	16.3
miR-338-3p	0.0	0.0	22.1	11.1	16.6
miR-129-5p	4.8	7.7	33.2	15.0	17.9

miR-34c-5p	25.1	19.5	52.2	28.9	18.3
miR-1981-5p	0.0	0.0	20.6	16.7	18.6
miR-24-2-5p	9.6	29.8	34.8	42.2	18.8
miR-872-5p	0.0	27.5	34.8	32.2	19.8
miR-338-5p	19.1	11.5	33.2	47.8	25.2
miR-351-3p	21.5	54.4	71.2	61.1	28.2
miR-28a-3p	40.6	80.2	91.7	91.1	31.0
miR-490-3p	7.2	73.9	55.4	91.1	32.7
miR-374c-5p	19.1	16.0	53.8	53.3	36.0
miR-130a-3p	15.5	4.0	45.9	46.7	36.5
let-7a-1-3p	4.2	9.7	42.7	44.5	36.6
miR-542-3p	0.0	6.3	36.4	46.7	38.4
miR-224-5p	206.8	300.0	283.1	303.4	39.8
miR-10a-3p	0.0	18.3	44.3	54.5	40.2
miR-378d	0.0	10.0	41.9	53.9	42.9
miR-30a-5p	880.9	1354.2	1149.7	1176.9	45.8
miR-103-3p	142.8	120.2	174.7	181.1	46.4
miR-185-5p	29.9	51.5	71.2	106.7	48.2
miR-1839-5p	20.3	47.0	50.6	118.9	51.1
miR-181d-5p	99.2	78.4	177.1	104.5	52.0
miR-744-5p	69.3	80.7	137.6	121.1	54.3
miR-378a-3p	548.0	1749.8	1133.1	1276.4	55.8
let-7b-3p	21.5	22.3	94.9	75.6	63.3
let-7d-3p	125.5	254.8	268.8	241.2	64.8
miR-139-5p	121.9	65.3	169.2	167.8	74.9
miR-133a-3p	21.5	34.3	86.2	129.5	79.9
miR-664-3p	25.1	5.2	106.0	101.1	88.4
miR-15b-5p	16.7	34.9	115.4	117.8	90.8
miR-24-3p	1642.3	812.8	1337.9	1315.8	99.3
miR-221-3p	70.5	14.3	166.1	123.4	102.3
miR-423-5p	554.6	498.2	667.4	597.9	106.2
miR-708-5p	34.7	64.7	158.1	161.1	110.0
let-7j	378.3	282.3	497.4	418.4	127.6
miR-328-3p	82.5	95.0	232.5	201.2	128.0
miR-129-3p	0.0	29.2	177.1	128.9	138.4
miR-320-3p	176.9	121.4	302.1	306.7	155.2
miR-16-5p	152.4	99.9	282.3	283.4	156.7
miR-361-5p	138.7	166.6	281.5	352.3	164.3
miR-7a-5p	72.3	47.0	240.4	236.7	178.9
miR-30e-3p	29.9	79.6	237.2	260.6	194.2
miR-365-3p	77.7	169.8	234.1	424.0	205.3
miR-98-5p	87.3	180.9	332.1	372.3	218.1

miR-29a-3p	163.8	217.6	457.0	423.4	249.6
miR-335-5p	199.6	91.6	392.2	452.3	276.6
miR-30a-3p	49.0	144.9	379.5	400.6	293.2
miR-7b-5p	124.3	111.1	442.8	423.4	315.4
miR-455-3p	175.7	234.2	512.4	663.5	383.0
miR-30d-5p	1436.7	1019.8	1764.9	1601.4	454.9
miR-146a-5p	192.4	399.1	786.0	1023.5	609.0
miR-30b-5p	66.9	114.5	838.2	740.1	698.4
miR-143-5p	279.7	463.8	950.4	1373.6	790.3
miR-26b-5p	187.7	218.0	1208.2	1165.0	983.8
miR-23b-3p	1840.1	1523.1	2422.8	2931.7	995.6
miR-30e-5p	388.5	795.3	1654.2	1688.1	1079.3
let-7i-5p	1850.9	2589.5	4329.2	3510.1	1699.4
let-7b-5p	4651.4	3523.2	6834.5	5361.6	2010.7
miR-26a-5p	7743.0	7815.9	9871.3	9807.8	2060.1
miR-23a-3p	1470.8	788.5	3025.3	3546.2	2156.1
miR-30c-5p	577.3	644.2	4022.4	4096.4	3448.6
let-7a-5p	6110.2	8602.1	10787.3	11192.5	3633.8
let-7d-5p	1695.3	2154.6	6216.6	6043.4	4205.0
let-7g-5p	2589.5	3695.5	7371.1	7998.5	4542.3
let-7c-5p	6305.1	5867.0	12948.8	12437.4	6607.1
miR-145a-5p	3563.1	6025.9	67932.3	91840.1	75091.7

Supplementary Table 2. Clinical characterization of patients with idiopathic and/or diabetic gastroparesis

Parameters	Healthy (n=18)	Idiopathic gastroparesis (n=14)	Diabetic gastroparesis (n=2)
Age (mean ± SEM)	45.1 ± 14.2	39.2 ± 3.56	60.2 ± 14.2
Gender (M:F)	0.39:0.61	0.22:0.78	1:1
BMI	26.9 ± 4.56	25.6 ± 1.1	24.6 ± 3.06
GES %2hr	-	59 ± 5	39.6 ± 7
GES %4hr	-	32 ± 5	15 ± 4
A1C	5.6 ± 0.83	5.2 ± 0.06	8.4 ± 2.16
Scoring Abdominal pain (0-5)	0	2.3 ± 1.2	-
GCSI-dd Aggregate	-	2.3 ± 0.18	-
GCSI-dd Nausea/Vomit	-	1.09 ± 0.16	-
GCSI-dd Fullness/Satiety	-	3.10 ± 0.22	-
GCSI-dd Bloating/Abd pain	-	2.43 ± 0.32	-

Supplementary Table 3. Expression levels of miRNAs in blood samples collected from healthy control (HC, n=2) subjects, idiopathic gastroparesis high insulin (IG-HI, n=2), idiopathic gastroparesis low insulin patients (IG-LI, n=2), and diabetic gastroparesis (DG, n=2) patients obtained by miRNA-seq.

miRNA Name	Normalized Reads (Number)							
	HC1	HC2	IG-H1	IG-H2	IG-L1	IG-L2	DG1	DG2
let-7a-2-3p	0.0	0.0	0.0	0.0	0.0	5.9	0.0	0.0
let-7a-3p	1752.5	2189.0	1345.6	1687.3	1362.4	1761.4	1289.2	1530.5
let-7a-5p	12089.7	11115.5	17102.2	13988.6	19944.5	14468.3	20675.0	23350.8
let-7b-3p	350.6	429.0	345.2	375.1	336.8	421.0	319.2	329.9
let-7b-5p	6543.2	6724.5	12581.4	7582.7	14706.2	11874.2	15930.8	17532.7
let-7c-3p	35.7	51.0	27.9	44.1	26.6	22.9	32.8	26.2
let-7c-5p	6271.2	5275.5	7664.9	7165.1	8875.9	6660.9	9170.3	10502.0
let-7d-3p	1559.1	2152.9	2627.1	1429.1	2671.9	2976.4	2739.7	2760.2
let-7d-5p	7099.3	7232.9	9813.1	7820.4	11855.4	8845.5	11380.9	12029.0
let-7e-3p	79.7	88.0	48.9	50.8	38.6	42.1	27.8	39.8
let-7e-5p	753.2	660.6	1340.7	856.5	1451.1	1049.5	1546.9	1667.7
let-7f-1-3p	136.1	121.0	183.6	113.0	176.5	202.4	186.0	224.1
let-7f-2-3p	582.5	676.1	507.0	532.7	556.0	622.2	523.4	512.3
let-7f-5p	31068.5	28211.6	68777.4	34764.5	78646.6	55069.0	75967.3	84434.8
let-7g-3p	17.9	20.0	229.5	16.9	290.5	259.2	294.4	286.2
let-7g-5p	90168.8	79510.2	210846.5	91764.8	258706.0	160957.6	230958.4	302196.1
let-7i-3p	126.5	172.0	344.2	139.0	386.5	394.4	422.6	365.8
let-7i-5p	30357.2	28285.4	48164.6	32001.4	52168.0	38300.9	48649.1	62525.1
miR-1-3p	1197568.1	786538.6	544298.3	782369.2	266289.8	208702.3	255561.2	305468.6
miR-1-5p	23.4	18.0	57.9	24.9	24.9	34.7	26.9	30.1
miR-100-5p	11820.1	10682.9	4612.6	9384.3	5298.8	3783.2	4314.0	4149.5
miR-101-3p	34885.5	31625.8	66706.2	36575.7	83171.2	83505.1	98553.1	81364.9
miR-101-5p	0.0	10.0	52.9	18.1	53.1	95.3	76.6	40.7
miR-103a-2-5p	0.0	0.0	0.0	5.6	5.1	7.4	10.9	0.0
miR-103a-3p	8471.0	7319.3	3194.1	8422.3	3142.8	3417.8	3254.5	3607.4
miR-106a-5p	2675.8	2470.4	2369.8	2958.1	2303.4	2558.0	2347.9	2400.6
miR-106b-3p	794.7	735.0	171.6	644.0	136.3	177.3	150.2	145.5
miR-106b-5p	4524.8	4132.8	6147.1	4617.3	5720.8	6206.1	6688.7	5386.6
miR-107	2430.4	2485.5	1690.5	2445.9	1985.5	1985.0	1919.0	2031.3
miR-10a-3p	237.9	279.0	249.4	223.7	189.4	199.4	239.7	184.3
miR-10a-5p	42542.3	39025.9	22461.2	32946.4	21720.5	20410.6	21483.4	31341.4

miR-10b-3p	33.0	23.0	0.0	35.0	0.0	0.0	0.0	0.0
miR-10b-5p	6235.2	5992.7	2620.1	4961.3	1028.3	1109.3	1079.0	1592.1
miR-1180-3p	6.9	0.0	0.0	0.0	0.0	0.0	0.0	0.0
miR-1197	0.0	0.0	0.0	0.0	4.3	0.0	0.0	0.0
miR-122-3p	1905.6	1985.9	1482.6	2033.6	2904.1	3082.0	3190.2	2473.0
miR-122-5p	153765.4	143244.1	868373.1	154302.7	1206260.9	917617.7	1158388.6	1454197.6
miR-124-3p	5.0	15.7	30.9	22.2	42.0	42.3	44.1	40.1
miR-1247-3p	0.0	0.0	0.0	0.0	4.3	3.7	0.0	0.0
miR-1247-5p	0.0	0.0	5.0	0.0	6.0	4.4	5.0	0.0
miR-1248	160.9	159.0	45.9	212.4	34.3	82.7	35.8	25.2
miR-1249-3p	24.7	25.0	74.8	23.7	89.1	112.3	113.4	98.0
miR-125a-3p	20.6	17.0	33.9	31.6	29.1	23.6	33.8	22.3
miR-125a-5p	5939.6	7244.6	1809.9	5198.0	1719.0	2001.5	1888.5	1694.0
miR-125b-1-3p	133.4	149.0	68.8	88.1	52.3	40.6	45.7	68.9
miR-125b-5p	20211.1	19924.9	3171.3	13522.0	2917.0	3264.4	3099.7	2533.2
miR-126-3p	157428.1	134624.6	144720.9	139821.6	134260.7	117966.7	138335.6	133138.7
miR-126-5p	31470.2	33763.1	48247.9	31306.6	48345.2	46626.3	49743.0	41700.2
miR-1260a	419.3	309.0	108.8	641.1	109.7	96.4	109.4	34.0
miR-1260b	881.3	614.0	163.6	718.0	132.0	146.6	152.2	71.8
miR-1268a	19.9	41.5	3.0	27.7	0.0	8.5	5.0	0.0
miR-1268b	6.2	5.5	3.0	5.1	0.0	2.6	0.0	0.0
miR-127-3p	1467.0	1569.9	1039.6	1229.2	984.6	993.4	915.9	934.3
miR-127-5p	127.9	128.0	186.6	149.1	229.7	240.0	189.9	195.0
miR-128-1-5p	0.0	13.0	9.0	11.3	0.0	0.0	0.0	0.0
miR-128-3p	134.1	148.0	30.4	108.5	25.7	59.8	45.2	25.2
miR-129-1-3p	20.6	17.0	11.0	12.4	17.1	20.7	34.8	34.9
miR-129-2-3p	61.9	63.0	82.8	70.0	84.8	109.3	69.6	89.3
miR-129-5p	16.5	17.5	20.0	11.3	32.6	34.0	17.4	31.0
miR-1296-5p	30.2	49.0	14.0	29.4	0.0	28.8	19.9	17.5
miR-1306-5p	22.0	27.0	5.0	23.7	0.0	0.0	0.0	0.0
miR-130a-3p	1116.4	1211.9	2689.9	1211.1	3143.2	3115.2	3396.1	3239.5
miR-130a-5p	23.4	20.0	31.9	14.7	30.0	35.5	16.9	41.7
miR-130b-3p	37.1	71.0	162.6	58.7	155.1	152.9	123.3	195.0
miR-130b-5p	35.7	61.0	10.0	31.6	9.4	6.6	0.0	4.9
miR-132-3p	129.2	154.0	192.6	125.4	216.8	154.4	206.8	188.2
miR-132-5p	30.2	42.0	22.0	28.2	18.0	23.6	18.9	14.6
miR-1323	0.0	0.0	0.0	0.0	0.0	13.3	0.0	0.0
miR-133a-3p	9954.8	11043.2	6893.4	10493.5	3418.9	3690.8	3680.0	3565.6
miR-133a-5p	2322.9	2088.9	1628.8	2194.5	940.9	921.3	982.5	892.1
miR-133b	1037.1	1201.3	984.8	1168.5	517.3	536.4	516.1	448.9
miR-134-3p	0.0	0.0	0.0	0.0	4.3	0.0	0.0	0.0
miR-134-5p	67.4	55.0	118.7	58.7	175.7	139.6	234.7	141.6

miR-135a-5p	103.1	94.0	108.8	107.3	72.0	80.9	85.0	91.2
miR-135b-5p	0.0	5.0	22.0	7.9	8.6	12.6	7.0	12.6
miR-136-3p	1256.7	1145.9	1544.5	1023.6	1457.6	1486.0	1394.2	1392.2
miR-136-5p	30.2	19.0	76.8	31.6	74.6	62.0	79.6	96.0
miR-137-3p	258.5	175.0	695.4	264.4	867.2	838.3	886.1	835.3
miR-137-5p	0.0	0.0	0.0	0.0	0.0	0.0	0.0	4.9
miR-138-5p	37.8	32.0	70.8	23.7	93.8	99.3	97.0	92.2
miR-139-3p	17.9	26.0	16.0	21.5	7.7	12.6	9.0	22.3
miR-139-5p	1204.4	1335.9	883.0	1265.3	800.4	840.5	879.1	870.3
miR-140-3p	12517.1	10731.4	9853.7	10492.0	9706.4	9279.2	9490.1	8783.2
miR-140-5p	1080.7	1087.9	1375.9	1208.8	1300.0	1325.7	1445.9	1558.1
miR-141-3p	3634.6	3661.8	5844.8	3741.2	6424.0	7127.4	7170.6	7615.6
miR-141-5p	28.9	28.0	29.9	29.4	38.6	46.5	42.8	34.9
miR-142-3p	8209.6	7042.6	6140.1	10077.4	2683.0	2906.9	3237.0	2948.4
miR-142-5p	60139.8	52483.1	41237.8	52009.3	15542.1	14867.1	14507.2	11501.7
miR-143-3p	3254629.9	2144140.2	1965522.1	1984982.2	1919795.7	1501545.0	1912538.6	1905224.5
miR-143-5p	5758.1	4915.7	6652.0	5013.8	6989.1	6515.5	7356.0	5806.7
miR-144-3p	6584.4	7065.6	8392.0	5887.1	6517.8	5488.9	7341.1	5383.6
miR-144-5p	2395.1	2496.9	2827.6	2874.1	2407.1	2509.6	2522.0	2730.1
miR-145-3p	17736.3	18728.0	19253.5	15978.1	18171.1	17488.9	17177.3	17853.6
miR-145-5p	64517.5	76116.8	26444.2	66928.8	24927.1	37576.8	25345.8	28365.8
miR-1469	1391.4	1944.9	191.6	1291.3	24.0	31.8	37.8	10.7
miR-146a-3p	9.6	7.0	0.0	0.0	11.1	8.1	5.0	4.9
miR-146a-5p	11022.6	9540.5	13481.0	11019.6	11184.6	8671.3	10712.8	12704.3
miR-146b-5p	1993.6	1697.9	1969.0	1873.1	1771.3	1403.2	1639.4	2247.5
miR-147b-3p	198.0	187.0	167.6	230.5	90.8	85.7	90.5	80.5
miR-147b-5p	52.2	56.0	37.9	59.9	14.6	35.5	15.9	10.7
miR-148a-3p	106051.3	116349.1	87320.6	92653.3	100500.4	94345.2	105292.1	101396.6
miR-148a-5p	662.7	719.0	718.4	568.3	781.5	793.9	788.6	794.6
miR-148b-3p	4407.3	5232.2	1090.0	4111.2	1115.7	1145.9	1121.8	1272.9
miR-148b-5p	86.6	75.0	126.7	70.0	134.5	135.9	141.2	160.1
miR-149-5p	919.8	978.9	438.0	829.2	389.9	369.3	336.1	273.6
miR-150-3p	64.6	69.0	25.9	52.0	4.3	0.0	0.0	0.0
miR-150-5p	4122.0	4508.8	1143.4	4005.0	405.3	510.3	407.7	335.7
miR-151a-3p	607.7	668.0	845.1	555.8	960.6	915.1	894.0	948.9
miR-151b	7843.2	7174.6	3100.0	7094.8	2646.2	2660.6	2878.0	2330.4
miR-152-3p	26403.7	22342.8	25365.2	24146.2	29916.2	31194.2	32099.7	26861.9
miR-152-5p	112.7	79.0	115.7	53.1	174.8	181.7	113.4	235.8
miR-153-3p	22.0	26.5	77.3	18.1	94.7	91.9	92.5	87.8
miR-154-3p	6.9	21.0	20.0	21.5	26.6	40.6	21.9	27.2
miR-154-5p	19.2	28.0	27.9	27.1	54.0	45.8	41.8	35.9
miR-15a-3p	119.6	103.0	140.7	82.5	162.0	168.4	132.3	147.5

miR-15a-5p	1324.0	1097.9	1212.3	1555.7	1575.0	1520.7	1977.0	1653.2
miR-15b-3p	382.2	477.0	176.6	488.1	205.7	195.0	171.0	143.6
miR-15b-5p	1209.9	1417.9	145.7	1282.3	207.4	211.2	240.7	177.5
miR-16-3p	427.6	408.0	478.9	439.5	496.2	536.2	517.1	492.9
miR-16-5p	12678.7	10790.9	8946.8	14095.4	9349.1	10471.2	10395.1	10481.6
miR-17-3p	228.2	283.0	152.7	198.8	156.0	186.1	160.1	140.7
miR-17-5p	2675.8	2470.4	2369.8	2958.1	2303.4	2558.0	2347.9	2400.6
miR-181a-3p	231.0	254.0	125.7	188.7	113.1	136.6	109.4	114.5
miR-181a-5p	1418.9	1430.4	264.4	1469.2	193.2	255.5	193.4	210.0
miR-181b-3p	0.0	11.0	0.0	9.0	0.0	0.0	0.0	0.0
miR-181b-5p	305.0	287.5	179.1	320.8	129.4	147.7	140.2	148.4
miR-181c-3p	187.0	146.0	40.9	113.0	16.3	28.1	27.8	27.2
miR-181c-5p	503.2	534.0	472.9	464.3	399.3	435.0	385.9	359.0
miR-181d-5p	162.7	198.0	34.9	188.1	31.7	40.6	34.8	36.9
miR-182-3p	0.0	5.0	0.0	0.0	0.0	3.7	0.0	0.0
miR-182-5p	3255.8	3262.8	4654.5	3072.9	4965.0	5300.6	5016.1	6489.7
miR-183-3p	6.9	8.0	0.0	0.0	4.3	0.0	0.0	0.0
miR-183-5p	1559.1	1899.9	2245.9	1380.6	2196.3	2240.8	2131.1	2402.2
miR-184	93.5	54.0	172.6	328.8	1913.5	166.2	367.0	136.8
miR-185-3p	0.0	8.0	15.0	0.0	8.6	19.9	17.9	0.0
miR-185-5p	5007.4	4272.8	7488.1	4870.4	7816.0	7293.2	7702.1	9219.8
miR-186-5p	4893.3	4605.7	3933.1	4523.5	3591.4	4065.7	3296.6	4195.1
miR-187-3p	110.0	99.0	55.9	135.6	66.8	93.1	59.7	71.8
miR-188-5p	0.0	0.0	14.0	5.6	12.9	17.7	14.9	12.6
miR-18a-3p	0.0	0.0	0.0	0.0	0.0	3.7	0.0	0.0
miR-18a-5p	225.5	276.0	375.2	346.8	353.1	394.0	393.3	418.2
miR-18b-5p	0.0	0.0	11.0	0.0	0.0	3.3	7.5	0.0
miR-190a-3p	0.0	0.0	12.0	5.6	31.7	17.7	22.9	17.5
miR-190a-5p	122.4	138.0	259.4	179.6	367.6	274.0	354.0	458.9
miR-190b-5p	0.0	0.0	0.0	0.0	10.3	0.0	6.0	6.8
miR-191-3p	8.2	14.0	11.0	5.6	0.0	3.7	0.0	5.8
miR-191-5p	22202.0	19767.9	7732.5	21021.3	8133.1	7532.5	7341.1	9133.5
miR-192-3p	185.6	201.0	775.2	192.1	1003.5	1006.6	996.5	1045.9
miR-192-5p	428947.4	420605.4	292064.3	339612.7	301890.2	296566.7	285734.2	316862.1
miR-193a-3p	70.1	91.0	525.8	92.6	640.1	645.5	675.2	544.3
miR-193a-5p	8.2	12.0	0.0	12.4	0.0	0.0	0.0	0.0
miR-193b-3p	88.0	113.0	114.7	80.2	75.4	187.6	114.4	145.5
miR-194-3p	180.1	186.0	302.3	180.8	438.7	404.7	445.5	461.8
miR-194-5p	104325.1	84406.4	85083.2	89888.2	100659.3	80404.7	101777.2	92654.6
miR-195-3p	33.0	33.0	29.9	30.5	37.7	17.0	26.9	25.2
miR-195-5p	3352.0	3147.8	3202.8	3324.9	3276.0	3127.8	3459.7	3721.7
miR-196a-5p	138.9	168.0	163.1	170.0	103.7	77.2	104.9	135.3

miR-196b-3p	0.0	0.0	0.0	5.6	0.0	4.4	0.0	4.9
miR-196b-5p	499.1	495.0	513.8	537.8	371.0	326.4	348.1	503.5
miR-197-3p	97.6	109.0	41.9	114.1	0.0	107.8	86.5	81.5
miR-199a-3p	9216.9	9228.5	10276.8	8804.5	10932.7	10559.3	10702.7	10110.5
miR-199a-5p	9051.0	8022.1	1875.9	6840.8	1708.4	2202.0	1783.2	1798.9
miR-199b-5p	3295.7	3127.8	4713.0	3254.4	5164.4	5871.5	5488.1	5569.6
miR-19a-3p	508.7	525.0	541.8	797.6	609.3	840.1	668.3	1068.2
miR-19b-1-5p	0.0	0.0	0.0	0.0	4.3	8.9	7.0	4.9
miR-19b-3p	1643.0	1425.9	1678.7	2171.4	1800.0	1793.2	1951.6	2395.9
miR-200a-3p	60367.3	54661.0	109701.5	60205.1	120697.7	128308.3	125533.4	131401.5
miR-200a-5p	536.2	554.0	549.8	468.8	641.8	653.6	571.8	487.0
miR-200b-3p	47878.4	40785.8	78815.3	43879.0	84183.2	82217.5	80705.0	91740.7
miR-200b-5p	515.6	409.0	388.1	396.5	457.6	381.8	436.6	386.1
miR-200c-3p	10766.9	8961.5	11656.7	10481.3	11344.4	11693.9	11060.9	12840.1
miR-200c-5p	0.0	0.0	11.0	10.2	6.0	5.2	7.0	6.8
miR-203a-3p	26928.9	24477.7	11887.1	26389.9	7838.3	6838.3	8050.2	7909.1
miR-203a-5p	0.0	15.0	13.0	7.9	17.1	5.2	0.0	13.6
miR-203b-3p	143.0	144.0	208.5	151.4	207.4	185.4	198.9	232.8
miR-204-5p	118.2	138.0	48.9	105.1	54.8	56.1	47.7	53.4
miR-205-3p	52.2	37.0	32.9	47.4	24.9	25.8	27.8	29.1
miR-205-5p	1849.2	2023.9	272.4	1959.0	191.1	237.1	209.8	186.3
miR-206	13.7	3.3	196.2	13.2	239.7	184.6	236.7	316.3
miR-208a-3p	796.1	675.0	728.4	669.9	530.4	479.3	565.8	584.1
miR-208a-5p	24.7	33.0	44.9	49.7	26.6	11.1	24.9	35.9
miR-208b-3p	17.9	14.0	19.0	15.8	13.7	6.6	22.9	19.4
miR-20a-3p	15.1	42.0	39.9	30.5	39.4	36.2	33.8	51.4
miR-20a-5p	15283.0	12190.3	12110.8	15832.7	11756.6	13898.8	12135.4	15012.2
miR-20b-5p	46.7	33.0	109.3	56.1	161.5	181.7	114.4	148.8
miR-21-3p	110.0	144.0	492.9	108.5	608.4	577.5	723.0	592.8
miR-21-5p	565817.9	475902.8	730471.8	500235.3	826813.7	821694.6	880560.9	906753.3
miR-210-3p	1253.9	1031.9	1218.2	1423.5	1335.1	1435.0	1604.1	1302.0
miR-210-5p	13.7	30.0	0.0	9.0	0.0	3.7	0.0	0.0
miR-2110	0.0	0.0	0.0	0.0	0.0	3.7	0.0	0.0
miR-212-3p	24.7	42.0	23.9	26.0	42.8	48.7	31.8	38.8
miR-212-5p	30.2	27.0	14.0	31.6	22.3	22.9	10.9	21.3
miR-214-3p	353.4	380.0	141.7	357.0	164.5	212.0	198.9	183.4
miR-214-5p	30.2	48.0	60.9	44.1	74.6	40.6	82.5	43.7
miR-215-5p	1605.9	1525.4	1471.2	1423.5	1551.9	1538.0	1776.6	1397.6
miR-216a-3p	0.0	0.0	5.0	0.0	12.0	14.8	20.9	20.4
miR-216a-5p	0.0	0.0	607.6	0.0	916.9	955.7	964.6	920.7
miR-216b-3p	0.0	0.0	179.6	0.0	438.7	433.5	474.4	433.7
miR-216b-5p	0.0	0.0	280.4	0.0	422.5	562.8	445.5	339.6

miR-217-3p	0.0	0.0	35.9	0.0	51.4	55.4	39.8	44.6
miR-217-5p	0.0	0.0	2435.5	0.0	3846.7	3923.2	3587.0	3612.1
miR-218-5p	209.0	223.5	219.0	220.3	239.9	196.5	263.0	223.6
miR-219a-5p	30.2	29.0	182.6	32.8	251.1	231.2	275.5	275.5
miR-22-3p	58374.4	52223.1	105777.9	51648.9	130161.2	115160.9	140412.0	133635.4
miR-22-5p	1531.6	1564.9	400.1	1827.9	418.2	462.3	503.2	377.4
miR-221-3p	2349.7	2601.9	1754.0	2530.6	1849.2	2135.9	1926.3	2154.8
miR-221-5p	156.7	172.0	59.9	177.4	60.0	62.8	46.7	62.1
miR-222-3p	398.7	452.0	410.1	338.9	452.5	391.4	434.6	413.3
miR-222-5p	0.0	7.0	9.0	7.9	15.4	24.4	18.9	28.1
miR-223-3p	416.6	451.0	462.0	477.9	466.2	534.7	470.4	403.6
miR-223-5p	49.5	47.0	5.0	49.7	15.4	8.1	0.0	9.7
miR-23a-3p	12090.9	14091.7	7469.1	13130.6	7905.6	8104.9	7770.2	7626.7
miR-23a-5p	0.0	0.0	5.0	0.0	0.0	0.0	0.0	0.0
miR-23b-3p	9646.3	11052.9	7964.0	10210.1	8199.5	8726.7	8048.7	8336.0
miR-23b-5p	0.0	12.0	5.0	0.0	9.4	3.7	7.0	5.8
miR-23c	0.0	0.0	0.0	0.0	0.0	2.2	0.0	0.0
miR-24-5p	1853.4	1825.9	1548.5	1687.9	1425.9	1501.5	1642.9	1392.2
miR-24-3p	15399.6	14872.7	13178.2	13323.2	12262.2	11341.6	11971.3	11272.8
miR-25-3p	5303.0	5267.7	4436.0	5318.9	4543.4	4703.8	4683.9	3765.3
miR-25-5p	39.9	48.0	40.9	50.8	25.7	23.6	14.9	23.3
miR-26a-3p	96.2	123.0	187.6	102.8	161.1	143.3	189.9	191.1
miR-26a-5p	106321.5	99394.0	49977.9	99383.2	49858.3	44822.8	48082.4	51603.5
miR-26b-3p	92.1	128.0	38.9	84.7	42.0	72.4	55.7	33.0
miR-26b-5p	37705.4	36126.0	25369.0	40063.3	26275.7	25029.3	28248.3	25950.0
miR-27a-3p	40904.8	44159.4	33794.8	35728.8	33685.9	32953.2	35655.6	29192.4
miR-27a-5p	232.4	230.0	237.5	224.8	212.5	192.8	223.8	225.1
miR-27b-3p	182460.4	180403.9	109309.6	152784.7	109662.8	105632.3	106898.8	99518.8
miR-27b-5p	82.5	111.0	231.5	93.8	207.4	144.0	193.9	199.9
miR-28-3p	338.2	307.0	428.0	378.5	453.3	506.6	516.1	537.5
miR-28-5p	1574.3	1312.6	1444.7	1332.4	1480.8	1531.0	1489.7	1523.2
miR-296-5p	13.7	21.0	5.0	12.4	6.0	12.6	9.9	7.8
miR-299-3p	48.1	75.0	104.8	53.1	137.1	141.8	177.0	182.4
miR-299-5p	9.6	0.0	12.0	5.6	18.9	21.4	5.0	11.6
miR-29a-3p	95034.9	91396.7	92324.3	93690.4	96056.8	86809.6	98647.6	84086.8
miR-29a-5p	37.1	59.0	123.7	79.1	132.8	152.1	158.1	118.4
miR-29b-5p	88.0	74.0	75.8	90.4	50.6	82.7	53.7	107.7
miR-29b-3p	1260.8	1467.7	1657.3	1281.7	2423.0	2371.3	2706.4	2267.4
miR-29c-3p	1522.0	1721.7	4973.8	1682.2	6459.1	6045.2	7290.4	5886.7
miR-29c-5p	122.4	135.0	187.6	127.7	236.5	262.2	256.6	259.0
miR-301a-3p	46.7	64.0	87.8	64.4	112.3	121.1	159.1	142.6
miR-301a-5p	33.0	35.0	16.0	32.8	11.1	9.6	9.0	0.0

miR-302a-3p	0.0	0.0	0.0	0.0	0.0	69.9	0.0	0.0
miR-302a-5p	0.0	0.0	0.0	0.0	0.0	711.2	0.0	0.0
miR-302b-3p	0.0	0.0	0.0	0.0	0.0	860.9	0.0	0.0
miR-302c-3p	0.0	0.0	0.0	0.0	0.0	29.5	0.0	0.0
miR-302c-5p	0.0	0.0	0.0	0.0	0.0	19.2	0.0	0.0
miR-302d-3p	0.0	0.0	0.0	0.0	0.0	86.9	0.0	0.0
miR-3065-5p	0.0	0.0	0.0	0.0	0.0	3.7	0.0	0.0
miR-3074-3p	0.0	7.0	0.0	0.0	0.0	0.0	0.0	0.0
miR-3074-5p	0.0	0.0	0.0	0.0	4.3	5.2	0.0	0.0
miR-30a-3p	1735.8	1758.9	1933.6	1694.6	2204.4	2010.7	2010.8	2165.0
miR-30a-5p	124659.3	101447.4	122295.1	108844.3	121838.7	106026.2	124617.0	132619.1
miR-30b-3p	360.2	344.0	441.0	275.7	403.6	375.9	382.9	516.1
miR-30b-5p	32267.7	32166.6	43627.4	35687.8	41513.8	35348.6	40677.8	40560.5
miR-30c-3p	749.3	782.0	1102.5	716.3	1234.8	1305.0	1234.1	1435.9
miR-30c-5p	51794.8	49390.1	25502.4	50080.2	24463.1	25152.5	24268.2	27682.1
miR-30d-3p	305.2	356.0	219.5	333.3	247.7	215.7	206.8	232.8
miR-30d-5p	64590.3	55335.5	27174.1	55016.7	24620.8	21624.1	24481.2	23750.5
miR-30e-3p	1590.1	1578.9	1701.2	1533.1	1422.1	1408.0	1359.4	1541.2
miR-30e-5p	200677.9	156494.9	183565.1	185730.8	155022.8	142837.1	154073.4	191750.9
miR-31-3p	16.5	36.0	273.4	37.3	347.1	349.3	309.3	321.1
miR-31-5p	966.6	817.0	2024.4	973.8	2837.3	2566.5	2817.3	2420.7
miR-32-3p	15.1	18.0	20.0	9.0	24.9	29.5	31.8	28.1
miR-32-5p	250.2	261.0	785.2	291.5	862.9	927.6	1074.0	945.9
miR-320a-3p	1174.2	1163.9	755.3	1082.4	759.0	821.5	900.3	981.2
miR-320b	8.2	9.5	5.0	7.4	11.3	4.7	4.3	6.1
miR-320c	0.0	0.0	0.0	0.8	0.9	0.0	0.0	0.0
miR-320d	0.0	0.0	0.0	0.8	0.0	0.0	0.0	0.0
miR-323a-3p	13.7	12.0	5.0	19.2	6.9	5.9	6.0	0.0
miR-324-3p	24.7	25.0	42.9	30.5	78.8	67.2	66.6	42.7
miR-324-5p	118.2	141.0	118.7	111.8	136.3	157.3	127.3	124.2
miR-326	123.7	111.0	127.7	110.7	172.2	174.3	184.0	137.8
miR-328-3p	736.9	771.0	415.1	578.4	546.7	671.3	555.9	456.0
miR-330-3p	28.9	15.0	13.0	13.6	16.3	13.3	5.0	16.5
miR-330-5p	83.9	62.0	112.7	63.3	92.5	116.0	88.5	93.1
miR-331-3p	181.5	190.0	76.8	146.9	77.1	75.3	87.5	74.7
miR-331-5p	16.5	8.0	10.0	0.0	19.7	13.3	10.9	10.7
miR-335-3p	290.1	333.0	116.7	238.4	156.0	123.3	104.4	156.2
miR-335-5p	1755.8	1605.9	1105.5	1774.8	1144.9	1116.7	1099.9	1546.5
miR-338-3p	68.7	95.0	103.8	101.7	114.8	74.6	126.3	111.6
miR-338-5p	30.2	37.0	38.9	23.7	35.1	37.7	26.9	25.2
miR-339-3p	0.0	11.0	0.0	0.0	0.0	0.0	0.0	0.0
miR-339-5p	2400.6	2841.8	1495.6	2258.4	1549.3	1739.3	1581.2	1045.9

miR-33a-3p	19.2	29.0	5.0	31.6	11.1	10.3	16.9	15.5
miR-33a-5p	242.0	221.0	711.4	229.3	862.1	791.0	1013.4	762.6
miR-340-3p	264.0	363.0	78.8	244.0	87.4	73.1	85.5	124.2
miR-340-5p	5264.5	5569.7	8344.1	5182.2	7551.2	6709.0	7458.5	8144.8
miR-342-3p	1062.8	1169.9	1297.1	1046.2	1167.1	1410.6	979.5	1281.6
miR-342-5p	0.0	0.0	0.0	0.0	0.0	3.7	0.0	11.6
miR-345-3p	228.2	188.0	183.6	189.8	175.7	219.3	176.0	162.0
miR-345-5p	0.0	0.0	0.0	0.0	0.0	3.7	0.0	0.0
miR-34a-3p	0.0	6.0	0.0	0.0	12.9	0.0	0.0	7.8
miR-34a-5p	284.6	253.0	721.4	340.1	960.6	922.5	1038.2	1154.5
miR-34b-3p	12.4	16.0	0.0	11.3	8.6	9.6	0.0	9.7
miR-34b-5p	0.0	0.0	0.0	0.0	0.0	4.4	5.0	6.8
miR-34c-5p	522.5	499.0	919.9	593.1	790.1	760.7	764.7	1024.5
miR-361-3p	247.5	228.0	67.8	265.5	74.6	109.3	82.5	97.0
miR-361-5p	963.8	1104.9	914.9	872.2	904.9	1024.4	927.8	978.9
miR-362-3p	1714.5	1739.9	2615.1	1771.5	2993.2	3321.3	3184.3	2737.9
miR-362-5p	301.1	302.0	129.7	319.7	132.8	143.3	138.2	157.2
miR-363-3p	92.1	45.0	61.9	30.5	94.3	186.1	84.5	103.8
miR-365b-3p	1103.4	1201.9	761.8	1131.4	949.5	1289.5	1112.8	1164.2
miR-365b-5p	15.1	20.0	20.0	22.6	18.0	22.2	17.9	19.4
miR-367-3p	0.0	0.0	0.0	0.0	0.0	4.4	0.0	0.0
miR-369-3p	94.9	78.0	162.6	68.9	200.5	160.3	200.9	141.6
miR-369-5p	12.4	28.0	12.0	19.2	22.3	17.0	20.9	11.6
miR-370-3p	9.6	8.0	5.0	11.3	9.4	5.9	9.0	18.4
miR-371a-5p	0.0	0.0	0.0	0.0	0.0	5.2	0.0	0.0
miR-372-3p	0.0	0.0	0.0	0.0	0.0	21.4	0.0	0.0
miR-374a-3p	0.0	0.0	0.0	7.9	0.0	5.2	0.0	10.7
miR-374a-5p	11.0	8.0	0.0	0.0	0.0	11.8	5.0	16.5
miR-374b-3p	44.0	53.0	23.9	37.3	20.6	22.2	25.9	17.5
miR-374b-5p	1975.7	1892.9	2376.6	2169.1	2444.8	2697.9	2344.9	2602.1
miR-375-3p	4084.8	4165.8	6776.7	3974.5	9679.8	9096.7	10570.1	8705.6
miR-376a-3p	0.0	6.0	10.0	0.0	17.1	13.3	12.9	4.9
miR-376a-5p	6.9	0.0	8.0	6.8	12.0	15.5	15.9	5.8
miR-377-3p	0.0	15.0	15.0	5.6	18.0	36.2	25.9	20.4
miR-377-5p	0.0	0.0	0.0	5.6	0.0	0.0	0.0	0.0
miR-378a-3p	46798.6	39390.8	31634.7	40998.4	31611.6	31492.2	30241.1	30880.0
miR-378a-5p	1152.2	1145.9	689.4	1110.5	587.9	737.8	630.5	590.9
miR-378b	0.0	3.5	0.0	0.0	0.0	0.0	0.0	1.2
miR-378c	6641.5	5976.7	4220.7	5983.4	3743.5	3837.8	4057.4	3151.7
miR-378d	7919.5	7085.5	5086.8	7058.6	4527.2	4625.0	5085.9	3665.3
miR-378e	5.0	1.6	5.2	1.6	2.6	3.0	3.2	1.9
miR-378f	0.0	0.0	2.5	3.4	0.0	1.3	0.0	0.0

miR-378g	0.0	3.0	19.0	13.0	10.3	10.0	8.5	10.7
miR-378h	4.4	6.8	3.6	6.8	3.3	3.7	4.5	1.6
miR-378i	1734.4	1489.4	1181.3	2381.5	1066.4	1073.1	1030.8	1040.5
miR-379-3p	57.7	65.0	46.4	41.2	55.7	58.0	53.7	55.8
miR-379-5p	356.1	316.0	947.9	342.3	1103.7	1002.2	1249.0	1193.3
miR-380-3p	19.2	20.0	34.9	14.7	55.7	35.5	42.8	61.1
miR-380-5p	0.0	7.0	12.0	6.8	18.9	11.1	13.9	21.3
miR-381-3p	254.4	250.0	483.9	205.6	500.4	618.9	599.7	574.4
miR-382-3p	42.6	54.0	75.8	39.5	71.1	83.5	84.5	80.5
miR-382-5p	23.4	15.0	19.0	14.7	24.9	17.0	14.9	16.5
miR-409-3p	17.9	12.0	49.9	21.5	48.0	56.1	31.8	41.7
miR-409-5p	130.6	157.0	71.8	108.5	99.4	87.1	84.5	71.8
miR-410-3p	121.0	148.0	191.6	151.4	241.7	224.5	244.6	191.1
miR-411-3p	59.1	95.0	63.4	70.6	78.8	69.1	85.5	83.0
miR-411-5p	324.5	240.0	456.0	266.6	561.3	499.3	526.1	464.7
miR-421	122.4	103.0	20.0	137.8	10.3	27.3	9.9	26.2
miR-422a	21.7	13.7	37.9	20.6	43.3	38.5	42.3	39.8
miR-423-3p	1358.4	1481.9	1231.2	1155.7	1205.7	1557.6	1249.0	1465.0
miR-423-5p	394.6	516.0	364.2	497.1	481.6	501.5	507.2	573.4
miR-424-5p	9.6	27.0	40.9	28.2	55.7	60.6	55.7	55.3
miR-425-3p	151.2	166.0	114.7	190.9	123.4	139.6	105.4	116.4
miR-425-5p	1208.5	988.9	874.0	1126.4	961.5	1072.4	1009.4	1036.2
miR-4286	411.1	455.0	572.7	437.2	591.3	551.0	649.4	294.0
miR-429	0.0	0.0	0.0	0.0	0.0	3.7	0.0	5.8
miR-431-5p	0.0	5.0	0.0	0.0	9.4	12.6	9.0	0.0
miR-433-3p	6.9	0.0	6.0	0.0	10.3	8.1	7.0	11.6
miR-433-5p	0.0	0.0	0.0	0.0	0.0	3.7	0.0	0.0
miR-4443	0.0	0.0	11.0	0.0	16.3	5.9	13.9	6.8
miR-4448	8.2	6.0	20.0	14.7	36.8	49.5	71.6	22.3
miR-4454	6040.0	3152.8	1633.3	5993.3	852.6	661.7	864.2	433.7
miR-449a	0.0	5.0	6.0	10.2	10.3	8.9	7.0	0.0
miR-4508	0.0	0.0	0.0	10.2	4.3	0.0	5.0	0.0
miR-450a-1-3p	0.0	0.0	13.0	0.0	45.4	32.5	43.8	46.6
miR-450a-5p	651.0	603.0	628.1	513.5	616.1	568.3	617.6	631.6
miR-4510	0.0	0.0	1.5	0.0	4.3	2.6	5.2	3.4
miR-451a	15363.2	16132.1	15309.4	17286.3	13235.2	17110.0	14160.1	16765.1
miR-452-5p	12.4	7.0	9.0	9.0	14.6	8.9	7.0	13.6
miR-455-3p	266.7	324.0	254.4	279.0	193.7	254.1	193.9	203.7
miR-455-5p	622.8	651.0	919.9	607.8	955.5	999.3	1067.1	1012.9
miR-4770	0.0	15.0	0.0	0.0	6.0	0.0	7.0	0.0
miR-4791	9.6	5.0	6.0	0.0	8.6	0.0	0.0	0.0
miR-483-3p	0.0	0.0	0.0	0.0	0.0	4.4	0.0	0.0

miR-484	1501.4	1516.9	1033.7	1300.3	1081.4	1145.5	1118.8	747.1
miR-485-3p	0.0	0.0	10.0	0.0	14.6	23.6	11.9	20.4
miR-485-5p	0.0	0.0	0.0	0.0	0.0	8.1	8.0	4.9
miR-486-3p	28.9	41.0	21.5	24.9	22.7	23.6	18.4	22.8
miR-486-5p	7570.9	8240.0	6282.8	6458.2	5215.7	4326.4	4919.1	4802.0
miR-487b-3p	26.1	32.0	12.0	18.1	0.0	13.3	13.9	6.8
miR-490-3p	724.6	578.0	927.9	535.5	782.4	951.3	878.1	892.6
miR-490-5p	11.0	9.0	18.0	18.1	27.4	29.5	17.9	16.5
miR-491-5p	0.0	0.0	0.0	6.8	4.3	6.6	8.0	6.8
miR-494-3p	56.4	54.0	43.9	46.3	44.6	35.5	21.9	41.7
miR-495-3p	20.6	35.0	48.9	47.4	56.6	59.1	41.8	56.3
miR-496	9.6	8.0	7.0	0.0	7.7	23.6	8.0	4.9
miR-497-3p	8.2	0.0	5.0	0.0	12.9	3.7	12.9	7.8
miR-497-5p	955.6	813.0	1349.9	971.6	1384.8	1392.2	1568.3	1334.0
miR-499a-3p	0.0	0.0	0.0	0.0	0.0	5.9	0.0	0.0
miR-499a-5p	7611.5	6955.6	1793.9	8005.4	720.7	813.9	755.8	707.3
miR-501-3p	55.0	42.0	19.0	23.7	27.4	36.9	20.9	25.2
miR-501-5p	0.0	0.0	0.0	0.0	0.0	3.7	5.0	0.0
miR-504-5p	23.4	62.0	5.0	33.9	0.0	36.2	12.9	9.7
miR-505-3p	12.4	11.0	6.0	5.6	17.1	27.3	11.9	32.0
miR-532-3p	59.1	67.0	11.0	64.4	22.3	26.6	26.9	14.6
miR-532-5p	1109.5	1024.9	726.4	935.4	792.7	860.4	832.4	778.1
miR-542-3p	618.7	546.0	620.6	590.9	695.0	601.2	747.8	746.1
miR-542-5p	0.0	0.0	0.0	0.0	0.0	0.0	5.0	0.0
miR-543	0.0	14.0	0.0	6.8	0.0	0.0	0.0	0.0
miR-574-3p	445.5	503.0	464.0	416.9	456.7	655.8	530.0	416.2
miR-574-5p	52.2	79.0	154.7	62.1	181.7	195.0	214.8	231.9
miR-582-5p	108.6	104.0	118.7	115.2	115.7	121.9	114.4	117.4
miR-592	23.4	14.0	81.8	21.5	133.7	145.5	148.2	144.6
miR-6128	0.0	0.0	0.0	0.0	0.9	0.0	0.0	0.0
miR-615-3p	41.2	30.0	18.0	19.2	4.3	15.5	11.9	0.0
miR-6516-3p	71.5	11.0	32.9	75.7	0.0	11.8	6.0	4.9
miR-652-3p	2447.3	2689.9	2478.4	2373.6	2462.8	2531.8	2626.4	2502.1
miR-652-5p	0.0	0.0	0.0	0.0	12.9	5.2	8.0	6.8
miR-664a-3p	0.0	0.0	0.0	0.0	0.0	3.7	0.0	0.0
miR-671-3p	61.9	87.0	30.9	56.5	36.8	30.3	15.9	15.5
miR-671-5p	68.7	57.0	157.6	81.3	167.1	188.3	192.9	163.0
miR-675-3p	0.0	0.0	0.0	0.0	0.0	0.0	6.0	0.0
miR-7-1-3p	160.9	158.0	53.9	151.4	41.1	59.1	24.9	34.9
miR-7-5p	4023.4	4201.4	11535.9	4381.6	14400.1	12116.4	14359.4	21608.6
miR-708-3p	199.4	190.0	50.9	144.6	123.4	110.0	154.1	74.7
miR-708-5p	741.1	623.0	534.8	803.3	560.4	517.7	530.0	482.2

miR-744-3p	34.4	34.0	28.9	36.2	26.6	30.3	36.8	27.2
miR-744-5p	627.0	518.0	460.0	561.5	554.4	585.7	541.0	636.5
miR-760	0.0	0.0	0.0	0.0	0.0	3.7	0.0	4.9
miR-766-3p	6.9	0.0	0.0	0.0	0.0	0.0	0.0	4.9
miR-7704	0.0	0.0	0.0	0.0	7.7	0.0	0.0	0.0
miR-7975	9.6	0.0	0.0	0.0	0.0	0.0	0.0	0.0
miR-7977	3111.4	1677.9	660.5	2996.1	445.6	424.7	455.5	132.9
miR-802	3556.9	3721.8	6238.9	3603.9	7766.3	8087.1	7874.1	8118.6
miR-873-5p	0.0	0.0	6.0	0.0	4.3	0.0	0.0	0.0
miR-874-3p	34.4	45.0	46.9	33.9	54.8	90.1	60.7	68.9
miR-874-5p	6.9	6.0	0.0	0.0	0.0	4.4	5.0	0.0
miR-877-3p	0.0	6.0	0.0	5.6	0.0	0.0	0.0	0.0
miR-877-5p	0.0	0.0	0.0	0.0	0.0	3.7	0.0	0.0
miR-885-5p	0.0	0.0	0.0	0.0	0.0	10.3	7.0	0.0
miR-9-3p	28.9	35.0	28.6	38.0	27.1	27.6	20.6	27.8
miR-9-5p	165.9	160.3	153.3	163.8	163.7	165.9	166.1	164.9
miR-92a-3p	2663.2	2982.3	3874.2	2569.6	4438.0	4873.3	4803.7	4448.4
miR-92b-3p	169.1	158.0	55.9	133.3	18.0	106.4	63.6	59.2
miR-93-3p	46.7	65.0	23.9	47.4	32.6	22.2	9.0	16.5
miR-93-5p	4819.0	3966.8	4247.4	4955.1	4234.1	4638.1	4513.9	4062.2
miR-96-3p	0.0	8.0	0.0	7.9	0.0	0.0	0.0	0.0
miR-96-5p	1049.1	1145.9	1140.4	1045.0	1177.4	1345.6	1191.4	1871.5
miR-98-3p	30.2	28.0	128.7	9.0	136.3	155.1	121.3	148.4
miR-98-5p	1037.2	1054.3	8218.7	1311.9	8873.1	6272.1	8244.6	11101.0
miR-9985	41.9	47.3	40.1	45.6	32.3	33.4	40.4	17.9
miR-99a-3p	0.0	7.0	54.9	0.0	61.7	63.5	64.6	75.7
miR-99a-5p	66021.6	58741.3	16198.4	52268.6	13576.7	12557.2	13478.9	13835.1
miR-99b-3p	22.0	26.0	20.0	38.4	6.0	12.6	33.8	17.5
miR-99b-5p	12313.7	11046.4	5563.4	9270.8	5237.5	5569.4	5055.8	4954.8
miRNA Name	**Change of Reads (Number)**							
	HC1	**HC2**	**IG-H1**	**IG-H2**	**IG-L1**	**IG-L2**	**DG1**	**DG2**
let-7a-2-3p	0	0	0	0	0	5.908417	0	0
let-7a-3p	-218.2496	218.2496	-625.1718	-283.5111	-608.4258	-209.3501	-681.6431	-440.3054
let-7a-5p	487.0827	-487.0827	5499.606	2386.059	8341.938	2865.711	9072.377	11748.23
let-7b-3p	-39.18767	39.18767	-44.5691	-14.71087	-53.01647	31.18593	-70.56659	-59.92058
let-7b-5p	-90.68423	90.68423	5947.531	948.8487	8072.36	5240.331	9296.914	10898.79
let-7c-3p	-7.624818	7.624818	-15.43553	0.687974	-16.80764	-20.47727	-10.55515	-17.17697
let-7c-5p	497.8415	-497.8415	1891.575	1391.774	3102.555	887.6361	3396.953	4728.735
let-7d-3p	-296.869	296.869	771.0491	-426.8756	815.8855	1120.352	883.729	904.2078
let-7d-5p	-66.76214	66.76214	2646.978	654.34	4689.279	1679.363	4214.777	4862.941
let-7e-3p	-4.125302	4.125302	-34.98037	-33.03099	-45.30815	-41.77239	-56.02494	-44.09164

let-7e-5p	46.33934	-46.33934	633.8164	149.6189	744.217	342.5795	839.9819	960.7746
let-7f-1-3p	7.561182	-7.561182	55.03049	-15.57927	47.97241	73.80873	57.40978	95.56178
let-7f-2-3p	-46.81379	46.81379	-122.2951	-96.63734	-73.31297	-7.085602	-105.8974	-117.0499
let-7f-5p	1428.486	-1428.486	39137.38	5124.447	49006.55	25428.99	46327.19	54794.71
let-7g-3p	-1.06256	1.06256	210.5449	-1.990051	271.5619	240.2954	275.4243	267.2728
let-7g-5p	5329.333	-5329.333	126007	6925.334	173866.5	76118.09	146118.9	217356.6
let-7i-3p	-22.74959	22.74959	194.981	-10.28138	237.2331	245.1458	273.4052	216.5246
let-7i-5p	1035.898	-1035.898	18843.28	2680.03	22846.65	8979.597	19327.72	33203.71
miR-1-3p	205514.7	-205514.7	-447755	-209684.2	-725763.6	-783351.1	-736492.1	-686584.7
miR-1-5p	2.687197	-2.687197	37.18298	4.16835	4.164673	14.02574	6.164254	9.390007
miR-100-5p	568.5779	-568.5779	-6638.917	-1867.2	-5952.683	-7468.258	-6937.517	-7101.943
miR-101-3p	1629.867	-1629.867	33450.59	3320.114	49915.56	50249.5	65297.5	48109.27
miR-101-5p	-4.999725	4.999725	47.88074	13.07632	48.12974	90.27349	71.57382	35.7487
miR-103a-2-5p	0	0	0	5.648763	5.141562	7.385521	10.93908	0
miR-103a-3p	575.8809	-575.8809	-4701.032	527.1607	-4752.366	-4477.373	-4640.604	-4287.778
miR-106a-5p	102.7162	-102.7162	-203.2706	384.9886	-269.6609	-15.10535	-225.1567	-172.481
miR-106b-3p	29.86809	-29.86809	-593.2156	-120.8687	-628.5763	-587.5752	-614.664	-619.2976
miR-106b-5p	196.0217	-196.0217	1818.31	288.5045	1392.05	1877.258	2359.954	1057.759
miR-107	-27.5771	27.5771	-767.4409	-12.03847	-472.4533	-472.9712	-538.9736	-426.6765
miR-10a-3p	-20.56295	20.56295	-8.985554	-34.7307	-69.04087	-59.01266	-18.75648	-74.08363
miR-10a-5p	1758.246	-1758.246	-18322.87	-7837.69	-19063.57	-20373.48	-19300.75	-9442.745
miR-10b-3p	4.999507	-4.999507	-27.99824	7.02409	-27.99824	-27.99824	-27.99824	-27.99824
miR-10b-5p	121.2645	-121.2645	-3493.858	-1152.626	-5085.623	-5004.63	-5034.944	-4521.836
miR-1180-3p	3.437266	-3.437266	-3.437266	-3.437266	-3.437266	-3.437266	-3.437266	-3.437266
miR-1197	0	0	0	0	4.284635	0	0	0
miR-122-3p	-40.13543	40.13543	-463.1069	87.79935	958.3699	1136.222	1244.477	527.2857
miR-122-5p	5260.629	-5260.629	719868.4	5797.991	1057756	769113	1009884	1305693
miR-124-3p	-5.312241	5.312241	20.57652	11.8649	31.63586	31.99009	33.73423	29.74806
miR-1247-3p	0	0	0	0	4.284635	3.69276	0	0
miR-1247-5p	0	0	4.988723	0	5.998488	4.431312	4.972308	0
miR-1248	0.936382	-0.936382	-114.0314	52.46586	-125.6506	-77.20981	-124.127	-134.7024
miR-1249-3p	-0.125157	0.125157	49.95738	-1.148663	64.24693	87.38645	88.49515	73.11678
miR-125a-3p	1.812264	-1.812264	15.11199	12.82174	10.32419	4.822337	15.00036	3.503282
miR-125a-5p	-652.5035	652.5035	-4782.19	-1394.106	-4873.103	-4590.622	-4703.616	-4898.128
miR-125b-1-3p	-7.812955	7.812955	-72.33448	-53.05815	-88.90632	-100.5585	-95.43363	-72.29462
miR-125b-5p	143.1082	-143.1082	-16896.68	-6546.004	-17151.03	-16803.61	-16968.28	-17534.82
miR-126-3p	11401.77	-11401.77	-1305.5	-6204.791	-11765.63	-28059.66	-7690.797	-12887.69
miR-126-5p	-1146.458	1146.458	15631.25	-1310.11	15728.56	14009.58	17126.28	9083.502
miR-1260a	55.18169	-55.18169	-255.4105	276.9699	-254.4781	-267.7837	-254.7739	-330.2077
miR-1260b	133.6743	-133.6743	-584.0104	-29.68276	-615.6738	-601.038	-595.488	-675.8457
miR-1268a	-10.78079	10.78079	-27.7237	-3.03799	-30.71693	-22.22358	-25.74462	-30.71693
miR-1268b	0.34369	-0.34369	-2.850154	-0.759501	-5.843388	-3.258456	-5.843388	-5.843388

miR-127-3p	-51.4444	51.4444	-478.8194	-289.2984	-533.8603	-525.1168	-602.5702	-584.1662
miR-127-5p	-0.063344	0.063344	58.64863	21.19773	101.7268	112.0998	62.01254	67.08068
miR-128-1-5p	-6.499643	6.499643	2.480059	4.797884	-6.499643	-6.499643	-6.499643	-6.499643
miR-128-3p	-6.969256	6.969256	-110.5914	-32.56636	-115.3148	-81.19989	-95.77461	-115.7974
miR-129-1-3p	1.812264	-1.812264	-7.836138	-6.38405	-1.672791	1.868128	15.99483	16.11589
miR-129-2-3p	-0.562879	0.562879	20.37915	7.611006	22.40211	46.87205	7.178651	26.82479
miR-129-5p	-0.500082	0.500082	2.955937	-5.70143	15.56427	16.97444	0.404121	14.04746
miR-1296-5p	-9.374685	9.374685	-25.6542	-10.24905	-39.62262	-10.81909	-19.73339	-22.15901
miR-1306-5p	-2.500008	2.500008	-19.50978	-0.773702	-24.49851	-24.49851	-24.49851	-24.49851
miR-130a-3p	-47.75478	47.75478	1525.741	46.91623	1979.029	1951.034	2231.908	2075.321
miR-130a-5p	1.687252	-1.687252	10.24168	-6.999369	8.306289	13.76435	-4.780307	20.03247
miR-130b-3p	-16.93682	16.93682	108.5731	4.687855	101.0445	98.821	69.25395	140.951
miR-130b-5p	-12.62454	12.62454	-38.39466	-16.73903	-38.94591	-41.72514	-48.3721	-43.5211
miR-132-3p	-12.37518	12.37518	50.94836	-16.21382	75.18615	12.74102	65.23165	46.60254
miR-132-5p	-5.874878	5.874878	-14.17243	-7.878998	-18.12735	-12.48915	-17.22804	-21.56981
miR-1323	0	0	0	0	0	13.29394	0	0
miR-133a-3p	-544.2236	544.2236	-3605.585	-5.483579	-7080.15	-6808.212	-6818.998	-6933.354
miR-133a-5p	117.0094	-117.0094	-577.0765	-11.35008	-1264.989	-1284.551	-1223.367	-1313.795
miR-133b	-82.06487	82.06487	-134.4285	49.33838	-601.9042	-582.7675	-603.0769	-670.323
miR-134-3p	0	0	0	0	4.284635	0	0	0
miR-134-5p	6.186713	-6.186713	57.54792	-2.436553	114.4863	78.40265	173.5092	80.46558
miR-135a-5p	4.561566	-4.561566	10.19777	8.770102	-26.57454	-17.68495	-13.52994	-7.357553
miR-135b-5p	-2.499863	2.499863	19.45052	5.408406	6.069407	10.05552	4.461368	10.11274
miR-136-3p	55.36363	-55.36363	343.2081	-177.7447	256.332	284.6661	192.9345	190.9371
miR-136-5p	5.62449	-5.62449	52.20289	7.009628	49.9292	37.41493	54.93348	71.4264
miR-137-3p	41.74599	-41.74599	478.6917	47.62575	650.4737	621.5202	669.3289	618.6063
miR-137-5p	0	0	0	0	0	0	0	4.851003
miR-138-5p	2.90584	-2.90584	35.93579	-11.17928	58.92942	64.43117	62.05592	57.26497
miR-139-3p	-4.062395	4.062395	-5.972261	-0.470875	-14.22383	-9.380791	-12.98602	0.378436
miR-139-5p	-65.75437	65.75437	-387.1682	-4.849234	-469.8025	-429.7	-391.0682	-399.9024
miR-140-3p	892.868	-892.868	-1770.552	-1132.265	-1917.867	-2345.11	-2134.131	-2841.053
miR-140-5p	-3.631964	3.631964	291.5817	124.5271	215.6499	241.3927	361.6389	473.8338
miR-141-3p	-13.6171	13.6171	2196.607	92.99426	2775.771	3479.215	3522.384	3967.407
miR-141-5p	0.437285	-0.437285	1.496594	0.937823	10.12597	18.09303	14.3261	6.491472
miR-142-3p	583.476	-583.476	-1485.968	2451.305	-4943.051	-4719.148	-4389.117	-4677.65
miR-142-5p	3828.328	-3828.328	-15073.66	-4302.151	-40769.36	-41444.39	-41804.24	-44809.72
miR-143-3p	555244.8	-555244.8	-733862.9	-714402.8	-779589.3	-1197840	-786846.5	-794160.6
miR-143-5p	421.1887	-421.1887	1315.045	-323.0762	1652.177	1178.588	2019.114	469.7315
miR-144-3p	-240.5929	240.5929	1567.012	-937.8777	-307.2326	-1336.1	516.0966	-1441.376
miR-144-5p	-50.88808	50.88808	381.6337	428.1161	-38.86697	63.62523	75.97985	284.1695
miR-145-3p	-495.8403	495.8403	1021.348	-2254.039	-60.99503	-743.2174	-1054.796	-378.5008
miR-145-5p	-5799.671	5799.671	-43872.92	-3388.338	-45390	-32740.35	-44971.3	-41951.39

miR-1469	-276.744	276.744	-1476.582	-376.8418	-1644.155	-1636.391	-1630.36	-1657.477
miR-146a-3p	1.312364	-1.312364	-8.311979	-8.311979	2.828071	-0.187907	-3.339672	-3.460977
miR-146a-5p	741.0737	-741.0737	3199.478	738.058	903.0608	-1610.21	431.2879	2422.741
miR-146b-5p	147.8537	-147.8537	123.2888	27.36956	-74.4924	-442.5114	-206.3904	401.7091
miR-147b-3p	5.498385	-5.498385	-24.867	37.98143	-101.6539	-106.8161	-101.9921	-111.9615
miR-147b-5p	-1.875243	1.875243	-16.20738	5.755212	-39.55392	-18.67118	-38.21029	-43.44947
miR-148a-3p	-5148.889	5148.889	-23879.6	-18546.94	-10699.83	-16854.99	-5908.117	-9803.592
miR-148a-5p	-28.12785	28.12785	27.54352	-122.5671	90.68471	103.1108	97.77539	103.7616
miR-148b-3p	-412.4753	412.4753	-3729.701	-708.5672	-3704.018	-3673.874	-3697.985	-3546.834
miR-148b-5p	5.811606	-5.811606	45.90609	-10.76282	53.73004	55.0861	60.40606	79.2756
miR-149-5p	-29.56697	29.56697	-511.3693	-120.1408	-559.4775	-580.1032	-613.2512	-675.7827
miR-150-3p	-2.187808	2.187808	-40.86704	-14.83978	-62.52377	-66.8084	-66.8084	-66.8084
miR-150-5p	-193.3917	193.3917	-3171.945	-310.3873	-3910.034	-3805.021	-3907.631	-3979.671
miR-151a-3p	-30.12737	30.12737	207.2538	-81.99761	322.7792	277.2301	256.185	311.0202
miR-151b	334.2734	-334.2734	-4408.886	-414.0324	-4862.689	-4848.245	-4630.907	-5178.458
miR-152-3p	2030.463	-2030.463	991.9284	-227.0319	5542.94	6820.988	7726.492	2488.706
miR-152-5p	16.87333	-16.87333	19.8694	-42.77061	78.94411	85.81483	17.49964	139.8897
miR-153-3p	-2.250022	2.250022	53.07669	-6.172479	70.4419	67.70121	68.2364	63.55462
miR-154-3p	-7.062157	7.062157	6.018205	7.528612	12.62805	26.68368	7.941466	13.22893
miR-154-5p	-4.374887	4.374887	4.313277	3.49049	30.36282	22.16665	18.14381	12.27384
miR-15a-3p	8.31125	-8.31125	29.37641	-28.83365	50.6536	57.08428	20.9578	36.16489
miR-15a-5p	113.0475	-113.0475	1.272602	344.6822	364.0445	309.6915	766.0024	442.2345
miR-15b-3p	-47.37493	47.37493	-252.9981	58.45429	-223.9364	-234.6211	-258.5515	-286.0092
miR-15b-5p	-104.0023	104.0023	-1168.249	-31.6505	-1106.543	-1102.694	-1073.26	-1136.373
miR-16-3p	9.809126	-9.809126	61.13074	21.68708	78.37398	118.4021	99.33331	75.07515
miR-16-5p	943.8953	-943.8953	-2788.026	2360.557	-2385.73	-1263.611	-1339.695	-1253.241
miR-17-3p	-27.37501	27.37501	-102.9545	-56.77297	-99.64874	-69.49432	-95.50113	-114.9304
miR-17-5p	102.7162	-102.7162	-203.2706	384.9886	-269.6609	-15.10535	-225.1567	-172.481
miR-181a-3p	-11.5009	11.5009	-116.7693	-53.81645	-129.3708	-105.853	-133.0944	-128.0015
miR-181a-5p	-5.75909	5.75909	-1160.26	44.58103	-1231.425	-1169.123	-1231.24	-1214.614
miR-181b-3p	-5.499698	5.499698	-5.499698	3.538324	-5.499698	-5.499698	-5.499698	-5.499698
miR-181b-5p	8.757914	-8.757914	-117.1469	24.60764	-166.8461	-148.5317	-156.023	-147.8014
miR-181c-3p	20.49763	-20.49763	-125.5821	-53.51435	-150.208	-138.4246	-138.6447	-139.324
miR-181c-5p	-15.37749	15.37749	-45.66219	-54.26482	-119.2652	-83.586	-132.7421	-159.619
miR-181d-5p	-17.64594	17.64594	-145.4221	7.760641	-148.6369	-139.7228	-145.537	-143.4756
miR-182-3p	-2.499863	2.499863	-2.499863	-2.499863	-2.499863	1.192898	-2.499863	-2.499863
miR-182-5p	-3.521389	3.521389	1395.18	-186.3721	1705.735	2041.289	1756.765	3230.372
miR-183-3p	-0.562515	0.562515	-7.437046	-7.437046	-3.152411	-7.437046	-7.437046	-7.437046
miR-183-5p	-170.376	170.376	516.4036	-348.9619	466.7841	511.2474	401.6115	672.6968
miR-184	19.74829	-19.74829	98.8645	255.0127	1839.773	92.42889	293.211	63.05294
miR-185-3p	-3.99978	3.99978	10.96639	-3.99978	4.569489	15.94113	13.90053	-3.99978
miR-185-5p	367.3216	-367.3216	2847.987	230.2769	3175.944	2653.115	3062.018	4579.729

miR-186-5p	143.7722	-143.7722	-816.4096	-225.9894	-1158.138	-683.7899	-1452.879	-554.3721
miR-187-3p	5.498969	-5.498969	-48.61983	31.07679	-37.65323	-11.43597	-44.82583	-32.69869
miR-188-5p	0	0	13.96843	5.648763	12.8539	17.72525	14.91692	12.61261
miR-18a-3p	0	0	0	0	0	3.69276	0	0
miR-18a-5p	-25.25011	25.25011	124.4173	96.09934	102.3192	143.2828	142.5748	167.4217
miR-18b-5p	0	0	10.97519	0	0	3.323484	7.458462	0
miR-190a-3p	0	0	11.97294	5.648763	31.7063	17.72525	22.87262	17.46361
miR-190a-5p	-7.812882	7.812882	129.2341	49.45114	237.4421	143.8233	223.8488	328.7253
miR-190b-5p	0	0	0	0	10.28312	0	5.966769	6.791404
miR-191-3p	-2.874897	2.874897	-0.149143	-5.475571	-11.12433	-7.431574	-11.12433	-5.303131
miR-191-5p	1217.036	-1217.036	-13252.43	36.35815	-12851.86	-13452.46	-13643.83	-11851.48
miR-192-3p	-7.688308	7.688308	581.947	-1.242695	810.1608	813.3458	803.1499	852.5755
miR-192-5p	4170.99	-4170.99	-132712.1	-85163.69	-122886.2	-128209.7	-139042.2	-107914.2
miR-193a-3p	-10.43739	10.43739	445.2538	12.08211	559.5668	564.9369	594.6818	463.7249
miR-193a-5p	-1.874952	1.874952	-10.12439	2.30289	-10.12439	-10.12439	-10.12439	-10.12439
miR-193b-3p	-12.4999	12.4999	14.24674	-20.28146	-25.08432	87.09833	13.86919	45.03618
miR-194-3p	-2.938533	2.938533	119.2654	-2.290821	255.6953	221.6753	262.4675	278.7642
miR-194-5p	9959.386	-9959.386	-9282.572	-4477.542	6293.602	-13961.06	7411.428	-1711.114
miR-195-3p	-0.000219	0.000219	-3.065628	-2.494646	4.706817	-16.01127	-6.147505	-7.772755
miR-195-5p	102.0972	-102.0972	-47.16379	74.9379	26.10746	-122.1562	209.8076	471.765
miR-196a-5p	-14.56262	14.56262	9.703106	16.59963	-49.73999	-76.24946	-48.51245	-18.08518
miR-196b-3p	0	0	0	5.648763	0	4.431312	0	4.851003
miR-196b-5p	2.059078	-2.059078	16.80663	40.73039	-125.9825	-170.5919	-148.9703	6.502185
miR-197-3p	-5.687835	5.687835	-61.4009	10.79884	-103.3062	4.522427	-16.78802	-21.80933
miR-199a-3p	-5.789948	5.789948	1054.067	-418.1638	1709.971	1336.622	1480.024	887.7566
miR-199a-5p	514.4742	-514.4742	-6660.607	-1695.693	-6828.107	-6334.54	-6753.298	-6737.62
miR-199b-5p	83.91104	-83.91104	1501.274	42.70168	1952.674	2659.75	2276.363	2357.859
miR-19a-3p	-8.127926	8.127926	24.93213	280.7622	92.43182	323.2598	151.435	551.3475
miR-19b-1-5p	0	0	0	0	4.284635	8.862625	6.961231	4.851003
miR-19b-3p	108.5456	-108.5456	144.2381	636.9173	265.5077	258.7371	417.1636	861.4429
miR-200a-3p	2853.162	-2853.162	52187.37	2690.926	63183.57	70794.12	68019.21	73887.37
miR-200a-5p	-8.878067	8.878067	4.665824	-76.24414	96.74678	108.5271	26.72392	-58.05084
miR-200b-3p	3546.3	-3546.3	34483.28	-453.0304	39851.16	37885.4	36372.97	47408.65
miR-200b-5p	53.30615	-53.30615	-74.161	-65.74049	-4.684699	-80.45226	-25.71505	-76.14388
miR-200c-3p	902.6915	-902.6915	1792.452	617.0813	1480.228	1829.665	1196.7	2975.92
miR-200c-5p	0	0	10.97519	10.16777	5.998488	5.169865	6.961231	6.791404
miR-203a-3p	1225.629	-1225.629	-13816.15	686.6084	-17864.97	-18865.03	-17653.12	-17794.21
miR-203a-5p	-7.499588	7.499588	5.471093	0.408681	9.638951	-2.329723	-7.499588	6.083219
miR-203b-3p	-0.50092	0.50092	65.03747	7.89569	63.88515	41.8854	55.40115	89.35695
miR-204-5p	-9.875241	9.875241	-79.22769	-23.05018	-73.27385	-71.98722	-80.38302	-74.75615
miR-205-3p	7.624235	-7.624235	-11.69663	2.82741	-19.77132	-18.77288	-16.77728	-15.51619
miR-205-5p	-87.31996	87.31996	-1664.185	22.4223	-1745.474	-1699.494	-1726.737	-1750.29

miR-206	5.207956	-5.207956	187.682	4.639342	231.1128	176.0969	228.1407	307.7443
miR-208a-3p	60.5539	-60.5539	-7.163193	-65.57348	-205.079	-256.1965	-169.6682	-151.4561
miR-208a-5p	-4.124937	4.124937	16.02526	20.83587	-2.308515	-17.79497	-4.01171	7.024169
miR-208b-3p	1.937275	-1.937275	3.020643	-0.119968	-2.225675	-9.289537	6.936111	3.467504
miR-20a-3p	-13.43686	13.43686	11.34896	1.942492	10.85781	7.628221	5.250863	22.8598
miR-20a-5p	1546.335	-1546.335	-1625.874	2096.066	-1980.056	162.1468	-1601.25	1275.571
miR-20b-5p	6.874312	-6.874312	69.38054	16.23855	121.6582	141.8113	74.49058	108.8916
miR-21-3p	-16.99979	16.99979	365.8936	-18.53604	481.4258	450.5554	595.9813	465.8002
miR-21-5p	44957.53	-44957.53	209611.4	-20625.1	305953.3	300834.2	359700.5	385892.9
miR-210-3p	110.9856	-110.9856	75.31737	280.5595	192.1633	292.0778	461.1376	159.0802
miR-210-5p	-8.124645	8.124645	-21.87371	-12.83569	-21.87371	-18.18095	-21.87371	-21.87371
miR-2110	0	0	0	0	0	3.69276	0	0
miR-212-3p	-8.62469	8.62469	-9.42713	-7.388691	9.473344	15.37143	-1.550232	5.435018
miR-212-5p	1.62471	-1.62471	-14.6548	3.009848	-6.343126	-5.728112	-17.68415	-7.278815
miR-214-3p	-13.31411	13.31411	-224.9853	-9.663167	-202.135	-154.7006	-167.7727	-183.2971
miR-214-5p	-8.874713	8.874713	21.73978	4.937704	35.42999	1.497714	43.41766	4.536373
miR-215-5p	40.23714	-40.23714	-94.4788	-142.165	-13.75865	-27.61863	210.9523	-168.0795
miR-216a-3p	0	0	4.988723	0	11.99698	14.77104	20.88369	20.37421
miR-216a-5p	0	0	607.6265	0	916.9118	955.6864	964.6277	920.7203
miR-216b-3p	0	0	179.594	0	438.7466	433.5301	474.3582	433.6796
miR-216b-5p	0	0	280.3663	0	422.465	562.7767	445.5188	339.5702
miR-217-3p	0	0	35.91881	0	51.41562	55.39141	39.77846	44.62922
miR-217-5p	0	0	2435.495	0	3846.745	3923.189	3587.023	3612.056
miR-218-5p	-7.250987	7.250987	2.768224	4.065037	23.70281	-19.78188	46.79836	7.394485
miR-219a-5p	0.624765	-0.624765	152.9641	3.139656	221.4564	201.5436	245.8427	245.9138
miR-22-3p	3075.632	-3075.632	50479.14	-3649.859	74862.44	59862.19	85113.25	78336.66
miR-22-5p	-16.63424	16.63424	-1148.184	279.66	-1130.099	-1085.946	-1045.082	-1170.872
miR-221-3p	-126.0711	126.0711	-721.7507	54.86009	-626.5376	-339.8933	-549.5138	-320.9705
miR-221-5p	-7.62562	7.62562	-104.5002	13.00624	-104.38	-101.588	-117.6252	-102.2721
miR-222-3p	-26.62618	26.62618	-15.27592	-86.42318	27.10843	-33.91638	9.230726	-12.04357
miR-222-5p	-3.499808	3.499808	5.479894	4.408461	11.92488	20.87241	15.39496	24.63601
miR-223-3p	-17.18932	17.18932	28.16988	44.09948	32.38235	100.9258	36.59443	-30.18249
miR-223-5p	1.249603	-1.249603	-43.2583	1.462097	-32.82234	-40.12295	-48.24702	-38.54502
miR-23a-3p	-1000.4	1000.4	-5622.209	39.22488	-5185.746	-4986.455	-5321.1	-5464.579
miR-23a-5p	0	0	4.988723	0	0	0	0	0
miR-23b-3p	-703.2753	703.2753	-2385.619	-139.4776	-2150.112	-1622.886	-2300.943	-2013.655
miR-23b-5p	-5.99967	5.99967	-1.010947	-5.99967	3.426526	-2.30691	0.961561	-0.178467
miR-23c	0	0	0	0	0	2.215656	0	0
miR-24-5p	13.73696	-13.73696	-291.1369	-151.7861	-413.7102	-338.1603	-196.7861	-447.3989
miR-24-3p	263.4772	-263.4772	-1957.948	-1812.987	-2873.964	-3794.585	-3164.831	-3863.4
miR-25-3p	17.65138	-17.65138	-849.3891	33.51363	-741.9353	-581.5238	-601.4479	-1520.014
miR-25-5p	-4.062541	4.062541	-3.02729	6.904048	-18.22701	-20.30116	-29.0179	-20.65001

miR-26a-3p	-13.3749	13.3749	77.95766	-6.810846	51.48392	33.66076	80.32382	81.51116
miR-26a-5p	3463.73	-3463.73	-52879.91	-3474.556	-52999.47	-58034.92	-54775.38	-51254.26
miR-26b-3p	-17.93712	17.93712	-71.1438	-25.32439	-68.06642	-37.67774	-54.36599	-77.06902
miR-26b-5p	789.7067	-789.7067	-11546.73	3147.567	-10640.06	-11886.44	-8667.377	-10965.77
miR-27a-3p	-1627.286	1627.286	-8737.345	-6803.316	-8846.18	-9578.912	-6876.53	-13339.76
miR-27a-5p	1.185895	-1.185895	6.289976	-6.352476	-18.65538	-38.41117	-7.419401	-6.086738
miR-27b-3p	1028.224	-1028.224	-72122.56	-28647.41	-71769.35	-75799.87	-74533.32	-81913.34
miR-27b-5p	-14.24976	14.24976	134.7326	-2.974666	110.6322	47.27352	97.17587	103.1172
miR-28-3p	15.6219	-15.6219	105.4274	55.86211	130.7093	184.0417	193.5205	214.8861
miR-28-5p	130.8365	-130.8365	1.30321	-111.0761	37.33865	87.58737	46.27236	79.78372
miR-296-5p	-3.624892	3.624892	-12.38523	-4.946675	-11.37547	-4.818569	-7.429338	-9.61235
miR-299-3p	-13.43708	13.43708	43.20439	-8.460423	75.54951	80.2432	115.4554	120.8389
miR-299-5p	4.812172	-4.812172	7.160764	0.836592	14.04022	16.60584	0.160136	6.830234
miR-29a-3p	1819.083	-1819.083	-891.5022	474.5783	2840.985	-6406.215	5431.795	-9129.017
miR-29a-5p	-10.93715	10.93715	75.66073	31.02307	84.76406	104.0821	110.0598	70.30485
miR-29b-5p	6.999032	-6.999032	-5.166371	9.385247	-30.43628	1.722866	-27.29404	26.69729
miR-29b-3p	-103.4402	103.4402	293.0247	-82.52478	1058.732	1007.077	1342.198	903.1294
miR-29c-3p	-99.8171	99.8171	3351.919	60.36343	4837.248	4423.395	5668.56	4264.853
miR-29c-5p	-6.312964	6.312964	58.89638	-1.017567	107.8322	133.5064	127.8915	130.3639
miR-301a-3p	-8.624836	8.624836	32.42988	9.024254	56.88578	65.75089	103.7422	87.24783
miR-301a-5p	-1.000164	1.000164	-18.034	-1.235086	-22.85786	-24.39674	-25.04776	-33.99791
miR-302a-3p	0	0	0	0	0	69.91626	0	0
miR-302a-5p	0	0	0	0	0	711.2256	0	0
miR-302b-3p	0	0	0	0	0	860.9055	0	0
miR-302c-3p	0	0	0	0	0	29.54208	0	0
miR-302c-5p	0	0	0	0	0	19.20235	0	0
miR-302d-3p	0	0	0	0	0	86.90296	0	0
miR-3065-5p	0	0	0	0	0	3.69276	0	0
miR-3074-3p	-3.499808	3.499808	-3.499808	-3.499808	-3.499808	-3.499808	-3.499808	-3.499808
miR-3074-5p	0	0	0	0	4.284635	5.169865	0	0
miR-30a-3p	-11.54212	11.54212	186.268	-52.73223	457.0833	263.3468	263.4401	417.6412
miR-30a-5p	11605.94	-11605.94	9241.694	-4209.042	8785.36	-7027.201	11563.61	19565.77
miR-30b-3p	8.122166	-8.122166	88.89988	-76.44361	51.50932	23.81974	30.76444	164.0434
miR-30b-5p	50.55415	-50.55415	11410.26	3470.637	9296.705	3131.459	8460.668	8343.406
miR-30c-3p	-16.31657	16.31657	336.8674	-49.37727	469.1912	539.3811	468.4864	670.2563
miR-30c-5p	1202.33	-1202.33	-25090.1	-512.2085	-26129.33	-25439.95	-26324.27	-22910.37
miR-30d-3p	-25.37563	25.37563	-111.101	2.672226	-82.95293	-114.9476	-123.7568	-97.75669
miR-30d-5p	4627.443	-4627.443	-32788.83	-4946.207	-35342.11	-38338.84	-35481.74	-36212.39
miR-30e-3p	5.582902	-5.582902	116.6585	-51.42177	-162.4259	-176.4466	-225.0672	-43.33263
miR-30e-5p	22091.49	-22091.49	4978.678	7144.386	-23563.59	-35749.31	-24512.96	13164.53
miR-31-3p	-9.749574	9.749574	247.1336	11.03339	320.807	323.0867	283.0291	294.8879
miR-31-5p	74.80198	-74.80198	1132.667	82.08971	1945.528	1674.711	1925.553	1528.893

miR-32-3p	-1.437521	1.437521	3.393404	-7.523468	8.289391	12.98059	15.26128	11.57433
miR-32-5p	-5.376363	5.376363	529.6158	35.86689	607.3161	672.0121	818.4092	690.3362
miR-320a-3p	5.116935	-5.116935	-413.7603	-86.69613	-410.1014	-347.5369	-268.7338	-187.8569
miR-320b	-0.62502	0.62502	-3.885734	-1.477268	2.408414	-4.196961	-4.565124	-2.729854
miR-320c	0	0	0	0.806966	0.856927	0	0	0
miR-320d	0	0	0	0.806966	0	0	0	0
miR-323a-3p	0.874861	-0.874861	-7.885478	6.331594	-6.018786	-6.965785	-6.907432	-12.8742
miR-324-3p	-0.125157	0.125157	18.02955	5.629853	53.96381	42.33477	41.75546	17.81535
miR-324-5p	-11.37516	11.37516	-10.88548	-17.77158	6.634288	27.6945	-2.326012	-5.431428
miR-326	6.373829	-6.373829	10.34359	-6.651969	54.87458	56.93056	66.60766	20.40074
miR-328-3p	-17.00395	17.00395	-338.8919	-175.5203	-207.2343	-82.60985	-198.0497	-297.9594
miR-330-3p	6.936927	-6.936927	-8.965422	-8.379071	-5.654492	-8.642166	-16.9638	-5.442695
miR-330-5p	10.93634	-10.93634	39.81221	-9.666787	19.61517	43.01974	15.57414	20.20631
miR-331-3p	-4.250969	4.250969	-108.9123	-38.87074	-108.6152	-110.4063	-98.22597	-111.0332
miR-331-5p	4.249657	-4.249657	-2.271771	-12.24922	7.460102	1.04472	-1.31014	-1.577012
miR-335-3p	-21.43825	21.43825	-194.8073	-73.16564	-155.5828	-188.2053	-207.125	-155.3412
miR-335-5p	74.92174	-74.92174	-575.3324	94.00794	-535.9791	-564.1428	-580.959	-134.3339
miR-338-3p	-13.12473	13.12473	21.8954	19.80769	32.95816	-7.276286	44.42657	29.70301
miR-338-5p	-3.375015	3.375015	5.28909	-9.898146	1.511052	4.043204	-6.772489	-8.397739
miR-339-3p	-5.499698	5.499698	-5.499698	-5.499698	-5.499698	-5.499698	-5.499698	-5.499698
miR-339-5p	-220.6288	220.6288	-1125.596	-362.8395	-1071.891	-881.9249	-1040.021	-1575.339
miR-33a-3p	-4.87486	4.87486	-19.13482	7.509528	-12.9835	-13.78382	-7.2177	-8.600339
miR-33a-5p	10.49782	-10.49782	479.9063	-2.145885	630.5828	559.5036	781.8707	531.0919
miR-340-3p	-49.49903	49.49903	-234.6592	-69.45445	-226.0745	-240.3644	-227.9573	-189.2954
miR-340-5p	-152.589	152.589	2927.034	-234.9295	2134.135	1291.902	2041.357	2727.728
miR-342-3p	-53.5666	53.5666	180.699	-70.21814	50.76537	294.2654	-136.8245	165.2658
miR-342-5p	0	0	0	0	0	3.69276	0	11.64241
miR-345-3p	20.12238	-20.12238	-24.52703	-18.3136	-32.44203	11.23791	-32.09235	-46.08857
miR-345-5p	0	0	0	0	0	3.69276	0	0
miR-34a-3p	-2.999835	2.999835	-2.999835	-2.999835	9.854069	-2.999835	-2.999835	4.761769
miR-34a-5p	15.80974	-15.80974	452.5736	71.25971	691.8192	653.6557	769.422	885.7428
miR-34b-3p	-1.812482	1.812482	-14.18664	-2.889112	-5.617369	-4.585461	-14.18664	-4.484633
miR-34b-5p	0	0	0	0	0	4.431312	4.972308	6.791404
miR-34c-5p	11.74589	-11.74589	409.2021	82.40168	279.3682	249.9902	254.0225	513.8133
miR-361-3p	9.747824	-9.747824	-169.8887	27.75658	-163.1827	-128.4296	-155.195	-140.7152
miR-361-5p	-70.56501	70.56501	-119.4424	-162.2052	-129.4594	-10.00254	-106.5416	-55.44196
miR-362-3p	-12.69817	12.69817	887.8826	44.24596	1266.04	1594.062	1457.06	1010.7
miR-362-5p	-0.439472	0.439472	-171.8371	18.17607	-168.7203	-158.2648	-163.3138	-144.3715
miR-363-3p	23.56059	-23.56059	-6.697952	-38.0548	25.70384	117.557	15.97111	35.25333
miR-365b-3p	-49.28586	49.28586	-390.87	-21.2008	-203.1731	136.8638	-39.84559	11.59251
miR-365b-5p	-2.437466	2.437466	2.393459	5.033619	0.434031	4.595127	0.338874	1.842575
miR-367-3p	0	0	0	0	0	4.431312	0	0

miR-369-3p	8.436408	-8.436408	76.20026	-17.51721	114.0888	73.83368	114.4491	55.21715
miR-369-5p	-7.812153	7.812153	-8.213373	-0.980513	2.093791	-3.199611	0.697384	-8.543903
miR-370-3p	0.812392	-0.812392	-3.823229	2.485575	0.614244	-2.903535	0.138202	9.621858
miR-371a-5p	0	0	0	0	0	5.169865	0	0
miR-372-3p	0	0	0	0	0	21.41801	0	0
miR-374a-3p	0	0	0	7.908269	0	5.169865	0	10.67221
miR-374a-5p	1.499845	-1.499845	-9.499405	-9.499405	-9.499405	2.317428	-4.527097	6.994004
miR-374b-3p	-4.500044	4.500044	-24.55117	-11.21521	-27.9308	-26.34048	-22.64104	-31.03343
miR-374b-5p	41.42213	-41.42213	442.3097	234.807	510.4944	763.6126	410.6223	667.7597
miR-375-3p	-40.46236	40.46236	2651.373	-150.8389	5554.538	4971.437	6444.823	4580.3
miR-376a-3p	-2.999835	2.999835	6.977612	-2.999835	14.1387	10.2941	9.928165	1.851167
miR-376a-5p	3.437266	-3.437266	4.544692	3.34125	8.559711	12.07233	12.47412	2.383938
miR-377-3p	-7.499588	7.499588	7.466582	-1.850825	10.49588	28.68946	18.35641	12.87462
miR-377-5p	0	0	0	5.648763	0	0	0	0
miR-378a-3p	3703.902	-3703.902	-11460.01	-2096.298	-11483.07	-11602.53	-12853.61	-12214.68
miR-378a-5p	3.117191	-3.117191	-459.6126	-38.50735	-561.2023	-411.2407	-518.5656	-558.2021
miR-378b	-1.749904	1.749904	-1.749904	-1.749904	-1.749904	-1.749904	-1.749904	-0.537153
miR-378c	332.4262	-332.4262	-2088.405	-325.6474	-2565.553	-2471.232	-2251.645	-3157.369
miR-378d	417.0058	-417.0058	-2415.731	-443.937	-2975.269	-2877.514	-2416.591	-3837.212
miR-378e	1.709248	-1.709248	1.879112	-1.727506	-0.738379	-0.354952	-0.126883	-1.368759
miR-378f	0	0	2.494362	3.389258	0	1.292466	0	0
miR-378g	-1.499918	1.499918	17.45723	11.49224	8.783206	8.470535	6.953006	9.172288
miR-378h	-1.199963	1.199963	-2.007782	1.178853	-2.343341	-1.882284	-1.124586	-4.047342
miR-378i	122.513	-122.513	-430.6015	769.5874	-545.4856	-538.815	-581.1717	-571.3911
miR-379-3p	-3.625184	3.625184	-14.97612	-20.13527	-5.670994	-3.394907	-7.67032	-5.584715
miR-379-5p	20.05904	-20.05904	611.8158	6.273384	767.6802	666.1735	913.0021	857.305
miR-380-3p	-0.375107	0.375107	15.29727	-4.937009	36.07646	15.82671	23.13805	41.49884
miR-380-5p	-3.499808	3.499808	8.473128	3.278708	15.35258	7.578473	10.42265	17.8446
miR-381-3p	2.185694	-2.185694	231.7342	-46.55697	248.2734	366.7347	347.4884	322.1867
miR-382-3p	-5.68747	5.68747	27.51903	-8.76822	22.81537	35.14682	36.21967	32.21708
miR-382-5p	4.187115	-4.187115	-0.229142	-4.499506	5.66459	-2.199593	-4.269367	-2.692882
miR-409-3p	2.93722	-2.93722	34.95067	6.52874	33.05135	41.1934	16.88621	26.78206
miR-409-5p	-13.18764	13.18764	-71.96612	-35.34748	-44.40021	-56.65459	-59.2745	-72.00889
miR-410-3p	-13.50006	13.50006	57.07517	16.89505	107.1616	90.02802	110.1457	56.63769
miR-411-3p	-17.93691	17.93691	-13.70109	-6.448332	1.779404	-8.003255	8.465822	5.89427
miR-411-5p	42.24553	-42.24553	173.737	-15.61071	279.0548	217.0289	243.8378	182.4937
miR-421	9.686157	-9.686157	-92.7256	25.14933	-102.3974	-85.35407	-102.7359	-86.48508
miR-422a	3.952764	-3.952764	20.21229	2.915977	25.5728	20.76425	24.56261	22.07621
miR-423-3p	-61.75561	61.75561	-188.946	-264.426	-214.4668	137.4434	-171.1192	44.83981
miR-423-5p	-60.68678	60.68678	-91.10806	41.80631	26.30807	46.19199	51.89054	118.1036
miR-424-5p	-8.687086	8.687086	22.5961	9.932387	37.38882	42.24984	37.37842	36.99
miR-425-3p	-7.375597	7.375597	-43.87464	32.31292	-35.2178	-19.02894	-53.20235	-42.19122

miR-425-5p	109.7985	-109.7985	-224.7198	27.6193	-137.2721	-26.3665	-89.36561	-62.56997
miR-4286	-21.93902	21.93902	139.6695	4.178302	158.2436	117.9239	216.3474	-139.0652
miR-429	0	0	0	0	0	3.69276	0	5.821203
miR-431-5p	-2.499863	2.499863	-2.499863	-2.499863	6.926334	10.05552	6.450292	-2.499863
miR-433-3p	3.437266	-3.437266	2.549202	-3.437266	6.845858	4.686807	3.523965	8.205141
miR-433-5p	0	0	0	0	0	3.69276	0	0
miR-4443	0	0	10.97519	0	16.28161	5.908417	13.92246	6.791404
miR-4448	1.124883	-1.124883	12.83034	7.562231	29.7233	42.35844	64.47668	15.19006
miR-4454	1443.568	-1443.568	-2963.087	1396.943	-3743.753	-3934.652	-3732.208	-4162.715
miR-449a	-2.499863	2.499863	3.486605	7.667911	7.78326	6.362762	4.461368	-2.499863
miR-4508	0	0	0	10.16777	4.284635	0	4.972308	0
miR-450a-1-3p	0	0	12.97068	0	45.41713	32.49629	43.75631	46.56962
miR-450a-5p	24.02561	-24.02561	1.087792	-113.5199	-10.86202	-58.67666	-9.43184	4.608051
miR-4510	0	0	1.496617	0	4.284635	2.584932	5.220923	3.395702
miR-451a	-384.4557	384.4557	-438.2635	1538.688	-2512.421	1362.378	-1587.519	1017.407
miR-452-5p	2.68727	-2.68727	-0.707184	-0.648864	4.880872	-0.824261	-2.725655	3.895921
miR-455-3p	-28.6252	28.6252	-40.93211	-16.30809	-101.6915	-41.29509	-101.437	-91.61489
miR-455-5p	-14.06586	14.06586	283.0222	-29.09144	318.5752	362.3626	430.1589	375.991
miR-4770	-7.499588	7.499588	-7.499588	-7.499588	-1.501099	-7.499588	-0.538357	-7.499588
miR-4791	2.312309	-2.312309	-1.325566	-7.312034	1.257235	-7.312034	-7.312034	-7.312034
miR-483-3p	0	0	0	0	0	4.431312	0	0
miR-484	-7.759526	7.759526	-475.4936	-208.8118	-427.7153	-363.6629	-390.3878	-762.1027
miR-485-3p	0	0	9.977447	0	14.56776	23.63367	11.93354	20.37421
miR-485-5p	0	0	0	0	0	8.124073	7.955693	4.851003
miR-486-3p	-6.062358	6.062358	-13.48388	-10.08083	-12.22683	-11.30172	-16.53785	-12.13568
miR-486-5p	-334.5631	334.5631	-1622.686	-1447.253	-2689.798	-3579.046	-2986.38	-3103.477
miR-487b-3p	-2.937512	2.937512	-17.08779	-10.98469	-29.06073	-15.76679	-15.13827	-22.26933
miR-490-3p	73.30367	-73.30367	276.6306	-115.7691	131.1024	299.9832	226.8377	241.3126
miR-490-5p	0.999872	-0.999872	7.960027	8.076665	17.42228	19.54271	7.900931	6.494031
miR-491-5p	0	0	0	6.778516	4.284635	6.646969	7.955693	6.791404
miR-494-3p	1.187061	-1.187061	-11.28333	-8.864235	-10.62389	-19.73359	-33.30594	-13.46547
miR-495-3p	-7.187242	7.187242	21.07865	19.63878	28.74634	31.27333	13.95655	28.46079
miR-496	0.812392	-0.812392	-1.827739	-8.811952	-1.09961	14.82171	-0.856259	-3.960949
miR-497-3p	4.124719	-4.124719	0.864005	-4.124719	8.729185	-0.431958	8.803282	3.636885
miR-497-5p	71.30225	-71.30225	465.691	87.32972	500.5363	507.9131	684.0083	449.7681
miR-499a-3p	0	0	0	0	0	5.908417	0	0
miR-499a-5p	327.9315	-327.9315	-5489.604	721.8781	-6562.874	-6469.665	-6527.758	-6576.273
miR-501-3p	6.499278	-6.499278	-29.53982	-24.77216	-21.07531	-11.56937	-27.61328	-23.27176
miR-501-5p	0	0	0	0	0	3.69276	4.972308	0
miR-504-5p	-19.31159	19.31159	-37.69628	-8.79242	-42.685	-6.495948	-29.757	-32.98299
miR-505-3p	0.68738	-0.68738	-5.700308	-6.038012	5.451763	15.63965	0.246763	20.32984
miR-532-3p	-3.937676	3.937676	-52.08345	1.337259	-40.77854	-36.47077	-36.20818	-48.50564

miR-532-5p	42.30282	-42.30282	-340.8884	-131.8113	-274.5891	-206.8333	-234.8822	-289.1457
miR-542-3p	36.3689	-36.3689	38.25829	8.521745	112.6288	18.84249	165.4962	163.7453
miR-542-5p	0	0	0	0	0	0	4.972308	0
miR-543	-6.999615	6.999615	-6.999615	-0.221099	-6.999615	-6.999615	-6.999615	-6.999615
miR-574-3p	-28.75137	28.75137	-10.26971	-57.34225	-17.47894	181.6133	55.82703	-58.00497
miR-574-5p	-13.37461	13.37461	89.02938	-3.484651	116.0475	129.3567	149.1827	166.2569
miR-582-5p	2.311653	-2.311653	12.42568	8.928833	9.379197	15.55515	8.057143	11.08832
miR-592	4.687087	-4.687087	63.12875	2.778982	114.9943	126.8084	129.4885	125.8736
miR-6128	0	0	0	0	0.856927	0	0	0
miR-615-3p	5.624417	-5.624417	-17.66336	-16.41697	-31.33813	-20.11318	-23.68923	-35.62277
miR-6516-3p	30.24786	-30.24786	-8.321685	34.44617	-41.24726	-29.43043	-35.28049	-36.39626
miR-652-3p	-121.2596	121.2596	-90.19486	-194.9823	-105.7846	-36.83612	57.7804	-66.44552
miR-652-5p	0	0	0	0	12.8539	5.169865	7.955693	6.791404
miR-664a-3p	0	0	0	0	0	3.69276	0	0
miR-671-3p	-12.56222	12.56222	-43.50291	-17.94537	-37.58514	-44.15236	-58.52161	-58.90979
miR-671-5p	5.874221	-5.874221	94.77257	18.4711	104.2297	125.4597	130.0545	100.1226
miR-675-3p	0	0	0	0	0	0	5.966769	0
miR-7-1-3p	1.436355	-1.436355	-105.5495	-8.040816	-118.2952	-100.3435	-134.5661	-124.5005
miR-7-5p	-89.00095	89.00095	7423.489	269.1226	10287.65	8004.004	10246.93	17496.19
miR-708-3p	4.685921	-4.685921	-143.7905	-50.06714	-71.278	-84.63122	-40.53394	-119.97
miR-708-5p	59.05434	-59.05434	-147.229	121.234	-121.5899	-164.2951	-151.9721	-199.8305
miR-744-3p	0.187262	-0.187262	-5.250798	1.966692	-7.620659	-3.904759	2.609685	-7.019779
miR-744-5p	54.49285	-54.49285	-112.5041	-10.97731	-18.03266	13.20741	-31.47729	63.98715
miR-760	0	0	0	0	0	3.69276	0	4.851003
miR-766-3p	3.437266	-3.437266	-3.437266	-3.437266	-3.437266	-3.437266	-3.437266	1.413737
miR-7704	0	0	0	0	7.712342	0	0	0
miR-7975	4.812172	-4.812172	-4.812172	-4.812172	-4.812172	-4.812172	-4.812172	-4.812172
miR-7977	716.7525	-716.7525	-1734.153	601.4438	-1949.058	-1969.993	-1939.197	-2261.743
miR-802	-82.45655	82.45655	2599.559	-35.42794	4126.99	4447.806	4234.808	4479.299
miR-873-5p	0	0	5.986468	0	4.284635	0	0	0
miR-874-3p	-5.312436	5.312436	7.208908	-5.792511	15.15823	50.41826	20.97706	29.19914
miR-874-5p	0.43743	-0.43743	-6.437101	-6.437101	-6.437101	-2.005788	-1.464793	-6.437101
miR-877-3p	-2.999835	2.999835	-2.999835	2.648928	-2.999835	-2.999835	-2.999835	-2.999835
miR-877-5p	0	0	0	0	0	3.69276	0	0
miR-885-5p	0	0	0	0	0	10.33973	6.961231	0
miR-9-3p	-3.062523	3.062523	-3.33354	6.099453	-4.799534	-4.362943	-11.38335	-4.123139
miR-9-5p	2.790414	-2.790414	-9.794838	0.699199	0.558106	2.813096	2.960147	1.81915
miR-92a-3p	-159.5714	159.5714	1051.478	-253.1423	1615.26	2050.571	1980.982	1625.605
miR-92b-3p	5.561073	-5.561073	-107.6787	-30.24158	-145.5569	-57.20089	-99.90685	-104.3702
miR-93-3p	-9.124808	9.124808	-31.92575	-8.422008	-23.3084	-33.71506	-46.92147	-39.37821
miR-93-5p	426.1321	-426.1321	-145.5151	562.181	-158.8382	245.1929	120.9469	-330.6846
miR-96-3p	-3.99978	3.99978	-3.99978	3.908488	-3.99978	-3.99978	-3.99978	-3.99978

miR-96-5p	-48.44179	48.44179	42.92693	-52.47402	79.92236	248.1466	93.86973	774.0215
miR-98-3p	1.124738	-1.124738	99.58586	-20.08518	107.1282	125.9727	92.20111	119.3175
miR-98-5p	-8.556406	8.556406	7172.937	266.0831	7827.35	5226.294	7198.798	10055.25
miR-9985	-2.698046	2.698046	-4.556608	0.934005	-12.35511	-11.27475	-4.191249	-26.68398
miR-99a-3p	-3.499808	3.499808	51.37615	-3.499808	58.19893	60.01567	61.14019	72.17583
miR-99a-5p	3640.175	-3640.175	-46183.06	-10112.87	-48804.73	-49824.22	-48902.51	-48546.39
miR-99b-3p	-2.000036	2.000036	-4.043642	14.41306	-18.00005	-11.44315	9.813158	-6.534926
miR-99b-5p	633.6336	-633.6336	-6116.602	-2409.276	-6442.489	-6110.605	-6624.184	-6725.213

Supplementary Table 4. Oligonucleotides (primers, miRNAs, and siRNAs) used in this study.

(A) Primers

Name	Sequence (5' to 3')	Orientation	Spices	Application
Hoxd4-1	GATGAAGAAGGTGCACGTGAATTCG	Forward	Mouse	Genotyping
Hoxd4-1r	GTGTGAGCGATTTCAATCCGACG	Reverse	Mouse	Genotyping
Hoxd3-1	GAATCCCGACAGAACTCCAAGC	Forward	Mouse	Genotyping
Hoxd3-1r	GAAGTGGAACTCCTTCTCCAGC	Reverse	Mouse	Genotyping
Hoxd10-1	CTTCCAGAAGACAGGAGCTGC	Forward	Mouse	Genotyping
Hoxd10-1r	GAGCCAATTGCTGGTTGGAGTATC	Reverse	Mouse	Genotyping
lacZ-1	CTGTTCCGTCATAGCGATAACGAG	Forward	Mouse	Genotyping
lacZ-1r	GTTGCACTACGCGTACTGTGAG	Reverse	Mouse	Genotyping
Hoxd4-I4	CTGAAAGATAGGCCATCGGAGACC	Forward	Mouse	Genotyping
10bWT-1r	GAAGTTGGATCTTTCTGCAGGAGG	Reverse	Mouse	Genotyping
LacZ-2	CCATTACCAGTTGGTCTGGTGTC	Forward	Mouse	Genotyping
10bWT-1r	GAAGTTGGATCTTTCTGCAGGAGG	Reverse	Mouse	Genotyping
10b-2	CTGCTTCAGGCGATGGTGAGTAAG	Forward	Mouse	Genotyping
10b-2r	CTTGCCATGCCACATTTGAGAGTC	Reverse	Mouse	Genotyping
10b-1a	AGAAGGTCCTGGCTGCTCAGCTAC	Forward	Mouse	Genotyping
10b-4r	GAATCTGTGACTATGTGGGTACCAC	Reverse	Mouse	Genotyping
Snord66	CTGAGACCACATGATGGGATTG	Forward	Mouse	qPCR
miR-10b-5p	TACCCTGTAGAACCGAATTTGTG	Forward	Mouse/Human	qPCR
miRTQ	CGAATTCTAGAGCTCGAGGCAGGC GACATGGCTGGCTAGTTAAGCTTGG TACCGAGCTCGGATCCACTAGTCCT TTTTTTTTTTTTTTTTTTTTTTTTVN	Forward	Mouse/Human	qPCR
miRTQ-rev	CGAATTCTAGAGCTCGAGGCAGG	Reverse	Mouse/Human	qPCR
10b-scram-f	CTAGAACAGTCTGAGTAGTACATTG ATCT	Forward	Mouse	Clone
10b-scram-r	CTAGAGATCAATGTACTACTCAGAC TGTT	Reverse	Mouse	Clone
10b-mKlf-Xf	CTAGACATGTTTTGTAGAAATGTGA CAGGGTACTAT	Forward	Mouse	Clone
10b-mKlf-Xr	ACATGTTTTGTAGAAATGTGACAGG GTACTATCTAG	Reverse	Mouse	Clone
10b-mKlf-f	CATGTTTTGTAGAAATGTGACAGGG	Forward	Mouse	Clone

10b-mKlf-r	CCCTGTCACA TTTCTACAAA ACATG	Reverse	Mouse	Clone
10b-mKlfMu-Xf	CTAGACATGTTTTGTAGAAATGTGC CTGAGCACTAT	Forward	Mouse	Clone
10b-mKlMu-Xr	CTAGATAGTGCTCAGGCACATTTCT ACAAAACATGT	Reverse	Mouse	Clone
10b-mKlfMu-f	GTTTTGTAGAAATGTGCCTGAGCAC	Forward	Mouse	Clone
10b-mKlfMu-r	GTGCTCAGGCACATTTCTACAAAAC	Reverse	Mouse	Clone
mKlf-1	GAGGTGGGCAAGCTGAACAGAATC	Forward	Mouse	Clone
mKlf-1r	CTTCCTCTCCAGGATCGACTCAC	Reverse	Mouse	Clone
10b-hKLF-Xf	CTAGAGATGTTTTGTAGAAATAAGA CAGGGTACTAT	Forward	Human	Clone
10b-hKLF-Xr n	CTAGATAGTACCCTGTCTTATTTCTA CAAAACATCT	Reverse	Human	Clone
10b-hKLF-f	GATGTTTTGTAGAAATAAGACAGGG	Forward	Human	Clone
10b-hKLF-r	CCCTGTCTTATTTCTACAAAACATC	Reverse	Human	Clone
hKLF-1	GCTGAACAGAATCGCCTCTGCAG	Forward	Human	Clone
hKLF-1r	GCTTCCTCTCCAGGATGGACTC	Reverse	Human	Clone
pLen-f	GAGTTGTGTTTGTGGACGAAGTAC	Forward	Plasmid	Clone
pLen-r	GCAGCGTATCCACATAGCGT	Reverse	Plasmid	Clone
pLen-1	CGTTTAGTGAACCGTCAGATCGC	Forward	Plasmid	Clone
Luc-1r	GTTGCTCTCCAGCGGTTCCATC	Reverse	Plasmid	Clone
Luc-2r	CGTTTCATAGCTTCTGCCAACC	Reverse	Plasmid	Clone
(B) miRNAs and siRNAs				
Name	**Sequence (5' to 3')**	**Orientation**	**Spices**	**Application**
miR-10b mimic	UACCCUGUAGAACCGAAUUUGUG	Sense	Mouse/Human	In vitro/In vivo
	TTAUGGGACAUCUUGGCUUAAAC	Antisense		
miR-10b inhibitor	UACCCUGUAGAACCGAAUUUGUG	Sense	Mouse/Human	In vitro/In vivo
	AUGGGACAUCUUGGCUUAAACAC	Antisense		
siKlf11-1	GUUCCUUCCCAAGUAGUUAtt	Sense	Mouse	In vitro/In vivo
	UAACUACUUGGGAAGGAACag	Antisense		
siKlf11-2	UCUGAUUUCUGUCCCUGUAtt	Sense	Mouse	In vitro/In vivo
	UACAGGGACAGAAAUCAGAgg	Antisense		
siKLF11-1	ACAGUUUACUCAGCACUAAtt	Sense	Human	In vitro
	UUAGUGCUGAGUAAACUGUcc	Antisense		
siKLF11-2	CACCUGAACUACCAAAAGAtt	Sense	Human	In vitro
	UCUUUUGGUAGUUCAGGUGtg	Antisense		

Supplementary Table 5. Primary antibodies used in this study.

Name	Vendor (Item #)	Host	Reactivity	Clonality	MW (kDa)	Concentration
KIT	antibodies.com (A11143)	Human, Mouse	Rabbit	Polyclonal	115	1:10 WES
KiT	R&D system (AF1356)	Human, Mouse	Goat	Polyclonal		1:20 IHC
KLF11	Antibodies-Online (ABIN324466)	Rabbit	Human, Mouse, Rat	Polyclonal	57	1:100
Insulin	Abcam (ab181547)	Rabbit	Human, Mouse, Rat	Monoclonal		1:100
APC-Cy7 anti-mouse CD45	Biolegend (103116)	Mouse	Rat	Polyclonal	NA	1:5000 FACS
GAPDH	Cell signaling (S2118)	Rabbit	Human, Mouse	Polyclonal	36	1:500
Alexa™ 594-anti-rabbit	Jackson ImmunoResearch (711-585-152)	Rabbit	Donkey	Polyclonal	NA	1:500 IHC

Supplementary Table 6. Drugs used in this study.

Group	Dose	Administration	Frequency	Class
Sitagliptin	10mg/kg body weight	Oral	Once per day till 4 weeks	Diabetes medication
Prucalopride	2mg/kg body weight	Oral	Once per day till 4 weeks	Chronic constipation medication
Metformin	250mg/kg body weight	Oral	Once per day till 4 weeks	Diabetes medication
Insulin	0.75U/Kg body weight	Intraperitoneal injection	Once per day till 4 weeks	Diabetes medication
Liraglutide	0.2mg/kg body weight	Subcutaneous Injection	Twice per day till 2 weeks	Diabetes medication
miR-10b mimic	500 ng/g body weight	Intraperitoneal injection	Once per week till 2 weeks	

CHAPTER FOUR: Diabetes and Gut Dysmotility is Linked to Gut Barrier Dysfunction in Mice Lacking miR-10b

Introduction

Globally, there are more than 451 million people diagnosed with diabetes.[1] This condition has been shown to have significant overlap with disorders of gut brain interactions (DGBIs), such as gastroparesis and slow transit constipation, with approximately 50-60% of diabetics experiencing at least one of these disorders.[2-4] Dysregulated gut-brain axis, altered gut motility, gut altered GI secretion, immune dysfunction, microbial dysbiosis, presence and degree of bile acid malabsorption, impaired glucose homeostasis, insulin resistance, and visceral hypersensitivity have all been attributed to the development of DGBIs, highlighting the heterogeneous nature of these disorders. Recent studies have highlighted gut barrier dysfunction as a possible core pathophysiological mechanism linking DGBIs to the diabetic condition.[2, 5, 6] This is likely mediated through gut microbiota-induced immune dysfunction, which is extremely prevalent in both conditions.[2, 7, 8] Therefore, it is of paramount importance that a treatment for gut barrier dysfunction become clinically available for patients with diabetes and DGBIs.

Normal glucose homeostasis and gut functions require a complex coordinated interplay between pancreatic cell types, for instance, pancreatic beta and alpha cells and GI cell types, for instance, interstitial cells of Cajal (ICCs), enteric neurons, smooth muscle cells (SMCs), enteroendocrine cells, enterocytes, and immune cells.[17,18] Functional defects of these cells lead to diabetes and gut dysmotility.[10,19–23] Proper functioning of these cells is regulated by molecular mechanisms at the transcriptional, post-transcriptional, translational, and post-translational levels. That is one of top reasons that the use of RNA based therapeutics offer significant advantages over many of the traditional small molecule and protein based therapeutic options.[9, 10] First, they typically are much cheaper to produce.[11] Second, they are much faster to produce.[9, 11] Additionally, it is much easier to deliver RNA based therapeutics to their target cells due to the advancement of

delivery mechanisms.[12, 13] Therefore, RNA based drugs, such as microRNAs (miRNAs), have immense potential for the treatment of diabetes, DGBIs, and the leaky gut.

miRNAs dysregulation has been linked to pathophysiological mechanisms of diabetes and gut dysmotility.[14, 15] Further, miRNAs have been associated with key gut pathophysiological mechanisms such as visceral hypersensitivity (miR-200a, -199a/b, -338, and -495), gut immune dysfunction (miR- 29, -155, -146a/b, -192, -146a, -155, and -122), gut barrier dysfunction (miR-16, -29a, -219a, and -122a), as well as gut motility (-10b, -143, -551b, -222, -145, let-7f, -375, and -128).[14, 16-21] These mechanisms are highly relevant to gut-metabolic health and dysregulation of these miRNAs might lead to the development of diabetes and gut dysmotility conditions.

We have previously reported that a conditional loss of miR-10b in KIT$^+$ cells, such as pancreatic beta cells and ICCs, led to the onset of diabetes and gut dysmotility.[20] Further, our previous study found a novel miR-10b-KLF11-KIT pathway responsible for the regulation of glucose homeostasis and gut motility. We demonstrated the targeting effect of miR-10b-5p on Krüppel-like factor-11 (KLF11), where miR-10b downregulates KLF11 expression, which is a transcription factor that then negatively regulates the expression of KIT. In the diabetic condition miR-10b is depleted leading to increased KLF11 expression, which leads to decreased KIT expression. Since KIT expression is essential for the functioning of ICCs,[22, 23] pacemaking cells in the gut, it is of no surprise that previous studies have reported that loss of KIT$^+$ ICCs lead to the development of gut dysmotility in both humans and mice.[24-26] Interestingly, when the KIT$^+$ cell-specific knockout (KO) mice were injected with the miR-10b mimic, there was restoration of KIT expression and the diabetes and gut dysmotility phenotypes were rescued.[20] Taken together, it is clear that loss of miR-10b plays a crucial role in the development of diabetes and gut dysmotility.

While our previous studies have elucidated the role of miR-10b in KIT$^+$ cells, in this study we aimed to elucidate if global loss of *mir-10b* led to the development of similar phenotypes as the cell-specific conditional KO as well as elucidating if the leaky gut is linked to the development of hyperglycemia and gut dysmotility. Additionally, loss of *mir-10b*, a key regulator of cell differentiation,[27-29] may impact the function and/or development of enteric neurons, resident

macrophages, enterocytes, enteroendocrine cells, SMC, and other cells important for maintaining gut homeostasis; therefore, further contributing to the development of diabetes and gut dysmotility. To test these hypotheses, we created a *mir-10b* global KO (gKO) mouse model using CRISPR-Mb3Cas12a/Mb3Cpf1. Using both loss-of-function and gain-of-function studies we found that the leaky gut phenotype is a core pathophysiological mechanism linking the hyperglycemic and gut dysmotility phenotypes. Finally, we found that treating the mice with a miR-10b mimic rescues these phenotypes and might have substantial therapeutic potential for the treatment of diabetes, gut dysmotility, and the leaky gut.

Materials and Methods

Animals

The Mb3Cas12a/Mb3Cpf1 endonuclease was used to generate *mir-10b* knockout mice like previously reported.[30] Since the Mb3Cas12a can process and utilize its own CRISPR RNA (crRNA), we used one crRNA harboring three 23nt spacers separated by three 20nt direct repeats (DRs) to target the *mir-10b* locus. One of the spacers was designed to target the TTV (V stands for A/C/G) protospacer adjacent motif (PAM) sequence (spacer 1) and the rest of the spacers (spacers 2 and 3) recognize the TTTV PAM sequence. Sequencing of PCR samples from the *mir-10b* KO mice were sent to the Nevada Genomics Center at the University of Nevada, Reno to confirm the presence of the *mir-10b* deletion. The founder with two deletions in both the 5p and 3p regions of miR-10b was selected for further breeding. PCR was then utilized to further confirm the deletion of *mir-10b* in the mice. The Institutional Animal Care and Use Committee at the University of Nevada, Reno approved all experimental procedures.

Automated Western Blot

Mucosa was separated from the smooth muscle tissue in the colon and was homogenized in radioimmunoprecipitation assay (RIPA) buffer using a Bullet Blender. The homogenate was then centrifuged at 12,000 rpm for 5 minutes at 4°C. The supernatant was then collected and stored at

-80°C. A detergent compatible Bradford assay was then performed to measure the protein concentration of each sample. The automated WES (protein simple) was used to analyze protein expression.

In Vivo Metabolic Screening

Body weight and 6-hour fasting blood glucose measurements of both male and female mice were conducted weekly between 6 and 30 weeks of age. A glucose tolerance test (GTT) was performed by measuring the 6-hour fasting blood glucose levels as well as blood glucose levels at 15-, 30-, 60-, 90-, and 120-minutes post glucose injection (2g/kg body weight). An insulin tolerance test (ITT) was performed by measuring the 6-hour fasting blood glucose levels as well as blood glucose levels at 30-, 60-, 90-, and 120-minutes post Lantus insulin glargine (0.6 IU/kg) injection.[20] Area under the curve analysis for both GTT and ITT was performed using GraphPad Prism 9 software.

In Vivo Functional Gastrointestinal Motility Procedures

Whole gut transit time was conducted by oral gavaging an Evans blue solution into the mice as previously reported.[20] The mice were then monitored every 10 minutes until a fecal pellet containing the Evans blue solution was expelled. The time from oral gavage until the time of Evans blue containing pellet expulsion was considered the whole gut transit time. Gastric emptying was measured following an oral gavage of a semi-solid solution containing Gastrosense™750.[20] Images were taken before the administration of Gastrosense™750 to ensure no autofluorescence and then 0-, 30-, and 60-minutes post-gavage using an IVIS Lumina III system (PerkinElmer). Fluorescence of the images from 0- and 30-minutes were quantified and compared to determine the percent of gastric emptying 30 minutes following the oral gavage using Living Image (PerkinElmer) software. Colonic transit time was measured by inserting a 3 mm glass bead 3 cm into the colon. The time from bead placement to bead expulsion is considered the bead expulsion time.

Pathological Analysis

To examine the microanatomy of the *mir-10b* gKO mice, colon cryostat sections were stained with Hematoxylin solution (ab220365) and Eosin Y Solution (ab246824) according to the manufacturers protocol. Slides were then visualized using Keyence BZ-X710 microscope.

Immunohistochemical and Confocal Microscopy Analysis

Murine colon tissue was analyzed through cryostat sectioned staining as previously described. Briefly, the slides were washed in 1X Tris-buffered saline (TBS), followed by blocking in 4% milk/1X TBS/0.1%–0.5% Triton X-114 (Sigma-Aldrich). The slides were then incubated at 4˚C with the primary antibody for 48 hours. Next, the slides were incubated with a secondary antibody at room temperature for 2 hours. After washing with 1X TBS and treated with Fluoroshield mounting medium with 40, 6-diamidino-2-phenylindole (Abcam). Fluoview FV10-ASW (Olympus) Viewer software (version 3.1) on an Olympus FV1000 confocal laser scanning microscope was used to image the slides.

Gut Permeability Assay

Mice are fasted overnight and then oral gavaged 600 mg/kg body weight of FITC-Dextran (4kDa).[31] 4 hours after the gavage, blood was collected by penetrating the retro-orbital sinus of the mice. The blood was stored in a vial containing EDTA to prevent blood clotting. The blood was then spun down at 15000 RPM for 15 minutes at 4˚C in order to collect the plasma. The plasma was diluted 1:5 with 1X PBS and then fluorescence was measured at 485 nm excitation and 528 nm emission using the GloMax® Explorer plate reader.

Rescue Experiments Through miR-10b Mimic Intervention

Intraperitoneal (IP) injection of either 500 ng/g of the miR-10b mimic (a chemically modified double-stranded RNA molecule that mimics endogenous miR-10b upregulates miRNA activity) or 500 ng/g of the scramble (SCR) RNA (a negative control miRNA mimic molecule with a random sequence that has been extensively tested and validated to ensure no identifiable effects) was

administered to male and female *mir-10b* gKO mice.[20] Body weight, blood glucose levels, functional gut motility assays, and gut permeability assays were performed 2-weeks post-injection.

miRNA Sequencing

Small RNA libraries were generated using an Illumina TruSeq Small RNA Preparation Kit (Illumina) following manufacturer's instructions. The cDNA libraries were sequenced following vendor's instructions.

Statistics

The experimental data are shown as the mean ± SEM. Two-tailed unpaired Student's t-test, Mann-Whitney U test, area under the curve calculations, and one-way or two-way ANOVA were used for all mouse and human experiments using GraphPad Prism 9 software.

Results

Generation of Global mir-10b Knockout Mice

In order to create a global (g) *mir-10b* knockout (KO) mouse model that did not disrupt the host gene exons (Figure 1*A*), we used the Mb3Cas12a/Mb3Cpf1 endonuclease and one crRNA harboring three 23nt spacers separated by three 20nt direct repeats (DRs) (Figure 1*B*) to target the *mir-10b* locus. Mice were then screened for deletion in the *mir-10b* gene using Sanger sequencing (Figure 1*C*). The founder was selected due to it having deletions in the portion of the *mir-10b* gene that encodes for the mature 3' and 5' miRNAs. Further confirmation of the KO mice was accomplished using PCR (Figure 1*D*). *mir-10b* gKO mice were observed to have increased body mass as compared to their wildtype (WT) counterparts (Figure 1*E*). We further confirmed the miR-10b deficiency (Figure 1*F*) through miRNA-seq analysis from colonic mucosa from *mir-10b* KO mice and healthy WT mice (Supplementary Table 1).

Global KO of mir-10b Leads to Body Weight Gain and Impaired Glucose Homeostasis

Further, we wanted to see if the global loss of miR-10b leads to obesity and hyperglycemia similar to the Kit+ cell specific conditional *mir-10b* KO mice. We found that male mice had significantly increased body weight gain when compared to their WT counterparts (Figure 2*A*). However, while we do see an increase in body weight in the female *mir-10b* gKO mice, the change was not significant compared to WT mice (Figure 2*A*). Additionally, we found that both male and female *mir-10b* gKO mice developed significantly increased blood glucose levels after 20 weeks of age, possibly indicating a hyperglycemic condition (Figure 2*B*). To further confirm if the *mir-10b* gKO mice developed impaired glucose homeostasis we performed glucose and insulin tolerance tests (GTT and ITT, respectively) (Figure 2*C*-*F*). While only males had significantly impaired glucose tolerance, both male and female *mir-10b* gKO mice developed insulin resistance, as evidenced by significantly increased area under the curve (AUC) (Figure 2*D*, *F*). Taken together, these data suggest that a global loss of miR-10b leads to the development of impaired glucose homeostasis.

Global mir-10b KO Mice Develop Delayed Gut Transit

It is well understood that the hyperglycemic condition is linked to gut dysmotility.[2] Therefore, we investigated whether *mir-10b* gKO mice also developed impaired gut motility. Interestingly, both male and female mice developed extensively delayed whole gut transit when compared to their WT counterparts, as evidenced by their significantly increased whole gut transit times (Figure 3*A*). Further, we found that both male and female *mir-10b* gKO mice developed slow transit constipation, which was indicated by significantly delayed colonic transit time (Figure 3*B*). Finally, significantly reduced percent of gastric emptying in both male and female *mir-10b* gKO mice (Figure 3*C*, *D*) indicated the development of impaired gastric emptying. Therefore, these data indicate that gKO of *mir-10b* causes the onset of gut dysmotility.

Leaky Gut Links Hyperglycemia and Gut Dysmotility Phenotypes

Intestinal barrier dysfunction, known as leaky gut, is a common co-occurrence with hyperglycemia and gut dysmotility.[32, 33] Recently, leaky gut has been proposed as a core

pathophysiological mechanism linking these two conditions.[2] Therefore, we hypothesized that *mir-10b* gKO mice may develop the leaky gut phenotype. First, we observed H&E staining of the distal colon in *mir-10b* gKO mice and found that the epithelium was extensively disorganized, likely caused by a breakdown of the epithelial barrier, when compared to their WT counterparts (Figure 4*A*). Additionally, we imaged cross sections stained with the Villin and DAPI antibodies of colon tissue from WT and *mir-10b* gKO mice (Figure 4*B*) and found that there was decreased Villin expression in the epithelium in *mir-10b* gKO mice when compared to their WT counterparts. To test the function of the epithelial barrier, we performed gut permeability assays and found that the *mir-10b* gKO mice had significantly increased gut permeability compared to WT mice as shown by increased FITC-dextran in the blood serum of the mice (Figure 4*C*). Further, we found that there was a significant reduction of the tight junction protein Tight junction protein-1, also known as Zonula occludens-1 (ZO-1), in the colon of *mir-10b* gKO mice (Figure 4*D*, *E*). Moreover, miRNA-seq analysis of differentially expressed miRNA from colonic mucosa from *mir-10b* KO mice and healthy WT mice revealed that overexpression of miR-21a-3p, miR-200b, and miR-30e (Supplementary Figure 1), which have been linked to the leaky gut phenotype in both *in vitro* and *in vivo* models of impaired barrier function highlighting their role in regulating tight junction proteins and gut immune function. Furthermore, GO terms associated with the depletion of miR-10b-5p in colonic mucosa of *mir-10b* KO vs. WT revealed the GO term ‘Cell junction’ was reduced in *mir-10b* KO mice as compared to WT mice (Supplementary Figure 2). Interestingly, we also found that patients with IBS-C, a known gut motility disorder that is linked to the leaky gut, had significantly reduced miR-10b expression as compared to healthy controls (HC) (Figure 4F). Taken together, these data suggest that global loss of *mir-10b* leads to the development of the leaky gut phenotype, and this may also be the case for a subset of patients with IBS-C.

Treatment with the miR-10b Mimic Rescues the Hyperglycemic, Gut Dysmotility, and Leaky Gut Phenotypes

For gain of function studies, a miR-10b-5p mimic was injected into 5-month-old mir-10b gKO mice. Additionally, a scramble (SCR) injection was given to mir-10b gKO mice as a negative

control. We analyzed body weight of the mice and discovered that mir-10b gKO mice did not have significant weight reduction two weeks after the mimic injection (Figure 5A); however, there was a significant reduction in blood glucose levels 2-weeks post-injection when compared to SCR injected mice (Figure 5B). Further, the gut dysmotility phenotype was rescued by the mimic injection as evidenced by significantly improved whole gut transit time (Figure 5C), colonic transit time (Figure 5D), and percent gastric emptying (Figure 5E) when compared to the SCR injected and mir-10b gKO mice. Interestingly, the mimic injection improved gut permeability of the mir-10b gKO mice to similar levels as their WT counterparts (Figure 5F). Further, the intestinal epithelial barrier integrity was restored following the mimic injection (Figure 5F,G). Moreover, ZO-1 expression was restored in mir-10b gKO mice following the mimic injection (Figure 5H, I). Further, we found that levels of the proinflammatory cytokine TNFα were reduced in mir-10b gKO mice injected with the mimic as compared to non-injected mir-10b gKO mice, suggesting the mimic injection decreased inflammation in the leaky gut (Figure 5J). Additionally, miRNA-seq analysis of colonic mucosa from mir-10b gKO mice injected with the mimic and mir-10b gKO mice that did not receive any injection confirmed that miR-10b was depleted in mir-10b gKO mice and slightly restored miR-10b-5p in mir-10b gKO mice following the miR-10b-5p mimic injection (Figure 5K). Interestingly, miR-10a-5p appeared to compensate for the loss of miR-10b in the mir-10b gKO mice; however, a miR-10b-5p mimic injection did not reduce miR-10a-5p levels (Figure 5L). In addition, leaky-gut associated miRNAs (miR-21a-3p and miR-200b) were upregulated in mir-10b gKO mice (Supplementary Figure 1A), highlighting the important role of miR-10b in maintaining barrier function and gut immune function. miR-21a-3p and miR-200b expression was decreased to normal levels, similar to those found in their WT counterparts, following injection with the miR-10b-5p mimic (Supplementary Figure 1B). These data suggest that the mimic injection is able to rescue impaired glucose homeostasis, gut dysmotility, and the leaky gut in *mir-10b* gKO mice. Additionally, the mimic might have potential for the treatment of diabetes, gut motility disorders, as well as other disorders linked to the leaky gut.

Discussion

It has been well established that hyperglycemia and gut dysmotility have a substantial co-occurrence; however, how these two disorders are related has been largely elusive.[34] Here we have identified a possible pathophysiological mechanism linking the two disorders, the leaky gut. Additionally, we have identified a potential treatment option for patients suffering from conditions linked to the leaky gut, such as IBS-C. Our data suggest that global loss of miR-10b leads to impaired gut barrier function, which links the hyperglycemia and gut dysmotility phenotypes.

mir-10b gKO mice have substantial weight gain likely due to the role of miR-10b in regulating expression of apolipoprotein L6 (Apol6), which is a lipid binding protein that has a key role in adipogenesis.[35] The observed increase in blood glucose levels, impaired glucose tolerance, as well as insulin resistance indicates the development of impaired glucose homeostasis, which is likely caused by the degeneration of pancreatic β-cells through the KLF11-KIT pathway.[20] Further, these mice develop severe gut dysmotility as evidenced by significantly increased whole gut transit time and colonic transit time, as well as reduced gastric emptying, which could be caused by the loss of KIT expression in ICCs,[20] along with degeneration of smooth muscle cells, macrophages, enteric neurons, along with other cells that function to maintain gut homeostasis. Most importantly, the diabetic and gut dysmotility phenotypes are linked by the development of the leaky gut phenotype as shown with the development of a disorganized epithelial barrier, increased gut permeability, and reduced ZO-1 expression. Leaky gut further led to gut immune dysfunction as evidenced by the increased TNFα expression in colonic tissue from mir-10b gKO mice. Overexpression of miR-21a-3p, miR-200b, and miR-30e in the colonic mucosa from mir-10b KO mice further reinforces that the leaky gut phenotype is associated with cellular remodeling of the epithelial barrier with the reduction of the GO term ‘cell junction’. Taken together, the *mir-10b* gKO mouse model is likely a great model for studying the leaky gut and its associated conditions (gut immune dysfunction, gut microbiota dysbiosis, etc.).

Additionally, we found that injection with a miR-10b mimic rescued the hyperglycemic, gut dysmotility, and leaky gut phenotypes. This was evidenced by significantly improved blood glucose levels, whole gut transit time, gastric emptying, colonic transit time as well as restored gut barrier

integrity, decreased gut permeability, and increased ZO-1 expression 2-weeks post-injection. This highlights the potential of the miR-10b mimic as a treatment option for patients suffering from conditions linked to the leaky gut, such as IBS and diabetic gastroparesis.

We found that patients with IBS had reduced miR-10b expression as compared to healthy controls (HC), likely contributing to the intestinal barrier dysfunction. Studies have shown miRNA dysregulation in patients with IBS elucidating how dysregulated miRNAs modulate the leaky gut phenotype. Recently, miRNA transcriptome data from colonic biopsies showed that miR-219-5p levels were downregulated in IBS as compared to HCs.[21] The authors demonstrated inhibition of miR-219a-5p in IECs altered the expression of permeability-associated genes including TJP1/ZO-1, E-cadherin (CDH1), carcinoembryonic antigen-related cell adhesion molecule 5 (CEA- CAM5), and catenin delta 1 (CTNND1). Another important study showed miR-29a is involved in the pathophysiology of IBS, by downregulating the expression of ZO-1 and CLDN1.[17] This study suggested that ZO-1 and CLDN1 expression in the colonic mucosa of an IBS murine model was significantly increased following intervention with a miR-29a inhibitor, suggesting miR-29a is critical to maintain intestinal barrier integrity. miR-29a is an important miRNA in regulating intestinal barrier integrity in patients with IBS through its interaction with the glutamine synthetase gene.[17] Upregulation of miR-29a leads to reduced glutamine synthetase (GLUL) levels resulting in impaired intestinal membrane permeability in patients with IBS. Exploring the interplay between miRNAs and tight junction proteins would open a window for putative therapeutic candidates that might reinforce the gut barrier integrity, consequently preventing or ameliorating inflammatory reactions and potentially re-establishing gut-metabolic homeostasis.

The leaky gut has also been associated with immune cell infiltration.[36, 37] The gut epithelial barrier is the front-line defender against pathogens and their associated molecules.[38] When there is breakdown in this defense it allows for infiltration of these harmful bacteria and molecules, leading to an inflammatory response.[17, 21, 38, 39] This chronic low-grade inflammatory response causes the development of diabetes, gut dysmotility, as well as Parkinson's disease and even has been implicated in the exacerbate the symptoms of Lupus.[40, 41] Therefore, it is imperative to focus

future research on elucidating if *mir-10b* gKO mice also develop this inflammatory response. Additionally, it is of paramount importance to uncover the role of miR-10b in other cells essential to proper gut function and maintenance, such as neurons, PDGFRα cells, smooth muscle cells, etc.[42-47] Further, the leaky gut phenotype should be assessed using an Ussing chamber, which is currently the gold standard for measuring epithelial barrier permeability. Moreover, validation of the leaky gut phenotype should be conducted using a larger number of patients.

Gut microbial alterations are extensively prevalent in patients with IBS and metabolic disorders.[2, 14, 48] Studies noted the role of host miRNAs in shaping the gut microbiota, which might further modulate the altered gut microbiota-linked pathophysiological mechanisms such as gut motility, gut immune dysfunction, impaired gut barrier function, and insulin resistance.[49-51] A landmark study showed that host fecal miRNA directly regulates gut microbial gene expression and growth.[49] This study showed that human and mouse feces contained specific miRNAs, such as miR-155 and miR-1224. Mice deficient in the miRNA-generating protein Dicer (restricted only to intestinal epithelial cells) had reduced levels of fecal miRNA, suggesting that IECs are a significant source of miRNA in feces. Further, the authors showed that mice with Dicer knocked out specifically in IECs had gut microbiota dysbiosis and were more susceptible to induced colitis than wild-type mice. This study provided evidence that the host can actively modulate gut microbes through miRNAs. Further, one study compared the miRNA profile of IECs from conventional and GF mice and demonstrated that miR-21-5p is induced by commensal bacteria, with implications for intestinal barrier function regulation.[52] miR-21-5p is also dysregulated in our mir-10b gKO mice and might involve in the gut microbiota dysbiosis. Future studies are warranted to provide significant clinical insights into different facets of the host miRNA-gut microbiota interplay and to elucidate the role of the host miRNAs in shaping gut microbial composition in gut and metabolic health.

Overall, our study has provided evidence linking diabetes and gut dysmotility to the leaky gut phenotype, with miR-10b being a key player. This may provide new treatment options for millions of patients suffering from conditions associated with the leaky gut.

References

1. Ogurtsova K, Guariguata L, Barengo NC, et al. IDF diabetes Atlas: Global estimates of undiagnosed diabetes in adults for 2021. Diabetes Res Clin Pract 2022;183:109118.
2. Singh R, Zogg H, Wei L, et al. Gut Microbial Dysbiosis in the Pathogenesis of Gastrointestinal Dysmotility and Metabolic Disorders. J Neurogastroenterol Motil 2021;27:19-34.
3. Singh R, Zogg H, Ghoshal UC, et al. Current Treatment Options and Therapeutic Insights for Gastrointestinal Dysmotility and Functional Gastrointestinal Disorders. Front Pharmacol 2022;13:808195.
4. Camilleri M, Kuo B, Nguyen L, et al. ACG Clinical Guideline: Gastroparesis. Am J Gastroenterol 2022;117:1197-1220.
5. Chen RY, Kung VL, Das S, et al. Duodenal Microbiota in Stunted Undernourished Children with Enteropathy. N Engl J Med 2020;383:321-333.
6. Thaiss CA, Levy M, Grosheva I, et al. Hyperglycemia drives intestinal barrier dysfunction and risk for enteric infection. Science 2018;359:1376-1383.
7. Gehrig JL, Venkatesh S, Chang HW, et al. Effects of microbiota-directed foods in gnotobiotic animals and undernourished children. Science 2019;365.
8. Martin A, Devkota S. Hold the Door: Role of the Gut Barrier in Diabetes. Cell Metab 2018;27:949-951.
9. Zogg H, Singh R, Ro S. Current Advances in RNA Therapeutics for Human Diseases. Int J Mol Sci 2022;23.
10. Matsui M, Corey DR. Non-coding RNAs as drug targets. Nat Rev Drug Discov 2017;16:167-179.
11. Winkle M, El-Daly SM, Fabbri M, et al. Noncoding RNA therapeutics - challenges and potential solutions. Nat Rev Drug Discov 2021;20:629-651.
12. Yu AM, Choi YH, Tu MJ. RNA Drugs and RNA Targets for Small Molecules: Principles, Progress, and Challenges. Pharmacol Rev 2020;72:862-898.

13. Paunovska K, Loughrey D, Dahlman JE. Drug delivery systems for RNA therapeutics. Nat Rev Genet 2022;23:265-280.
14. Singh R, Zogg H, Ro S. Role of microRNAs in Disorders of Gut-Brain Interactions: Clinical Insights and Therapeutic Alternatives. J Pers Med 2021;11.
15. Mori MA, Ludwig RG, Garcia-Martin R, et al. Extracellular miRNAs: From Biomarkers to Mediators of Physiology and Disease. Cell Metab 2019;30:656-673.
16. Mazzone A, Strege PR, Gibbons SJ, et al. microRNA overexpression in slow transit constipation leads to reduced NaV1.5 current and altered smooth muscle contractility. Gut 2020;69:868-876.
17. Zhou Q, Costinean S, Croce CM, et al. MicroRNA 29 targets nuclear factor-kappaB-repressing factor and Claudin 1 to increase intestinal permeability. Gastroenterology 2015;148:158-169 e8.
18. Zhou Q, Yang L, Larson S, et al. Decreased miR-199 augments visceral pain in patients with IBS through translational upregulation of TRPV1. Gut 2016;65:797-805.
19. Martinez C, Rodino-Janeiro BK, Lobo B, et al. miR-16 and miR-125b are involved in barrier function dysregulation through the modulation of claudin-2 and cingulin expression in the jejunum in IBS with diarrhoea. Gut 2017;66:1537-1538.
20. Singh R, Ha SE, Wei L, et al. miR-10b-5p Rescues Diabetes and Gastrointestinal Dysmotility. Gastroenterology 2021;160:1662-1678 e18.
21. Mahurkar-Joshi S, Rankin CR, Videlock EJ, et al. The Colonic Mucosal MicroRNAs, MicroRNA-219a-5p, and MicroRNA-338-3p Are Downregulated in Irritable Bowel Syndrome and Are Associated With Barrier Function and MAPK Signaling. Gastroenterology 2021;160:2409-2422 e19.
22. Beckett EA, Ro S, Bayguinov Y, et al. Kit signaling is essential for development and maintenance of interstitial cells of Cajal and electrical rhythmicity in the embryonic gastrointestinal tract. Dev Dyn 2007;236:60-72.

23. Neve B, Fernandez-Zapico ME, Ashkenazi-Katalan V, et al. Role of transcription factor KLF11 and its diabetes-associated gene variants in pancreatic beta cell function. Proc Natl Acad Sci U S A 2005;102:4807-12.
24. Grover M, Bernard CE, Pasricha PJ, et al. Clinical-histological associations in gastroparesis: results from the Gastroparesis Clinical Research Consortium. Neurogastroenterol Motil 2012;24:531-9, e249.
25. Sanders KM, Ordog T, Ward SM. Physiology and pathophysiology of the interstitial cells of Cajal: from bench to bedside. IV. Genetic and animal models of GI motility disorders caused by loss of interstitial cells of Cajal. Am J Physiol Gastrointest Liver Physiol 2002;282:G747-56.
26. Pasricha PJ, Grover M, Yates KP, et al. Progress in Gastroparesis - A Narrative Review of the Work of the Gastroparesis Clinical Research Consortium. Clin Gastroenterol Hepatol 2022.
27. Gong X, Chao R, Wang P, et al. Interplay of transcription factors and microRNAs during embryonic hematopoiesis. Sci China Life Sci 2017;60:168-177.
28. Ge G, Yang D, Tan Y, et al. miR-10b-5p Regulates C2C12 Myoblasts Proliferation and Differentiation. Biosci Biotechnol Biochem 2019;83:291-299.
29. Yang J, Wang S, Wang F, et al. Downregulation of miR-10b promotes osteoblast differentiation through targeting Bcl6. Int J Mol Med 2017;39:1605-1612.
30. Wang Z, Wang Y, Wang S, et al. Efficient genome editing by CRISPR-Mb3Cas12a in mice. J Cell Sci 2020;133.
31. Rao M, Rastelli D, Dong L, et al. Enteric Glia Regulate Gastrointestinal Motility but Are Not Required for Maintenance of the Epithelium in Mice. Gastroenterology 2017;153:1068-1081 e7.
32. You Q, Shen Y, Wu Y, et al. Neutrophil Extracellular Traps Caused by Gut Leakage Trigger the Autoimmune Response in Nonobese Diabetic Mice. Front Immunol 2021;12:711423.
33. Camilleri M, Vella A. What to do about the leaky gut. Gut 2022;71:424-435.

34. Bytzer P, Talley NJ, Leemon M, et al. Prevalence of gastrointestinal symptoms associated with diabetes mellitus: a population-based survey of 15,000 adults. Arch Intern Med 2001;161:1989-96.
35. Tan Y, Gan M, Fan Y, et al. miR-10b-5p regulates 3T3-L1 cells differentiation by targeting Apol6. Gene 2019;687:39-46.
36. Jang YJ, Kim WK, Han DH, et al. Lactobacillus fermentum species ameliorate dextran sulfate sodium-induced colitis by regulating the immune response and altering gut microbiota. Gut Microbes 2019;10:696-711.
37. Niesler B, Kuerten S, Demir IE, et al. Disorders of the enteric nervous system - a holistic view. Nat Rev Gastroenterol Hepatol 2021;18:393-410.
38. Shin A, Preidis GA, Shulman R, et al. The Gut Microbiome in Adult and Pediatric Functional Gastrointestinal Disorders. Clin Gastroenterol Hepatol 2019;17:256-274.
39. Ghoshal UC. Marshall and Warren Lecture 2019: A paradigm shift in pathophysiological basis of irritable bowel syndrome and its implication on treatment. J Gastroenterol Hepatol 2020;35:712-721.
40. Chen QQ, Haikal C, Li W, et al. Gut Inflammation in Association With Pathogenesis of Parkinson's Disease. Front Mol Neurosci 2019;12:218.
41. Charoensappakit A, Sae-Khow K, Leelahavanichkul A. Gut Barrier Damage and Gut Translocation of Pathogen Molecules in Lupus, an Impact of Innate Immunity (Macrophages and Neutrophils) in Autoimmune Disease. Int J Mol Sci 2022;23.
42. Yarandi SS, Kulkarni S, Saha M, et al. Intestinal Bacteria Maintain Adult Enteric Nervous System and Nitrergic Neurons via Toll-like Receptor 2-induced Neurogenesis in Mice. Gastroenterology 2020;159:200-213 e8.
43. Drumm BT, Cobine CA, Baker SA. Insights on gastrointestinal motility through the use of optogenetic sensors and actuators. J Physiol 2022;600:3031-3052.
44. Ha SE, Jin B, Jorgensen BG, et al. Transcriptome profiling of subepithelial PDGFRalpha cells in colonic mucosa reveals several cell-selective markers. PLoS One 2022;17:e0261743.

45. Ji S, Traini C, Mischopoulou M, et al. Muscularis macrophages establish cell-to-cell contacts with telocytes/PDGFRalpha-positive cells and smooth muscle cells in the human and mouse gastrointestinal tract. Neurogastroenterol Motil 2021;33:e13993.
46. Park C, Hennig GW, Sanders KM, et al. Serum response factor-dependent MicroRNAs regulate gastrointestinal smooth muscle cell phenotypes. Gastroenterology 2011;141:164-75.
47. Lee MY, Ha SE, Park C, et al. Transcriptome of interstitial cells of Cajal reveals unique and selective gene signatures. PLoS One 2017;12:e0176031.
48. Barbara G, Feinle-Bisset C, Ghoshal UC, et al. The Intestinal Microenvironment and Functional Gastrointestinal Disorders. Gastroenterology 2016.
49. Liu S, da Cunha AP, Rezende RM, et al. The Host Shapes the Gut Microbiota via Fecal MicroRNA. Cell Host Microbe 2016;19:32-43.
50. Aguilar C, Mano M, Eulalio A. MicroRNAs at the Host-Bacteria Interface: Host Defense or Bacterial Offense. Trends Microbiol 2019;27:206-218.
51. Liu S, Weiner HL. Control of the gut microbiome by fecal microRNA. Microb Cell 2016;3:176-177.
52. Nakata K, Sugi Y, Narabayashi H, et al. Commensal microbiota-induced microRNA modulates intestinal epithelial permeability through the small GTPase ARF4. J Biol Chem 2017;292:15426-15433.

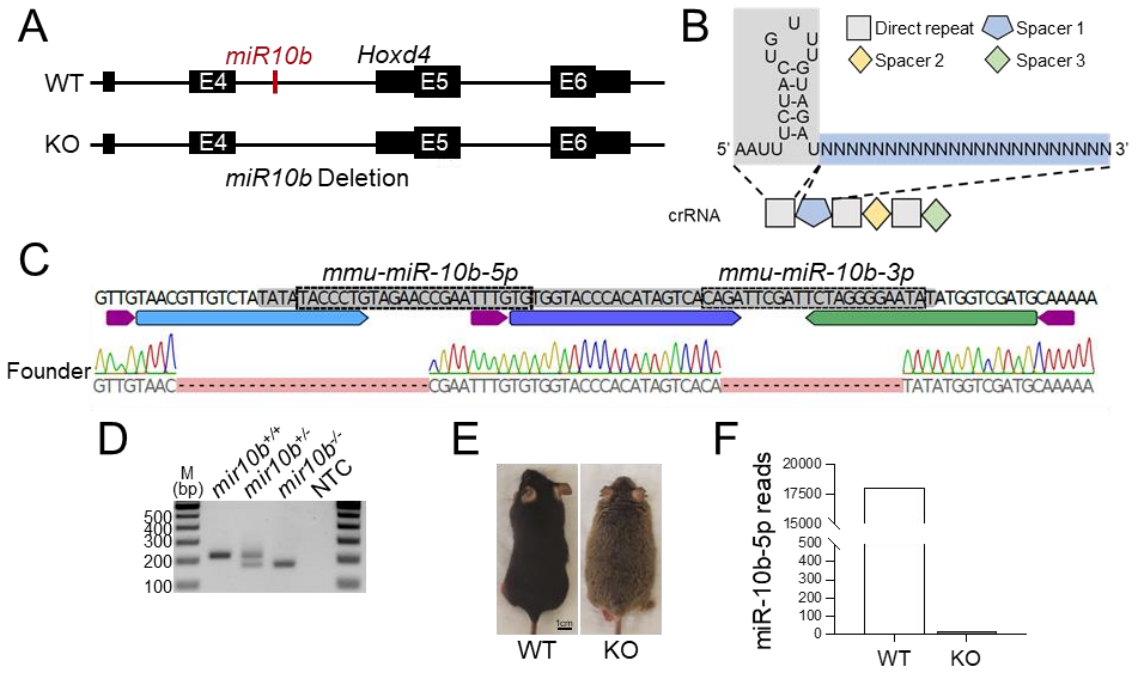

Figure 1: Generation of Global *mir-10b* Knockout Mice. (A) Schematic of the deletion of *mir-10b*. *mir-10b* is located within the intron of *Hoxd4.* (B) Schematic of the crRNA used to create the *mir-10b* gKO mouse model. (C) Sequencing results confirming deletion of both *miR-10b-5p* and *miR-10b-3p*. (D) PCR confirmation of the *mir-10b* gKO mice. (E) Gross body image comparison of the WT and *mir-10b* gKO (KO) mice. (F) miR-10b miRNA reads in WT vs. KO mice.

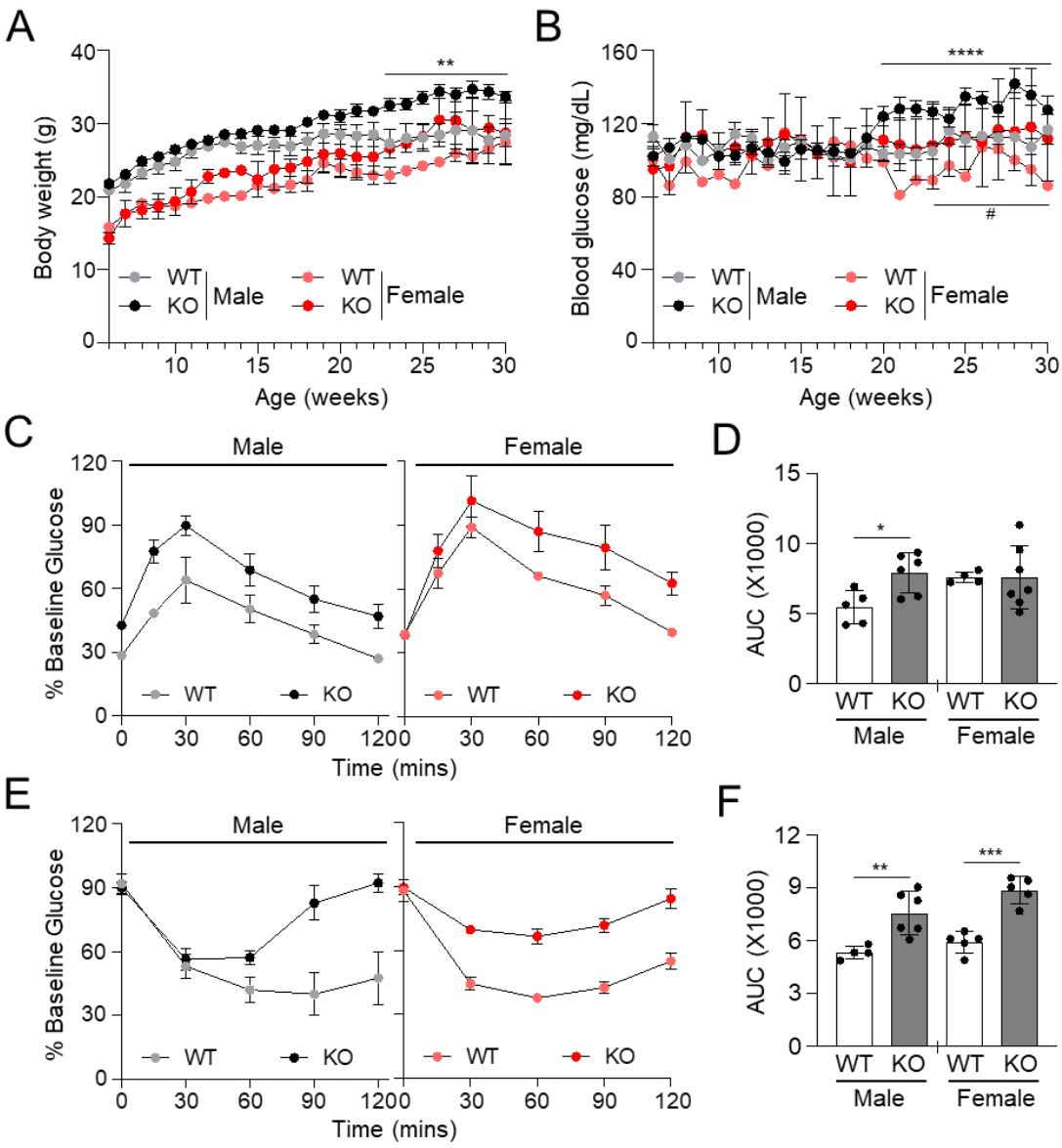

Figure 2: Global KO of *miR-10b* Leads to Body Weight Gain and Impaired Glucose Homeostasis. (A) Body weight comparison of both male and female *mir-10b* gKO (KO) and WT mice. (B) Blood glucose comparison of both male and female KO and WT mice. (C) Glucose tolerance tests of both male and female KO and WT mice. (D) AUC from C. (E) Insulin tolerance tests of both male and female KO and WT mice. (F) AUC from E.

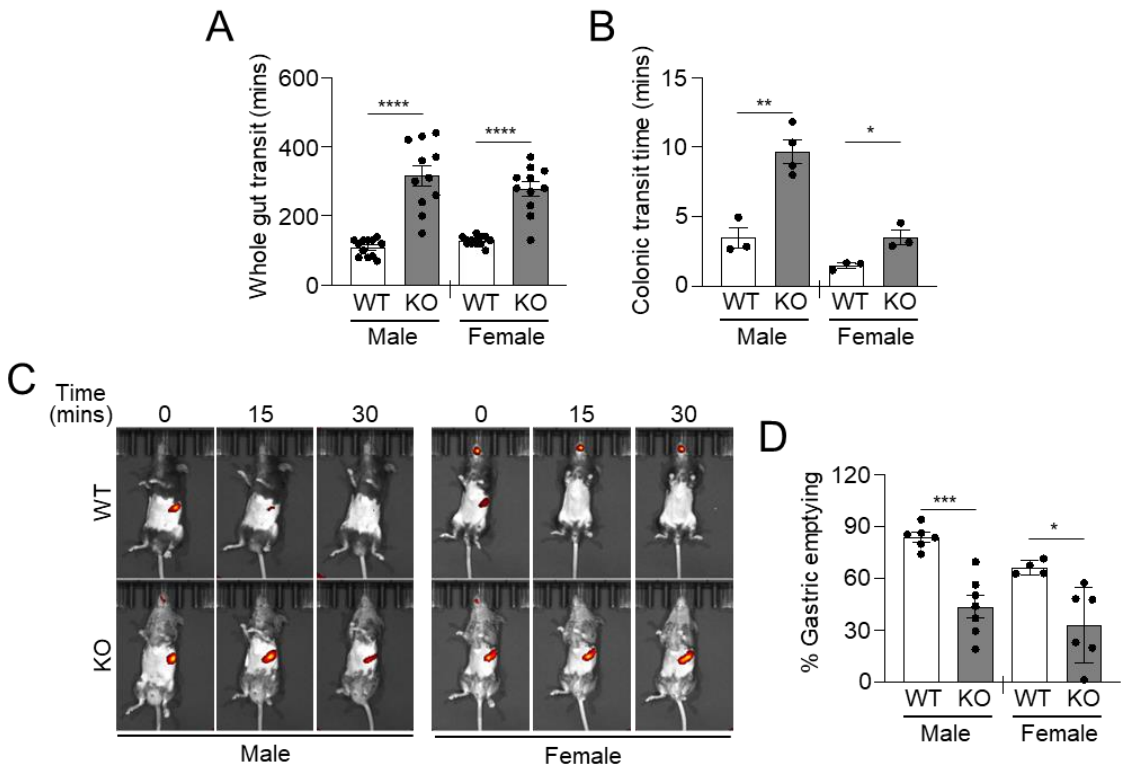

Figure 3: Global *mir-10b* KO Mice Develop Delayed Gut Transit. (A) Whole gut transit time comparison of both male and female *mir-10b* gKO (KO) and WT mice. (B) Colonic transit time comparison of both male and female KO and WT mice. (C) Gastric emptying images of both male and female KO and WT mice. (D) Quantification of percent gastric emptying after 30 minutes of both male and female KO and WT mice..

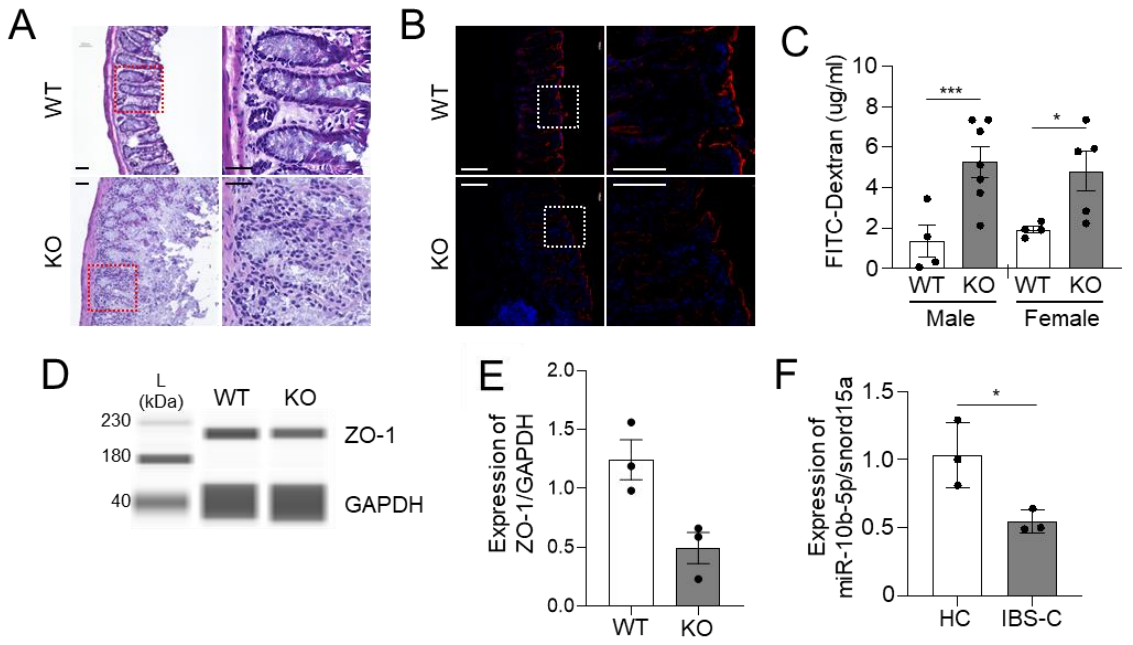

Figure 4: Global *mir-10b* KO Mice Develop the Leaky Gut Phenotype. (A) H&E staining of colon cross sections from *mir-10b* gKO (KO) and WT mice. (B) Villin (red) and DAPI (blue) staining of colon cross sections from KO and WT mice. (C) Amount of FITC-Dextran found in serum from KO and WT mice. (D, E) Western blot and quantification of ZO-1 expression from the colon of KO and WT mice. (F) miR-10b-5p expression from patients with IBS-C and healthy controls (HC) normalized by snord15a expression.

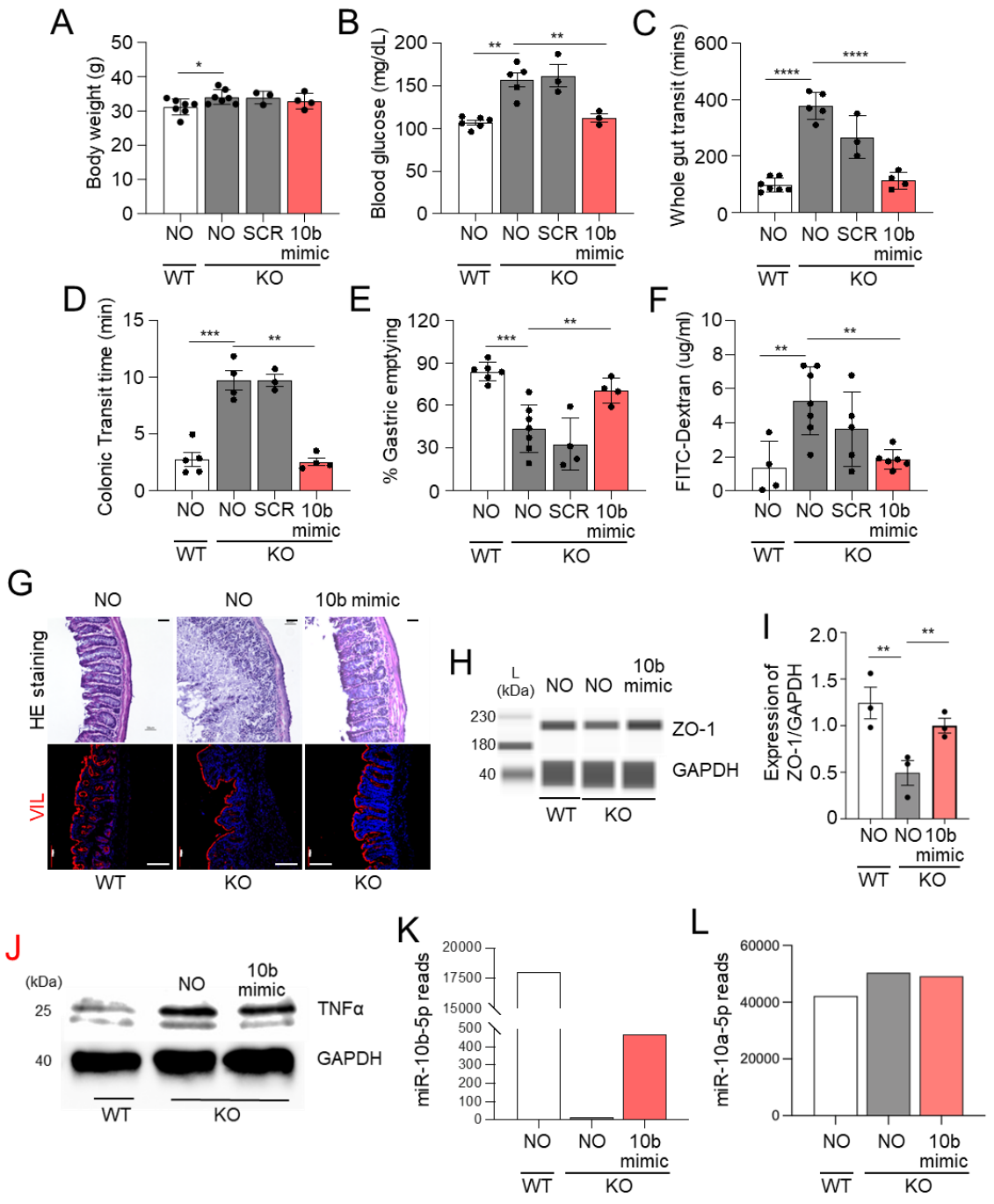

Figure 5: Treatment with the miR-10b Mimic Rescues the Hyperglycemic, Gut Dysmotility, and Leaky Gut Phenotypes. (A) Confirmation of the restoration of miR-10b in colonic mucosa following 10b mimic injection in mice. (B) Body weight comparison between WT non-injected (NO) mice, *mir-10b* gKO (KO) mice either injected with the scramble (SCR) RNA or the miR-10b (10b)

mimic, and NO KO mice. (C) Blood glucose comparison between NO WT, NO KO, SCR KO, and 10b mimic injected KO mice. (D) Comparison of whole gut transit time between NO WT, NO KO, SCR KO, and 10b mimic injected KO mice. (E) Colonic transit time comparison between NO WT, NO KO, SCR KO, and 10b mimic injected KO mice. (F) Comparison of percent gastric emptying between NO WT, NO KO, SCR KO, and 10b mimic injected KO mice. (G) Amount of FITC-Dextran found in serum from NO WT, NO KO, and 10b mimic injected KO mice. (H) Top: H&E staining of colon cross sections from WT, KO, and mimic injected KO mice. Bottom: Villin (red) and DAPI (blue) staining of colon cross sections from WT, KO, and mimic injected KO mice. (I, J) Western blot and quantification of ZO-1 expression from the colon of WT, KO, and mimic injected KO mice. (K) Top 10 differentially expressed miRNAs in WT, KO and 10b mimic injected mice. (L) TNFα expression in WT, KO and 10b mimic injected mice.

Table 1: Differentially expressed miRNAs in colonic mucosa from WT, KO, and 10b injected mice

miRNA name	miRNA reads in colonic mucosa			Changes in miRNA reads	
	WT	KO	KO+10b	KO-WT	(KO+10b)-KO
miR-145a-5p	261,621	83,319	529,831	-178,302	446,512
miR-378a-3p	211,958	153,738	66,829	-58,220	-86,909
miR-23a-3p	118,055	77,778	68,171	-40,277	-9,607
miR-429-3p	83,919	46,991	74,855	-36,928	27,864
miR-23b-3p	75,844	41,292	51,637	-34,552	10,345
miR-27a-3p	96,824	64,676	111,800	-32,148	47,124
miR-27b-3p	299,991	277,980	567,023	-22,011	289,043
miR-10b-5p	18,057	14	469	-18,043	455
miR-142a-5p	31,674	14,200	47,347	-17,474	33,147
miR-141-3p	54,818	43,461	51,514	-11,357	8,053
miR-16-5p	19,832	11,045	15,507	-8,787	4,462
miR-29a-3p	101,418	95,703	255,114	-5,715	159,411
miR-24-3p	30,796	26,266	36,240	-4,530	9,974
miR-106b-5p	12,265	8,351	8,926	-3,914	575
miR-378c	14,557	10,964	10,241	-3,593	-723
let-7d-3p	14,833	11,921	2,284	-2,912	-9,637
miR-574-3p	5,710	2,813	954	-2,897	-1,859
miR-215-3p	4,718	1,875	3,846	-2,843	1,971
miR-29c-3p	4,730	2,314	6,116	-2,416	3,802
let-7c-3p	4,669	2,398	6,158	-2,271	3,760
miR-99b-5p	23,690	21,848	22,007	-1,842	159
miR-345-5p	4,250	2,432	4,234	-1,818	1,802
miR-182-5p	19,307	17,564	19,337	-1,743	1,773
miR-362-3p	4,081	2,463	3,679	-1,618	1,216
miR-342-3p	4,674	3,074	1,174	-1,600	-1,900
miR-130a-3p	2,722	1,234	1,945	-1,488	711
miR-378a-5p	4,742	3,258	857	-1,484	-2,401
miR-125a-5p	8,251	6,833	6,918	-1,418	85
miR-136-3p	3,725	2,310	2,047	-1,415	-263
miR-195a-5p	7,192	5,894	6,458	-1,298	564
miR-145a-3p	11,099	9,886	24,569	-1,213	14,683
miR-210-3p	9,973	8,888	10,020	-1,085	1,132
miR-194-3p	1,945	1,039	1,696	-906	657
miR-133b-3p	2,158	1,286	1,726	-872	440
miR-196b-5p	9,152	8,294	4,556	-858	-3,738
miR-30e-3p	3,650	2,828	8,105	-822	5,277
miR-1839-5p	3,865	3,086	1,595	-779	-1,491
miR-451a	1,615	849	2,164	-766	1,315
miR-365-3p	1,957	1,200	1,649	-757	449
let-7b-3p	1,551	870	980	-681	110

miR-145b	759	78	1,443	-681	1,365
miR-18a-5p	1,827	1,158	1,071	-669	-87
miR-328-3p	1,533	895	245	-638	-650
miR-500-3p	1,237	609	595	-628	-14
let-7f-3p	1,285	687	1,828	-598	1,141
miR-150-5p	1,187	613	410	-574	-203
miR-329-3p	916	357	111	-559	-246
miR-582-5p	1,087	537	918	-550	381
miR-350-3p	1,112	563	382	-549	-181
miR-214-3p	2,749	2,211	371	-538	-1,840
miR-541-5p	2,949	2,412	306	-537	-2,106
miR-192-3p	1,679	1,147	1,487	-532	340
miR-425-5p	3,595	3,109	3,872	-486	763
miR-22-5p	1,165	682	1,654	-483	972
miR-154-5p	732	256	114	-476	-142
miR-149-5p	982	513	271	-469	-242
miR-382-3p	950	495	315	-455	-180
miR-16-3p	849	436	553	-413	117
miR-425-3p	899	489	722	-410	233
miR-7a-3p	916	509	915	-407	406
miR-10a-3p	788	382	397	-406	15
miR-199b-5p	18,511	18,221	10,158	-290	-8,063
miR-193a-3p	549	262	288	-287	26
miR-181d-5p	2,574	2,296	2,338	-278	42
miR-495-3p	606	336	76	-270	-260
miR-223-3p	1,438	1,179	1,821	-259	642
miR-28c	3,478	3,227	5,739	-251	2,512
miR-320-3p	3,880	3,640	963	-240	-2,677
miR-92b-3p	1,165	947	259	-218	-688
miR-26a-3p	368	158	560	-210	402
miR-212-3p	393	201	170	-192	-31
miR-337-3p	256	71	61	-185	-10
miR-5099	892	717	530	-175	-187
miR-193b-3p	414	241	162	-173	-79
miR-369-3p	518	350	189	-168	-161
miR-29b-3p	1,249	1,086	2,808	-163	1,722
miR-139-5p	6,964	6,801	2,620	-163	-4,181
miR-140-3p	7,968	7,806	5,233	-162	-2,573
miR-652-3p	5,850	5,689	3,592	-161	-2,097
miR-15b-3p	560	418	1,101	-142	683
miR-98-3p	175	39	182	-136	143
miR-196a-3p	502	367	733	-135	366
miR-511-3p	427	293	449	-134	156
miR-137-3p	420	289	719	-131	430

miR-333	273	153	224	-120	71
miR-652-5p	175	60	33	-115	-27
miR-664-3p	360	247	69	-113	-178
let-7i-3p	537	427	327	-110	-100
miR-669o-3p	155	49	30	-106	-19
miR-181b-5p	2,562	2,460	1,474	-102	-986
miR-93-3p	218	118	220	-100	102
miR-124-3p	168	77	100	-91	23
miR-204-5p	204	121	79	-83	-42
miR-300-3p	2,291	2,208	1,356	-83	-852
let-7g-3p	250	170	204	-80	34
miR-3068-3p	405	326	454	-79	128
miR-490-3p	295	217	402	-78	185
miR-674-5p	280	204	37	-76	-167
miR-1843a-3p	84	10	12	-74	2
miR-26b-3p	221	149	204	-72	55
miR-501-5p	112	40	0	-72	-40
miR-872-5p	1,980	1,908	4,574	-72	2,666
miR-1839-3p	384	315	432	-69	117
miR-324-3p	122	53	17	-69	-36
miR-29a-5p	219	151	418	-68	267
miR-376b-5p	124	60	58	-64	-2
miR-125a-3p	102	39	41	-63	2
miR-9-5p	514	452	440	-62	-12
miR-490-5p	61	0	64	-61	64
miR-29c-5p	287	230	302	-57	72
miR-187-3p	479	424	221	-55	-203
miR-671-3p	145	92	104	-53	12
miR-1843b-3p	50	0	8	-50	8
miR-15a-3p	220	170	142	-50	-28
miR-181b-1-3p	95	49	198	-46	149
miR-154-3p	186	141	53	-45	-88
miR-30b-3p	232	187	408	-45	221
miR-744-3p	177	135	162	-42	27
miR-335-3p	127	85	273	-42	188
miR-450a-5p	937	896	359	-41	-537
miR-487b-3p	102	60	59	-42	-1
miR-3105-3p	196	156	309	-40	153
miR-191-3p	80	40	61	-40	21
miR-130a-5p	55	15	23	-40	8
miR-1247-5p	46	7	0	-39	-7
miR-101a-5p	38	0	26	-38	26
miR-34b-3p	50	13	67	-37	54
miR-676-3p	153	116	115	-37	-1

miR-20a-3p	98	61	120	-37	59
miR-708-5p	320	284	725	-36	441
miR-188-5p	108	72	69	-36	-3
miR-30a-3p	2,202	2,167	6,155	-35	3,988
miR-384-3p	41	7	90	-34	83
miR-133a-5p	70	36	205	-34	169
miR-378b	194	160	131	-34	-29
miR-802-5p	68	35	26	-33	-9
miR-671-5p	137	106	64	-31	-42
miR-103-5p	31	0	0	-31	0
miR-669c-5p	89	59	8	-30	-51
miR-421-3p	270	240	399	-30	159
miR-323-3p	91	61	47	-30	-14
let-7e-3p	154	124	142	-30	18
miR-337-5p	244	215	62	-29	-153
miR-466c-3p	47	18	15	-29	-3
miR-132-3p	699	671	217	-28	-454
miR-8103	27	0	0	-27	0
miR-141-5p	349	323	301	-26	-22
miR-7033-5p	26	0	0	-26	0
miR-138-5p	66	42	65	-24	23
miR-125b-3p	249	224	736	-25	512
miR-450a-3p	45	24	0	-21	-24
miR-450b-3p	45	24	0	-21	-24
miR-467d-3p	32	12	8	-20	-4
miR-708-3p	107	86	455	-21	369
miR-214-5p	264	244	126	-20	-118
miR-130b-3p	590	570	412	-20	-158
miR-129-3p	171	152	117	-19	-35
miR-467b-5p	39	20	65	-19	45
miR-190a-3p	44	25	41	-19	16
miR-210-5p	44	26	161	-18	135
miR-34c-3p	17	0	14	-17	14
miR-551b-3p	17	0	9	-17	9
miR-203-5p	41	25	19	-16	-6
miR-3105-5p	26	10	12	-16	2
miR-129-5p	63	47	56	-16	9
miR-129-3p	95	81	58	-14	-23
miR-30c-3p	381	367	215	-14	-152
miR-330-5p	158	145	128	-13	-17
miR-326-3p	825	811	257	-14	-554
miR-598-3p	172	159	195	-13	36
miR-12191-3p	12	0	0	-12	0
miR-211-5p	12	0	0	-12	0

miR-212-5p	158	146	118	-12	-28
miR-542-5p	19	7	0	-12	-7
miR-297b-5p	11	0	9	-11	9
miR-381-5p	11	0	0	-11	0
miR-27b-5p	252	241	246	-11	5
miR-669d-5p	30	20	20	-10	0
miR-6418-3p	10	0	0	-10	0
miR-540-3p	17	7	0	-10	-7
miR-540-5p	147	138	28	-9	-110
miR-504-5p	9	0	0	-9	0
miR-544-3p	9	0	0	-9	0
miR-297a-5p	8	0	6	-8	6
miR-297b-3p	22	14	22	-8	8
miR-1a-5p	8	0	12	-8	12
miR-201-5p	8	0	0	-8	0
miR-222-5p	8	0	23	-8	23
miR-3098-5p	8	0	0	-8	0
miR-3110-5p	8	0	14	-8	14
miR-18a-3p	31	24	0	-7	-24
miR-34a-3p	15	7	14	-8	7
miR-758-3p	21	14	19	-7	5
miR-1198-3p	7	0	0	-7	0
miR-188-3p	7	0	12	-7	12
miR-206-3p	7	0	0	-7	0
miR-23a-5p	7	0	8	-7	8
miR-3072-3p	7	0	0	-7	0
miR-467d-5p	7	0	41	-7	41
miR-672-3p	7	0	0	-7	0
miR-873a-5p	7	0	12	-7	12
miR-1306-5p	31	25	0	-6	-25
miR-1943-5p	20	14	20	-6	6
miR-301b-3p	27	21	47	-6	26
miR-100-3p	6	0	0	-6	0
miR-146a-3p	6	0	14	-6	14
miR-375-5p	6	0	12	-6	12
miR-500-5p	6	0	0	-6	0
miR-541-3p	6	0	0	-6	0
miR-433-5p	12	7	0	-5	-7
miR-377-3p	214	209	61	-5	-148
miR-122-5p	11	7	47	-4	40
miR-3090-3p	11	7	12	-4	5
miR-466h-3p	6	2	0	-4	-2
miR-20b-5p	42	39	23	-3	-16
miR-668-3p	11	8	0	-3	-8

miR-376c-5p	3	0	0	-3	0
miR-466a-5p	3	0	4	-3	4
miR-466p-5p	3	0	4	-3	4
miR-196b-3p	230	227	84	-3	-143
miR-669a-5p	8	5	2	-3	-3
miR-296-5p	18	15	0	-3	-15
miR-369-5p	25	22	28	-3	6
miR-1943-3p	19	17	31	-2	14
miR-298-5p	13	11	0	-2	-11
miR-9-3p	34	32	105	-2	73
miR-344d-3p	2	0	0	-2	0
miR-669b-5p	2	0	0	-2	0
miR-106a-5p	22	21	19	-1	-2
miR-466c-5p	6	4	0	-2	-4
miR-669-5p	4	3	0	-1	-3
miR-874-3p	77	77	17	0	-60
miR-505-3p	16	15	9	-1	-6
miR-184-3p	6	7	0	1	-7
miR-376a-5p	6	7	0	1	-7
miR-677-5p	6	7	8	1	1
miR-1964-3p	12	14	0	2	-14
miR-1193-3p	64	66	25	2	-41
miR-1197-3p	8	10	8	2	-2
miR-99a-3p	22	25	22	3	-3
miR-331-5p	23	26	33	3	7
miR-19b-1-5p	7	10	0	3	-10
miR-503-3p	7	10	0	3	-10
miR-666-5p	17	21	0	4	-21
miR-182-3p	7	11	26	4	15
miR-467e-5p	30	35	79	5	44
miR-3073a-3p	16	21	0	5	-21
miR-299a-5p	131	137	44	6	-93
miR-8112	8	14	0	6	-14
miR-338-5p	71	78	61	7	-17
miR-664-5p	17	24	44	7	20
miR-7219-3p	6	13	8	7	-5
miR-219a-3p	7	14	9	7	-5
miR-493-5p	7	15	8	8	-7
miR-499-5p	7	15	34	8	19
miR-376a-3p	76	85	65	9	-20
miR-676-5p	15	24	92	9	68
miR-31-5p	27	36	25	9	-11
miR-374c-3p	52	63	122	11	59
miR-1968-5p	22	33	0	11	-33

miR-346-5p	0	11	0	11	-11
miR-365-5p	0	11	22	11	11
miR-491-5p	8	20	0	12	-20
miR-186-3p	31	43	9	12	-34
miR-377-5p	6	18	0	12	-18
miR-3547-3p	0	13	0	13	-13
miR-485-5p	29	43	0	14	-43
miR-195a-3p	114	128	103	14	-25
miR-99b-3p	93	107	48	14	-59
miR-125b-3p	156	171	304	15	133
miR-673-5p	12	28	8	16	-20
miR-532-3p	136	152	36	16	-116
miR-34b-5p	0	17	26	17	9
miR-431-3p	0	17	0	17	-17
miR-452-5p	7	24	19	17	-5
miR-543-3p	103	120	34	17	-86
miR-200c-5p	11	29	26	18	-3
miR-384-5p	0	18	8	18	-10
miR-380-3p	30	49	56	19	7
miR-665-3p	66	85	8	19	-77
miR-301a-5p	49	68	62	19	-6
miR-380-5p	7	28	20	21	-8
miR-144-5p	22	45	62	23	17
miR-467c-5p	17	40	48	23	8
miR-582-3p	58	82	209	24	127
miR-363-3p	8	32	0	24	-32
miR-879-5p	23	49	78	26	29
miR-32-3p	65	91	19	26	-72
miR-350-5p	29	56	31	27	-25
miR-1981-3p	20	47	28	27	-19
miR-135a-5p	17	45	38	28	-7
miR-409-3p	367	394	89	27	-305
miR-25-5p	16	43	26	27	-17
miR-3102-3p	52	81	0	29	-81
miR-299a-3p	296	326	123	30	-203
miR-488-3p	25	56	232	31	176
miR-667-3p	15	49	0	34	-49
miR-433-3p	71	106	25	35	-81
miR-486b-5p	237	272	178	35	-94
miR-92a-5p	16	52	51	36	-1
miR-205-3p	17	53	25	36	-28
miR-193a-5p	11	47	45	36	-2
miR-335-5p	185	223	574	38	351
miR-3081-3p	26	66	8	40	-58

miR-152-5p	211	251	118	40	-133
miR-485-3p	55	98	0	43	-98
miR-222-3p	765	811	591	46	-220
miR-382-5p	322	369	44	47	-325
miR-96-3p	15	67	45	52	-22
miR-181c-3p	644	697	890	53	193
miR-877-3p	55	112	0	57	-112
miR-139-3p	65	124	44	59	-80
miR-134-5p	455	516	291	61	-225
miR-376c-3p	55	116	69	61	-47
miR-322-3p	1,230	1,294	669	64	-625
miR-1981-5p	8	72	8	64	-64
miR-147-5p	113	180	748	67	568
miR-140-5p	1,192	1,260	1,122	68	-138
miR-672-5p	185	254	28	69	-226
miR-148b-5p	99	169	165	70	-4
miR-132-5p	56	128	94	72	-34
miR-379-3p	124	206	78	82	-128
miR-153-3p	170	252	182	82	-70
miR-155-5p	605	693	422	88	-271
miR-450b-5p	176	265	53	89	-212
miR-431-5p	48	137	51	89	-86
miR-29b-5p	32	121	51	89	-70
miR-330-3p	27	116	28	89	-88
miR-219a-5p	74	168	25	94	-143
miR-496a-3p	44	138	44	94	-94
miR-324-5p	256	351	243	95	-108
miR-1843b-5p	253	350	356	97	6
miR-196a-5p	1,894	1,992	680	98	-1,312
miR-700-5p	215	315	98	100	-217
miR-6538	52	156	104	104	-52
miR-340-3p	57	163	373	106	210
miR-434-3p	1,343	1,455	747	112	-708
miR-221-5p	67	190	268	123	78
miR-28a-3p	589	719	556	130	-163
miR-224-5p	1,049	1,179	265	130	-914
miR-374b-5p	2,309	2,439	9,151	130	6,712
miR-136-5p	300	440	268	140	-172
miR-674-3p	751	896	603	145	-293
miR-339-3p	39	194	173	155	-21
miR-331-3p	629	785	344	156	-441
miR-1198-5p	213	374	44	161	-330
miR-1983	232	396	209	164	-187
miR-700-3p	425	591	117	166	-474

miR-345-3p	509	680	730	171	50
miR-130b-5p	179	354	165	175	-189
miR-128-3p	863	1,042	263	179	-779
miR-27a-5p	161	343	726	182	383
miR-338-3p	118	318	443	200	125
miR-411-3p	209	410	323	201	-87
miR-183-3p	29	231	83	202	-148
miR-361-3p	343	555	151	212	-404
miR-494-3p	31	247	65	216	-182
miR-410-3p	304	523	458	219	-65
miR-181a-3p	558	790	804	232	14
miR-106b-3p	1,022	1,256	566	234	-690
miR-329-5p	73	307	65	234	-242
miR-361-5p	2,001	2,246	1,325	245	-921
miR-574-5p	485	751	41	266	-710
miR-221-3p	3,635	3,911	3,654	276	-257
miR-362-5p	1,185	1,464	1,565	279	101
miR-190a-5p	21	304	97	283	-207
miR-30d-3p	190	473	889	283	416
miR-17-3p	672	958	616	286	-342
miR-503-5p	359	651	128	292	-523
miR-15a-5p	1,742	2,035	2,443	293	408
miR-351-5p	272	604	316	332	-288
miR-144-3p	324	689	725	365	36
miR-34a-5p	1,526	1,893	564	367	-1,329
miR-542-3p	90	466	125	376	-341
miR-301a-3p	146	523	309	377	-214
miR-218-5p	507	885	666	378	-219
miR-127-5p	292	675	344	383	-331
miR-34c-5p	282	668	882	386	214
miR-434-5p	805	1,245	717	440	-528
miR-148a-5p	928	1,391	1,963	463	572
miR-381-3p	719	1,225	641	506	-584
miR-501-3p	456	991	215	535	-776
miR-423-3p	791	1,331	390	540	-941
miR-21a-3p	462	1,062	840	600	-222
miR-409-5p	295	914	362	619	-552
miR-339-5p	3,102	3,722	3,049	620	-673
miR-3068-5p	1,264	1,893	2,681	629	788
miR-497a-5p	3,229	3,874	2,697	645	-1,177
miR-872-3p	225	894	815	669	-79
miR-33-5p	164	848	137	684	-711
miR-24-5p	1,608	2,311	4,405	703	2,094
miR-181c-5p	2,788	3,492	3,659	704	167

miR-484	6,606	7,343	5,256	737	-2,087
miR-19b-3p	5,820	6,562	3,425	742	-3,137
miR-532-5p	781	1,545	528	764	-1,017
miR-322-5p	1,029	1,841	606	812	-1,235
miR-32-5p	736	1,624	706	888	-918
miR-455-3p	726	1,623	271	897	-1,352
miR-93-5p	16,824	17,740	7,958	916	-9,782
miR-423-5p	1,302	2,226	320	924	-1,906
miR-379-5p	417	1,579	620	1,162	-959
miR-142a-3p	1,587	2,753	1,804	1,166	-949
miR-7b-5p	873	2,099	3,249	1,226	1,150
miR-185-5p	1,964	3,400	2,670	1,436	-730
miR-151-3p	2,498	4,008	1,062	1,510	-2,946
miR-455-5p	1,390	2,987	1,048	1,597	-1,939
miR-200a-5p	595	2,237	2,028	1,642	-209
miR-200b-5p	912	2,681	783	1,769	-1,898
miR-26a-5p	120,950	122,738	128,088	1,788	5,350
miR-20a-5p	14,812	16,650	9,899	1,838	-6,751
miR-127-3p	10,203	12,073	2,006	1,870	-10,067
miR-15b-5p	3,230	5,119	2,770	1,889	-2,349
miR-19a-3p	634	2,633	627	1,999	-2,006
miR-107-3p	2,974	4,998	3,959	2,024	-1,039
miR-98-5p	1,662	3,821	3,057	2,159	-764
miR-744-5p	479	2,646	401	2,167	-2,245
miR-146b-5p	1,173	3,405	2,583	2,232	-822
miR-26b-5p	46,415	48,655	72,583	2,240	23,928
miR-186-5p	3,876	6,184	8,655	2,308	2,471
miR-147-3p	5,398	7,883	8,857	2,485	974
miR-183-5p	24,064	26,951	13,434	2,887	-13,517
miR-92a-3p	2,717	5,644	973	2,927	-4,671
miR-205-5p	6,205	9,595	2,282	3,390	-7,313
miR-143-5p	1,387	4,827	13,503	3,440	8,676
miR-126a-5p	21,218	24,824	40,238	3,606	15,414
miR-22-3p	18,186	22,016	43,298	3,830	21,282
let-7e-5p	2,350	6,493	1,268	4,143	-5,225
miR-17-5p	4,346	8,688	3,593	4,342	-5,095
miR-1a-3p	2,989	7,441	22,584	4,452	15,143
miR-7a-5p	3,110	7,580	7,875	4,470	295
miR-340-5p	6,842	11,537	9,605	4,695	-1,932
miR-148b-3p	4,603	10,136	11,624	5,533	1,488
miR-199b-3p	34,591	40,360	32,452	5,769	-7,908
miR-25-3p	12,505	18,788	9,657	6,283	-9,131
miR-96-5p	4,062	10,364	9,602	6,302	-762
miR-181a-5p	7,924	14,379	4,051	6,455	-10,328

let-7d-5p	9,713	16,641	13,073	6,928	-3,568
miR-151-5p	8,997	16,079	13,073	7,082	-3,006
miR-215-5p	85,529	92,654	175,976	7,125	83,322
miR-10a-5p	42,206	50,417	49,136	8,211	-1,281
miR-199a-5p	15,354	24,214	19,856	8,860	-4,358
miR-125b-5p	7,257	16,539	17,321	9,282	782
miR-100-5p	14,536	24,780	38,282	10,244	13,502
miR-99a-5p	14,536	24,780	38,282	10,244	13,502
miR-203-3p	2,687	13,832	9,570	11,145	-4,262
miR-146a-5p	9,351	20,555	12,452	11,204	-8,103
miR-101a-3p	42,718	54,813	56,691	12,095	1,878
let-7b-5p	20,853	33,448	8,691	12,595	-24,757
miR-126a-3p	38,616	53,124	82,351	14,508	29,227
miR-152-3p	34,337	50,079	26,964	15,742	-23,115
miR-103-3p	9,567	27,480	14,302	17,913	-13,178
miR-191-5p	21,335	42,182	40,269	20,847	-1,913
miR-200c-3p	17,423	39,162	13,609	21,739	-25,553
miR-375-3p	93,198	115,315	54,757	22,117	-60,558
miR-30b-5p	11,103	36,242	19,843	25,139	-16,399
miR-30c-5p	9,266	34,410	28,435	25,144	-5,975
let-7i-5p	37,176	63,556	34,098	26,380	-29,458
let-7a-5p	19,060	53,329	24,447	34,269	-28,882
let-7c-5p	30,393	79,683	32,094	49,290	-47,589
let-7f-5p	51,022	105,438	112,419	54,416	6,981
miR-30d-5p	7,003	65,605	43,133	58,602	-22,472
miR-30a-5p	19,934	85,382	81,404	65,448	-3,978
let-7g-5p	50,354	124,550	97,101	74,196	-27,449
miR-194-5p	85,675	169,274	165,965	83,599	-3,309
miR-30e-5p	24,946	113,295	57,750	88,349	-55,545
miR-200b-3p	171,853	334,093	139,362	162,240	-194,731
miR-148a-3p	37,461	209,390	173,201	171,929	-36,189
miR-200a-3p	380,522	754,583	498,181	374,061	-256,402
miR-192-5p	656,011	1,081,718	1,341,381	425,707	259,663
miR-143-3p	294,225	954,512	1,655,929	660,287	701,417
miR-21a-5p	319,136	1,360,772	626,341	1,041,636	-734,431

Supplementary Materials

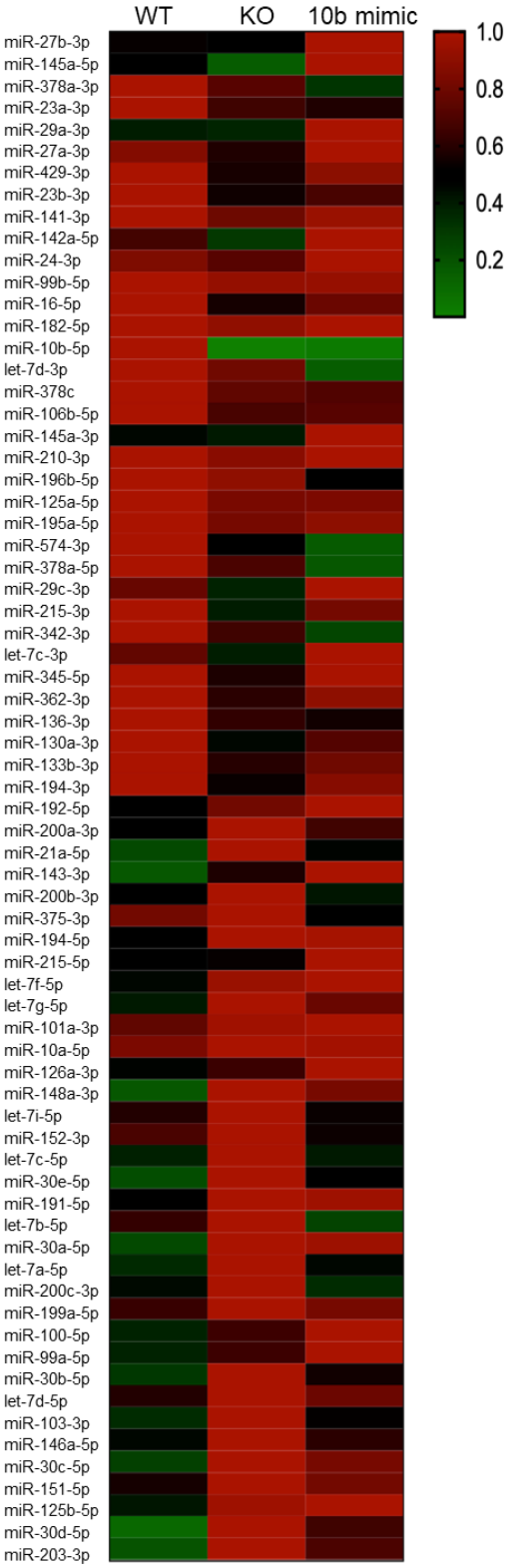

Supplementary Figure 1: Heat map showing the normalized expression of differentially expressed miRNAs in colonic mucosa from WT, KO and 10b mimic injected mice obtained by miRNA-seq analysis. Heat map colors range from dark green to dark red, representing low and high expression, respectively.

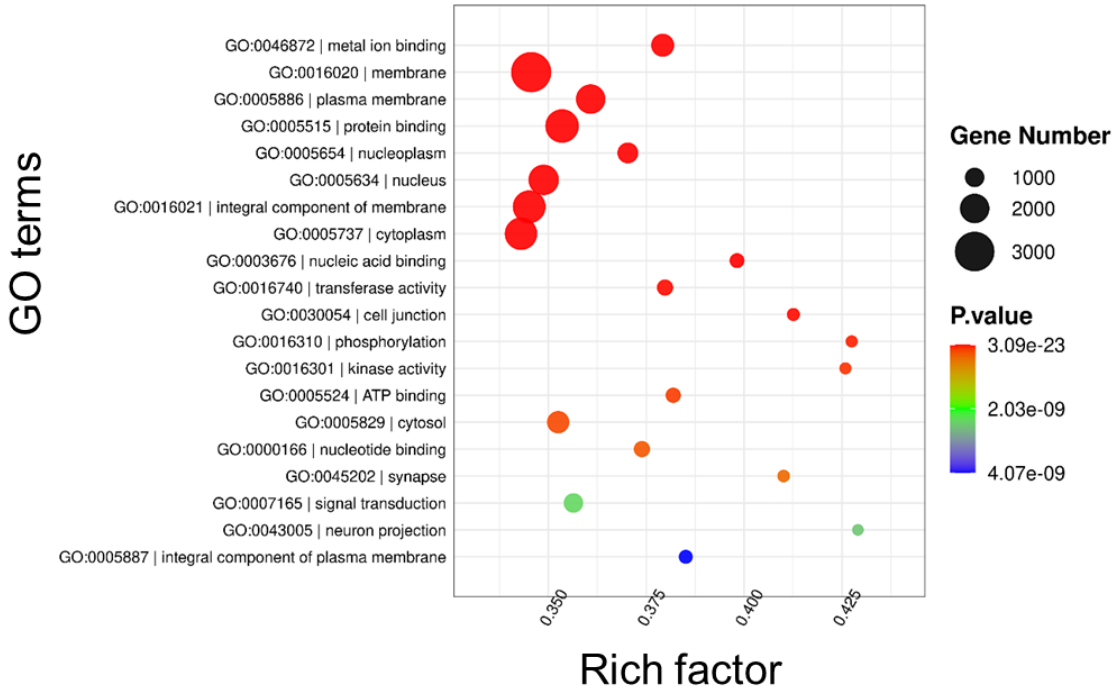

Supplementary Figure 2: Scatter plot of enriched GO terms associated with the depletion of miR-10b-5p in colonic mucosa of mir-10b KO vs. WT.